An Optical and Infrared Study of Blazars

Andrew Robert Graham Mead

Presented for the Degree of Doctor of Philosophy
at the University of Edinburgh

August, 1988.

This thesis is my own composition, except where specifically indicated in the text.

August, 1988.

Table of Contents

Chapter 2: Polarimetric Observations of Blazars

Chapter 3: The Cluster Environments of Blazars

Abstract

This thesis presents a study of some of the optical and infrared properties of blazars. A review of previous observations of blazars is given. The evidence for bulk relativistic flows in quasars and blazars is also discussed. The observational study has two parts. First a series of infrared and optical polarization measurements of blazars are presented. Second a study of the cluster environments of blazars is reported.

The polarization study consisted of 156 observations of 37 blazars and candidate blazars at infrared and optical frequencies. The observations of the quasar $1253-055$ (3C 279) showed a U polarization of $45.5 \pm 0.9\%$. This is the highest ever seen in a blazar. The effect of the proposed 'blue bump' on the observations of $1641+399$ (3C 345) is discussed, as are other sources of unpolarized contaminating flux. The interpretation of the observed spectrum is discussed in terms of shock acceleration models and the synchrotron-self-Compton jet pictures. It is shown that frequency dependence is a common feature of the polarization behaviour with the polarization generally increasing towards higher frequencies. Position angle frequency-dependence is an infrequent phenomenon. No evidence is found to support the claim that frequency dependence is related to high levels of polarization. No characteristic form of blazar variability is evident in the data. The possible explanations of the observed frequency dependence are discussed. The frequency-dependent polarization can be interpreted as a result of the spectral curvature which in turn is explained as being the result of an inhomogeneous source. However the structure of this source is unknown. A second picture explains the observed behaviour in terms of a polarized cut-off component (which is identified with emission from a shock) and an unpolarized steep spectrum component. This can explain the observations of $1253-055$ (3C 279) and many other of the observed cases of frequency-dependent polarization.

The study of the cluster environments of blazars was formulated as a test of a unified scheme. Deep CCD observations were obtained for a sample of blazars and quasars with extended radio structure. The unified scheme predicts that these are distinguished only by their relative orientation. The strength of the cluster environment was parameterised by the amplitude of the quasar-galaxy spatial correlation function B_{gq}. The evaluation of this quantity is subject to large systematic errors as a result of the uncertainty in the galaxy luminosity function. Previously published data had to be re-evaluated so as to be comparable with the data presented here. No evidence was found for a difference in the environments of blazars relative to those of extended quasars. A previously reported correlation between B_{gq} and redshift was confirmed, but cannot be distinguished from an apparent relationship due to a correlation between B_{gq} and radio power since radio power is known to be correlated with redshift.

Introductory Comments

This thesis consists of the investigation of two aspects of blazars. Chapter 1 contains a review of the current state of blazar studies and includes a brief description of the relevant pieces of synchrotron physics. Chapter 2 presents a series of polarimetric IR/optical observations of blazars, which were obtained at UKIRT in 1986 and 1987. Chapter 3 presents a study of the galaxy clusters around blazars and their possible relevance to unified schemes relating blazars to other quasars.

The observations listed in Chapter 2 were conducted as part of a collaboration including Dr. P. Brand (Univ. of Edinburgh), Dr. J. Hough (Hatfield Polytechnic), Dr. J. Bailey (Anglo-Australian Observatory) and Dr. D. Axon (University of Manchester). The observations described in Chapter 3 were conducted in collaboration with Dr. P. Brand (Univ. of Edinburgh) and Dr. L. Miller (Royal Observatory Edinburgh).

This opportunity will be taken to outline some terminology which will be consistently used throughout this thesis. The term quasar will be used throughout to refer to both radio and optically selected objects. The term QSO (quasi-stellar object) will not be used. Quasars (and hence blazars) will all be assumed to have cosmological redshifts. The standard Friedmann cosmology will be assumed (with no cosmological constant). Distances, luminosities and other quantities which were calculated using this cosmology will, where possible, be quoted independently of the value of H_0. The chosen value of q_0 (or equivalently Ω_0) will be specified at the appropriate part of the text.

Blazar optical spectra are often fitted by power-law spectra. These power-laws will be parameterised as $S_\nu(\nu) \propto \nu^{-\alpha}$. This ensures that most blazar spectra have positive spectral indices. The following symbol conventions are used; $S_\nu(\nu)$ is the spectral flux density, $p(\nu)$ the polarization, $P_\nu(\nu)$ the polarized spectral flux density and $\theta(\nu)$ is the polarization position angle. When referred

to, the symbols for the Stokes' parameters are S_ν, Q_ν, U_ν and V_ν. Following the common practice, the values of $p(\nu)$ have been expressed as percentage values when explicitly quoted.

Physical quantities are referred to in terms of SI units and derived units (e.g flux density in milliJanskies - mJy). The only exceptions are the common astronomical units such as parsecs and magnitudes and units of time (e.g. days).

Much mention of the frequency dependence properties of the polarization behaviour will be made. To avoid tedious repetition the convenient short-hands of FDP and FDθ will be used. FDP refers to the 'frequency dependence of the degree of polarization'. FDθ refers to the 'frequency dependence of the position angle of polarization'. Another abbreviation which is frequently used in Chapter 3 is LF which refers to the luminosity function.

Acknowledgements

First I must thank my supervisor and co-observer Peter Brand for his help over the last few years. Lance Miller and Alan Heavens have also been a great source of help and were volunteered to read parts of this manuscript. I must also thank John Peacock, Chris Collins and Klaus Meisenheimer for many useful discussions, Jim Hough, Jeremy Bailey and Dave Axon for their help with the UKIRT observations and Howard Yee for a copy of his incredible PPP code.

All my fellow students (and some other itinerants) have contributed to the successful (and delayed) completion of this thesis. In particular I must especially thank James Dunlop (for many a pint in the Argyle and the consequent ulcers), James More (for his truly wonderful orange vehicle), Crispin Keable (for his cool), Phil Puxley (for at least one friendly elbow in the throat), Toby Moore (for his example of extreme hard work), the Guppy (for the breathing exercises), Neil H... (for his positive attitude towards astronomy), John Rayner (for his praise on the football field), Mark Yates (for confirming my suspicions about Guildford), Steve Torchinsky (because he asked to be mentioned), Paul Mitchell (for his incredibly annoying Star Trek door noises and, of course, the fish) and Stuart Lumsden (for the squid).

Other people, places and things who deserve mention; Tracey, Sue , John, Ruth, Joan, The Argyle, Diggers, Kenny Dalglish, Midweek Sportsound, McEwan's and Belhaven 70\− and 80\−.

Much encouragement was offered by my parents and all my family.

Lastly I must acknowledge the receipt of an S.E.R.C. research studentship.

Chapter 1

A Review of Blazars

This chapter contains a overview of the observational characteristics of blazars (§1.1), a review of the observations of jets in active galactic nuclei (AGN) together with a discussion of the evidence for bulk relativistic motion in blazars (§1.2), and a discussion of the possible emission mechanisms in blazars (§1.3).

1.1 Observations of Blazars

1.1.1 DEFINITION OF A BLAZAR

Blazars are a class of extragalactic radio-source. The defining characteristics are:

1. Core-dominated radio emission which has a flat spectrum and is variable.
2. An unresolved non-stellar optical continuum source.
3. Significant optical and infrared polarization.
4. Rapid and extreme optical variability.

This includes all the major features which led to the invention of this class as a unification of two existing groupings of objects (Angel & Stockman 1980). These were the BL Lac objects (e.g. Stein, O'Dell & Strittmatter 1976) and the OVV (optically violently variable) quasars. The term HPQ (highly polarized quasar, Moore & Stockman 1981) will be used in preference to the term OVV quasar (see §1.1.3).

The motivation for the unification of these two groups was the recognition of the fact that they are indistinguishable in terms of their continuum properties at frequencies from the radio through to the optical. The sole characteristic which, historically, would have led to an object being classified as a BL Lac object rather than as a quasar (or a radio galaxy) is the presence or absence of emission lines in its optical spectrum. However, some HPQ's can be seen to appear to be lineless at times of peak optical luminosity (e.g. $1921-293$ [1] Wills & Wills 1981 and $2223-052$ Barbieri *et al.* 1985). Conversely, many BL Lac objects are now known to have emission line features (e.g. Miller, French & Hawley 1978). Given that the one known distinction is now no longer as sharp as it was thought to be, and that the continuum properties of these objects are so similar, some degree of unification into the class blazars is certainly secure. In §1.1.5 attempts to find some differences among the class of blazars are discussed.

1.1.2 A CATALOGUE OF BLAZARS

Table 1.1a lists all known blazars and Table 1.1b lists those objects which have been proposed as candidate blazars. No distinction has been made between objects which have been classified as BL Lac objects or HPQ's. The main sources for these tables are the original list of blazars given by Angel & Stockman (1980) and the more recent compilation of Ledden & O'Dell (1985). Some of the information about these objects has been obtained from the catalogue of Hewitt & Burbidge (1987).

The criterion for inclusion in Table 1.1a as a confirmed blazar is that the object displays all the characteristics of blazar emission described in §1.1.1. Because the optical polarization is the most difficult property to measure, and is often subject to large errors, Moore & Stockman (1981) and Moore & Stockman (1984) arbitrarily adopted the classification criteria that a definite HPQ would

[1] All blazars will be referred to by their IAU designations.

Table 1.1a : *Confirmed Blazars*

IAU Designation	Other Name	z	Pol. Ref.	z Ref.
0048 − 097	OB–081		(1,2)	
0106 + 013	PKS	2.107	(3)	(4)
0109 + 224	GC		(1)	
0118 − 272	PKS		(5,6)	
0138 − 097			(5)	
0215 + 015	PKS	1.721	(1)	(7)
0219 + 428	3C 66A	0.444 (?)	(1)	(8)
0219 − 164	PKS		(9)	
0229 + 341	3CR 68.1	1.238	(3)	(10)
0235 + 164	AO	0.9399	(1)	(11)
0300 + 470	4C 47.08		(1)	
0317 + 186	1E	0.190	(12)	(12)
0323 + 022	1H	0.1471	(13)	(14)
0336 − 019	CTA 26	0.852	(3)	(15)
0338 − 214			(6)	
0403 − 132	PKS	0.571	(16)	(17)
0420 − 014	PKS	0.915	(1)	(15)
0422 + 004	OF 038		(1)	
0454 − 234		1.009 (?)	(5)	(18)
0458 − 020	PKS	2.286	(3)	(19)
0521 − 365	PKS	0.0554	(1,20)	(21)
0537 − 441	PKS	0.8940	(20,5)	(22)
0548 − 322	PKS	0.0690 (g)	(1)	(23)
0716 + 714	S5		(24)	
0735 + 178	PKS	$\geq$0.424	(1)	(8)
0736 + 017	PKS	0.191	(1)	(17)
(0752 + 258)	OI 287	0.446	(1)	(25)
0754 + 100	OI 090.4		(1)	
0808 + 019	PKS		(1)	
0818 − 128	OJ–131		(1)	
0823 + 033			(5)	
0823 − 233			(5)	
0829 + 046	OJ 049		(1)	
0836 + 182			(26)	
0846 + 513	W1	1.860	(3,27)	(28)
0851 + 202	OJ 287	0.306	(1)	(29)
0906 + 430	3CR 216	0.670	(1)	(30)
0906 + 015	PKS	1.018	(3)	(31)
0912 + 297	OK 222		(1)	
1034 − 293	PKS		(5)	
1057 + 100	HM		(1)	
1101 + 384	Mkn. 421	0.0308	(1)	(8)
1133 + 704	Mkn. 180	0.0458	(1)	(8)

Table 1.1a : *Confirmed Blazars (Contd.)*

IAU Designation	Other Name	z	Pol. Ref.	z Ref.
1144 − 379	PKS		(5)	
1147 + 245	OM 280		(1)	
1156 + 295	4C 29.45	0.729	(1)	
1215 + 303	ON 325		(1)	
1218 + 304	2A	0.130	(26)	
1219 + 285	W Coma	0.102	(1)	
1244 − 255		0.638	(5)	
1253 − 055	3C 279	0.538	(1)	(32)
1308 + 326	B2	0.997	(1)	(8)
1335 − 127	PKS	0.541 (?)	(5)	(18)
1349 − 439			(5)	
1400 + 162	MC3	0.244	(1)	(33)
1418 + 546	OQ 530		(1)	
1424 + 240			(5)	
1424 − 418			(5)	
1510 − 089	PKS	0.361	(16,34)	(35)
1514 + 197	GC		(1)	
1514 − 241	AP Libra	0.049	(1)	(8)
1519 − 273			(5)	
1522 + 155	MC3	0.628	(1)	(36)
1532 + 017		1.420	(5)	
1538 + 149	4C 14.60		(1,20)	
1546 + 027	PKS	0.413	(14)	(31)
1641 + 399	3C 345	0.595	(1)	(37)
1652 + 398	Mkn. 501	0.034	(1)	(8)
1717 + 178	OT 129		(1,6)	
1727 + 502	I Zw 186	0.055	(1)	(8)
1749 + 701	W1		(26)	
1749 + 096	OT 081	0.32	(1)	(38)
1921 − 293	OV–236	0.3525	(39,40)	(40)
1954 − 388		0.626	(5)	(41)
2155 − 304	PKS	0.117 (g)	(1)	(42)
2200 + 420	BL Lacertae	0.0690	(1)	(8)
2208 − 137	PKS	0.392	(1)	(43)
2223 − 052	3C 446	1.404	(1)	(37)
2230 + 114	CTA 102	1.037	(1)	(44)
2234 + 282	B2	0.795	(3)	(3)
2243 − 123		0.630	(5)	(41)
2251 + 158	3CR 454.3	0.859	(1)	(17)
2254 + 074	OY 091	0.190	(1)	(38)
2254 − 204			(5)	
2345 − 167	PKS	0.600	(1)	(45)

Table 1.1b : *Candidate Blazars*

IAU Designation	Other Name	z	Blazar Ref.	Pol. Ref.	z Ref.
0019 + 058			(46)		
0110 − 131	H		(47)		
0212 + 735	S5	2.367		(24)	(48)
0306 + 102	OE 110		(49)		
0208 − 512		1.003		(5)	(5)
0301 − 243				(5)	
0332 − 403		1.455		(5)	(5)
0414 + 009	H			(5)	
0420 + 022			(46)		
0431 − 531	H		(47)		
0438 − 436		2.852		(5)	(5)
0503 − 044			(46)		
0605 − 085		0.870		(5)	(5)
0743 − 006			(46)		
0855 + 143	3CR 212	1.048 (?)		(16)	(30)
1011 + 496	5C 12.123			(50)	
1055 + 018		0.888		(5)	(5)
1100 − 230	H			(5)	
1150 + 497	4C 49.22	0.334		(16)	
1207 + 397		0.59		(12)	(12)
1217 + 348				(50)	
1225 + 206	4C 20.29			(51)	
1235 + 632	1E	0.297		(12)	(12)
1301 − 192	PKS		(52)		
1307 + 121	4C 12.46			(53)	
1309 − 216		1.491		(5)	(5)
1402 + 042			(12)		
1408 + 020			(54)		
1413 + 135	OQ 122	0.260		(55)	(55)
1415 + 256		0.237		(5)	(5)
1502 + 106		1.839		(5)	(5)
1504 − 167		0.876		(5)	(5)
1548 + 056				(5)	
1604 + 159	MC3			(53)	
1610 − 771		1.710		(5)	(5)
1622 + 238	3CR 336	0.927		(14)	(56)
1704 + 607			(54)		
1803 + 784	S5			(24)	
2005 − 489	PKS	0.071	(57)		(58)
2007 + 776	S5			(24)	
2010 − 697	H		(47)		
2032 + 107	MC	0.601	(1)	(43)	
2131 − 021	PKS	0.557 (?)	(4)		
2155 − 152	OX-192			(59)	
2201 + 171	MC3	1.080		(14)	(36)
2206 − 260				(5)	
2229 − 542	1H		(47)		
2233 − 148			(18)		
2240 − 260				(5)	
2335 + 031	4C 03.59		(51)		
2355 − 534		1.006		(5)	(5)

Table 1.1: *References*

(1) Angel & Stockman (1980)
(2) Bailey, Hough & Axon (1983)
(3) Moore & Stockman (1984)
(4) Wills & Lynds (1978)
(5) Impey & Tapia (1988)
(6) This work
(7) Boissé & Bergeron (1988)
(8) Miller, French & Hawley (1978)
(9) Meisenheimer & Röser (1984)
(10) Boksenberg, Carswell & Oke (1976)
(11) Cohen *et al.* (1987)
(12) Stocke *et al.* (1984)
(13) Feigelson *et al.* (1986)
(14) Filippenko *et al.* (1986)
(15) Bolton & Wall (1970)
(16) Moore & Stockman (1981)
(17) Lynds (1967)
(18) Wilkes *et al.* (1983)
(19) Strittmatter *et al.* (1974)
(20) Brindle *et al.* (1986)
(21) Danziger *et al.* (1979)
(22) Peterson *et al.* (1976)
(23) Fosbury & Disney (1976)
(24) Biermann *et al.* (1981)
(25) Wills & Wills (1976)
(26) Wills *et al.* (1980)
(27) Sitko *et al.* (1984)
(28) Arp *et al.* (1979)
(29) Sitko & Junkkarinen (1985)
(30) Smith & Spinrad (1980)
(31) Burbidge & Strittmatter (1972)
(32) Burbidge & Rosenberg (1965)
(33) Baldwin *et al.* (1977)
(34) Smith *et al.* (1987)
(35) Burbidge & Kinman (1966)
(36) Smith *et al.* (1977)
(37) Burbidge (1965)
(38) Stickel, Fried & Kühr (1988a)
(39) Wills & Wills (1981)
(40) Impey *et al.* (1982)
(41) Browne, Savage & Bolton (1975)
(42) Bowyer *et al.* (1984)
(43) Antonucci *et al.* (1987)
(44) Schmidt (1965)
(45) Folsom, Smith & Hackney (1970)
(46) Fricke *et al.* (1983)
(47) Buckley, Tuohy & Remillard (1985)
(48) Lawrence *et al.* (1986)
(49) Wills & Wills (1979)
(50) Wisniewski, Sitko & Sitko (1986)
(51) Stein, O'Dell & Strittmatter (1976)
(52) Jauncey *et al.* (1978)
(53) Zotov & Tapia (1979)
(54) Chanan *et al.* (1982)
(55) Bregman *et al.* (1981)
(56) Lynds *et al.* (1966)
(57) Wall *et al.* (1986)
(58) Falomo *et al.* (1987)
(59) Wardle, Moore & Angel (1984)

be an object with two or more measured optical (or infrared) polarizations (p) greater than 3% and with $p/\sigma_p > 3$. The use of 3% as the significant level is discussed in §1.1.3. These restrictions have been imposed on the objects listed in Table 1.1a where the polarization reference refers either to the seminal list of Angel & Stockman (1980) or to the first two recorded polarization measurements. Some of the objects listed as candidate blazars in Table 1.1b have a solitary significant polarization measurement which is referenced. Others have no recorded polarization measurements and the 'blazar reference' refers to the original suggestion that the object might be a blazar. This is usually a lineless optical spectrum and a consequent classification as a BL Lac object. Where known, the redshifts of these objects are also given. The lower limit to the redshift of $0735+178$ is obtained from an absorption line spectrum. The redshifts of $0548-322$ and $2155-304$ are flagged by the code '(g)', which refers to redshifts obtained from features in the starlight of the host galaxy of the blazar rather than from emission lines from the nucleus. No references to featureless spectra have been given. As mentioned in §1.1.1 these are susceptible to the brightness state at the time of observation and thus cannot be relied on as evidence that the spectrum of the blazar is truly lineless.

While every object in Table 1.1a exhibits the characteristic blazar emission properties listed in §1.1.1, this catalogue can in no way be regarded as a statistically complete sample of blazars. This list is compiled from the observations of a wide range of authors using different instruments to investigate sources from different surveys (both radio and X-ray) at various flux limits and degrees of completeness. Consequently the set of blazars as defined above is subject to a wide a variety of unquantifiable selection effects. A further cause of incompleteness is the variability of these objects, which can cause an object, capable of showing blazar emission at some periods in its history, to be totally missed by a survey carried out at a single epoch. The list of blazars will undoubtedly increase as more blazars are discovered as the result of polarization surveys of complete radio samples. The 17 blazars and 17 blazar candidates discovered by

Impey & Tapia (1988) in their observations of a sample of Parkes radio sources are included in Table 1.1a. Wills *et al.* (1987) also report the discovery of 23 new HPQ's but do not give names and coordinates.

Another source of incompleteness is the arbitrary way in which objects are assigned to or excluded from the class of blazars at low redshifts and low luminosities. In their original list, Angel & Stockman (1980) included three objects not listed in Table 1.1. These are the radio-galaxies 0316 + 413 (NGC 1275), 1807 + 698 (3CR 371) and 1845 + 797 (3CR 390.3). Angel & Stockman (1980) regarded the latter object as a key in 'making the bridge between double lobe radio sources and those with variable stellar polarized nuclei'. However, these objects are dominated in the optical by the emission of the galaxy and have often been left out of subsequent lists of blazars. Furthermore 1845 + 797 is not even a core-dominated radio source and consequently does not agree with the definition of a blazar presented in §1.1.1. This exclusion (though followed here) is somewhat arbitrary as some of the objects listed in Table 1.1 are also located in bright galaxies (e.g. 0521 − 365) and little thought has been devoted to a criterion for defining a limit to the blazar class at these low luminosities. It may be possible that no physically justifiable limit can be imposed as blazar emission is claimed to be detected in more radio-galaxies (e.g. Cygnus A : Bailey *et al.* 1986, IC 5063 : Hough *et al.* 1987). What becomes more important is an observationally based criterion, which excludes those objects where an underlying galaxy can significantly hamper the study of the blazar nuclear emission. However, such a criterion would remove from consideration some of the famous BL Lac objects such as Mkn 421 (e.g. Kikuchi & Mikami 1987).

Finally, there is one other anomalous object. This is the HPQ 0752 + 258 (OI 287). This has been considered a blazar primarily on the basis of its high (8%) polarization (Moore & Stockman 1981). However there is little evidence of optical variability. Ulvestad & Antonucci (1988) consider the radio morphological properties of this source, and conclude that it is probably not a

blazar. Extrapolation of the radio core flux to infrared frequencies underpredicts the measured K flux by at least an order of magnitude. This would require a radio–IR spectrum quite unlike that seen in other blazars (§1.1.5). They further suggest that the optical polarization can probably be explained by scattering within a thin disc.

1.1.3 THE POLARIZATION PROPERTIES OF BLAZARS

The most characteristic feature of blazars is the high optical and infrared linear polarization. The polarization properties of blazars are briefly reviewed in this section. The following sections refer only to the optical and infrared polarization properties. There have been no detections of significant circular polarization in quasars, so all the results refer to linear polarization.

1.1.3.1 The Polarization Properties of the General Population of Quasars

BL Lac objects have long been known to be *appreciably* polarized (e.g. Stein, O'Dell & Strittmatter 1976). The HPQ's are solely distinguished from the general population of quasars on the basis of their *significant* polarization. On what objective criteria are these statements based?

Stockman (1978) reported the results of a polarization survey of quasars taken from the catalogue of Burbidge, Crowne & Smith (1977). This survey was extended by Moore & Stockman (1981), Moore & Stockman (1984) and Stockman, Moore & Angel (1984) who defined the class of HPQ's. They found that the distribution of their quasars with respect to 'white light' polarization was distinctly bimodal, with $p = 3\%$ being a suitable point to use to distinguish the HPQ's from the LPQ's (low polarization quasars). This is the origin of the classification criteria used to compile Table 1.1. Moore & Stockman (1984) studied a group of 186 radio-selected quasars and 53 optically-selected quasars. The numbers of HPQ's are 20 and 2 respectively. The two optically-selected

(and radio-quiet) HPQ's are both broad-absorption line (BAL) quasars (see e.g. Turnshek 1984). There were 10 other BAL quasars in Moore & Stockman's (1984) sample, and none of these were found to be highly polarized (according to the 3% criterion), though they did have polarizations somewhat higher than the average for the LPQ's. On this admittedly marginal evidence, the BAL polarization mechanism is assumed to be intrinsic to the BAL's and not related to blazar emission. This decision is made in the belief that the polarization mechanism seen in these objects is not that seen in the other HPQ's, which is intimately connected with blazar behaviour and radio emission in particular. (See also the attempts at optical-selection of blazars, Impey & Brand 1982; Borra & Corriveau 1984). Though the samples on which Moore & Stockman (1984) conducted their polarimetry were also poorly defined, they attempted to compare statistically the properties of the radio-loud LPQ's and the HPQ's. They found that the HPQ's were (*a*) associated with compact flat-spectrum radio-sources (*b*) large-amplitude photometric variability and (*c*) steep, smooth optical continua. They could *not* distinguish the HPQ's from the LPQ's on the basis of redshift, optical emission line equivalent-width, and optical or X-ray luminosity.

Recently, attempts have been made to study complete radio-selected samples of objects for optical polarization. Impey & Tapia (1988) present the results of such a study of a sample of stellar objects associated with a sample of sources brighter then 2 Jy at 5 GHz. Their results imply that at least 40% of sources in this sample are blazars (i.e. were highly polarized at the 3% limit). This is a lower limit to the fraction of compact radio sources which are blazars. The blazar polarization is known to be variable and can drop below the 3% HPQ classification criterion. Consequently a survey, which is limited to a small number of 'snapshots' of each blazar will inevitably miss a potentially significant fraction of blazars. The possibility remains that *all* compact radio sources will eventually be seen to be blazars (Impey 1987).

1.1.3.2 *The Frequency Dependence of the Polarization of Blazars*

In their review article, Angel & Stockman (1980) noted that the optical polarization of the continuum emission of a blazar was usually independent of frequency. However, small rotations in position angle and changes in polarization degree were noted in some objects. Since this date, improved polarimetric techniques over a wider frequency range have shown more examples of these phenomena than were discussed by Angel & Stockman (1980). Following Björnsson (1986), frequency dependence of the degree of polarization will be referred to as FDP and frequency dependence of the position of polarization as FDθ . Puschell & Stein (1980), Impey *et al.* (1982), Bailey, Hough & Axon (1983), Puschell *et al.* (1983), Impey *et al.* (1984), Holmes *et al.* (1984a), Holmes (1985), Sitko, Schmidt & Stein (1985), Brindle *et al.* (1986) and Smith *et al.* (1987) all report multifrequency observations of the polarization behaviour of blazars, and include many more cases of FDP and FDθ . The majority of these observations are concentrated in the optical wavebands, but include a substantial number of infrared measurements.

These observations indicate that FDP with $dp/d\nu > 0$ is more common than with $dp/d\nu < 0$. Where the latter occurs, it can often be explained in terms of dilution of a polarized continuum by unpolarized optical and near-UV emission (e.g. Smith *et al.* 1986, Chapter 2). Bailey, Hough & Axon (1983) reported a correlation between p(IR)/p(OPT) and p(OPT) which was also found in the data of Holmes *et al.* (1984a) and Holmes (1985).

FDθ seems to be much rarer. In most of these cases, the rotations are only of a few degrees. There is one case of a rotation of the position angle of the orientation of the order of 90° between the infrared and the optical for 0851+202 (OJ 287) in 1983 January (Holmes *et al.* 1984b). They use these observations to justify a model consisting of two polarized components of different spectral shapes to account both for the observed FDP and the FDθ . However, this model cannot explain all the observed cases of strong FDP (especially where this

occurs in the absence of FDθ). This and other explanations for the frequency-dependent polarization behaviour of blazars (§1.3.1) will be the subject of a large part of Chapter 2.

1.1.3.3 The Variability of the Polarization of Blazars

The most detailed study of the variability of the polarization in blazars has been that of $2200+420$ (BL Lac). There have been three major investigations of the behaviour of this object by Moore *et al.* (1982), Brindle *et al.* (1985) and Moore, Schmidt & West (1987). The first of these reported a week of continuous optical polarimetry, using a range of observatories allowing a coverage of 18 hours a day. Expressing the polarization behaviour in terms of the Stokes' parameters (Q,U) they found that the polarization behaviour could be characterised as a random walk in the $Q-U$ plane. Analysing the power spectrum of the variability, they found flat spectrum ('white noise') below 0.05 cycles per day, steepening to a power law of index -2 above this frequency. The model, which was advocated to explain these results, was that the polarization was a result of a large number of randomly oriented sub-components, each of which would be highly polarized ($\sim$ 70%), turning on rapidly at a rate of about 10 per day, and decaying after about 5 days. This would explain the absence of photometric variations accompanying the polarimetric variations. Brindle *et al.* (1985) observed BL Lac at a time when it was faint, and, in contrast, found that position angle variability in the polarization was much smaller. On this basis, they reject the Moore *et al.* (1982) model as an explanation of their data and propose a new component in addition to some randomly oriented components. The new component would have constant polarization, while the random components would now only require $\sim$ 25% polarizations. Moore, Schmidt & West (1987) investigated the higher (temporal) frequency variability of BL Lac, and found an even steeper power spectrum. They also interpret the variability behaviour in terms of random sub-components and the possibility of a constant component.

Though the observations of BL Lac (2200 + 420) represent the most thorough examination of the polarization variability of any blazar, this object does not show the full variety of behaviour seen in all blazars. An example of another well studied polarization event in a blazar is that seen by Holmes *at al.* (1984b) in the 1983 January observations of 0851 + 202 (OJ 287). These were mentioned in the last section (§1.1.3.2), as showing some quite extreme frequency dependent behaviour. However, the most extreme behaviour was only seen on one night. These data were interpreted as evidence for two components, one of which was rotating with respect to the other. This resulted in a minimum in the polarization at the frequency where their polarized fluxes were equal, when the position angles of the two polarizations were at 90° to each other. The less extreme FDP and FDθ seen on the other nights was interpreted as being the result of different relative orientations of the two components. While extreme, this behaviour has certain characteristics in common with those often seen in other blazars.

Kikuchi *et al.* (1988) present the first example of a correlated variation of the polarization of a blazar at both radio and optical frequencies. The particularly important results are the amplitudes of the observed position angle swings which can severely constrain the emission model. For example, Björnsson (1982) discusses the allowed variation in the position angle of an accelerating relativistic emitter. Their preferred explanation is a shock illuminating a helical magnetic field (c.f. Königl & Choudhuri 1985b and see §1.3.4).

1.1.4 THE RADIO PROPERTIES OF BLAZARS

1.1.4.1 Core Emission

This section will briefly review the core radio properties of blazars. The spectral shape will be discussed in §1.1.5, where the whole frequency range from radio through to X-ray will be discussed. Also the phenomenon of superluminal

motion, which occurs in at least 8 blazars, and maybe many more, will be deferred to §1.2. Angel & Stockman (1980) note that (with the exception of a BAL quasar; PHL 5200) all their original blazars show flat-spectrum core radio emission. They also note that the radio powers cover a wide range in luminosity.

The variability and polarization behaviour of the integrated cores of many blazars have been studied by Aller *et al.* (1985) (and references therein) using the University of Michigan 26 m radio telescope. Their observations include measurements at 8.0 GHz (since 1965), 14.5 GHz (since 1974) and 4.8 GHz (since 1977). The amount of data they have collected is vast and cannot be adequately described here. The major characteristic they find is that for most of their sources (not all of which are blazars) the timescale of the variability is of the order of months. Only a few blazars (0235 + 164, 0851 + 202 and 2200 + 420) show variability at these frequencies on timescales of the order of weeks. Typically, the amplitude of the variability increases with frequency (which Aller *et al.* 1985 interpret as an opacity effect). They find that the signature of both flux density and polarization variability is complicated and use this to advance a "shock in jet" model of the variability (§1.3.4). Higher frequency variability studies have been performed at 87 GHz by Barvainis & Predmore (1984) and in the sub-mm region by Gear *et al.* (1986). These show variability on timescales of months to week. The latter also interpret their results by a shock model.

VLBI milliarcsecond maps have been made of many blazars. Many of these can be interpreted in terms of a core and a series of knots, thought to be features in a jet (§1.2.1). Rusk & Seaquist (1985) have investigated the correlation of the VLBI structure axis with both the radio and optical core polarization position angle. Not all their objects were blazars, but they found that there was a strong tendency for the radio polarization to be perpendicular to the VLBI axis, while the optical polarization tended to be parallel to this axis. This latter relation has been re-investigated by Impey (1987). He considers only blazars, and concludes that, for those objects which can be considered to have

a preferred position angle, there is still a peak in the distribution of differences in angle at 0°. However, he also notes that there is the possibility of second, smaller amplitude peak at 90°.

Recently, the first measurements of VLBI polarization of quasars have been reported. Wardle *et al.* (1986) measured the polarization of 1641+399 (3C 345) and found that the optically thick core was essentially unpolarized, while two of the knots in the jet were highly polarized (11% and 6%). The position angles were 22° and 83° respectively. The jet P.A. is −75°. Roberts & Wardle (1987) report two observations of the blazar 0851 + 202 (OJ 287). In contrast, these are interpreted in terms of a moderately polarized core, a strongly polarized inner knot and a weakly polarized outer component. This 'jet' is at a position angle of about −110°. The core polarization position angle varied by 61° over a year, while the knot polarizations were roughly constant and aligned parallel to the jet.

The low-frequency variability which tested theories about the origin of the radio emission to their limits, is now thought to be the result of interstellar scintillation (e.g. Cawthorne & Rickett 1985 and references therein). This variability is thus thought not to be intrinsic to the source emission process and will not be discussed further.

1.1.4.2 Extended Emission

Since the construction of the VLA aperture synthesis telescope in New Mexico, high quality maps of the extended emission around blazars have appeared. These are contained in Hintzen & Owen (1981), Ulvestad, Johnston & Weiler (1983), Ulvestad & Johnston (1984), Wardle, Moore & Angel (1984), Antonucci & Ulvestad (1984), Antonucci & Ulvestad (1985), Antonucci (1986), Antonucci *et al.* (1986) and Ulvestad & Antonucci (1986). Of these, Antonucci & Ulvestad (1985; AU85) describe VLA observations of all of the original Angel & Stock-

man (1980) blazars. These observations show that extended emission can be seen around most blazars, the major exceptions being $0422+004$, $0735+178$, $0851+202$, $1219+285$ and $1749+096$. AU85 find a variety of morphologies and interpret these as being broadly consistent with the known types of extended radio sources (e.g. Miley 1980). This is important for the validity of the 'unified schemes' (§1.2.4). AU85 compare their extended powers with those for the general population of extragalactic radio sources and find that these span the full range of observed luminosities. Peacock (1986) has pointed out that if the AU85 extended powers are plotted separately for the BL Lac objects and the HPQ's, then most of the BL Lac objects are associated with extended emission of FR I power (according the Fanaroff & Riley 1974 classes). All of the AU85 HPQ's fall into the more powerful FR II division.

AU85 considered a variety of correlations of their radio properties with the other features of blazars. They found that there was a tendency for the the extended radio emission of the more core dominated sources to be one-sided. Core dominance also appeared to be correlated with radio variability amplitude, possibly anti-correlated with variability timescale, marginally correlated with optical variability but no strong evidence for correlations with preferred position angles or emission line widths. Similarly no strong evidence was found for a correlation between any extended radio structure axis and the optical polarization position angle.

1.1.5 THE SPECTRAL SHAPES OF BLAZARS

This section will consider the multifrequency spectrum of blazars from radio to X-ray frequencies. Because variability is a common feature of blazar emission at all frequencies, multifrequency spectra can only be reliably obtained by simultaneous observations at all the frequencies being considered. Many attempts at simultaneous or nearly simultaneous coverage have been reported. The objects studied include $0323+022$ (Feigelson *et al.* 1986), $0422+004$ (Worrall *et*

al. 1986), 0537 − 441 (Tanzi *et al.* 1986), 0735 + 178 (Bregman *et al.* 1984), 0851 + 202 (Worrall *et al.* 1982), 0912 + 297 (Worrall *et al.* 1986), 1101 + 384 (Makino *et al.* 1987, Brodie, Bowyer & Tennant 1987), 1156 + 295 (Wills *et al.* 1983, Glassgold *et al.* 1983), 1215 + 303 (Worrall *et al.* 1985), 1219 + 285 (Worrall *et al.* 1986), 1413 + 135 (Beichman *et al.* 1981, Bregman *et al.* 1981), 1418 + 546 (Worrall *et al.* 1984), 1641 + 399 (Bregman *et al.* 1986), 1727 + 502 (Bregman *et al.* 1982) and 2223−052 (Brown *et al.* 1986, Bregman *et al.* 1988). The details of these observations are beyond the scope of this chapter, but the broad features of the characteristics of the multifrequency blazar spectrum will be discussed. Added to this are the attempts to compile multifrequency spectra of large data sets from nearly simultaneous data (e.g. Cruz-Gonzalez & Huchra 1984, Ghisellini *et al.* 1986, Maraschi *et al.* 1986, Landau *et al.* 1986 and Impey & Neugebauer 1988). The validity of these may, in some cases, be compromised by variability considerations, as the simultaneity timescale used is often quite generous. Figure 1.1 shows an idealised representation of a 'typical' blazar spectrum. This should not be taken too seriously as a representation of an individual blazar, but it does indicate many of the gross features of blazar emission.

Detailed descriptions of the particular spectral behaviour of various blazars can be found in the above references. What follows is a brief description of the basic features of blazar emission. At radio frequencies blazars generally have flat spectra ($\alpha \sim 0$). In §1.2.1, VLBI observations of compact radio sources will be described, which will show that blazar radio cores are usually composed of a number of discrete components. One of these usually has a flat spectrum at high radio frequencies, while the remainder are optically thin. Note that the optically thick synchrotron spectral index of -2.5 (see §1.3.1) is not seen. The observed flat spectrum results from the superposition of these components. This is the so-called 'Cosmic Conspiracy' (Cotton *et al.* 1980). At frequencies higher than the radio the observed spectrum is observed to be steep ($\alpha \sim 1.0$) and can often be described locally by a power-law (e.g. Allen, Ward & Hyland

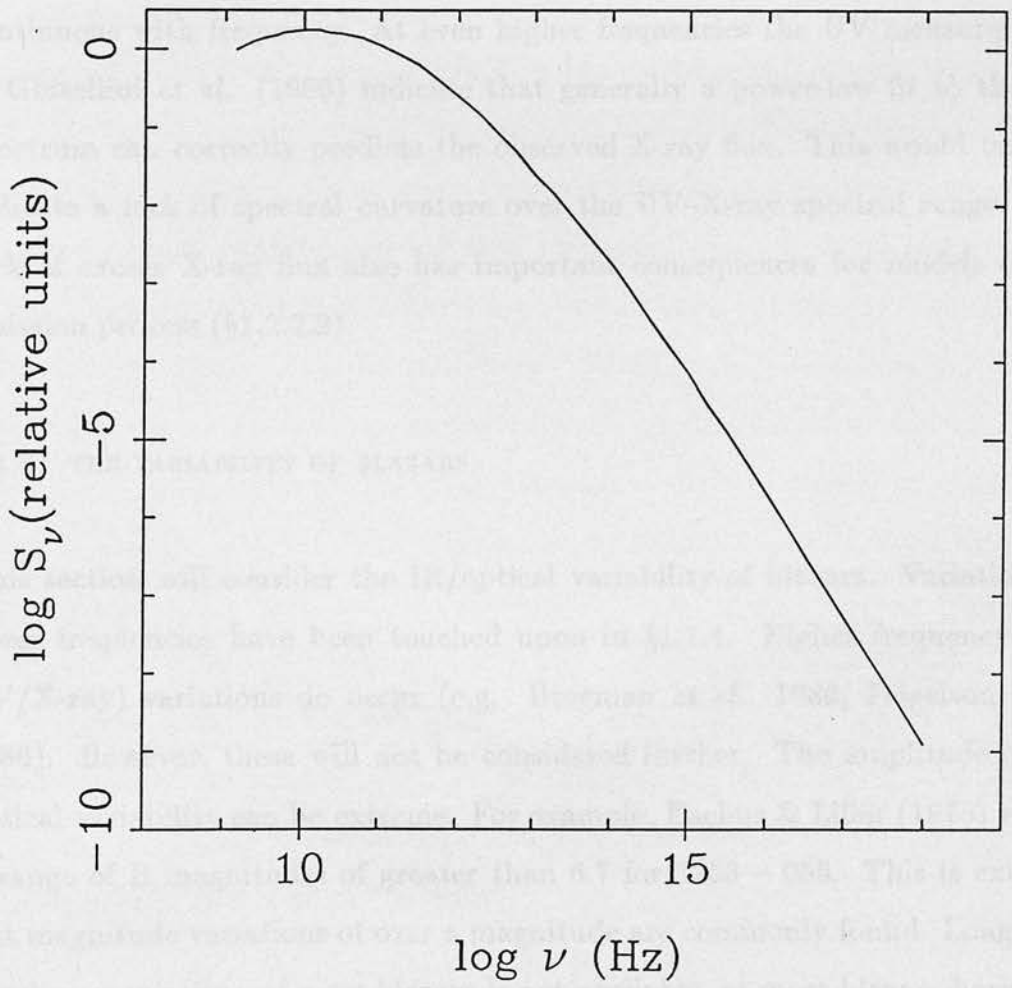

Figure 1.1: An idealised representation of a blazar spectrum.

1982, Moles *et al.* 1985). It is well known that the blazar spectrum steepens with increasing frequency in these regions. However, there is some controversy as to whether the spectrum is best described by a series of power-laws with spectral breaks or a gradual steepening with frequency. Gear *et al.* (1985) in their study of the 1 μmto 2mm spectral shape of blazars argue that power-laws are the best description of the IR and mm/sub-mm continua, and that there is some evidence for a break at 10 μm. Breaks at 3×10^{14}Hz (1 μm) are suggested by Cruz-Gonzalez & Huchra (1984) in their spectra. In contrast, Landau *et al.* (1986) fit all their multifrequency spectra (1400Å–20 cm) with parabolae in $\log S_\nu(\nu) - \log \nu$ space implying that the variations in spectral slope are continuous with frequency. At even higher frequencies the UV measurements of Ghisellini *et al.* (1986) indicate that generally a power-law fit to the UV spectrum can correctly predicts the observed X-ray flux. This would tend to indicate a lack of spectral curvature over the UV–X-ray spectral range. The lack of excess X-ray flux also has important consequences for models of the emission process (§1.2.2.2).

1.1.6 THE VARIABILITY OF BLAZARS

This section will consider the IR/optical variability of blazars. Variations at lower frequencies have been touched upon in §1.1.4. Higher frequency (e.g. UV/X-ray) variations do occur (e.g. Bregman *et al.* 1986, Feigelson *et al.* 1986). However, these will not be considered further. The amplitude of the optical variability can be extreme. For example, Eachus & Liller (1975) report a range of B magnitudes of greater than 6.7 for 1253 − 055. This is extreme but magnitude variations of over a magnitude are commonly found. Long time baseline monitoring of most blazars is not available, as most blazars have only been identified relatively recently, and archive material has not been searched. Nevertheless visual light-curves of a few of the more famous blazars, covering several decades or more, do exist (e.g. 0829 + 046 Liller & Liller 1975; 0851 + 202 Sillanpää *et al.* 1988; 1253 − 055 Eachus & Liller 1975; 1641 + 399

Babandzhanyants *et al.* 1985, Kidger *et al.* 1986 & Bregman *et al.* 1986; $2223 - 0\dot{2}3$ Barbieri *et al.* 1985). These show that large flares are a repeated feature of the blazar's history. Barbieri *et al.* (1984) claim that long-timescale (> 50 day) periodicity is evident in their data. A similar claim is also put forward by Sillanpää *et al.* (1988) who argue that their periodicity (11.65 years) in the visual variations of $0851 + 202$ (OJ 287) can be explained by a model involving accretion onto a binary pair of supermassive black holes. The observations of Corso, Ringwald & Harris (1988) appear to support the ~ 11 year periodicity in this object.

More attention has been focussed on the *short* timescale variability in these objects. This is because such variations can set important limits on the size and physical characteristics of the emission region. The shortest variability timescale (τ_{min}) is used to estimate the size of the emitting region, through the argument that the emitting region must have dimensions of the order of ($c\tau_{min}$) or less. Since substantial photometric variations have been seen on time-scales of hours (e.g. $0851 + 202$; Holmes *et al.* 1984b), a substantial fraction of the blazar flux can be assumed to originate from a region with linear dimensions of around 10^{12} m. Holmes (1985) shows that some of these variations violate the Elliot & Shapiro (1974) criterion for spherical accretion onto a black hole, and then goes onto to argue that this is consistent with non-spherically symmetric accretion. An alternative explanation is provided by relativistic beaming where the apparent fluxes are boosted(§1.2.2.4). In this case the variability argument says nothing about the proximity of the emitting region to the 'central engine' of the blazar, as the emission could originate from a small region of a jet-like outflow some distance from the centre.

Small amplitude, high (temporal) frequency *periodic* variations have been claimed to be seen in both the optical and radio observations of blazars. Since the claimed timescales are similar, both will be considered here. The observations are all of the blazar $0851 + 202$. Carrasco, Dultzin-Hacyan & Cruz-Gonzalez (1985) report periodicity on a timescale of 138 s with an amplitude

of 0.03 magnitudes. In contrast, a 15.7-minute periodicity was reported at 22 GHz, 37 GHz and at optical frequencies (Valtaoja *et al.* 1985). Dreher, Roberts & Lehár (1986) do not find any periodicity in their analysis of short-timescale variations at 5 GHz. Komesaroff, Roberts & Murray (1988) have also analysed this object at 8.4 GHz and find no evidence of 15.7-minute periodicity at any level greater than 0.7% of the total flux density.

The preceding parts of this section have been concerned about the amplitude and timescales of the variations in the flux levels. A potentially important diagnostic of the emission process in blazars is the behaviour of the spectral slope during flares. Gear, Robson & Brown (1986) present an analysis of the IR behaviour of $0851+202$ after its flare in 1983. They find a highly significant correlation between the IR spectral index and the flux density. This is in the sense that the spectrum flattens with increasing flux. This is similar to the correlation found by Hanson & Coe (1985) in their UV data. However, this correlation only existed during the flare. Counter-examples of behaviour where the spectral index remains essentially constant during a flare have also been seen ($1156+295$; Wills *et al.* 1983).

1.1.7 THE HOMOGENEITY OF THE CLASS OF BLAZARS

The question of whether the class of blazars can be meaningfully sub-divided has been often raised since the invention of the class at the 1978 Pittsburgh Conference. The most obvious potential difference is the emission lines. This opportunity will be taken to mention some proposed explanations for the lack of emission lines in some blazars. The most common explanation is that of relativistic beaming. The arguments for bulk relativistic flows in blazars are reviewed in §1.2.2. Essentially this explanation proposes that the emission lines in some blazars are swamped by a relativistically boosted continuum. Other explanations include those of Guilbert, Fabian & McCray (1983) who argue that the spectral slope of X-ray emission in BL Lac objects may account for their lack

of emission lines. They analyse the probable effect of the X-ray emission on gas accreting onto a compact object and find that the slope of the typical BL Lac X-ray spectrum may be too steep to account for the formation of the broad line emitting region. Ostriker & Vietri (1985) propose that the lineless appearance of BL Lac objects is a result of gravitational microlensing by compact objects in a foreground galaxy. This implies that the BL Lac objects seen in some galaxies are at much greater distances. They explain the lack of any emission lines being associated with the BL Lac continuum as being a result of the fact that the continuum source is expected to be much smaller in size than the line-emitting regions, and hence are more susceptible to gravitational lensing. This latter idea has received some support from Stickel, Fried & Kühr (1988b) who report that $0235+164$ is found in a galaxy cluster of lower redshift ($z \approx 0.52$) and has properties consistent with the Ostriker & Vietri (1985) model. However, this idea remains largely unverified and it and its implications will not be considered for the remainder of this thesis. Nevertheless, the consequences are potentially quite important. This is especially relevant for the clustering study of Chapter 3, where it is assumed that any detected galaxy clusters are associated with the blazar. The probability of chance superpositions of foreground clusters is small (Yee & Green 1987). However, if the Ostriker & Vietri (1985) model were correct, then BL Lac emission would preferentially select the presence of lower redshift clusters.

Returning to the question of whether there is a potential division of the blazar population in terms of their emission line properties, Moore & Stockman (1984) argue on the basis of equivalent widths that the HPQ emission lines are substantially stronger than those of the BL Lac objects. their conclusions are thoroughly criticised by Antonucci & Ulvestad (1985), who include the point that some HPQ's are known to appear lineless at some periods. Antonucci & Ulvestad (1985) propose that a more likely division is to be made between broad-line and narrow-line objects as in other branches of AGN study. In this picture most of the BL Lac objects would appear to be narrow-lined objects.

A more certain division of the blazar population is that furnished by X-ray studies. Ledden & O'Dell (1985) study the properties of X-ray selected blazars compared with those of radio-selected blazars and find that, in general, the X-ray emission of the former sample is very strong relative to their radio emission when compared. They refer to these objects as 'X-ray strong'. In contrast Maraschi *et al.* (1986) refer to these objects as 'radio weak'. Their motivation for this is that they observe groups of X-ray selected and radio selected blazars to span similar ranges of X-ray luminosity. The important question is whether the blazar can really be divided into two distinguishable classes on the basis of their radio/X-ray properties. The possibility remains that the bimodality seen by Ledden & O'Dell (1985) is a result of the two selection techniques searching out different regions of a homogeneous blazar parameter space, i.e. that this bimodality is a selection effect.

1.2 Jets and Relativistic Motion

1.2.1 JETS IN AGN

The observations of jets in extragalactic radio sources are reviewed by Bridle & Perley (1984; hereafter BP84). They define a jet in observational terms as being a feature which (*i*) is at least four times as long as it is wide (*ii*) is separable from the surrounding emission, either spatially or by its brightness, and (*iii*) is aligned with the compact radio core. Note that this definition does not include any direct evidence of outflow or indeed any motion at all. In fact, the only such evidence is from the superluminal VLBI knots which form the pc-scale jets (§1.2.2.1). The main motivation for believing that jets are outflows is the need to supply energy for the lobes of extended radio sources. The lifetimes of the synchrotron emitting electrons in these lobes are found to be less than the light-travel times from the radio cores (e.g. Miley 1980 and references therein). According to most models of AGN the source of power is

a 'central engine' (usually thought to be a black hole) located at the nucleus of a galaxy (Begelman, Blandford & Rees 1984). Consequently some method of moving energy from this central engine to power the extended emission is needed. Indeed, jets were suggested, as a method of powering the hot-spots in extended sources before the first radio jets were detected (e.g. Blandford & Rees 1974).

According to the above criteria, BP84 found kpc-scale jets in 65–80 % of weak radio galaxies, 40–70 % of distant extended quasars but in $< 10\%$ of distant radio-galaxies of the same power. They also found a tendency for jet detection rate to increase with radio core dominance. Not all of these jets are two sided, despite the fact that the extended emission, which they are supposed to power, is usually symmetric. Most, if not all, VLBI (i.e. pc-scale) jets are one-sided. The kpc-scale jets seen in the weaker radio sources tend to be two-sided and have magnetic fields oriented perpendicular to the jet axis (or changing from perpendicular to parallel towards the edges of the jet). The kpc-scale jets in the stronger sources are predominantly one-sided with magnetic fields oriented parallel to the jet axis (though some knots may have perpendicular fields). The break between these two types of jet behaviour appears to coincide with the Fanaroff & Riley (1974) morphological division at $P_{tot}^{1.4} \approx 10^{25}$ W Hz^{-1} (H_0 =100 km s^{-1} and $\Omega_0 = 1$). The method of confinement of these jets is not clear. BP84 report that some jets have been resolved and seen not to be freely expanding. They discuss whether the jets could be confined either by external pressure or by magnetic fields.

1.2.2 BULK RELATIVISTIC MOTION

The possibility of bulk relativistic motions being present in quasars has important consequences for the interpretation of their observed emission. The arguments for such flows are reviewed here.

1.2.2.1 *Superluminal Motion*

In VLBI radio observations of strong compact radio sources significant changes in the angular separation of components are often seen. These changes can be converted into apparent velocities using the optical redshift as an indicator of cosmological distance. These apparent velocities are often greater than the speed of light. This phenomenon is known as superluminal motion. The current state of observations of superluminal motion is reviewed by Zensus & Pearson (1987), and an up to date list of superluminal sources is presented by Porcas (1987). The various models proposed to explain these motions are reviewed by Marscher & Scott (1980) and Scheuer (1984), but the 'standard' interpretation is that the motions are a result of features travelling at relativistic velocities close to the line-of-sight. It was first noted by Rees (1966) that this geometry would result in apparent superluminal speeds. The apparent speed (in units of c) is given by;

$$\beta_{app} = \frac{\beta \sin\theta}{1 - \beta \cos\theta} \tag{1.1}$$

where β is the velocity of the feature and θ is the orientation of this velocity with respect to the line-of-sight. This has a maximum apparent velocity of $\gamma\beta$ for $\sin\theta = 1/\gamma$.

In the orthodox interpretation of the observed VLBI features, the unresolved flat spectrum component is known as the core. In the Blandford & Königl (1979) picture, the core is interpreted as the unresolved base of a relativistic jet, with the superluminal 'knots' being interpreted as features in this flow. This view strongly depends on the core being observed to be stationary. Because of the loss of phase information in VLBI measurements, this is difficult to verify. The core has only been confirmed to be stationary in one superluminal source (1641 + 399; Bartel *et al.* 1986). However, it must be noted that this simple picture has problems in interpreting new observations of some superluminal sources. For example two stationary components with superluminal

motion occurring between them are seen in 0923 + 392 (4C 39.25; Marscher *et al.* 1987) and in 1901 + 319 (3C 395; Simon *et al.* 1987), and accelerations and position angle changes are seen in 1641 + 399 (Biretta, Moore & Cohen 1986). Some of these problems are discussed by Marscher (1987).

1.2.2.2 The Compton Flux Problem

The evidence of superluminal motion argues only for relativistic *pattern* speeds (Lind & Blandford 1985). What is the evidence that there is bulk relativistic motion present in the pc-scale jets in the superluminal sources? An argument comes from the X-ray fluxes seen from the VLBI knots. This is reviewed by Marscher (1987). If the VLBI knots are assumed to be spherically symmetric synchrotron emitters then both the synchrotron emission (§1.3.1) and inverse Compton emission (§1.3.2) can be calculated (Marscher 1983 and Gould 1979). The predicted inverse Compton flux exceeds the observed X-ray luminosities for many of these objects (Marscher 1987 and references therein). This situation can be resolved if the emitter is moving relativistically close to the line-of-sight (i.e. has a high value of δ). However, the derivations of the observed fluxes make very simple assumptions about the structure of the 'knots' and depend very strongly on some of the observed parameters (particularly the angular size of the knot), so uncertainties in both the model and the observations may lead to over-estimations of δ. Conversely, the interpretation of the observed X-ray emission from the sources as being inverse-Compton emission is not at all secure (Marscher 1987). The main problem being that of uncorrelated variability between the synchrotron (i.e. radio) emission and the X-rays. If this flux were not all due to the inverse-Compton scattering of the synchrotron photons, then the application of this simple model would tend to under-estimate δ.

1.2.2.3 Beaming and One-Sided Jets

Another facet of bulk relativistic motion is the beaming of the emission seen in the observer's frame. If the emission is isotropic in the (primed) rest-frame of the emitting fluid, then the observed flux is ,

$$S_\nu(\nu) = S'_\nu(\nu)\,\delta^{3+\alpha}\,, \tag{1.2}$$

where,

$$\delta = \frac{1}{\gamma(1-\beta\cos\theta)}\,. \tag{1.3}$$

α is the source spectral index of the (assumed) power-law emission. The 3 in the exponent of the denominator is correct for an individual knot. However the correct value for a stream of knots (with finite lifetimes) is 2. For high values of γ, most of the radiation is concentrated within $1/\gamma$ of the direction of motion. The pc-scale structures seen in the VLBI sources are one-sided. There has never been a secure detection of a counter-jet at the opposite side of the flat-spectrum VLBI core from the superluminal knots. This is entirely consistent with the picture of superluminal sources presented above (§1.2.2.1), given the limited dynamic range of the VLBI observations. However one-sided jets are also seen on kpc-scales (§1.2.1). It is natural to interpret these too as being the result of Doppler boosting. This would imply that all the one-sided jets are pointed towards us. Evidence supporting this is provided by the polarization studies of extended radio emission by Garrington *et al.* (1988) and Laing (1988) who show that the lobes containing the one-sided jets are less depolarized than the counter lobes. If the depolarization arises in a hot gas halo surrounding the radio source then this implies that the lobes containing the observed jet are closer to the observer.

There are a number of problems with reconciling the jets and extended structure with superluminal motion. These are discussed in BP84 and are only briefly repeated here. The bending seen in the supposedly beamed jets in the

weaker sources should be accompanied by brightness changes if these jets were relativistically beamed. This appears to rule out $v_j \approx c$ in these sources. The situation in the more powerful sources is unclear, it may be possible that these jets are free and that a wobbling jet may be able to explain the observed bends without severe brightness changes. In order for appreciable boosting to be seen, the jet axis must be oriented close to the line-of-sight. There may be a problem with the deprojected sizes of the extended emission of some of the superluminal sources being comparable to or larger than the largest "normal" extended radio sources (Schilizzi & de Bruyn 1983, but see also Browne 1987). The frequency of detection of one-sided jets may also be a problem given the $1/\gamma$ beaming cone. However this may be eased by the fact that only the most naïve picture gives such a beaming cone. More complicated source models can widen the angles over which beaming is seen (Lind & Blandford 1985). Finally, the last problem is the detection of counter-jets. These are seen in some sources (Bridle 1988 and references therein), but in others the lack of a counter-jet may constrain the amount of beaming required. The most critical example is 3C 273 where no counter-jet is detected within a factor of 5500 of the observed jet. What is more no extended emission is seen within a factor of at least 50 of that associated with the observed jet (Davis 1986). These arguments have been used to argue that the kpc-scale jets are intrinsically one-sided and have to flip at occasional periods to supply the counter-lobes (BP84 and references therein).

1.2.2.4 Arguments for Relativistic Motion in Blazars

The arguments for relativistic motion being important in blazars, were first elaborated by Blandford & Rees (1978). The most recent review is due to Impey (1987). The latter author starts from the point of view that many of the superluminal radio sources show high IR/optical polarization and variability. That is to say that many superluminal sources are blazars (see definitions in §1.1). Using lists of blazars and superluminal sources available at the time, Impey (1987) found that "13 out of 21 of the probable and 9 out of 10 of the possible

superluminal sources are highly polarized in the optical." Given the possibility that the vast majority of compact radio sources could show both superluminal and blazar properties, Impey (1987) argued for a connection between the two processes.

The above evidence argues merely for a connection between the origin of superluminal motion and blazar emission, irrespective of whether bulk relativistic motion is involved in either. There is other evidence for relativistic motion in blazars. Impey *et al.* (1984) have shown that some blazars can exceed the Elliot & Shapiro (1974) variability limit for spherical accretion onto a black hole. This problem can be alleviated with the assumption of relativistic motion. This causes the timescales of variability to be modified by a factor of δ^{-1} and the observed fluxes to be multiplied by a factor of $\delta^{3+\alpha}$. Further problems exist in the construction of an emission region, which is small enough to satisfy the time variability constraint and has a small enough density of non-relativistic electrons to avoid Faraday effects destroying the observed polarization (Blandford & Rees 1978). Construction of synchrotron-self-Compton (SSC) (§1.3.3) models of the observed multifrequency spectra of blazars are also eased if some degree of relativistic boosting is allowed. Madau, Ghisellini & Persic (1987) present a set of fits to the multifrequency spectra of a variety of blazars. They find that all of the HPQ's require Doppler boosting factors $\delta > 1$. However, only half the BL Lac objects in their sample require boosting.

1.2.3 UNIFIED SCHEMES

The possibility of bulk relativistic flows being important in quasars, means that, for each population of sources where beaming plays a large part in the observed characteristics, there is a fraction of sources which are not identified as they are pointing away from us. The so called 'unified schemes' attempt to identify these misdirected counterparts with other known populations of extragalactic object which have (already) been selected on the basis of their unbeamed char-

acteristics.

The first of the unified schemes was presented by Scheuer & Readhead (1979). They suggested that the population of compact radio sources could be identified with the radio-quiet optically selected quasars. This supposed that the latter were misaligned such that the relativistically boosted radio emission is invisible in radio surveys. This scheme has since been rejected. The main evidence for this is the detection of steep-spectrum radio emission around the compact radio sources (e.g. Perley, Fomalont & Johnston 1982 and Antonucci & Ulvestad 1985). This emission is unlikely to be beamed and hence should also appear around the optically-selected quasars. This does not appear to be the case (e.g. Condon *et al.* 1981).

An alternative unified scheme was proposed by Orr & Browne (1982). They suggested that the compact flat-spectrum radio sources could be aligned steep-spectrum extended radio sources. This is broadly consistent with the detection of extended structure about the compact sources, and with the idea that the compact radio emission is relativistically beamed. Orr & Browne (1982) attempted to justify their picture by predicting the relative numbers of the two populations of radio source, assuming Lorentz factors from superluminal motion.

Lind & Blandford (1985) showed that tests of beaming models using the statistics of aligned and misaligned sources could be extremely dependent on the model of relativistic motion employed. The important factors are the strength of the boosting and the angular size of the cone over which the emission is visible. Lind & Blandford (1985) discussed the 'standard' relativistic jet model of Blandford & Königl (1979). In this model the superluminal features could possibly be shocks. The inferred pattern speed and Lorentz factor would then relate to the shock speed, *not* to the velocity of the emitting fluid. Furthermore, not all shocks are expected to be one dimensional. If oblique shocks provide important sources of enhanced emission in the flow, then the beaming-cone

could be much wider than would be predicted for the simple unidirectional flow. The status of the statistical tests, in the light of these problems, is discussed by Peacock (1986). He concludes that this scheme cannot be rejected by our current knowledge of the radio luminosity functions of steep and flat spectrum quasars.

An alternative method of examining the validity of these schemes is to look for differences in the orientation independent (ie. unbeamed) properties of the beamed sources and the candidate misdirected population. This was the basis of the criticism of the unified scheme by Heckman (1983), who argued that the emission line properties of the lobe-dominated radio quasars were significantly different from those of the compact radio quasars. If so, this would appear to conclusively invalidate the scheme. However some of these objections have been countered by Wills & Browne (1986), who find a anti-correlation between the Hβ line width and radio core-to-lobe flux ratio R. This would be consistent with beaming models if the line-emitting gas were confined to a disc (perpendicular to the radio axis). They also point out that care must be taken to compare populations with equivalent extended radio powers. Any correlations of the unbeamed properties with this unbeamed flux could lead to apparent differences between extended and compact sources obtained from flux-limited surveys. Wills & Browne (1986) argue that this effect could be responsible for the differences noted by Boroson & Oke (1984) and Boroson, Persson & Oke (1985).

Miller (1984) showed for a given X-ray power that the radio cores of compact quasars are $\sim$ 30 times more luminous than the extended radio quasars. On the basis of a correlation between Hβ luminosity and X-ray luminosity, he argued that the X-ray emission would be unbeamed, which imply that the X-ray brightness of the compact radio quasars would be an intrinsic property and not an orientation effect. However this result is strongly dependent on the strength of the $H\beta$ flux – X-ray luminosity correlation which is questionable. Since this date, Browne & Murphy (1987) have studied the R-dependence of X-ray lumi-

nosity of a sample of radio sources with high quality maps. They argue for both an isotropic and a beamed component to the X-ray emission.

Possible tests of unified schemes using the cluster environments of quasars (e.g. Peacock & Prestage 1987) will be the subject of Chapter 3 of this thesis.

1.3 Continuum Emission Mechanisms

1.3.1 SYNCHROTRON EMISSION

Synchrotron emission is the radiation of a relativistic charged particle as it is accelerated in a magnetic field. The basics of this emission are described by Rybicki & Lightman (1979) and a fuller mathematical treatment is given by Pacholczyk (1970 & 1977). The efficiency of synchrotron radiation as an energy-loss mechanism is inversely dependent on the fourth power of the particle mass and hence is more important for electrons than for protons. Only electron (or positron) synchrotron radiation will be considered here.

The average energy lost by an electron through synchrotron radiation is given by:

$$\frac{dE}{dt} = -\frac{4}{3}\sigma_T\, c\beta^2\gamma^2 U_B\,, \tag{1.4}$$

where σ_T is the Thomson cross-section of the electron, β is its velocity in units of c, γ is the electron Lorentz factor and U_B is the magnetic energy density ($B^2/2\mu_0$). The energy loss rate is dependent on the pitch angle (ϑ) of the electron, that is the angle between the electron velocity and the magnetic field. An isotropic pitch angle distribution has been assumed.

The expressions for the emission coefficients in the I and Q Stokes parameters are (Pacholczyk 1977) :

$$\varepsilon_I = \sqrt{3}\,\frac{e^2}{4\pi\epsilon_0 m_e}\,eB\sin\vartheta\;\phi(\vartheta)\int_0^\infty N(E)\,F(x)\,dE\;, \tag{1.5a}$$

and,

$$\varepsilon_Q = \sqrt{3}\,\frac{e^2}{4\pi\epsilon_0 m_e}\,eB\sin\vartheta\;\phi(\vartheta)\int_0^\infty N(E)\,G(x)\,dE\;. \tag{1.5b}$$

Where,

$$x = \frac{\nu}{\nu_c}\;, \tag{1.5c}$$

$$\nu_c = \frac{3\gamma^2}{4\pi m_e}\,eB\sin\vartheta, \tag{1.5d}$$

$$F(x) = x\int_x^\infty K_{\frac{5}{3}}(z)\,dz\;, \tag{1.5e}$$

and,

$$G(x) = xK_{\frac{2}{3}}(x). \tag{1.5f}$$

Here e is the electron charge, m_e is the electron mass, B is the magnetic field, ϕ is the electron pitch angle distribution, $N(E)$ is the electron energy distribution, ν is the frequency, ν_c is the critical frequency, and the K_μ are the modified Bessel functions. The electron distribution function has been assumed to be separable:

$$N(E,\theta) = \phi(\theta)N(E), \tag{1.6}$$

and the coordinate system has been chosen such that the Stokes' U parameter is identically zero. The synchrotron radiation of a single electron is elliptically polarized, but, to first order in γ, the circular component vanishes for an isotropic distribution of electron velocities (Pacholczyk 1970). The second order term (e.g. Pacholczyk 1977) is small and will be ignored. There remains the possibility that if anisotropic electron energy distributions are important then appreciable circular polarization may result (see §1.3.4). Figure 1.2 shows the functions $F(x)$ and $G(x)$. These functions represent the frequency dependence of the emission of a monoenergetic distribution of electrons. It can be seen

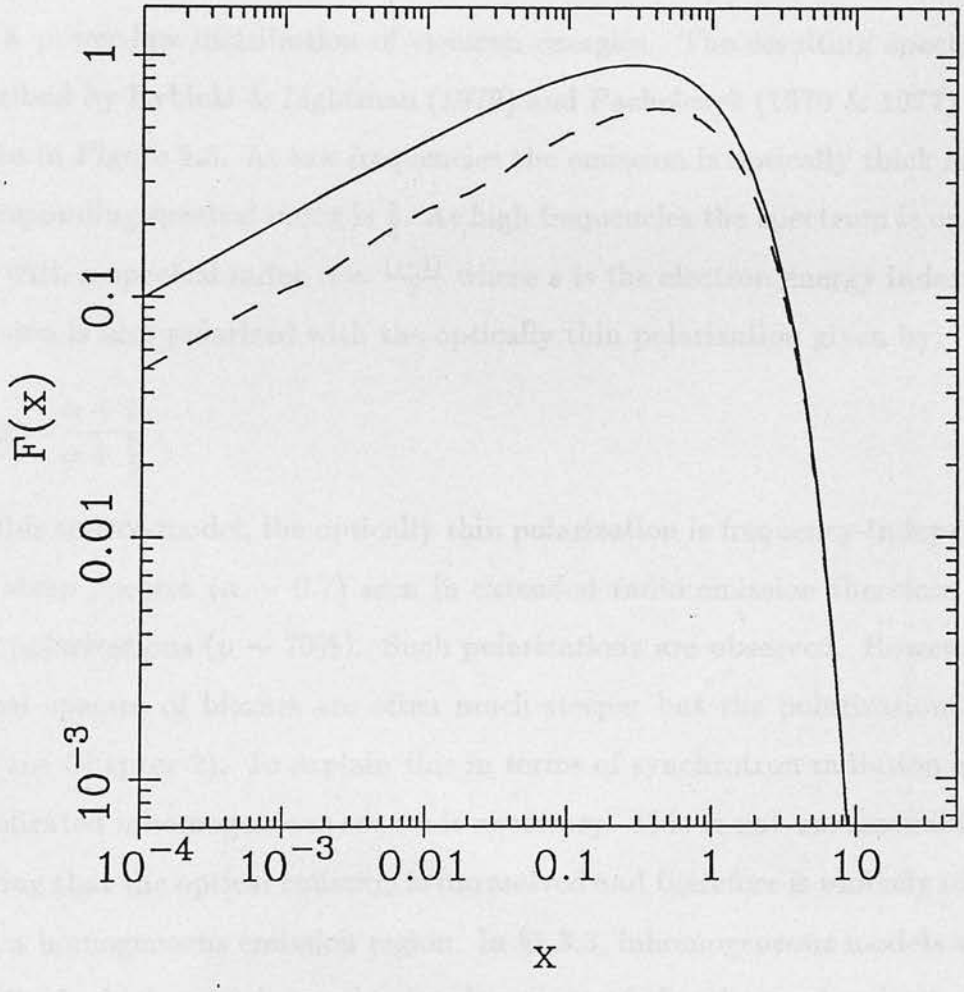

Figure 1.2: The synchrotron functions $F(x)$ (solid line) and $G(x)$ (dashed line).

that the emission is highly polarized. The asymptotic values of the degree of polarization are 50 % for $x \ll 1$ and 100 % for $x \gg 1$. The plane of this polarization is that of the projection of the **B**-field onto the plane perpendicular to the line-of-sight.

The canonical synchrotron source model, that has had great success in explaining the observed features of the extended emission of radio sources, consists of a uniform magnetic field with an isotropic distribution of electron velocities and a power-law distribution of electron energies. The resulting spectrum is described by Rybicki & Lightman (1979) and Pacholczyk (1970 & 1977) and is shown in Figure 1.3. At low frequencies the emission is optically thick and the corresponding spectral index is $\frac{5}{2}$. At high frequencies the spectrum is optically thin with a spectral index $\alpha = \frac{(s-1)}{2}$ where s is the electron energy index. This emission is also polarized with the optically thin polarization given by:

$$p = \frac{\alpha + 1}{\alpha + \frac{5}{3}} \, . \tag{1.7}$$

For this source-model, the optically thin polarization is frequency-independent. The steep spectra ($\alpha \sim 0.7$) seen in extended radio emission therefore imply high polarizations ($p \sim 70\%$). Such polarizations are observed. However, the optical spectra of blazars are often much steeper but the polarizations much less (see Chapter 2). To explain this in terms of synchrotron radiation a more complicated inhomogeneous source is necessary. This is not unreasonable considering that the optical emission is unresolved and therefore is unlikely to come from a homogeneous emission region. In §1.3.3, inhomogeneous models will be described which are advanced as explanations of the observed radio to X-ray spectra of compact radio sources. What is not considered by these models is the polarization characteristics.

The polarization characteristics of inhomogeneous sources are considered in the work of Nordsieck (1976), Björnsson & Blumenthal (1982) and Björnsson (1986). Their results will be considered in more detail in the discussion of the

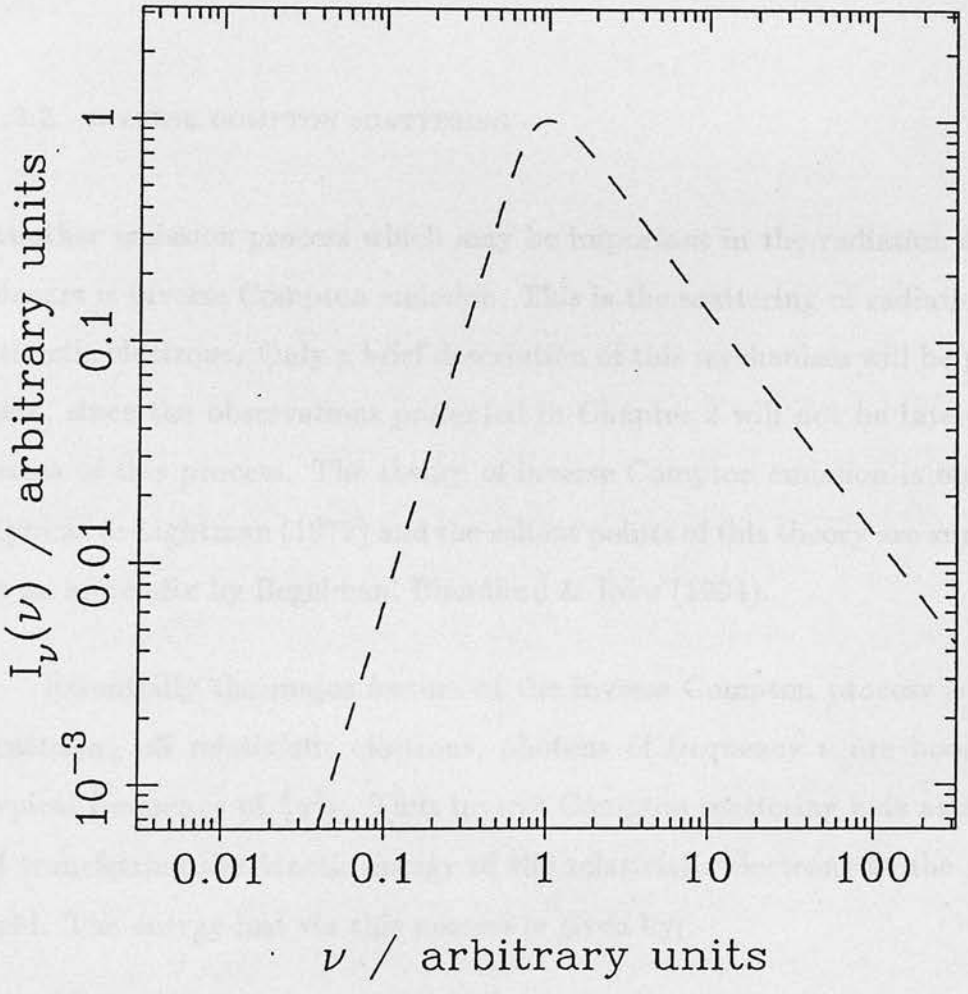

Figure 1.3: The synchrotron emission of the 'standard' synchrotron source with an electron energy index (s) of 3.

observed FDP and FDθ in Chapter 2. In short, the major results of Nordsieck (1976) and Björnsson & Blumenthal (1982) are that the FDP can be modelled as:

$$p(\nu) = \Pi(\nu)\,\frac{\alpha(\nu)+1}{\alpha(\nu)+\frac{5}{3}}\,, \tag{1.8}$$

where $\Pi(\nu)$ is a function of the magnetic field geometry, and the remaining frequency dependence has been parameterised in terms of the local synchrotron spectral index.

1.3.2 INVERSE COMPTON SCATTERING

Another emission process which may be important in the radiation seen from blazars is inverse Compton emission. This is the scattering of radiation by relativistic electrons. Only a brief description of this mechanism will be presented here, since the observations presented in Chapter 2 will not be interpreted in terms of this process. The theory of inverse Compton emission is outlined by Rybicki & Lightman (1979) and the salient points of this theory are summarised in an appendix by Begelman, Blandford & Rees (1984).

Essentially the major feature of the inverse Compton process is that, by scattering off relativistic electrons, photons of frequency ν are boosted to a typical frequency of $\frac{4}{3}\gamma^2\nu$. Thus inverse Compton scattering acts as a method of transferring the kinetic energy of the relativistic electrons to the radiation field. The energy lost via this process is given by;

$$\frac{dE}{dt} = -\frac{4}{3}\sigma_T c\gamma^2\beta^2 U_{ph}\,, \tag{1.9}$$

where U_{ph} is the photon energy density. Comparison with the equivalent equation for synchrotron radiation gives the result that the ratio of the synchrotron power emitted by an electron to the inverse Compton power is given by,

$$\frac{P_s}{P_c} = \frac{U_B}{U_{ph}} . \tag{1.10}$$

This depends only on the assumptions that the scattering is Thomson scattering in the rest-frame of the electrons and the isotropy of the magnetic and radiation fields. A consequence of this result is that if physical models of the emitting region are advanced which imply that the synchrotron radiation density is comparable to the magnetic energy density then the predicted Compton flux must also constrain the model. This is the origin of the Compton flux problem in superluminal sources (§1.2.2.2).

1.3.3 SYNCHROTRON-SELF-COMPTON MODELS

The combination of synchrotron emission and inverse Compton scattering of the synchrotron photons have been combined to create the so called synchrotron-self-Compton (SSC) models of the multifrequency emission from idealised jets. Many authors have presented such models based on the original Blandford & Königl (1979) idea that the core emission is the unresolved base of the jet that is responsible for the superluminal features. Examples of these models are due to Marscher (1980), Königl (1981), Reynolds (1982a & b) and Ghisellini, Maraschi & Treves (1985) among others.

These assume a simple jet morphology, either a constant opening angle or with the width being a power-law function of distance from the nucleus. Simple assumptions are also made about the evolution of magnetic field density and energetic electron density along the jet. The resulting synchrotron and inverse-Compton emission are then integrated along the length of the jet. The observed emission is, of course, dependent on the viewing angle and boosting factor of the jet.

An important question to be answered when interpreting the observed power-law spectra as synchrotron radiation is the origin of the power-law spectral index. What mechanism accelerates the electrons to produce a power-law spectrum? The different ideas which have been advanced are briefly reviewed in Begelman, Blandford & Rees (1984). The time for a relativistic electron to lose half its energy via synchrotron losses is given by;

$$\tau_{\frac{1}{2}} = 3\varepsilon_0 c^3 \sqrt{\frac{3m_e^5}{\pi\, e^7 (B \sin\vartheta)^3\, \nu}}\,, \tag{1.11}$$

where this has found by integrating eqn. 1.4 and replacing the electron energy by the frequency corresponding to its synchrotron emission through eqn. 1.5d. Putting in an estimate of the magnetic field strength ($B \sim 10^{-5}$ T; Gear *et al.* 1985) and considering those electrons which radiate at IR/optical frequencies, gives lifetimes of the order of days. This implies that, if SSC models are correct, *in situ* acceleration of the electrons must occur. The most developed theory of acceleration in jets is that of particle acceleration by Fermi processes in magneto-hydrodynamic (MHD) shocks.

The basic Fermi process is outlined by Longair (1981). The (original) second-order Fermi process is the acceleration of relativistic particles by collision with a distribution of clouds with random velocities. By consideration of the one-dimensional problem, Longair (1981) shows that the average energy gained per collision is $4\gamma_V^2\,(V/c)^2$, where V is the velocity of the cloud. The second-order dependence on (V/c) results from the possibility of 'following' (i.e. energy losing) collisions as well as 'head-on' (i.e. energy gaining) collisions. If only the latter occurred then the energy gain per particle would be first order in (V/c). Such a first-order Fermi process is shock acceleration. What is necessary for this mechanism to work is a scattering process either side of the shock which is able to deflect the accelerated particles such that they cross the shock many times before being convected downstream. Drury (1983) reviews the processes

of particle acceleration in MHD shocks, where the scattering is assumed to result from magnetic irregularities. The basic reason for considering these Fermi processes is that they all result in the production of power-law particle energy distributions (Longair 1981).

A strong non-relativistic shock produces an electron distribution giving rise to a synchrotron spectrum with $\alpha = 0.5$. Consideration of the effects of synchrotron energy losses on this spectrum can then give rise to a steepening of this (and any other) spectrum by 0.5 (Kardashev 1962, Pacholczyk 1970). This would give an observed spectrum with an index of 0.5 at low frequencies and 1.0 at higher frequencies up to a cutoff frequency corresponding to the energy at which the energy losses dominate the ability of the Fermi process to accelerate the electrons. This together with the effects of a finite emission region convolved with the beam size of the observations was used by Meisenheimer & Heavens (1986) and Heavens & Meisenheimer (1987) to explain the observed spectrum of the radio hot-spot in 3C 273. However these results refer to non-relativistic shock fronts. In §1.2 the evidence for relativistic flows being important in radio sources was reviewed. The acceleration of particles at relativistic shock fronts is discussed by Kirk & Schneider (1987) and Heavens & Drury (1988). The results of these calculations and other scenarios are reviewed by Heavens (1988). A major result of this work is that the particle velocity distributions are significantly anisotropic in both the upstream and downstream frames. The consequences of this over the traditional assumption of isotropy in the calculation of synchrotron spectra are a subject for future work.

An important consequence of particle acceleration mechanisms is the possibility of an upper cut-off in the electron energy distribution. There is observational evidence for sharp cut-offs in the infrared–optical spectra of some quasars (e.g. Rieke, Lebofsky & Kinman 1979, Bregman *et al.* 1981), and in jets and hot-spots (e.g. Röser & Meisenheimer 1986). Biermann & Strittmatter (1987) argue that the cutoffs resulting from synchrotron losses and photon interactions give an observed cut-off frequency between 3×10^{14} Hz and 2×10^{15} Hz. Though

this result is strongly model dependent, it does raise the possibility that cut-offs will be important in determining the infrared and optical flux and polarization behaviour of blazars. This will be discussed in Chapter 2 with reference to observations of the polarization behaviour of blazars.

Non-relativistic and relativistic MHD shocks can also amplify the magnetic field strength perpendicular to the shock normal (e.g. de Hoffman & Teller 1950). Shocks can then be used to compress tangled magnetic fields so that they are confined to a plane. Laing (1980) has shown how compression of a tangled field into a plane can explain the high polarizations observed in some radio sources without requiring initially ordered magnetic fields. Alternatively, if the magnetic field in the jet is ordered (e.g. Chan & Henriksen 1980 and Königl & Choudhuri 1985a), then time-dependent polarization changes (particularly position angle rotations) can result from the passage of a shock down such a magnetized jet (Königl & Choudhuri 1985b, Kikuchi *et al.* 1988).

Finally, shocks may be able to explain the behaviour of flares. Marscher & Gear (1985) used a shock-model to explain the behaviour of 3C 273 at mm wavelengths. They characterised the evolution of the flare maximum with time, in terms of the competing electron energy loss mechanisms (Compton, synchrotron and "adiabatic"). This model was also used by Gear *et al.* (1986) to model their observations of the variability in other blazars. A similar model has been proposed to explain the radio variability of 2200 + 420 (BL Lac) by Aller, Aller & Hughes (1985) and Hughes, Aller & Aller (1985). They proposed shocks in an unconfined jet to compress a random magnetic field and used this to explain both the flux and polarization variability.

1.3.5 ALTERNATIVE EMISSION MECHANISMS

The above sections have concentrated on the processes by which the various emission mechanisms may produce the observed characteristics of the emission

seen in blazars. This has all assumed the basic jet model of Blandford & Königl (1979). This is not the only view of the origin of the polarized variable emission seen in blazars. Some of the alternative emission mechanisms and locations are discussed in Begelman, Blandford & Rees (1984).

One alternative mechanism is that advanced by Begelman & Sikora (1987). This considers an isotropic radiation field and a uni-directional relativistic beam of cold electrons. In the rest frame of the beam, the cold electrons see a uni-directional beam of radiation, which is then Compton-scattered. The resultant scattered radiation field in the comoving frame of the blazar is highly beamed and polarized. This polarization is strongly dependent on small changes in the orientation of the electron beam with respect to the line-of-sight. The spectrum of the radiation depends essentially on the spectrum of the isotropic radiation field. This then makes it difficult for the mechanism to produce FDP and FDθ from a single beam. This can, of course, be overcome by a superposition of differing components. However this mechanism does not offer any major advantages over synchrotron emission as an explanation of the observed features of IR/optical blazar emission, and does not fit into the models advanced to explain the emission at other frequencies.

All the above sections considered that the origin of the emission was a jet-like flow. The evidence for such flows being important for the observed IR/optical emission is essentially the arguments of Blandford & Rees (1978 see §1.2.3). Nevertheless, some authors have advanced the opinion that some of the observed characteristics of blazar emission are associated with an accretion disc. It is possible that the emission from such discs can be significantly polarized. This polarization can result from electron scattering (e.g Pineault 1981, Phillips & Mészáros 1986 or Webb & Malkan 1986), or perhaps from synchrotron radiation (e.g. Pineault 1981). The theory of accretion discs is reviewed by Rees (1984), but an important point is that, like relativistic flows, thick accretion discs (Abramowicz, Calvani & Nobili 1980) can radiate at super-Eddington luminosities. Consequently, accretion disc radiation can potentially provide an

alternative explanation to some aspects of blazar emission. However, given the uncertainty as to whether such discs are stable (discussed in Rees 1984 and references therein), these ideas will not be considered in the following chapters.

Chapter 2

Polarimetric Observations of Blazars

2.1 Observational Techniques

This section describes the operation and data reduction of the Hatfield polarimeters, which were used to obtain the data presented in this chapter. There are two such devices, which are described separately below. The Mark I Hatfield Polarimeter was used for the observations of 1986 July 31 – August 7. The Mark II instrument was used for the observations of 1987 July 27–30 and 1987 September 18–21 (dates given are the UT dates). Both devices operate at the $f/35$ Cassegrain focus of UKIRT, where they require the removal of the standard UKIRT instrument platform (ISU2).

2.1.1 THE MARK I HATFIELD POLARIMETER

The Mark I Hatfield Polarimeter was constructed by Drs. J. Hough and J. Bailey at the Hatfield Polytechnic. Since its construction this device has undergone several major modifications. The original version of this instrument was described by Bailey and Hough (1982). A full description of a later version was given by Brindle (1986). The description given here differs in the addition of an extra optical channel. Nevertheless the basic operation of the instrument is the same as that described by Brindle (1986), and consequently only a brief description is given here. The optical layout of the device is shown in Figure 2.1. The extra channel is provided by the addition of an optical dichroic, which splits the optical beam into 'blue' and 'red' channels. This improvement allows si-

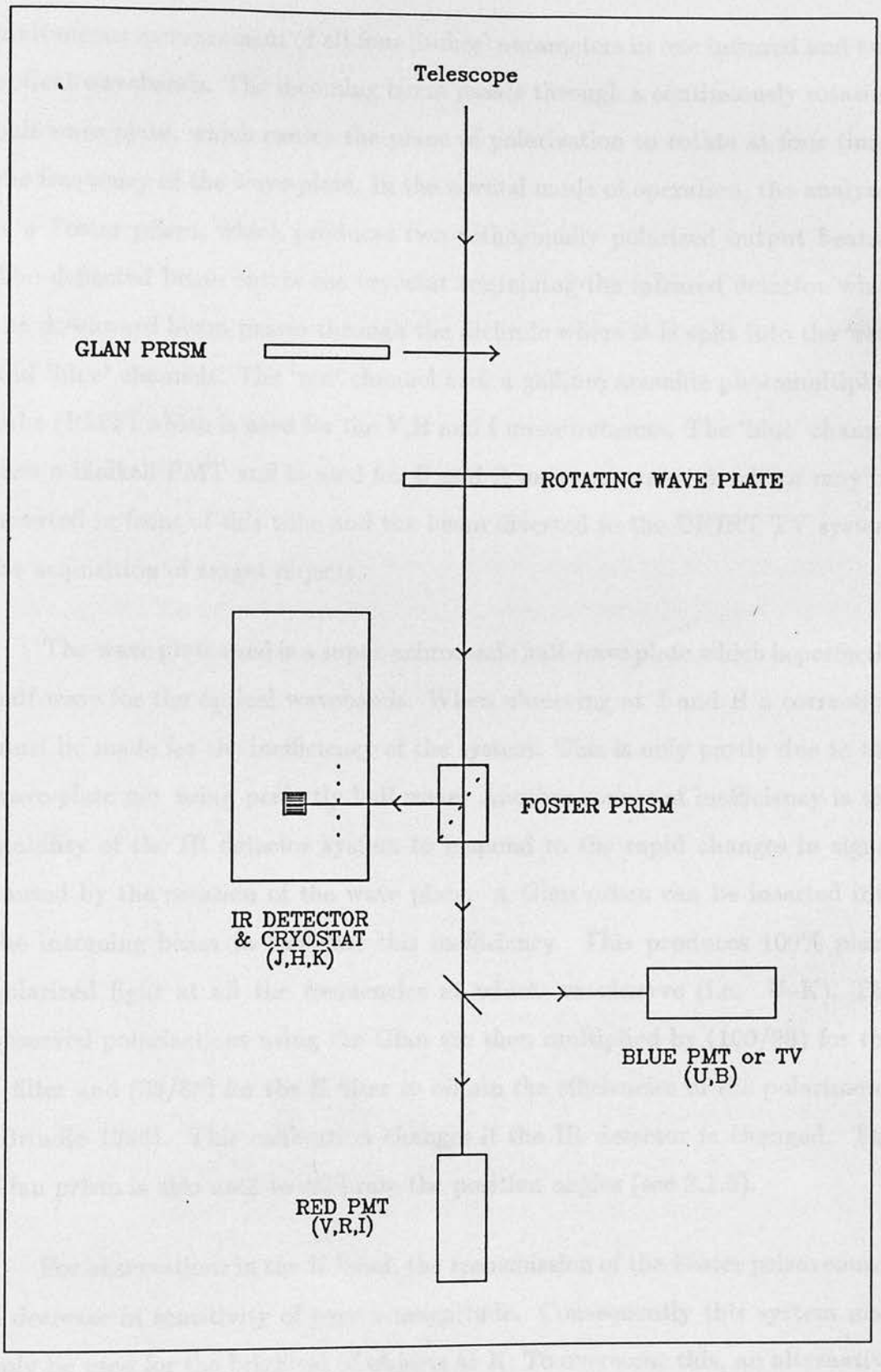

Figure 2.1: The Mark I Hatfield Polarimeter

multaneous measurement of all four Stokes' parameters in one infrared and two optical wavebands. The incoming beam passes through a continuously rotating half-wave plate, which causes the plane of polarization to rotate at four times the frequency of the wave-plate. In the normal mode of operation, the analyser is a Foster prism, which produces two orthogonally polarized output beams. The deflected beam enters the cryostat containing the infrared detector while the downward beam passes through the dichroic where it is split into the 'red' and 'blue' channels. The 'red' channel uses a gallium arsenide photomultiplier tube (PMT) which is used for the V,R and I measurements. The 'blue' channel uses a bialkali PMT and is used for U and B measurements. A mirror may be inserted in front of this tube and the beam diverted to the UKIRT TV system for acquisition of target objects.

The wave plate used is a super-achromatic half-wave plate which is perfectly half-wave for the optical wavebands. When observing at J and H a correction must be made for the inefficiency of the system. This is only partly due to the wave-plate not being perfectly half-wave. Another source of inefficiency is the inability of the IR detector system to respond to the rapid changes in signal caused by the rotation of the wave plate. A Glan prism can be inserted into the incoming beam to calibrate this inefficiency. This produces 100% plane polarized light at all the frequencies at which we observe (i.e. U–K). The observed polarizations using the Glan are then multiplied by (100/98) for the J filter and (93/88) for the H filter to obtain the efficiencies of the polarimeter (Brindle 1986). This calibration changes if the IR detector is changed. The Glan prism is also used to calibrate the position angles (see 2.1.5).

For observations in the K band, the transmission of the Foster prism causes a decrease in sensitivity of over a magnitude. Consequently this system may only be used for the brightest of objects at K. To overcome this, an alternative mode of operation is available, using a wave-plate which is achromatic between 1.0 and 2.5 μm. The prism is replaced by a dichroic and a wire-grid analyser is inserted in front of the cryostat. When configured in this way there is no

analyser in the path of the optical channels, so only infrared polarizations can be measured. This mode was only used for the observations of 1641 + 399 (3C 345) on 1986 August 5.

When using the Hatfield polarimeter, the chopping facility of UKIRT is disabled. One 'cycle' consists of four complete rotations of the wave-plate. Sky subtraction is performed by nodding the telescope, after the first and third rotations. The sequence of observation is then *OBJECT-SKY-SKY-OBJECT*. The counts from each detector are summed over periods of 1/16 a rotation of the wave-plate. In the absence of noise, any sequence of four of these measurements would be sufficient to calculate the flux and polarization parameters. On-line software calculates the polarization parameters and the instrumental magnitude after each cycle and writes these and the raw counts to a disc file on the UKIRT VAX computer. A run is terminated by the observer when the required signal-to-noise ratio is achieved.

2.1.2 THE MARK II HATFIELD POLARIMETER

The Mark II Hatfield Polarimeter was constructed by Dr. J. Hough at the Hatfield Polytechnic and first used in 1987 July at UKIRT. The optical layout is shown in Figure 2.2. This device is a twin-beam instrument with the two beams separated by 51.0 mm. This corresponds to an angular separation on the sky of 81.3 arcsec at the $f/35$ focus of UKIRT. The advantage of this set-up is that the optical and infrared measurements are now performed on separate beams so the wave-plates and other optics have been optimised for the appropriate wavelength ranges.

The infrared beam passes through an IR-achromatic wave-plate and then an IR/optical dichroic. The IR beam is then deflected through a wire-grid analyser and into the cryostat. The downwards beam is sent to the UKIRT TV camera and is used for acquisition and guiding. An efficiency correction must

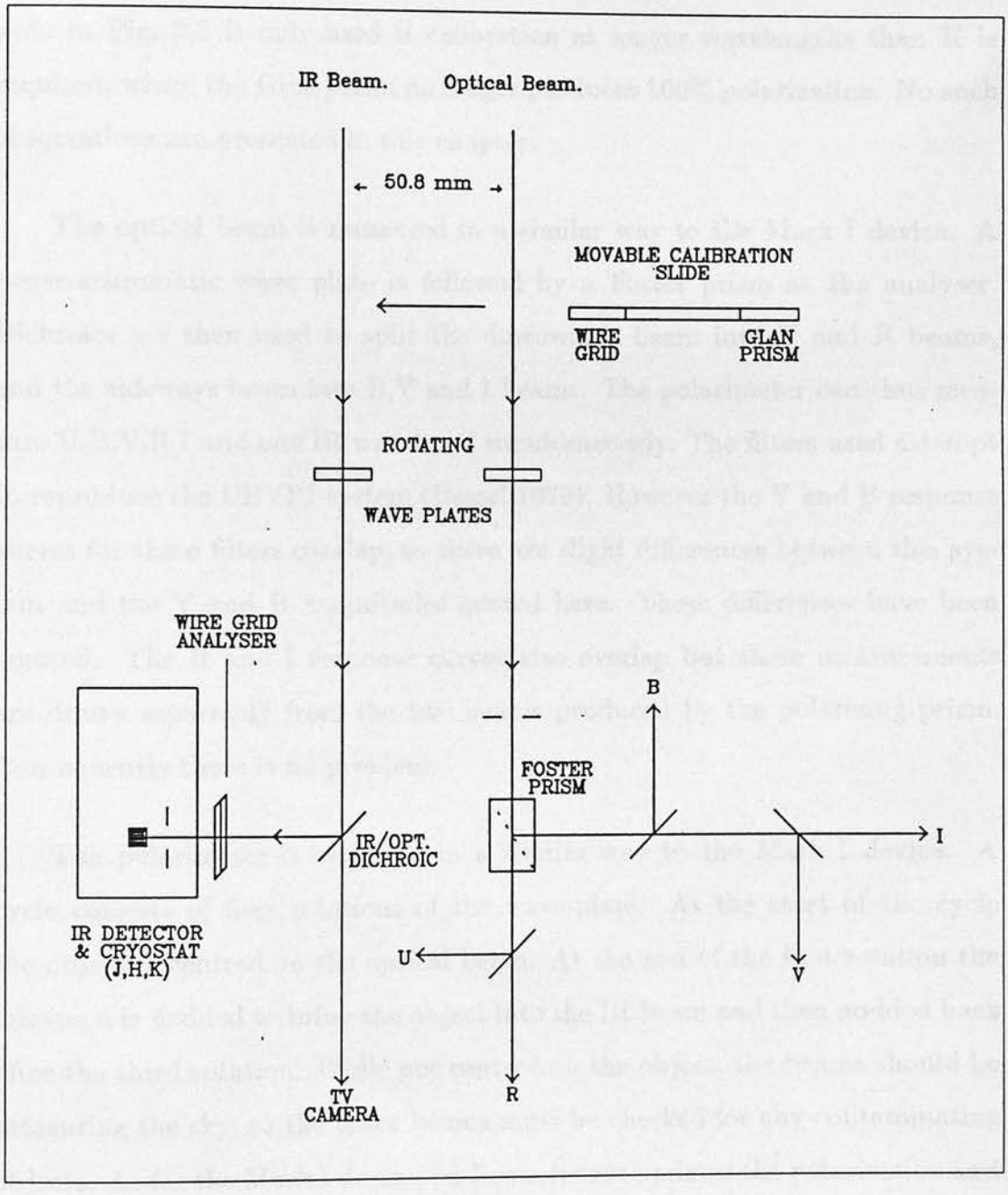

Figure 2.2: The Mark II Hatfield Polarimeter

still be applied to the infrared polarization measurements, but this is no longer a result of the wave plate characteristics. The inefficiencies result from the frequency response of the detector and the wire-grid analyser. The appropriate efficiency to correct the measurements is the measured polarization with the Glan prism inserted into the IR beam. The wire grid shown on the calibration slide in Fig. 2.2 is only used if calibration at longer wavelengths than K is required, where the Glan prism no longer produces 100% polarization. No such observations are presented in this chapter.

The optical beam is measured in a similar way to the Mark I device. A super-achromatic wave plate is followed by a Foster prism as the analyser. Dichroics are then used to split the downwards beam into U and R beams, and the sideways beam into B,V and I beams. The polarimeter can thus measure U,B,V,R,I and one IR waveband simultaneously. The filters used attempt to reproduce the UBVRI system (Bessel 1979). However the V and B response curves for these filters overlap, so there are slight differences between this system and the V and B magnitudes quoted here. These differences have been ignored. The R and I response curves also overlap but these measurements are drawn separately from the two beams produced by the polarizing prism. Consequently there is no problem.

The polarimeter is operated in a similar way to the Mark I device. A cycle consists of four rotations of the wave-plate. At the start of the cycle the object is centred on the optical beam. At the end of the first rotation the telescope is nodded to bring the object into the IR beam and then nodded back after the third rotation. While not centred on the object, the beams should be measuring the sky, so the offset beams must be checked for any contaminating objects. As for the Mark I device, on-line software updates the polarization and flux measurements at the end of each cycle. The data is also written to disc. The raw counts are now written as a file accessible using the FIGARO data reduction system, which is available on STARLINK.

2.1.3 THE INFRARED DETECTORS

Two infrared detectors have been used to make the observations presented here. These are the UKIRT common-user photometers, UKT 6 and UKT 9. Both are indium antimonide (InSb) detectors in liquid nitrogen cooled cryostats. The output voltages from these are fed to a voltage-frequency converter to provide the counts analogous to the photomultiplier signals needed by the reduction system. Both of these detectors have a problem in that they generate random 'spikes' in the output signal. These spikes, which are believed to be a result of vibration, can seriously degrade the signal-to-noise ratios of the data. The spikes were detected by selecting cycles of the raw sky-subtracted counts, where one or more phases differed by more than 4 standard deviations from the mean. These cycles were then removed and the polarization parameters recalculated accordingly. This process assumes that the sky-subtracted signal does not vary significantly over the duration of a run. If source variability or poor observing conditions caused this to be so, then only the very largest spikes would have been detected and removed.

2.1.4 THE CORRECTION OF BIAS IN THE MEASUREMENT OF POLARIZATION

The degree of polarization observed is subject to a statistical bias which must be corrected. This is inherent in the measurement of a vector quantity in the presence of noise. The analytic expression for the expected value of the polarization involves an intractable integral (Vinokur 1965). Wardle & Kronberg (1974) give the expression for the modal value, which is used to relate the true polarization p to the measured polarization p'.

$$p = p' \sqrt{1 - \left(\frac{\sigma_p}{p'}\right)^2} \tag{2.1}$$

The best estimate of the error on p is the error on the measured polarization σ_p. The measured position angle is the best estimate of the true position angle,

but the error is underestimated in the case of poor signal-to-noise (Wardle and Kronberg 1974).

2.1.5 THE CALIBRATION OF THE POSITION ANGLES

The on-line reduction system produces a set of measurements of the polarization and position angle for each waveband at the end of each run. However all the position angles are measured relative to different arbitrary zero points. For the Mark I polarimeter this is entirely a result of the special construction of the wave plate. This is also the case for the Mark II system where extra 90° differences are introduced into the optical results by the different polarizations of the two output beams from the Foster prism. The infrared position angles are all measured relative to the same zero point but this should differ from that of the optical measurements.

To calibrate the position angles relative to each other, the measurements with the polarizing Glan prism in the appropriate beam are used. After passing through the Glan prism, the light will be polarized with a wavelength independent position angle which depends only on the structure of the crystal. Consequently the Glan measurements can be used to transform the position angles such that all wavebands are measured with respect to a common zero point.

The zero point measured in the above procedure does not refer to a standard position angle on the sky. Furthermore there is an ambiguity as to the sense in which the rotations are measured. Astronomical position angles are conventionally measured with North as 0° and increasing from North through East. In fact the position angles returned for the Mark I system have the correct sense, while those for the Mark II system do not. In order to calibrate the position angle zero point and to check the sense, measurements of two or more polarized standard stars are used. These are bright stars whose (interstellar)

polarization properties are already known and are time-invariant. Those used in reducing the data in this chapter were taken from Serkowski (1974). These position angles are only quoted to one degree accuracy and no errors are given. Consequently for many of the measurements given, the position angle error is presumably dominated by the unknown error in these angles.

2.1.6 PHOTOMETRY

In addition to the polarimetric data for the blazars we are interested in the flux densities. The polarimeter returns instrumental magnitudes for each waveband, which are then calibrated in the usual way by observations of standard stars. The infrared magnitudes were calibrated by observations of standard stars from the UKIRT standard list. The optical standards were obtained from the catalogue of Landolt (1983). Airmass corrections were performed using observationally determined extinctions. The wavebands used in the infrared, are those given by the standard filters, but the optical wavebands are complicated by both the dichroic and photomultiplier response functions. The responses of the instrument correspond to the U,B,V,R,I system as described by Bessel (1979), except for B and the V. These are always drawn from the same beam and the filter responses overlap, so the instrumental responses are slightly different from standard. Nevertheless, the differences are small enough to be ignored for the work presented here. Table 2.1 shows the effective wavelengths and corresponding frequencies for each waveband together with the zero magnitude flux density in Janskys. These were obtained from Bessel (1979) and Campins, Rieke and Lebofsky (1985), and are used in the assumption that the slightly different filter responses of the polarimeter systems do not greatly affect these flux densities.

The fluxes have all been corrected for interstellar extinction. The values of $E(B-V)$, taken from Burstein and Heiles (1982) are given in the Appendix. The extinction curve is taken from Rieke and Lebofsky (1985).

Table 2.1: Effective wavelelengths and zero-magnitude flux densities.

Filter	$\lambda/\,\mu$m	$\nu/10^{14}$ Hz	S_o/kJy
K	2.18	1.38	0.667
H	1.64	1.83	1.075
J	1.23	2.44	1.603
I	0.80	3.75	2.55
R	0.64	4.68	3.08
V	0.55	5.45	3.64
B	0.44	6.81	4.26
U	0.36	8.33	1.81

2.2 The Observations

The observations obtained at UKIRT, using the methods described in §2.1 are tabulated and displayed in the Appendix. Table 2.2 summarises the observations. In all 37 objects were observed, giving 102 sets of simultaneous photometric and polarimetric data, 27 sets of polarimetric data without photometric calibration, 20 sets of photometric data with no polarization at the 3 σ level, and 7 sets of uncalibrated data without any polarization. The data which lack photometric calibration come from poor observing conditions during the 1987 September run. Consequently, for those objects where no polarization was detected (at 3 σ), some of the upper limits are quite high. In the sections that follow, brief descriptions of the observations of each object are given. These data constitute the largest such set of observations yet obtained.

The observing strategy used to obtain the data discussed in this chapter was to observe sources from a catalogue of known blazars and blazar candidates. This was an earlier version of Table 1.1. The main difference was the lack of the blazars and blazar candidates discovered by Impey & Tapia (1988). The objects were given a priority for each observing run. This priority was based on previous records of significant polarization flares and photometric variability. However, the period of time needed to ascertain the current state of each object was short ($\sim \frac{1}{2}$ hour) and there existed gaps in R.A., where there were no 'interesting' objects. This allowed the observation of a number of blazars and candidates for which there is little published polarimetry. Because of this, one candidate was confirmed to be a blazar ($0338-214$). Some others ($0118-272$ and $0138-097$) had been observed as candidate blazars, but have been independently shown to be blazars by Impey & Tapia (1988).

Table 2.2: Summary of the polarimetric observations at UKIRT

IAU Name	1986 Jul./Aug.	1987 Jul.	1987 Sep.
$0048-097$	HJIRVB	KHJIRVBU	HIRVBU
$0106+013$	HIB	HIRVBU	HIRVBU
$0109+224$	HJIRVB	HIRVBU	HIRVBU
$0118-272$	HJIRVB	HIRVBU	HIRVBU
$0138-097$	HIB	HIRVBU	KHIRVBU
$0219-164$		KHJIRVBU	
$0219+428$	HIB	HIRVBU	HIRVBU
$0235+164$		KHJIRVBU	KHJIRVBU
$0300+470$			HIRVBU
$0323+022$	HIB		HIRVBU
$0336-019$	HIB		
$0338-214$	HIB		HIRVBU
$0403-132$			HIRVBU
$0414+009$			HIRVBU
$0735+178$			HIRVBU
$0736+017$			HIRVBU
$1253-055$	HJIRVBU	KHJIRVBU	
$1413+135$	HIB		
$1418+546$	HIB	HJIRVBU	HIRVBU
$1510-089$	HIB		
$1514-241$	HIB	KHJIRVBU	
$1538+149$	HIB		
$1641+399$	KHJIRVBU	KHJIRVBU	HIRVBU
$1652+398$			KHJIRVBU
$1717+178$	HIB	HIRVBU	HIRVBU
$1727+502$	HIB		HIRVBU
$1749+096$	HIB	JIRVBU	
$1921-293$	HIB	JIRVB	
$2032+107$		JIRVBU	HIRVBU
$2155-304$	HJIRVB	KHJIRVBU	KHJIRVBU
$2200+420$	HJIRVB	KHJIRVBU	HIRVBU
$2208-137$	HIB		
$2223-052$	HIB	HJIRVBU	HIRVBU
$2230+114$	HIB		
$2251+158$	HIB	HIRVBU	HIRVBU
$2254+074$	HJIRVBU	HIRVBU	HIRVBU
$2345-167$			HIRVBU

2.2.1 0048 – 097 OB–081

An AS80 blazar, 0048 – 097 was observed extensively in all three runs. It consistently showed FDP, but not FDθ , in 1986 August. No such behaviour was observed in 1987 July or September. Typically the position angle changed from night to night by a few degrees.

2.2.2 PKS 0106 + 013

This HPQ (confirmed by Moore & Stockman 1984) was observed on one night in each of the three runs. No significant polarizations were recorded during the 1986 July/August and the 1987 September runs. The only significant polarization measured was the U polarization of 1987 July 28 ($p(U) = 14.37 \pm 2.39\,\%$).

2.2.3 GC 0109 + 224

An AS80 blazar, 0109+224 was observed during all three runs. The polarization in 1986 August was highly variable and displayed both FDP and FDθ . Both $dp/d\nu > 0$ and $dp/d\nu < 0$ were observed on successive nights. The polarization observed in 1987 July was $\sim 10\%$ but essentially constant. The 1987 September data showed more variation but only one case of FDP.

2.2.4 PKS 0118 – 272

This object was a radio source identification with a smooth IR/optical spectrum (Wilkes *et al* 1983). Impey & Tapia (1988) measured one significant (i.e. $> 3\%$) polarization. The observations presented here confirm that this object is a blazar. The polarization was high ($p \sim 17\%$) but constant through 1987 August. FDP was seen in 1987 July with $dp/d\nu > 0$. The polarization signature in 1987 September was more complicated.

2.2.5 0138 – 097

This was another radio source identification with a smooth IR/optical spectrum (Fricke *et al.* 1983), which was confirmed to be a blazar by Impey & Tapia (1988). The polarization in 1986 August was $\sim 6\%$ with marginal indications of $dp/d\nu < 0$. The 1987 July data showed higher polarization ($\sim 20\%$) without FDP, while the 1987 September polarizations were of similar amplitude but with $dp/d\nu > 0$.

2.2.6 PKS 0219 – 164

This object was identified as a blazar by Meisenheimer & Röser (1984). It was only observed once (1987 July 28), when it had (frequency averaged) polarization of $12.63 \pm 0.18\%$ at a position angle of $160.9 \pm 0.5\,°$. This position angle is consistent with the range predicted by their 'oblique rotator' model, though of course without some variability data, this model cannot be confirmed.

2.2.7 0219 + 428 3C 66A

An AS80 blazar which was observed in all three runs. the polarization behaviour in 1986 August was fairly constant with no marked frequency dependence, which was also the case in 1987 July. Marginal evidence for FDP was seen in 1987 September. Inoue (personal communication) reports 10 GHz observations of this object on 1987 September 17 which show 2.8% polarization at 5°.

2.2.8 AO 0235 + 164

This is the object for which Impey, Brand & Tapia (1982) measured their record polarization of $p(V) = 43.9 \pm 1.4\%$. Three observations of this object were made. For the two photometric nights, the spectrum was very steep $\alpha(B) =$

4.61, but the polarizations were always of the order of 10%. Inoue (personal communication) reports 10 GHz observations on 1987 September 17 which show polarization at 1.5% and at 14°. This position angle is consistent with the IR/optical data.

2.2.9 0300 + 470 4C 47.08

This AS80 blazar was only observed once on 1987 September 20 in poor photometric conditions. The data were consistent with $p = 8.91 \pm 0.64\%$ and $\theta = 9.42 \pm 1.92\%$, independent of frequency.

2.2.10 1H 0323 + 022

This X-ray selected object was classified as a blazar by Feigelson *et al.* (1986) who, in particular, noted its extremely rapid X-ray variability. They observed it to be optically polarized (2 – 9%) in 1983 and 1984. No significant polarization was observed on 1986 August 1 ($p < 6.3\%; 3\sigma$ upper limit at I). Polarization was measured on 1987 September 21, with the average over all wavebands being 3.56 ± 0.45 %.

2.2.11 0336 – 019 CTA 26

This Moore & Stockman (1981) HPQ was only observed once on 1986 August 5, and no significant polarization was measured as the object was faint and the integration was accordingly terminated early.

2.2.12 0338 – 214

This is a smooth optical spectrum radio source identification (Wilkes *et al.* 1983). The polarization was observed to be $\sim$ 10% in both 1986 August and

1987 September with no frequency dependence.

2.2.13 PKS 0403 – 132

This is a Moore & Stockman (1981) HPQ, which was observed only once on 1987 September 19 in poor photometric conditions. The 3σ upper limit to the R polarization is 3.48 %.

2.2.14 1H 0414 + 009

This X-ray selected object is a candidate blazar. Ulmer *et al.* (1983) classified this as a BL Lac object and Impey & Tapia (1988) report an optical polarization of $2.76 \pm 0.29\%$. This object was observed on 1987 September 21 in poor photometric conditions and a 3σ upper limit to the R polarization of 3.9 % was obtained.

2.2.15 PKS 0735 + 178

This well known blazar was only observed once (1987 September 19) in poor photometric conditions. The measured polarization was frequency independent ($p = 6.9 \pm 0.4$ %) but the position angle was marginally frequency-dependent (average value 136°). Inoue (personal communication) reports polarization of 1.2% at 72° (10 GHz).

2.2.16 PKS 0736 + 017

This AS80 blazar was observed on 1987 September 19 and 20 in poor photometric conditions. A significant polarization was measured at R of $6.32 \pm 1.50\%$ on the first night. The 3σ upper limit on the polarization on the second night

was 2.4% at R. The 10 GHz polarization was 4.5% at 2° on 1987 September 17 (Inoue; pèrsonal communication).

2.2.17 1253 − 055 3C 279

This object is a well studied superluminal radio source, which has long been known to be a blazar. The observations of 1986 August show a polarization flare, with the degree of polarization increasing during the course of the run, and consistently showing $dp/d\nu > 0$. The U data of 1986 August 5 show a polarization of $45.92 \pm 0.98\%$. This is the largest polarization ever seen in the IR/optical for a blazar (c.f. 0235 + 164; Impey, Brand & Tapia 1982). On 1987 July 28 the polarization was still high, but not at the record level.

2.2.18 1413 + 135 OQ 122

This is a radio source with a very steep IR/optical spectrum (Beichman *et al.* 1981 and Bregman *et al.* 1981). The latter gives the only recorded significant polarization of $19 \pm 3\%$ at H. This object was observed in 1986 August, but was too faint for IR polarimetry to be feasible in the time available. The spectrum was so steep that only an upper limit is available for the optical flux.

2.2.19 1418 + 546 OQ 530

This AS80 blazar was observed during all three runs. In 1986 August the polarization showed FDP with $dp/d\nu > 0$, which was repeated in the measurements of 1987 July 30, where the polarization increased from 2.5% at H to 8.7% at U. This latter was accompanied by significant FDθ . The data of 1987 September were all obtained in poor photometric conditions. However the polarization data still showed FDP but no FDθ .

2.2.20 PKS 1510 – 089

This object was confirmed to be a blazar by Moore & Stockman (1981) and Smith *et al.* (1987). It is one of the most violently variable HPQ's with $\Delta m =$ 5.4 (Moore & Stockman 1981). This object was observed only once on 1986 August 1. The 3σ upper limit to the the I polarization was 6.3 %.

2.2.21 1514 – 241 *AP Lib*

One of the original BL Lac objects, 1514 – 241 was observed only twice (1986 August 1 and 1987 July 27). The polarization of this object is typically quite low compared to most other blazars (e.g. AS80). These observations are consistent this. FDP was seen on 1987 July 27.

2.2.22 1538 + 149 4C 14.60

An AS80 blazar which was observed on 1986 August 1 when no significant polarization was observed. The 3 σ upper limit was high (27 %) as the object was faint.

2.2.23 1641 + 399 3C 345

The behaviour of this object will be discussed at length in §2.3.1.

2.2.24 1652 + 398 MKN. 501

This BL Lac object was observed only once on 1987 September 21. Both the degree and position angle of polarization were observed to be frequency dependent (at the 0.5 % level of significance).

2.2.25 1717 + 178 OT 129

This AS80 blazar was observed twice in 1986 August with strong $dp/d\nu < 0$ on the second night. No significant polarization was measured on 1987 July 30 ($p < 21\%$) nor on 1987 September 20 ($p < 8\%$) (both upper limits at R).

2.2.26 1727 + 502 I Zw. 186

An AS80 blazar which was observed twice in 1986 August, when it showed variable FDP and FDθ . It was also observed on 1987 September 21 when $dp/d\nu > 0$ was observed (without FDθ).

2.2.27 1749 + 096 OT 081

An AS80 blazar which was extensively observed in 1986 August. No FDP was seen but significant variations were seen in the polarization behaviour. FDθ was seen on 1986 July 31. On 1987 July 27, 1749 + 096 was faint but $dp/d\nu > 0$ was seen. The observations of 1987 September 19 were made in poor photometric conditions and the polarization data obtained were very noisy.

2.2.28 1921 – 293 OV–236

This blazar was first classified as such by Wills & Wills (1981). Confirmation of it being polarized was provided by Impey *et al.* (1982). The observations of 1986 August indicate appreciable photometric variability (a factor of two from 1986 August 6 to August 7). Appreciable FDP was seen on 1986 August 6.

2.2.29 2032 + 107 MC

This candidate blazar was first classified by Zotov & Tapia (1979), who have published the only polarization measurement. Antonucci *et al.* (1987) have confirmed its extragalactic nature. Two observations of this object were made on 1987 July 27 and September 19 (in poor photometric conditions). In neither case was any polarization detected. The 3 σ upper limits were respectively 1.32% and 1.47% at R.

2.2.30 PKS 2155 – 304

This is one of the brightest of the AS80 BL Lac objects, and was observed as a part of all three runs, but its polarization is typically quite low (3 – 7%; AS80). The data of 1986 August showed polarization at about this level and exhibited variability in both amplitude and frequency dependence. The data of 1987 July 27 showed a higher polarization ($\sim$ 10%) and both FDP and FDθ . The data of 1987 September 21 were obtained in poor conditions, but the polarization showed FDP.

2.2.31 2200 + 420 *BL Lac*

BL Lac was observed more often than any other object in this programme. Photometric variability was small over the three runs. Instances of both FDP and FDθ were observed in all three periods. The position angle of the polarization was in the range 10–40° for all the observations. This is essentially the same position angle seen by Brindle *et al.* (1985). Inoue (personal communication) reports a high 10 GHz polarization of 9.2% at 21° on 1987 September 17. This position angle is somewhat different from that seen in the IR/optical on 1987 September 19 ($\sim$ 40°).

2.2.32 PKS 2208 – 137

This is an AS80 blazar which was observed four times in the 1986 august run. On each occasion it was observed to have an abnormally flat IR/optical spectrum and no polarization. The lowest 3σ upper limit was 1.78% at B on 1986 August 4.

2.2.33 2223 – 052 3C 446

2223 – 052 is a well known violently variable HPQ. During the 1986 August observations this object was faint and no reasonable limits on the optical polarization were obtained. In 1987 July frequency independent polarization was seen varying from 12% to 8%. The observations of 1987 September were obtained in poor photometric conditions. The noisy data showed some evidence for FDP. The 10 GHz polarization data of 1987 September 17 ($p \approx 4\%$ and $\theta \approx 2°$), showed a position oriented roughly at 90° from the IR/optical data (Inoue, personal communication).

2.2.34 2230 + 114 CTA 102

This object is an AS80 blazar and a well known superluminal radio source. It was observed twice in 1986 August and no polarization was measured. the upper limits at B being 3.6% and 5.7%.

2.2.35 2251 + 158 3CR 454.3

Another superluminal radio source and AS80 blazar, this object was observed once in each of the three runs. No polarization was observed in the first two runs, but frequency-independent polarization was observed on 1987 September 20 of $p = 3.8 \pm 0.3\%$. This position angle was oriented somewhat differently from

the 10 GHz data of Inoue (perosnal communication) who measured $p \approx 3.2\%$ and $\theta \approx 11°$, on 1987 September 1987.

2.2.36 2254 + 074 OY 091

This AS80 blazar was extensively observed in all three runs. The polarization behaviour was characterised by strong FDP with little evidence for FDθ in all three runs. On all dates except for 1986 August 6, the FDP was such that $dp/d\nu > 0$.

2.2.37 PKS 2345 – 167

This AS80 blazar was only observed on 1987 September 20 in poor photometric conditions. Only the H polarization was significant at the 3σ level ($p = 25 \pm 6\%$).

2.3 Contamination by Unpolarized Components

This section considers the effects of non-synchrotron components in the observed polarization signature of blazars. Some of this section has appeared in the Monthly Notices of the Royal Astronomical Society as Mead *et al.* (1988).

This problem is very important in the study of the blazar emission process. Contamination of single-aperture photometry by emission from other components of the blazar can easily lead to erroneous conclusions about the nature of the emission process.

2.3.1 THE OBSERVATIONS OF 1641 + 399 (3C 345) AND THE 'BLUE BUMP'

1641 + 399 (3C 345) is a well studied superluminal radio source and optically violently variable quasar. It has long been known to be a highly polarized quasar (AS80). Recently Smith *et al.* (1986) (hereafter referred to as SBHE) reported observations of the polarization behaviour of this object over a range of dates in 1983 and 1984. They found that the polarization always decreased with increasing frequency from the infrared into the optical region. They were able to model their observations by including an unpolarized black-body in addition to the typical power-law continuum emission of a blazar. This black-body dilutes the polarized flux of the power-law component and causes the decrease in polarization observed. Such black-bodies have been proposed by Malkan & Sargent (1982), who used them to fit 'bumps' observed in the optical–ultraviolet continua of quasars. They proposed that these black-bodies were the radiating accretion discs around the black holes, which are believed to be at the centre of all active galactic nuclei. Malkan (1983) improved upon this model of quasar continua by considering more realistic accretion disc spectra, which allowed for temperature gradients across the surface of the disc. Malkan & Moore (1986) have also applied this model to observations of two blazars PKS 0736 + 017 and PKS 1510 − 089. SBHE then predicted that the black-body component seen in the polarization data for 1641 + 399 should remain stable for at least a few years, since the size of the proposed accretion disc indicates the minimum variability time-scale.

2.3.1.1 The Polarization Data of 1986 August

The mean B magnitude for the period August 1 to August 7 was 16.69 ± 0.02. Babandzhanyants *et al.* (1985) list photographic B magnitudes over the period 1973–1983, which peak at B= 14.70 in September 1982. The faintest magnitude recorded was in 1973 with B= 17.15. 1641 + 399 was thus two magnitudes below its peak B flux, during the 1986 August observations. There is

no evidence for any photometric variability over the period of these observations. There is marginal evidence that the polarization may have increased in the infrared wavebands until August 6 before dropping slightly to the August 7 value. However, the difference between the H polarizations on August 1 and August 6 is $3.9 \pm 1.8\%$, a 2.2σ result. Given this low significance, the possibility of variability over the period of observations has been discounted and the data were combined to give the mean flux and polarization values listed in Table 2.3, and shown in Fig. 2.3. There is no evidence that the position angle depends on frequency on any night. However the position angle increased by six degrees over the period of the observations. Table 2.4 shows the mean position angle for each night.

Qualitatively the frequency behaviour of the degree of polarization that we observe is similar to that seen by SBHE. There is no evidence that the degree of polarization depends on frequency for the infrared data, but it steadily decreases with increasing frequency for the optical measurements. This behaviour cannot be simply explained in terms of the synchrotron emission mechanism thought to be responsible for the polarization of the power-law continuum in blazars. A simple uniform synchrotron emitter should show no frequency dependence of polarization (§1.3.1).

SBHE considered a variety of methods of reproducing their data and concluded that dilution by an unpolarized component in the optical frequencies was the most probable explanation. There are likely to be several such optical components in a blazar spectrum. These are the stellar emission of an underlying galaxy, the quasar line emission, the Balmer and Paschen continua and the thermal 'blue bump' as proposed by Malkan & Sargent (1982). SBHE constructed a model in which the contribution of the first two of these components was estimated, and then a polarized power-law continuum and a black-body component were fitted to the remaining flux and the corrected polarization data. In order to compare the 1986 August data with those of SBHE a similar model has been constructed. The galaxy flux is estimated from the C model

Table 2.3: Averaged flux and polarization measurements for 3C 345 for the 1986 August run. Errors are given in parentheses.

Filter	Flux (mJy)		Polarization (%)	
K	8.02	(0.74)	17.93	(1.57)
H	4.13	(0.08)	17.98	(0.46)
J	2.54	(0.07)	17.21	(0.54)
I	1.44	(0.03)	14.89	(0.32)
R	1.07	(0.04)	13.53	(0.37)
V	0.89	(0.04)	11.76	(0.33)
B	0.90	(0.04)	8.42	(0.16)
U	0.60	(0.04)	7.92	(0.67)

Table 2.4: Mean position angles for each night.

U.T. Date	Position angle (°)	
01.08.86	53.16	(0.73)
02.08.86	53.15	(0.53)
04.08.86	55.75	(0.47)
05.08.86	58.99	(1.20)
06.08.86	58.30	(0.71)
07.08.86	59.08	(1.13)

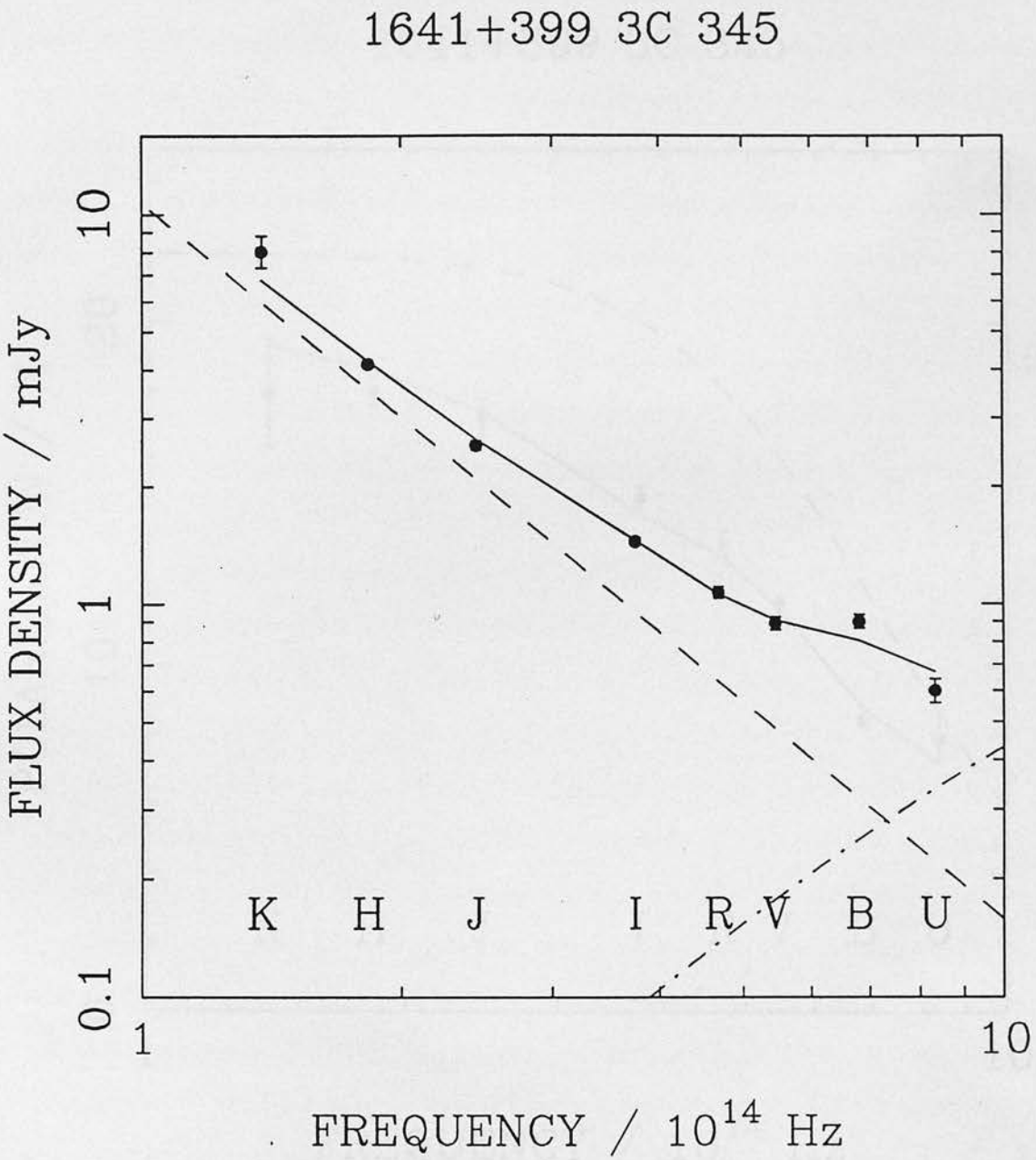

Figure 2.3: (*a*) The averaged flux density versus frequency. The solid line connects the model estimates for the flux density at each observed frequency. The dashed lines show the fitted power-law and black-body components.

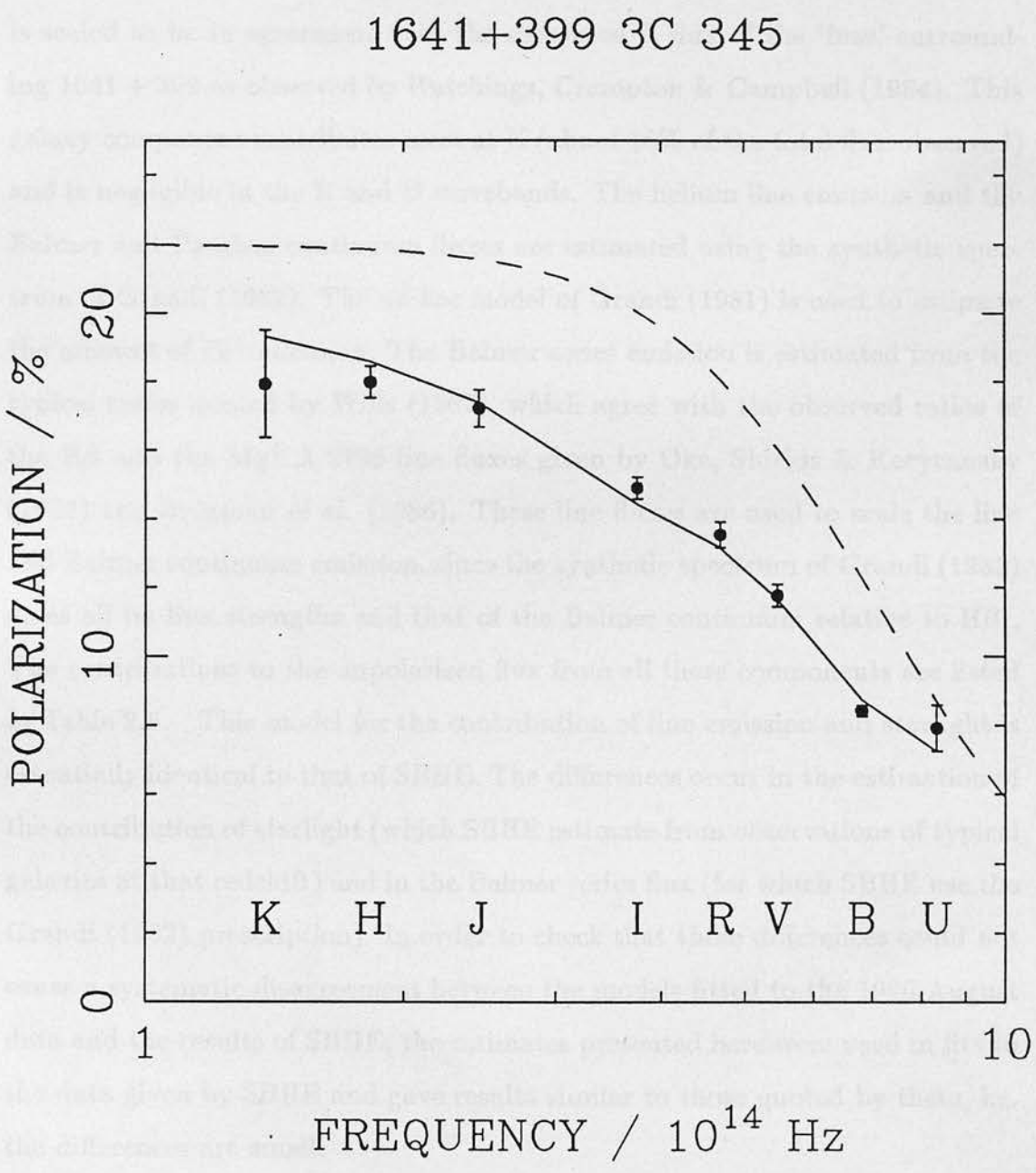

Figure 2.3: (*b*) The averaged polarization versus frequency. The dashed line shows the polarization predicted for the combination of the power-law component and the black-body. The difference between this curve and the observed values is due to the significant amount of line emission and starlight.

of an evolving elliptical galaxy developed by Bruzual (1983). This is evaluated at z=0.595, the redshift of 1641 + 399, taking H_0 = 100 km s^{-1} Mpc^{-1} and Ω_0=0. These values are fixed by the tables offered by Bruzual (1983). The flux is scaled to be in agreement with the measured R flux of the 'fuzz' surrounding 1641 + 399 as observed by Hutchings, Crampton & Campbell (1984). This galaxy component contributes most at K (about 10% of the total flux observed) and is negligible in the B and U wavebands. The helium line emission and the Balmer and Paschen continuum fluxes are estimated using the synthetic spectrum of Grandi (1982). The *ad hoc* model of Grandi (1981) is used to estimate the amount of Fe^+ emission. The Balmer series emission is estimated from the typical ratios quoted by Wills (1987), which agree with the observed ratios of the Hβ and the Mg^+ λ 2798 line fluxes given by Oke, Shields & Korycansky (1984) and Bregman *et al.* (1986). These line fluxes are used to scale the line and Balmer continuum emission, since the synthetic spectrum of Grandi (1982) gives all its line strengths and that of the Balmer continuum relative to Hβ . The contributions to the unpolarized flux from all these components are listed in Table 2.5. This model for the contribution of line emission and starlight is essentially identical to that of SBHE. The differences occur in the estimation of the contribution of starlight (which SBHE estimate from observations of typical galaxies at that redshift) and in the Balmer series flux (for which SBHE use the Grandi (1982) prescription). In order to check that these differences could not cause a systematic disagreement between the models fitted to the 1986 August data and the results of SBHE, the estimates presented here were used in fits to the data given by SBHE and gave results similar to those quoted by them, i.e. the differences are small.

These components do not appear to provide a sufficient amount of non-polarized flux to explain the polarization behaviour, and a further component of non-polarized radiation is required. Following SBHE, a power-law component with a frequency independent polarization and a non-polarized thermal component have been fitted as shown in Fig. 2.3. The best fitting parameters

Table 2.5: Model contributions to observed fluxes in mJy. Bruzual (1983) does not give a V–I colour for his model. The value shown here for the galaxy contribution in I is an interpolation between the J and R values.

Filter	Strong lines	Fe^+ lines	Balmer & Paschen continuum	Underlying galaxy
K	0.000	0.000	0.000	0.818
H	0.072	0.000	0.000	0.555
J	0.000	0.000	0.100	0.409
I	0.114	0.006	0.089	0.243
R	0.041	0.011	0.101	0.135
V	0.007	0.019	0.194	0.029
B	0.060	0.031	0.136	0.006
U	0.007	0.024	0.080	0.001

are a power-law component with a 10^{14} Hz flux density of 10.7 mJy, a spectral index of 1.8 and a polarization of 22.0 %. The fitted black-body has a temperature of 62000 K (this temperature is the temperature of the emitting material, the apparent temperature being T/(1+z)), and an angular diameter of 0.2×10^{-6} arcsec. This angular diameter corresponds to a projected diameter of ~ 0.003 pc or $\sim 10^{14}$ m (using the cosmological parameters assumed above). The χ^2 for this fit is 21.9 (10 degrees of freedom), implying a significance level of 0.016. The value of the fitted temperature is very high when compared to the values found by both Malkan & Sargent (1982) and SBHE. The peak flux for this black-body lies at an observer's wavelength of 746 Å, well beyond the 3600 Å effective wavelength of the U filter. Consequently only the Rayleigh-Jeans ($B_\nu \propto \nu^2$) portion of the black-body spectrum is being fitted. A temperature fixed at 26,000 K, was also fitted as this corresponds to the typical value found in observations of quasars and active galaxies (Edelson & Malkan 1986). For this fit the parameters of the power-law were essentially unchanged, while the fitted angular diameter was 0.4×10^{-6} arcsec, which corresponds to a projected diameter of ~ 0.006 pc or $\sim 2 \times 10^{14}$ m. Both of these fits give a V flux density of $\sim$ 0.2 mJy for the black-body component. The χ^2 for the 26,000 K fit is 31.0 (9 degrees of freedom), which implies a significance level of 0.003. This level is totally unacceptable (assuming Gaussian statistics) and is due to the appreciable amount of curvature of this black-body in the optical region. A Rayleigh-Jeans fit is all that is permitted by these data. A more simple unpolarized component was also tried of a flat ($\alpha = 0$) component but this could not provide a reasonable fit ($\chi^2 = 101$; 12 degrees of freedom).

2.3.1.2 The Polarization Data of 1987 July and September

1641 + 399 was also observed in both 1987 July and September. During these periods, the polarization was observed to have decreased dramatically compared to that described in the previous section. On 1987 July 28 no FDP was seen and the frequency averaged polarization was $2.13 \pm 0.36\%$. No 3σ polarizations

were observed on 1987 July 30, 1987 September 19 or 1987 September 20.

The flux was observed to be much less than that observed in 1986 August. No evidence for variability was seen between 1987 July and September. The September flux densities were all slightly lower than the July data, but this was not statistically significant (even at the 10% level). The B magnitude averaged over the two periods was 17.49 ± 0.03. This is fainter than the minimum of the monitoring data of Babandzhanyants *et al.* (1985) (see §2.3.1.1). Table 2.6 shows the averaged flux data and the corrected values when the §2.3.1.1 model for starlight, line emission and Balmer and Paschen continua have been removed. These data is shown in Fig. 2.4 with the best-fit combination of a power-law and a black-body. The parameters for the fit are a χ^2 of 4.8 (4 degrees of freedom) which corresponds to the 31% level of significance. The power-law component had a 10^{14} Hz flux density of 7.6 mJy and a spectral index of 2.4. The black-body was at a temperature of 26,000 K and had an angular size of 0.4×10^{-6} arcsec. This fit was performed on the flux density data alone, as the low level and noisy characteristics of the polarization data rendered this unusable. Comparison of this fitted black-body with that of §2.3.1.1 shows that, although a lower temperature has been fitted, the model black-body flux at V is comparable to that found for the 1986 August data ($\sim$ 0.2 mJy).

2.3.1.3 Discussion

SBHE found that their best fit black-body parameters were an apparent temperature of $\sim$ 16000 K (corresponding to an emission temperature of 25 000 K) and an angular diameter of 0.6×10^{-6} arcsec. This angular diameter corresponds to a projected diameter of $\sim$ 0.008 pc (given the cosmological parameters assumed in §2.3.1.1). The V flux density for this black body is $\sim$ 0.4 mJy , i.e. a factor of two greater than that estimated for either the 1986 August data or the 1987 July/September data. It is not unreasonable that this variability is due to a real variation of the parameters describing an accretion disc, given the

Table 2.6: Averaged flux densities for the 1987 July/September data of 1641 + 399, and the values corrrected for starlight, line emission etc.

Filter	Flux density (mJy)	Corrected Flux density (mJy)
K	5.36 (0.75)	4.54
H	2.38 (0.09)	1.75
J	1.39 (0.09)	0.88
I	0.88 (0.04)	0.43
R	0.62 (0.04)	0.33
V	0.47 (0.04)	0.22
B	0.48 (0.04)	0.25
U	0.36 (0.04)	0.25

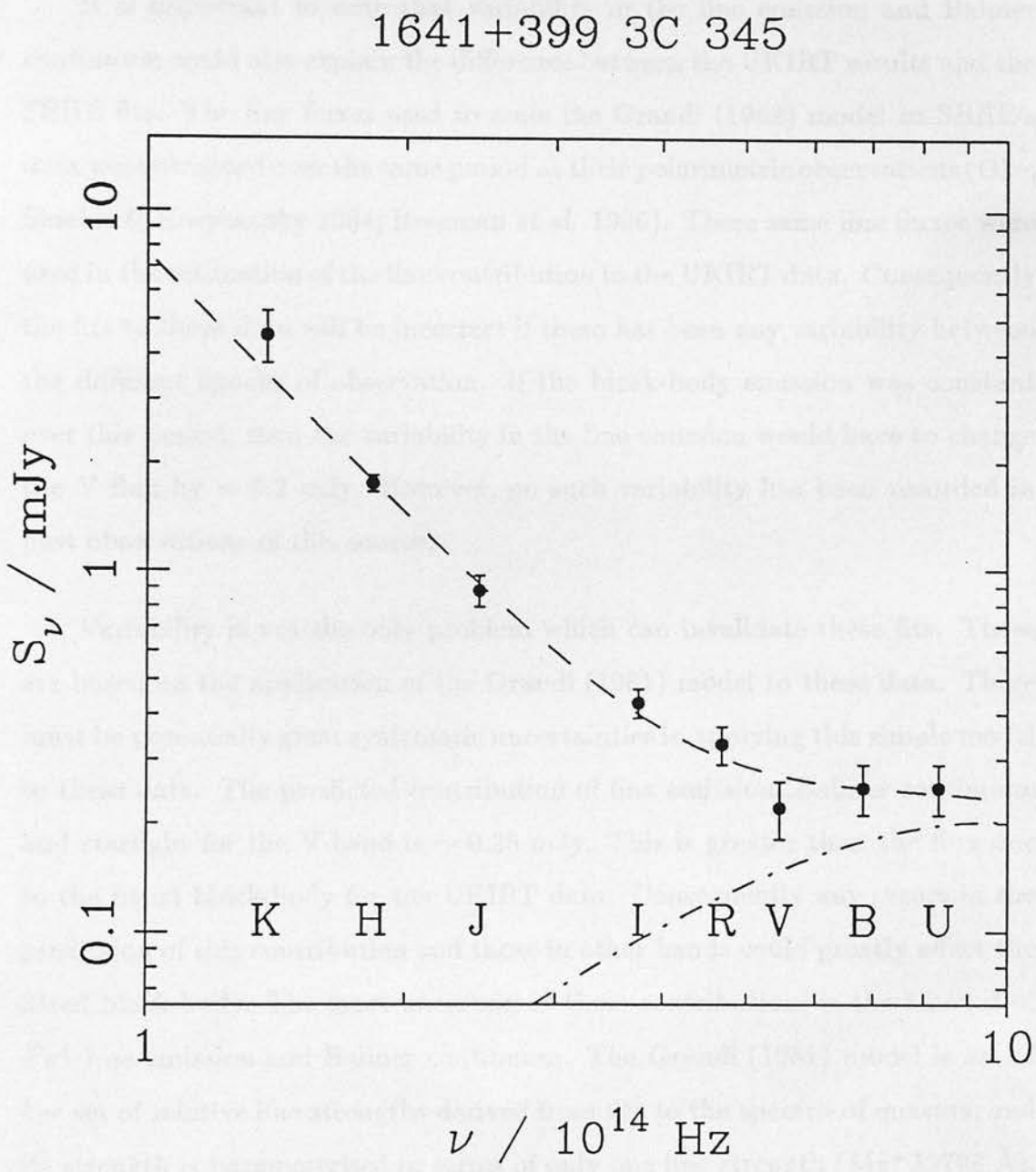

Figure 2.4: This plot shows flux density versus frequency for the 1987 July/September data. The data has been corrected to remove the contribution of starlight, line emission etc. (according to prescription described in §2.3.1.1). The fitted curve represnts the best fit combination of a power-law and a black-body to the remaining flux. The fitted black-body is also shown.

expected variability timescale of about a year.

It is important to note that variability in the line emission and Balmer continuum could also explain the difference between the UKIRT results and the SBHE fits. The line fluxes used to scale the Grandi (1982) model to SBHE's data were obtained over the same period as their polarimetric observations (Oke, Shields & Korycansky 1984; Bregman *et al.* 1986). These same line fluxes were used in the estimation of the line contribution to the UKIRT data. Consequently the fits to these data will be incorrect if there has been any variability between the different epochs of observation. If the black-body emission was constant over this period, then the variability in the line emission would have to change the V flux by $\sim$ 0.2 mJy. However, no such variability has been recorded in past observations of this source.

Variability is not the only problem which can invalidate these fits. These are based on the application of the Grandi (1981) model to these data. There must be potentially great systematic uncertainties in applying this simple model to these data. The predicted contribution of line emission, Balmer continuum and starlight for the V band is $\sim$ 0.25 mJy. This is greater than the flux due to the fitted black-body for the UKIRT data. Consequently any errors in the prediction of this contribution and those in other bands could greatly affect the fitted black-body. The most uncertain of these contributions is the amount of Fe^{+} line emission and Balmer continuum. The Grandi (1981) model is an *ad hoc* set of relative line strengths derived from fits to the spectra of quasars, and its strength is parameterised in terms of only one line strength ($Mg^{+}\lambda 2798$ Å). Wills, Netzer & Wills (1985) present a set of fits to the optical/UV spectra of quasars using the model of Netzer & Wills (1983). This model should be an improvement on the Grandi (1981) model as it incorporates more Fe^{+} multiplets. They found that they could fit all the excess flux above that which can be explained by a power-law continuum. This model is also used by Neugebauer *et al.* (1987) in analysing their $0.3 - 2.2\,\mu$m observations of the Palomar-Green sample of quasars. Neither of these investigations require black-bodies to ex-

plain continuum features in their spectra. However, the power-law components of these non-blazar spectra are much flatter ($\alpha \sim 0.3$), than the steep spectra of blazars (c.f. $\alpha = 1.8$ for the 1986 August model). Moreover, for the Wills, Netzer & Wills (1985) data, these power-laws are fitted, over a much smaller range of frequency. It cannot be ruled out that these flatter power-laws contain a contribution from an accretion disc, this being much broader than the unrealistic black-body shapes being considered here. Nevertheless, the error in the estimation of the line emission and Balmer continuum contributions to the observed fluxes may be large enough that the required black-body contribution is drastically reduced or perhaps eliminated altogether. The fit to SBHE's data uses contemporaneous line flux data and hence the uncertainty in their fit lies entirely in this uncertainty in the ability of the Grandi (1981) model to predict accurately the emission line contribution to the broad-band colours. The fitted black-body is more luminous than that fitted to the 1986 August data, but the uncertainties in the model implied by the above results still apply.

Since the publication of the SBHE, Smith *et al.* (1988) have extended their work to cover fits to observed $dp/d\nu < 0$ in three more HPQ's $0420 - 014$, $1156 + 295$ and $2251 + 158$. Only one of these ($2251 + 158$) was observed extensively as part of the programme of observations reported in this chapter and evidence of $dp/d\nu < 0$ was seen. For these data, Smith *et al.* (1988) employ a slightly different model for the unpolarized optical emission. They use the Wills, Netzer & Wills (1985) parameters to fit the emission lines etc. Rather than fit an unpolarized black-body as an approximation to an accretion disc, they use an unpolarized component with a flat optical to near-UV spectrum. They argue that this is more consistent with the more sophisticated accretion disc models of Malkan (1983). The 1986 August UKIRT data cannot be fitted with such a component in place of a black-body. However, this result is based on the Grandi (1981) etc. prescription for the remaining unpolarized flux.

The basic problem with attempting to determine the origin of the unpolarized flux in $1641 + 399$ is that only 16 data points are available (8 flux densities

and 8 polarizations). Since these data provide no information on such aspects as the amount of line emission, this must be assumed to be consistent with a 'best guess' taken from model fits to other quasars. This induces the potential systematic uncertainties described above. Add to this the variety of possible spectral shapes of the thermal accretion disc radiation and it becomes very hard to obtain meaningful parameters from such a limited data set. A further problem is that polarimetry can only be used to aid these decompositions in the assumption that the degree of polarization of the synchrotron component is frequency independent. As will be shown in §2.5, this is often not the case. What can be said is that spectrophotometry is really essential in determining the parameters of the (supposed) accretion disc radiation. Spectrophotopolarimetry (as employed by Antonucci 1988) may provide useful constraints if FDP can be neglected.

2.3.2 CONTAMINATION IN OTHER OBJECTS

The observations of $1641+399$, described in the previous section, represent the most extreme example of contamination of the blazar component seen in the UKIRT data set. Nevertheless, the possibility that the data on other objects does not solely represent the behaviour of the blazar component must be considered.

In addition to $1641+399$, the following instances of significant FDP with $dp/d\nu < 0$ were seen;

$0109+224$ 1986 August 4 (1.0% significance)

$0138-097$ 1986 August 5 (3.0% significance)

$1717+178$ 1986 August 7 (0.01% significance)

$1921-293$ 1986 August 6 (0.5% significance)

$2251+158$ 1987 September 20 (3.0% significance)

In addition the following objects also showed flux behaviour which could not be characterised as either power-laws or as convex ($d\alpha/d\nu > 0$) spectra;

0106 + 013 1987 July 18 (2.5% significance)

0118 − 272 1987 July 27 (0.01% significance)

1418 + 546 1986 August 6 (0.01% significance)

1749 + 096 1986 August 5 (0.01% significance)

1921 − 293 1987 July 27 (<0.01% significance)

2032 + 107 1987 July 27 (<0.01% significance)

2208 − 137 1987 August 3,4,6 & 7 (all <0.01% significance)

These significances are the χ^2 levels of significance (assuming a normal error distribution) for a fit to a frequency-independent polarization (for the FDP cases) and to a power-law flux distribution (for the abnormal spectra cases). These observations represent examples of behaviour which runs against the trends seen in the observations of blazar behaviour (see later sections).

The examples of FDP may be a result of a contaminating flux in the optical wavelengths. However, an alternative explanation could be that this behaviour is a result of the superposition of misaligned polarized components as in the 0851 + 202 (OJ 287) model of Holmes *et al.* (1984b). The FDθ seen in the behaviour of 0109+224 on 1986 August 4 could lend weight to this explanation for this object.

The examples of unusual spectral flux density distributions are more complicated to interpret. Objects showing either $d\alpha/d\nu < 0$ or not showing monotonic spectral index variation have been picked out. As can be seen they represent a very small subset of the observations of blazars. Many of these observations showed little or no significant polarization measurements and therefore cannot be assumed to represent the blazar component at all.

These objects have all been picked out because, as will be shown (§2.4 and §2.5), they display unusual behaviour when compared to other observations of blazars. However, one of the important potential causes of contaminating unpolarized flux is the starlight of the host galaxy. Since this will be expected to peak in the IR rather than in the optical, this can be expected to cause different

changes in the observed behaviour than that caused by the 'blue bump'. In fact, such emission will cause behaviour not dissimilar from that which is observed to be the general trend for blazars. If the continuum emission is dominated by starlight the spectrum will be both curved ($d\alpha/d\nu > 0$) and very steep. In this case the polarization will be low. However, contamination of a polarized synchrotron component by starlight can result in spectra that are more curved and steeper than the blazar component. Since the starlight also peaks in the IR, FDP will occur with $dp/d\nu > 0$, which is also a common (and expected) feature of blazar emission. Consequently care must be taken to ensure that behaviour which will be interpreted as being characteristic of the blazar emission process is not the result of contaminating starlight. This implies that all those blazars known to be located in low-redshift galaxies ($0521-365$, $0548-022$, $1101+384$, $1133+704$, $1514-241$, $1652+398$ and $2200+420$), must be studied with multi-aperture photometry, in order to separate out the galaxy component (c.f. Kikuchi & Mikami 1987). Other objects may also exhibit continuum properties which are affected by their relatively weaker underlying galaxies.

2.4 The Flux Density Data

The aim of the UKIRT observations was to obtain simultaneous multifrequency photopolarimetry of blazars. The primary requirement was to obtain high signal-to-noise measurements of flaring blazars, so as to constrain specific models of blazar behaviour. In this and the following section, the statistical properties of the flux and polarization data sets will be analysed separately.

2.4.1 SPECTRAL CURVATURE AND THE DISTRIBUTION OF SPECTRAL INDEX

The shape of the spectrum will be characterised by the use of the (local) spectral index;

$$\alpha(\nu) = -\frac{d\log S_\nu(\nu)}{d\log \nu}. \tag{2.2}$$

The motive for using this parameter is that the spectral flux distributions for blazars (and other AGN) are often characterised as power-law distributions, and hence have frequency-independent spectral indices (§1.1.5). The condition of a frequency-dependent spectral index is referred to as spectral curvature as this case results in curvature in the $\log S_\nu(\nu) - \log \nu$ plane.

In order to test for spectral curvature a power-law was fitted to all the UKIRT photometric data. All the Mark I Hatfield Polarimeter data consist of at least measurements at H, I and B. The Mark II data all has one infrared and at least four optical measurements[1]. Consequently all the data can be fitted by a power-law with at least one degree-of-freedom. These fits were achieved by minimising the χ^2 statistic, which was then used to test the goodness-of-fit. The goodness-of-fit is expressed as a level of significance. This is defined as the probability that a valid model of the data (the null hypothesis) has been rejected (e.g. Conover 1980). A low value of the significance level implies that this model can be confidently rejected. A note of caution must be sounded here. The use of the χ^2 distribution in testing this parameter is only valid if the errors concerned are distributed normally (e.g. Mathews & Walker 1970). Unfortunately, this is certainly *not* the case here. The errors on the photometry are not simply the random errors associated with photon counting, but include the (in some cases substantial) systematic uncertainties in the photometric calibration. It is most unlikely that these latter errors are distributed normally. The results presented in this and following sections are obtained by testing the data against a variety of null hypotheses (e.g. a power-law flux distribution). Where the data concerned include flux data the true level of the significance is likely to be different from that calculated in the case of normally distributed errors. In principle the true level could be either higher or lower than the calculated value. The conservative

[1]For some high airmass ($\sec z > 1.5$) observations, it was necessary to reject the U data because of differential refraction effects.

assumption (to avoid rejecting valid null hypotheses) is to assume that the true level of significance is higher than that calculated.

The fits to the 106 photometric data sets are shown in Table 2.7. These fits are separated into polarized and unpolarized samples. This is because it is only when polarizations in excess of the 3% limit are seen, that we can be sure that the observed flux contains a blazar contribution. The fits were all tested at the 5% significance level. If a power-law was rejected at this level, then the spectral flux distribution is characterised as having either a convex spectrum ($d\alpha/d\nu > 0$), a concave spectrum ($d\alpha/d\nu < 0$) or a 'complex' spectrum. The use of this level of significance is very lenient given the likely non-normal errors involved (it corresponds to a 1.96σ point of the normal distribution). Its use here is perhaps justified as the aim is to obtain some idea of the frequency of spectral curvature within the blazar population rather than to reject a power-law fit for any one individual object. The total numbers of the various types of fit given in Table 2.7 can nevertheless be misleading. For example, of the 11 concave spectra observed 6 were obtained for observations of $1641+399$ during 1986 August.

This brings up a number of points about the nature of the data which are studied in this and the following sections. The UKIRT data form an inhomogeneous sample of observations, which are subject to some known (but unquantifiable) selection effects. The strategy used to obtain these data was to observe as many blazars as possible. However, repeat observations were only made for those objects which showed 'interesting behaviour'. This interesting behaviour consists of variability, high polarizations, FDP or FDθ . Consequently there are in-built biasses in this sample of observations which will necessarily affect the conclusions drawn from these data if each observation of an object is treated as an independent data point. Even if the observing strategy had avoided these problems, it would still be questionable as to whether the individual observations were independent. This problem is related to the timescales associated with variations in the flux and polarization properties. It is known that in many

Table 2.7: Fits to the Spectral Flux Distributions

Name	Power-Law Spectra	Concave Spectra	Convex Spectra	Complex Spectra
Polarized Observations				
0048 − 097	7	2		
0106 + 013		1		
0109 + 224	6		3	
0118 − 272	3		2	1
0138 − 097	7		1	
0219 − 164	1			
0219 + 428	3		4	
0235 + 164			2	
0338 − 214			1	
1253 − 055	6			
1418 + 546		1	3	
1514 − 241			2	
1641 + 399		6		
1717 + 178	1		1	
1749 + 096	1	1	3	
1921 − 293			3	
2155 − 304	4		1	
2200 + 420			11	
2223 − 052	3			
2251 + 158	1			
2254 + 074	1		7	1
Totals	44	11	44	2
Unpolarized Observations				
0106 + 013	1			
0323 + 022			1	
0336 − 019			1	
1413 + 135	1			
1510 − 089	1			
1538 + 149	1			
1641 + 399		2		1
1717 + 178	1		1	
1921 − 293				1
2032 + 107			1	
2208 − 137		4		
2223 − 052	1			
2230 + 114	2			
2251 + 158			1	
Totals	8	6	5	2

cases these properties can be constant over periods of several nights, thus observations over one run would not be independent. To try avoid the effects of these biasses, the following results (and those in §2.5) will refer to the median and maximum values of the parameters for each object. Unfortunately, this loses some information. In these sections ν_f will refer to the effective frequency of the waveband f (see Table 2.1). These frequencies are all quoted in the observer's frame. The lack of complete redshift information for the blazar sample makes it impossible to transform these measurements to the emission frame.

Figure 2.5 shows the distribution of spectral indices at I. Both median and maximum values for each object are shown. The data used are the polarized observations as in Table 2.7. If the spectrum is fitted by a power-law at the 5% level, then the value of the frequency independent spectral index is used. Otherwise, a parabola in the $\log S_\nu(\nu) - \log \nu$ plane is fitted, and is used to derive the spectral index at I.

$$\log S_\nu(\nu) = \log S_{14} - a \log \nu_{14} + b(\log \nu_{14})^2 \tag{2.3}$$

There is no theoretical justification for choosing such a form, which is simply chosen as an empirical fit to the data. There is a problem with those observations which were made with the Mark I Hatfield polarimeter at H, I and B only. Such three-point data sets uniquely define the coefficients of a three-parameter fit such as the parabola given by equation 2.3. That is they are fitted with zero degrees-of-freedom. However the data are subject to observational error so that the fitted parabolae may be quite different from the true flux distribution. Higher degrees-of-freedom constrain the model to be more representative of the true flux distribution. Consequently, if a power-law fit to a three-point data set was rejected, then no information from this data set was included in Figure 2.5. Figure 2.6 shows the degree of spectral curvature for all the UKIRT data, again showing the median and maximum values for each object. The statistic used, $\Delta\alpha_{(B-H)}$, is the difference in the spectral indices at B and H;

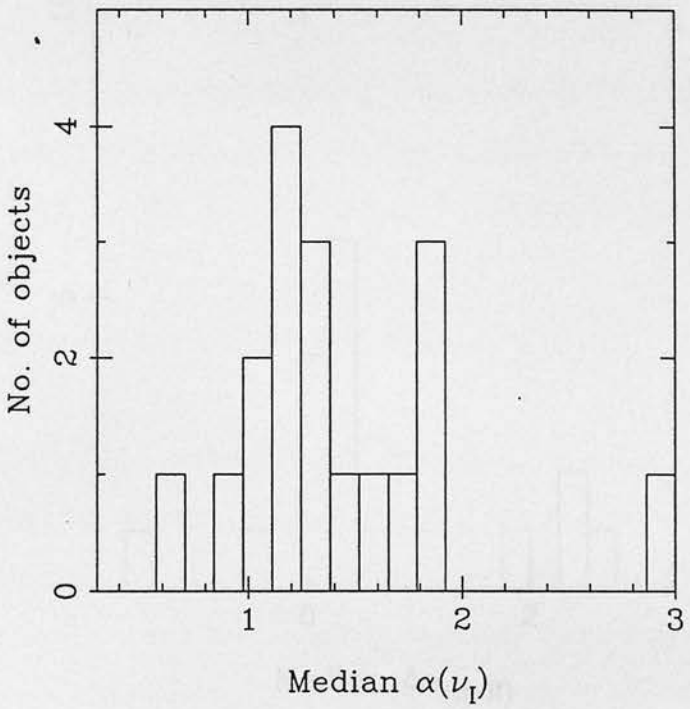

Figure 2.5: *(a)* This figure shows the median spectral index at I.

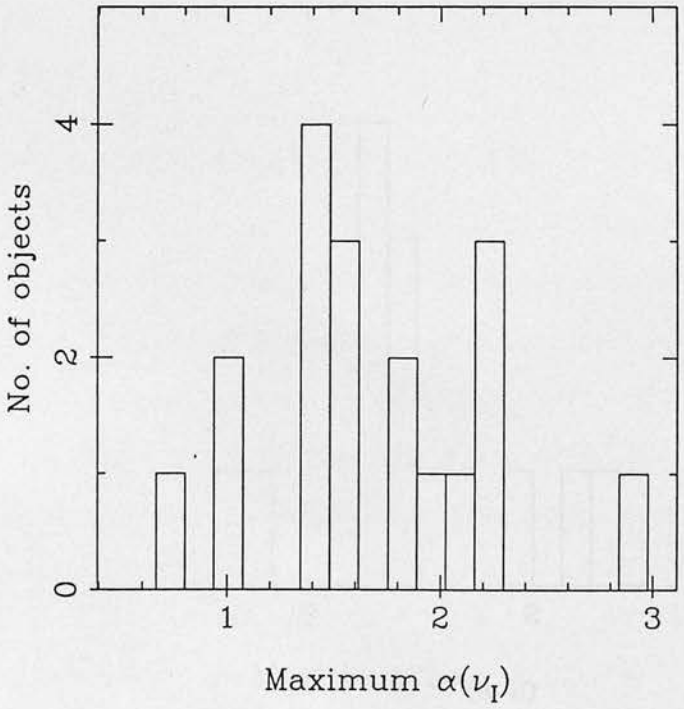

Figure 2.5: *(b)* This figure shows the maximum spectral index at I.

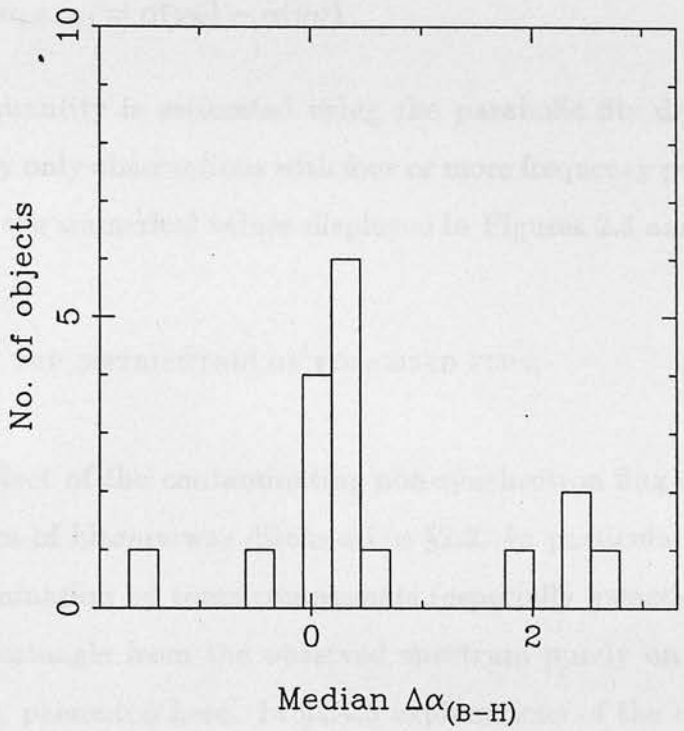

Figure 2.6: *(a)* This figure shows the distribution of the median value of $\Delta\alpha_{(B-H)}$.

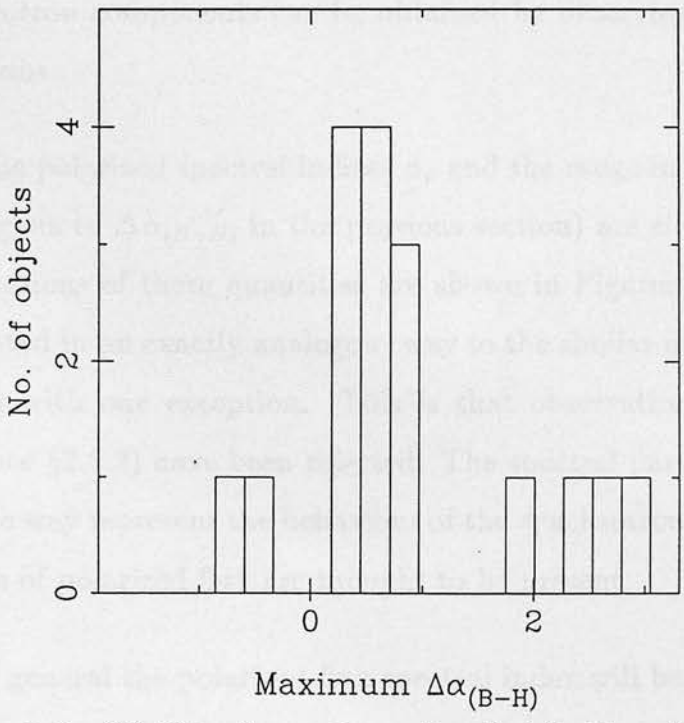

Figure 2.6: *(b)* This figure shows the distribution of the maximum value of $\Delta\alpha_{(B-H)}$.

$$\Delta\alpha_{(B-H)} = \alpha(\nu_B) - \alpha(\nu_H)\,. \tag{2.4}$$

This quantity is estimated using the parabolic fits described earlier. Consequently only observations with four or more frequency points are used. Table 2.8 shows the numerical values displayed in Figures 2.5 and 2.6.

2.4.2 THE DISTRIBUTION OF POLARIZED FLUX

The effect of the contaminating non-synchrotron flux on the observed characteristics of blazars was discussed in §2.3. In particular, it was mentioned that contamination by some components (especially galactic starlight) was difficult to disentangle from the observed spectrum purely on the basis of the observations presented here. In §2.4.3 explanations of the observed spectra will be discussed, this will tacitly assume that the observed spectra are all representative of the synchrotron component. A partial indication of whether the range of spectral indices given in the previous section is truly representative of the synchrotron components can be obtained by observing the polarized flux distributions.

The polarized spectral indices α_p and the range in this quantity $\Delta\alpha_{p,(B-H)}$ (analogous to $\Delta\alpha_{(B-H)}$ in the previous section) are shown in Table 2.9. The distributions of these quantities are shown in Figures 2.7 and 2.8. These are calculated in an exactly analogous way to the similar quantities of the previous section with one exception. This is that observations showing evidence for FDθ (see §2.5.2) have been rejected. The spectral parameters so derived must in some way represent the behaviour of the synchrotron component, as no other sources of polarized flux are thought to be present.

In general the polarized flux spectral index will be different from the total flux spectral index. Only in the special case of frequency independent polarization will the two parameters be equal. Björnsson & Blumenthal (1982) considered the polarization properties of an inhomogeneous source. They found

Table 2.8: Spectral Indices at I and Spectral Curvature Parameters

Object Name	$\alpha(\nu_I)$ Median	$\alpha(\nu_I)$ Maximum	No. of Obs.	$\Delta\alpha_{(B-H)}$ Median	$\Delta\alpha_{(B-H)}$ Maximum	No. of Obs.
$0048-097$	1.32	2.29	9	0.02	0.42	7
$0106+013$	1.36	1.36	1	−0.43	−0.43	1
$0109+224$	1.24	1.55	7	0.42	0.85	5
$0118-272$	1.18	1.98	5	0.00	0.62	4
$0138-097$	1.25	1.45	7	0.45	0.70	5
$0219-164$	1.00	1.00	1	0.35	0.35	1
$0219+428$	1.21	1.44	3	0.01	0.72	3
$0235+164$	1.84	2.23	2	2.44	2.49	2
$1253-055$	1.16	1.47	6	0.43	0.95	5
$1418+546$	1.59	1.59	1	0.58	0.58	1
$1514-241$	0.99	0.99	1	1.99	1.99	1
$1641+399$	1.87	2.07	6	−1.46	−0.62	6
$1717+178$	1.83	1.83	1			
$1749+096$	2.89	2.89	1	0.28	0.28	1
$2155-304$	0.62	0.71	2	0.02	0.42	2
$2200+420$	1.38	1.52	5	2.73	2.87	5
$2223-052$	1.71	1.78	3	0.28	0.50	3
$2254+074$	0.92	2.23	5	2.39	2.69	4

Table 2.9: The polarized flux spectral indices

Name	$\alpha_p(\nu_I)$		No. of	$\Delta\alpha_{p,(B-H)}$		No. of
	Median	Maximum	Obs.	Median	Maximum	Obs.
$0048-097$	1.16	0.18	9	1.28	1.68	7
$0106+013$	0.64	0.64	1	–2.67	–2.67	1
$0109+224$	1.40	1.59	5	–0.03	–0.03	4
$0118-272$	1.06	1.11	5	–0.39	1.08	4
$0138-097$	1.17	2.08	7	0.33	0.76	5
$0219-164$	1.07	1.07	1	0.04	0.04	1
$0219+428$	1.19	1.38	5	0.35	0.36	3
$0235+164$	2.32	3.41	2	1.60	2.50	2
$0338-214$	2.03	2.03	1			
$1253-055$	1.03	1.78	2	1.11	1.11	1
$1418+546$	1.61	1.61	1			
$1514-241$	1.79	1.79	1	1.33	1.33	1
$1641+399$	1.76	2.29	7	0.06	0.46	6
$1717+178$	1.62	1.62	1			
$1727+502$	3.45	3.45	1			1
$1749+096$	1.77	2.33	4	1.86	1.86	1
$1921-293$	2.57	2.77	3			
$2200+420$	2.66	2.66	1			
$2223-052$	1.66	1.43	3	1.96	2.00	3
$2254+074$	1.68	1.96	6	0.59	0.93	3

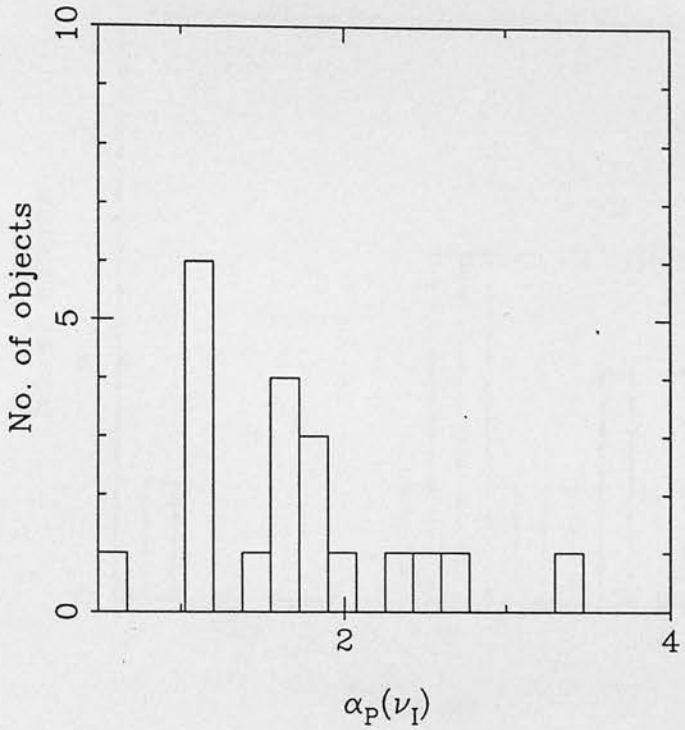

Figure 2.7: *(a)* The distribution of the median value of α_p.

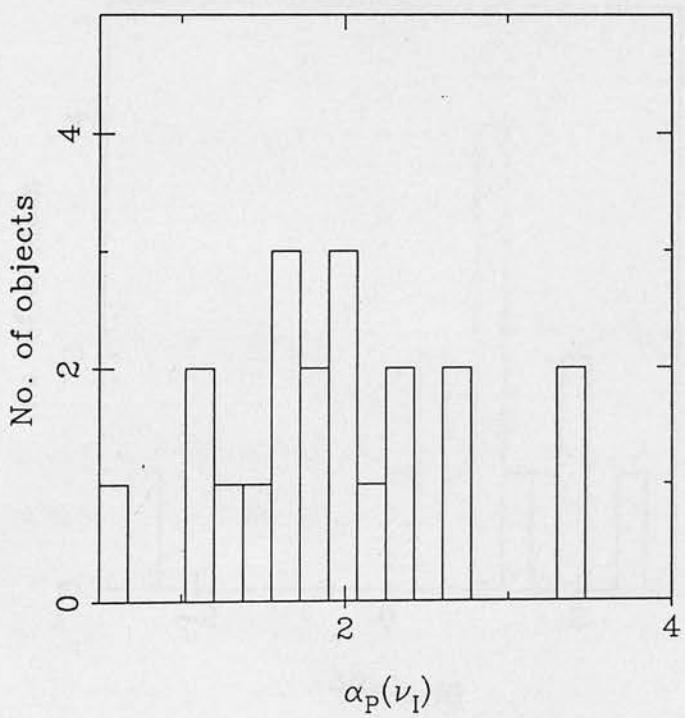

Figure 2.7: *(b)* The distribution of the maximum value of α_p.

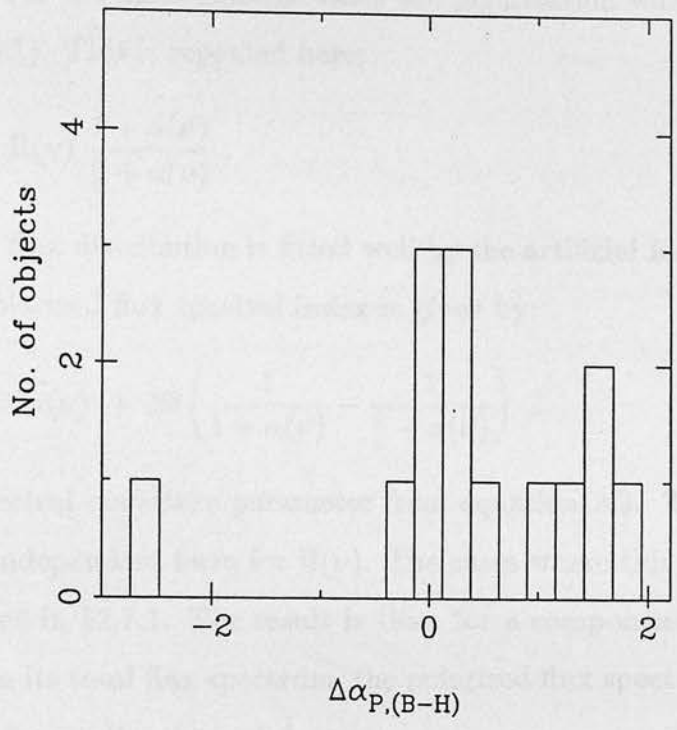

Figure 2.8: *(a)* The distribution of the median value of $\Delta\alpha_{p,(B-H)}$.

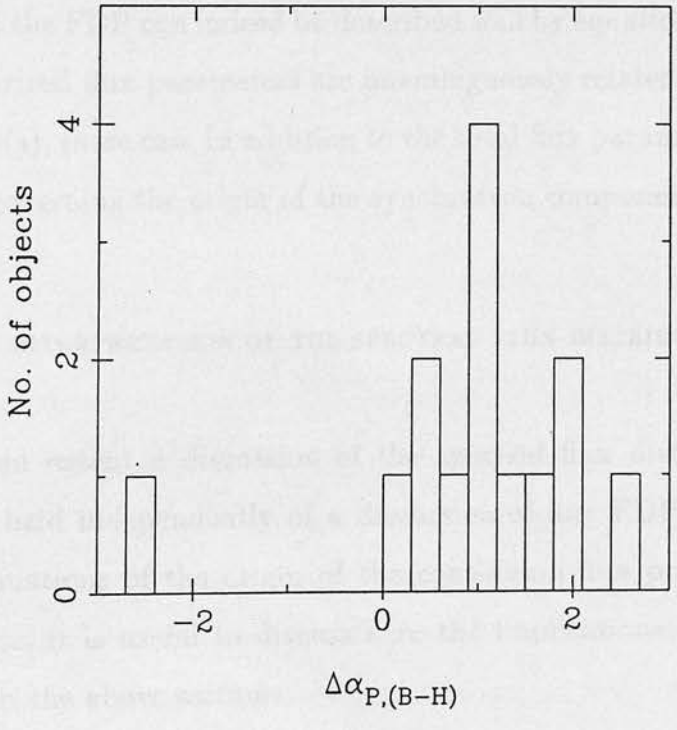

Figure 2.8: *(b)* The distribution of the maximum value of $\Delta\alpha_{p,(B-H)}$.

that in all but the most extreme cases the polarization was given by equation 1.8 (in §1:3.1). This is repeated here;

$$p(\nu) = \Pi(\nu) \, \frac{1 + \alpha(\nu)}{\frac{5}{3} + \alpha(\nu)} \, . \tag{2.5}$$

If the total flux distribution is fitted well by the artificial form of equation 2.3, then the polarized flux spectral index is given by;

$$\alpha_p(\nu) = \alpha(\nu) \; + \; 2b \left(\frac{1}{1 + \alpha(\nu)} - \frac{1}{\frac{5}{3} + \alpha(\nu)} \right) \, . \tag{2.6}$$

b is the spectral curvature parameter from equation 2.3. This has assumed a frequency-independent form for $\Pi(\nu)$. The cases where this assumption is true are discussed in §2.7.1. The result is that, for a component displaying convex curvature in its total flux spectrum, the polarized flux spectral index $\alpha_p(\nu)$ will be marginally smaller than $\alpha(\nu)$.

The above result only applies if the Björnsson & Blumenthal (1982) formalism is correct. This will be the subject of a later section (§2.7), where it will be shown that the FDP can indeed be described well by equation 2.5. Nevertheless, as the polarized flux parameters are unambiguously related to the synchrotron component(s), these can, in addition to the total flux parameters, constrain the processes governing the origin of the synchrotron component.

2.4.3 THE INTERPRETATION OF THE SPECTRAL FLUX DISTRIBUTION

To a certain extent a discussion of the spectral flux distribution of blazars cannot be held independently of a discussion of any FDP, as this constrains most explanations of the origin of the continuum flux properties of blazars. Nevertheless, it is useful to discuss here the implications of the observations described in the above sections.

The main candidate for the process whereby the electrons (or positrons) are accelerated to produce the observed synchrotron emission is first-order particle

acceleration at shock fronts (see §1.3.4). This process makes specific predictions about the range of the observed spectral index. These are reviewed by Heavens (1988). In summary, strong non-relativistic shocks produce observed spectra of 0.5, fast to relativistic strong shocks produce spectra between 0.4 and 0.65, while weak shocks can produce any spectral index greater than 0.5. These spectral indices should be constant over many decades of frequency. In the high frequency domain, synchrotron energy losses may become important (compared to other mechanisms such as free-free emission). This causes the injected electron energy spectrum to steepen by 1.0 and hence the observed synchrotron spectral index to increase by 0.5 (Kardashev 1962). Another feature of these theories is a high energy cut-off beyond which the Fermi process cannot accelerate electrons (see §1.3.4). Figure 2.9 shows the curvature in the observed synchrotron spectrum caused by such a sharp cut-off in a power-law electron distribution. Such a sharp cut-off is unlikely to be realistic, but it does indicate the gross features of the observed emission.

The weak shocks would appear to be able to explain any observed spectral index seen in a blazar. There are two reasons why such shocks are generally rejected. First, the observed spectral index is a strong function of shock speed. This would imply that even the range of spectral indices shown in Figure 2.5 (and Figure 2.7) would correspond to a narrow range of shock speeds. There is no known reason why this would occur. Second, strong shocks are expected to be a common feature of the hydrodynamic flows which are thought to be the origin of the blazar emission. As these should amplify the emissivity of the fluid, by accelerating particles and compressing the magnetic field, it may be reasonable to expect such shocks to play an important part in the origin of the observed emission. It should be noted that the first objection can be overcome if selection effects are important in determining the observed IR/optical spectral indices in blazars. There is an obvious bias against very steep optical spectra, as most blazar identifications are made on the basis of their optical emission. To resolve this a complete survey of the spectral behaviour of a sample of compact

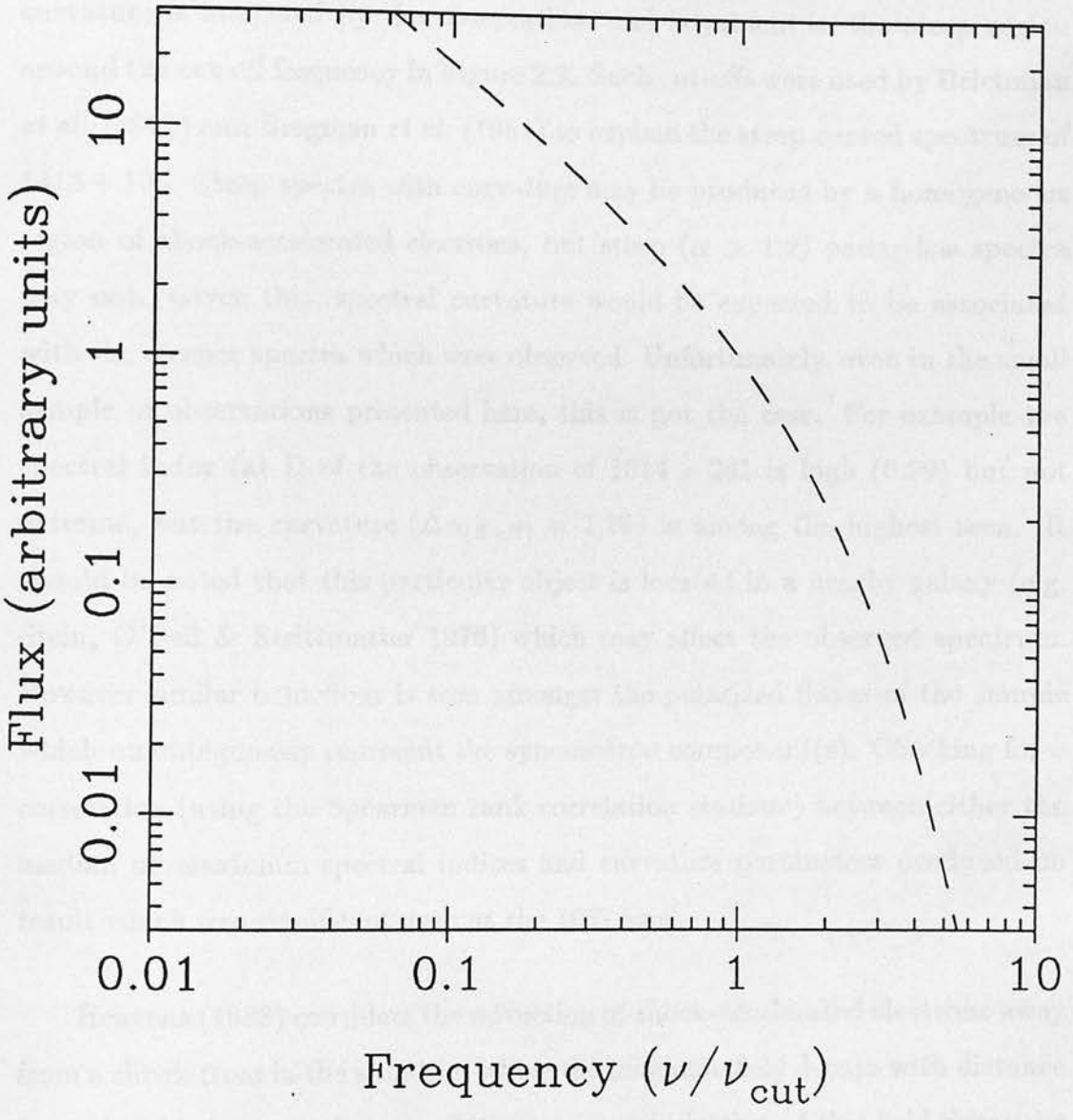

Figure 2.9: The observed synchrotron emission from an electron energy distribution of index 3, resulting in an observed spectral index of 1.0 below the cut-off. The energy spectrum is cut off at an upper energy corresponding to the critical frequency ν_{cut} (via eqn. 1.5c).

radio sources is needed.

If weak shocks are rejected, then the range of spectral indices observed cannot be consistent with the power-law spectra predicted by Fermi acceleration at strong shocks. Spectral indices of order 3 are too large. However, spectral curvature is indicated by the observations and is present in the steep region around the cut-off frequency in Figure 2.9. Such cut-offs were used by Beichman *et al.* (1981) and Bregman *et al.* (1981) to explain the steep curved spectrum of $1413+135$. Steep spectra with curvature may be produced by a homogeneous region of shock-accelerated electrons, but steep ($\alpha > 1.2$) *power-law* spectra may not. Given this, spectral curvature would be expected to be associated with the steeper spectra which were observed. Unfortunately, even in the small sample of observations presented here, this is not the case. For example the spectral index (at I) of the observation of $1514-241$ is high (0.99) but not extreme, but the curvature ($\Delta\alpha_{(B-H)} = 1.99$) is among the highest seen. It should be noted that this particular object is located in a nearby galaxy (e.g. Stein, O'Dell & Strittmatter 1976) which may affect the observed spectrum. However similar behaviour is seen amongst the polarized fluxes of the sample which unambiguously represent the synchrotron component(s). Checking for a correlation (using the Spearman rank correlation statistic) between either the median or maximum spectral indices and curvature parameters produced no result which was significant even at the 10% level.

Heavens (1988) considers the advection of shock-accelerated electrons away from a shock-front in the situation where the magnetic field decays with distance from the shock. Assuming an arbitrary parameterisation of this field decay, he shows that the resulting spectrum may have spectral indices which are steeper than those predicted by the simple shock theory. In fact, the observed spectrum is gradually curved but it can be approximately described by a power-law for observations spanning single decades of frequency if these are well below the cut-off. This is not the only inhomogeneous source model which produces power-law spectral flux distributions with spectral indices which are much steeper than

that derived from the electron spectral index. For example, the synchrotron self-Compton (SSC) model of Ghisellini, Maraschi & Treves (1985) gives rise to steep optical-IR continua as a result of the integration of the luminosity of an inhomogeneous jet. Their formula for this spectral index is;

$$\alpha = \alpha_0 + \frac{1 + 2\varepsilon - \varepsilon(n + m(1 + \alpha_0))}{\varepsilon(2e + m)}. \tag{2.7}$$

Here, α_0 is the spectral index calculated from the electron energy index in the usual manner. The jet perpendicular dimension (r) is related to the distance from the core (R) by $r \propto R^{\varepsilon}$. The magnetic field is assumed to decay as $B \propto r^{-m}$ and the electron energy density (normalisation factor) as $N \propto r^{-n}$. Finally the maximum electron energy is assumed to be radially dependent as $\gamma_{max} \propto r^{-e}$. This equation is only valid for a jet viewed at an angle to the line of sight which is greater than its opening angle. Nevertheless, it serves to show that there is a class of inhomogeneous source models, including also those of Marscher (1980) and Königl (1981), which can produce power-law flux distributions which have steeper spectral indices than those calculated from the electron energy spectral index. However, there are a large number of free parameters which go into determining this spectral index. Ghisellini, Maraschi & Treves (1985) attempt fits to the IR/optical continua of two blazars (2155 − 304 and 0537 − 441) using this model by varying some of these parameters. Fitting such models to the UKIRT data is not possible, given the limited number of frequency points. Marscher (1980) in his version of the SSC-model makes specific assumptions about some of these parameters, based on (necessarily naïve) physical reasoning about the behaviour of magnetic fields in such a jet. Nevertheless, other parameters are unknown, particularly ε which characterises whether the jet is freely expanding, 'parabolic' or has some other form.

The shape of the IR/optical spectrum has received much attention in the past. However, all the data discussed in this section were obtained with simultaneous polarimetry. This polarimetry can constrain the models of the origin of the spectral behaviour of the blazar emission region. Consequently, this

discussion will now be postponed until after the frequency dependence of the polarization properties has been considered.

2.5 Analysis of the Polarization Properties

2.5.1 FREQUENCY DEPENDENCE OF THE DEGREE OF POLARIZATION

In §1.1.3.2 the frequency-dependent properties of the IR/optical blazar emission were reviewed. This section will describe the characteristics of the frequency dependence of the UKIRT data in this context. The canonical synchrotron emitter described in §1.3.1, will exhibit a constant degree of polarization, whose value is dependent on the the spectral index of the power-law slope (eqn. 1.12). Both the range of polarizations and the occurrence of frequency dependence of the degree of polarization (FDP) indicate that this simple model is false. These data must contain information about the complex nature of the blazar emission region.

All the data which had two or more polarization measurements were tested for FDP. The weighted mean of the measured polarizations was calculated and this was then tested against all the measured polarizations by use of the χ^2 statistic with the loss of one degree-of-freedom. In §2.4 it was argued that the use of this test statistic was not strictly correct as the true distribution of the photometric errors was unknown. In the case of polarimetric errors, it is known that these should follow the Rice distribution and should have an approximately normal error distribution in the case of high signal-to-noise (Vinokur 1965; Wardle & Kronberg 1974). Consequently, the levels of significance quoted in these fits to the polarization data can be taken at face value. These authors also show that the position angle error distribution is similarly approximately normal for high signal-to-noise observations.

Table 2.10 lists all the polarimetric observations of blazars and whether

Table 2.10: A summary of the polarization observations

Object Name	$p(\nu) = p_0$	FDP $dp/d\nu > 0$	FDP $dp/d\nu < 0$	FDP Complex
$0048-097$	6	5		
$0106+013$	1			
$0109+224$	6	3	1	
$0118-272$	3	3		1
$0138-097$	5	2	1	
$0219-164$	1			
$0219+428$	8	1		1
$0235+164$	1			
$0300+470$	1			
$0323+022$	1			
$0338-214$	2			
$0735+178$	1			
$1253-055$	1	5		
$1418+546$		5		1
$1514-241$	1			1
$1641+399$	1		1	5
$1652+398$				1
$1717+178$	1		1	
$1727+502$	1	2		
$1749+096$	3	2		
$1921-293$	3		1	
$2155-304$	3	2		1
$2200+420$	1	1	2	9
$2223-052$	4	1		
$2251+158$			1	
$2254+074$	2	5		4
Totals	57	37	8	24

they were fitted (at the 5% level of significance) by a constant polarization or FDP (either with $dp/d\nu > 0$, $dp/d\nu < 0$ or with more complex behaviour). In order to assign the FDP categories, a power-law polarization behaviour was fitted to these data ($p(\nu) \propto \nu^{\beta}$). This was entirely an empirical fit whose form was chosen for two reasons. First, it allowed the same code as used to fit the flux data to be used. Second, the polarization was constrained to be positive definite and this form allowed for an unconstrained minimisation to be performed with respect to $\log p_{14}$ and β. The two FDP categories ($dp/d\nu > 0$ and $dp/d\nu < 0$) were assigned on the basis of the sign of the fitted value of β. Those objects not fitted (at the 5% level) by this functional form, are described as having 'complex' polarization behaviour. In principle it is possible that this procedure would classify as complex some behaviour which was monotonic with frequency. In practice, this does not appear to be the case. However, this procedure does flag behaviour, such as that seen in $1641+399$ and $2200+420$, where the FDP is only significant over a narrow range of the observed frequencies.

Figure 2.10 shows the distribution of the median and maximum degrees of polarization at I. Figure 2.11 shows the median and maximum changes in polarization over the observed frequency range. This is expressed in terms of the ratio of the B polarization to the H polarization ($p(\nu_B)/p(\nu_H)$). The data displayed in these figures is listed in Table 2.11. Figure 2.10 shows a wide range of both median and maximum polarizations. The largest polarization is that seen in the 'record-breaking' series of observations of $1253-055$ (3C 279) (see §2.2.17 and §2.7.2). As one would expect from the fits described in Table 2.10, Figure 2.11 shows a common tendency for the B polarization to be higher than that at H. Only three objects show the median value of ($p(\nu_B)/p(\nu_H)$) as being significantly less than one. These are the HPQ's $1641+399$ (3C 345), $1921-293$ and $2251+158$. The probable reason for this behaviour is contamination of the blazar flux by unpolarized optical components, which was discussed at length in §2.3.

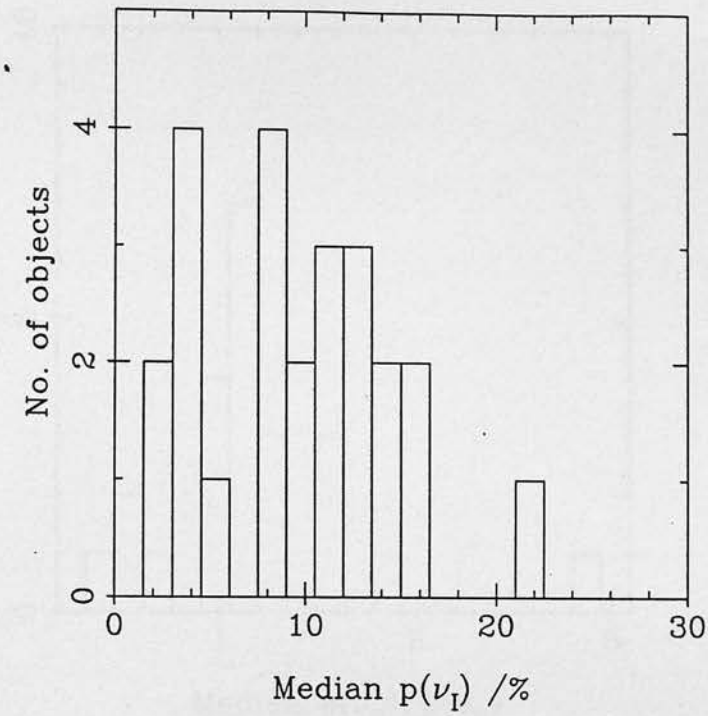

Figure 2.10: *(a)* The distribution of the median polarization at I.

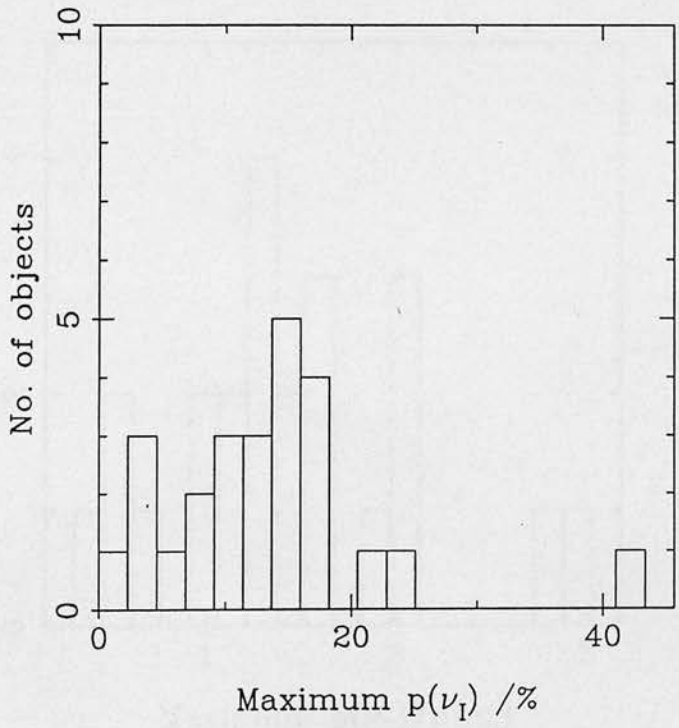

Figure 2.10: *(b)* The distribution of the maximum polarization at I.

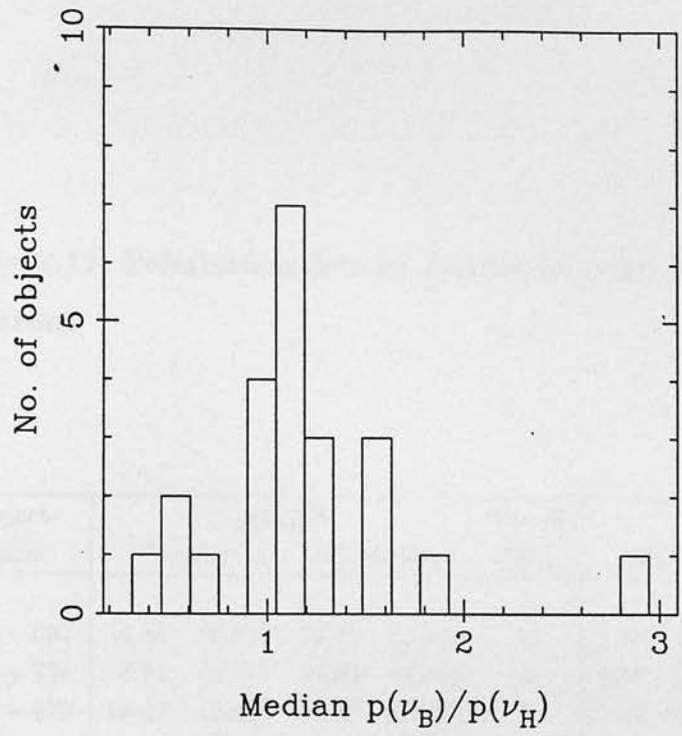

Figure 2.11: *(a)* The distribution of the median value of $(p(\nu_B)/p(\nu_H))$.

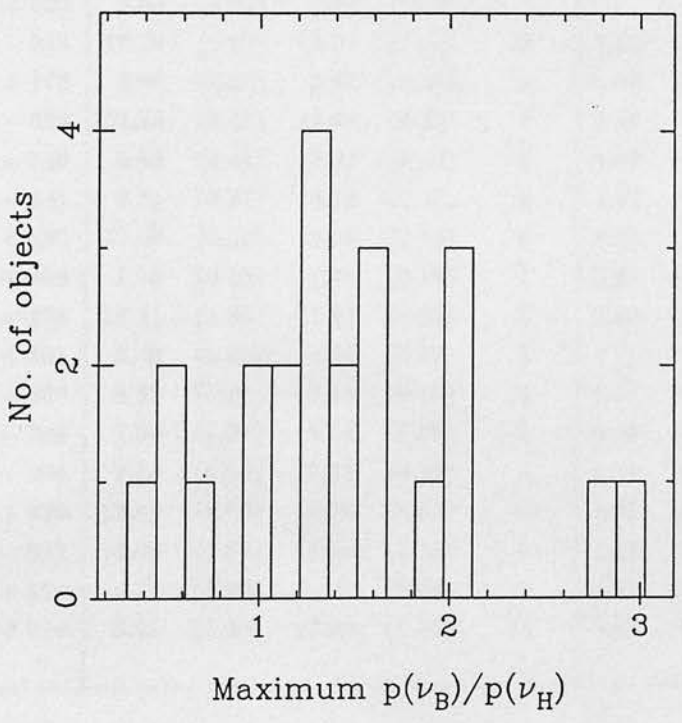

Figure 2.11: *(b)* The distribution of the maximum value of $(p(\nu_B)/p(\nu_H))$.

Table 2.11: Polarization data for Figures 2.10 and 2.11. Numbers in brackets are errors.

Object Name	$p(\nu_I)/\%$ Median		Maximum		No. of Obs.	$p(\nu_B)/p(\nu_H)$ Median		Maximum		No. of Obs.
0048 − 097	14.55	(0.61)	21.17	(1.02)	11	1.24	(0.13)	1.64	(0.17)	10
0109 + 224	8.91	(0.85)	14.04	(0.90)	9	1.09	(0.10)	1.20	(0.05)	7
0118 − 272	16.49	(0.68)	17.82	(0.58)	7	1.17	(0.04)	1.29	(0.08)	7
0138 − 097	22.16	(1.13)	24.80	(1.08)	6	1.09	(0.15)	1.42	(0.05)	8
0219 − 164	12.45	(0.42)	12.45	(0.42)	1	0.93	(0.04)	0.93	(0.04)	1
0219 + 428	11.46	(0.84)	15.46	(0.55)	10	1.08	(0.13)	1.29	(0.06)	10
0235 + 164	13.28	(0.90)	15.52	(1.59)	2	1.52	(0.38)	2.02	(0.24)	2
0300 + 470	9.44	(1.52)	9.44	(1.52)	1	0.69	(0.52)	0.69	(0.52)	1
0323 + 022	3.84	(1.02)	3.84	(1.02)	1					
0338 − 214	10.76	(1.05)	11.07	(1.56)	2	1.00	(0.25)	1.08	(0.13)	2
0735 + 178	8.08	(0.88)	8.08	(0.88)	1	0.99	(0.20)	0.99	(0.20)	1
1253 − 055	34.50	(0.41)	41.58	(0.55)	6	1.16	(0.04)	1.29	(0.06)	6
1418 + 546	4.89	(0.41)	15.37	(2.82)	6	1.52	(0.14)	2.92	(0.17)	4
1514 − 241	3.31	(0.21)	4.76	(0.30)	2	1.53	(0.14)	1.66	(0.07)	2
1641 + 399	15.00	(0.50)	16.09	(1.14)	6	0.48	(0.16)	0.52	(0.15)	6
1652 + 398	1.56	(0.16)	1.56	(0.16)	1	2.85	(0.11)	2.85	0.11	1
1717 + 178	16.11	(1.85)	17.82	(3.62)	2	0.93	(0.50)	1.35	(0.27)	2
1727 + 502	2.48	(0.49)	2.51	(0.82)	2					
1749 + 096	8.89	(0.58)	16.53	(0.95)	4	1.21	(0.21)	1.39	(0.13)	4
1921 − 293	7.56	(1.23)	8.13	(1.65)	2	0.41	(0.79)	0.41	(0.79)	1
2155 − 304	3.10	(0.12)	10.29	(0.23)	5	1.14	(0.06)	1.99	(0.04)	6
2200 + 420	12.02	(0.50)	14.15	(0.37)	13	1.21	(0.06)	1.88	(0.13)	13
2223 − 052	11.64	(1.87)	11.90	(1.21)	3	1.12	(0.23)	1.57	(0.14)	4
2251 + 158	4.18	(0.96)	4.18	(0.96)	1	0.47	(0.29)	0.47	(0.29)	1
2254 + 074	9.65	(1.45)	12.06	(1.26)	11	1.82	(0.16)	2.09	(0.19)	6

2.5.2 FREQUENCY DEPENDENCE OF THE POSITION ANGLE OF POLARIZATION

Analogous to Table 2.10, Table 2.12 presents the results of testing for frequency dependence of the position angle of polarization (FDθ). Again the χ^2 statistic has been used to test the goodness-of-fit at the 5% significance level. FDθ is seen to be much rarer than FDP. There is no evidence suggesting any preference for clockwise over counter-clockwise variations with frequency. There is a possible systematic origin for the cases where no preferred trend of position angle with frequency is fitted. This occurs as a result of the way multifrequency data was compiled using the Mark I Hatfield polarimeter data. If more than three frequency points were measured, then not all the data points would be strictly simultaneous. For example an integration using H, I and B filters lasting tens of minutes might be followed by one using J, V and U filters, which have been combined as if they were simultaneous in the data presented here. The evidence for such rapid rotations in position angle will be discussed in §2.6.3 with reference to the observations of $1253-055$ (3C 279) where this procedure has given rise to a spurious frequency dependence.

2.5.3 CORRELATION OF FREQUENCY DEPENDENCE WITH OTHER PROPERTIES

It has been suggested (Bailey, Hough & Axon 1983, Holmes *et al.* 1984a, Holmes 1985, Brindle *et al.* 1986), that there is a tendency for frequency dependence to be associated with high polarization (the so called '$p(\lambda) - p$' effect). The evidence for this effect in our data has been approached in two ways. Figure 2.12 shows histograms of the I polarizations where the objects which show evidence either for FDP (Figure 2.12a) or for FDθ (Figure 2.12b) have been flagged. This leaves two samples of objects (one showing frequency dependence and the other not). The distributions were then tested under the null hypothesis that the frequency-independent data had the same polarization distribution as the frequency-dependent data. The test used was the two-sample Kolmogorov-Smirnov test (e.g. Conover 1980). When considering FDP, the

Table 2.12: A summary of the position angle observations

Object Name	$\theta(\nu) = \theta_0$	FDθ		
		$d\theta/d\nu > 0$	$d\theta/d\nu < 0$	Complex
$0048-097$	11			
$0106+013$	1			
$0109+224$	7		2	1
$0118-272$	6			1
$0138-097$	7	1		
$0219-164$	1			
$0219+428$	9	1		
$0235+164$	2			
$0300+470$	1			
$0323+022$	1			
$0338-214$	2			
$0735+178$			1	
$1253-055$	2		3	1
$1418+546$	4			2
$1514-241$	2			
$1641+399$	6	1		
$1652+398$			1	
$1717+178$	2			
$1727+502$	2		1	
$1749+096$	4	1		
$1921-293$	3	1		
$2155-304$	3		2	1
$2200+420$	1	7	2	3
$2223-052$	5			
$2251+158$	1			
$2254+074$	7	1		3
Totals	89	13	12	12

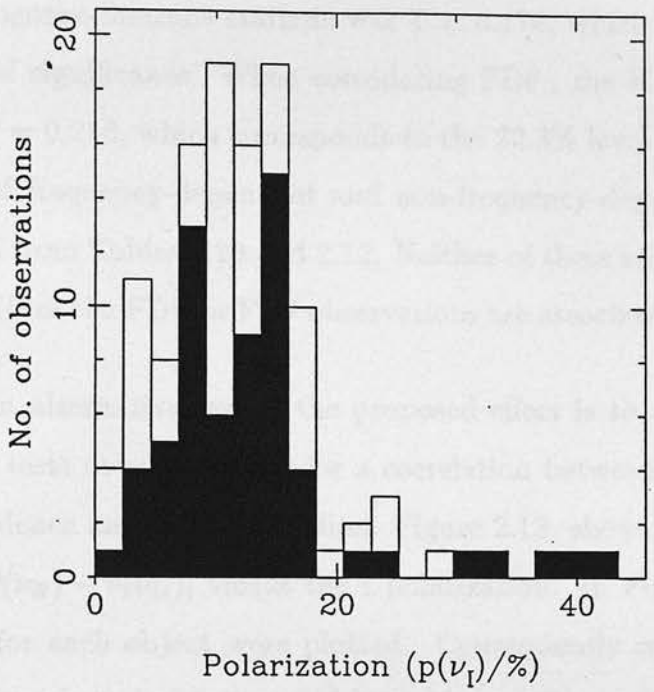

Figure 2.12: *(a)* The distribution of the I polarizations with each observation treated as being independent. The shaded areas represent those objects exhibiting FDP at the 5% level of significance. Of the 115 observations shown 64 show evidence of FDP.

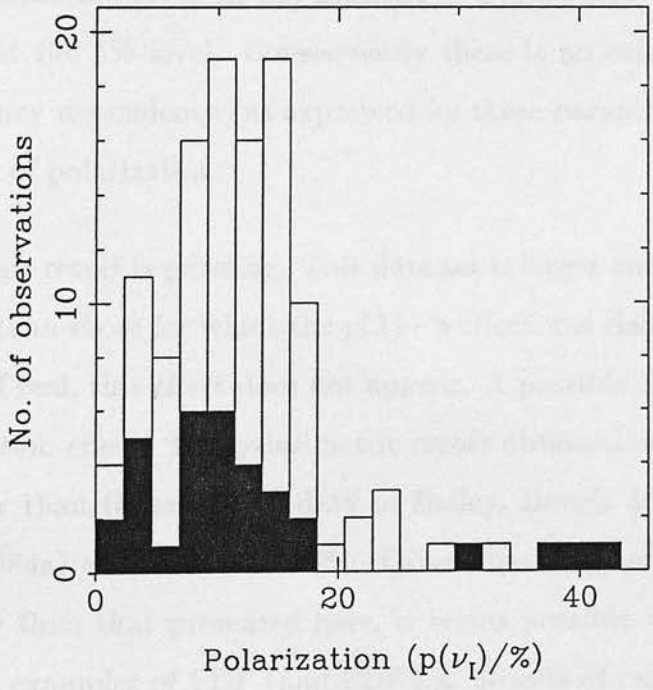

Figure 2.12: *(b)* The distribution of the I polarizations with each observation treated as being independent. The shaded areas represent those objects exhibiting FDθ at the 5% level of significance. Of the 115 observations shown 33 show evidence of FDθ .

Kolmogorov-Smirnov statistic was $T = 0.178$, which corresponds to the 32.8% level of significance. When considering FDθ , the Kolmogorov-Smirnov result was $T = 0.216$, which corresponds to the 22.3% level of significance. The numbers of frequency-dependent and non-frequency-dependent results can be obtained from Tables 2.10 and 2.12. Neither of these results provide any evidence that either the FDP or FDθ observations are associated with high polarizations.

An alternative test of the proposed effect is to use non-parametric correlation tests to test directly for a correlation between the amount of frequency dependence and the polarization. Figure 2.13 shows plots of $\log(p(\nu_B)/p(\nu_H))$ and $|\theta(\nu_B) - \theta(\nu_H)|$ versus the I polarization. In Figure 2.12 all the observations for each object were plotted. Consequently repeated observations of a small number of objects could have biassed the result. This problem was discussed in §2.4 with reference to the flux density data. In the correlation analysis all the observations for each object have been combined into a single value (either the median or maximum). The values of the Spearman rank correlation coefficients are given in the captions to Figure 2.13. None of these are significant at the 5% level. Consequently there is no evidence that the amount of frequency dependence (as expressed by these parameters) is dependent on the degree of polarization.

This result is puzzling. This data set is larger and covers a wider frequency range than those for which the $p(\lambda) - p$ effect was claimed. Thus it is surprising that, if real, this effect does not appear. A possible explanation is provided by a selection effect. The polarimetric errors obtained on these data are certainly smaller than those on the data of Bailey, Hough & Axon (1983), Holmes *et al.* (1984a) and Holmes (1985). Given that most of these data are of poorer quality than that presented here, it seems possible that these authors simply missed examples of FDP (and FDθ) in objects of moderately low polarization that would have been detected in this work. However, this would not explain the significant correlation found between $p(\nu_H)/p(\nu_K)$ and $p(\nu_J)$ by Holmes (1985). However, he does note that, in some of his samples, this correlation

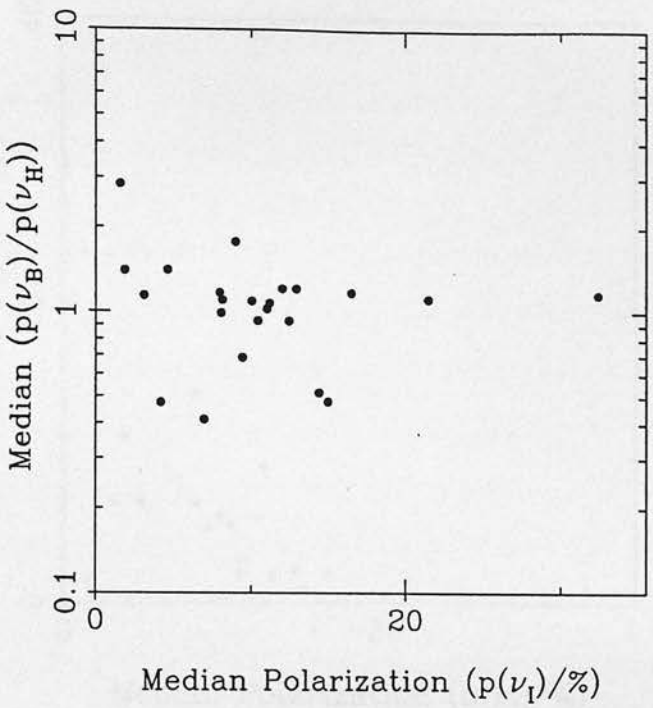

Figure 2.13: *(a)* A plot of $\log(p(\nu_B)/p(\nu_H))$ versus $p(\nu_I)$ is shown. The values shown are the median values for each object. The Spearman rank correlation coefficient is -0.174 for 23 objects.

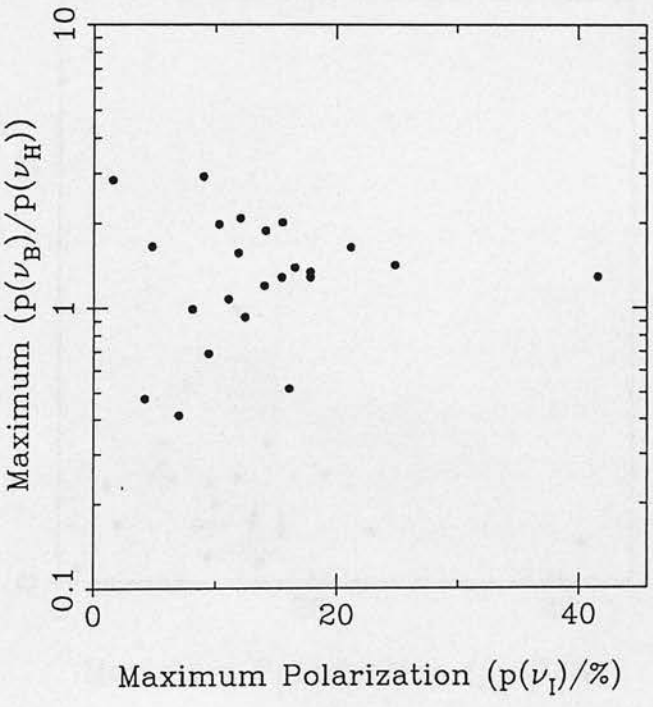

Figure 2.13: *(b)* A plot of $\log(p(\nu_B)/p(\nu_H))$ versus $p(\nu_I)$ is shown. The values shown are the maximum values for each object. The Spearman rank correlation coefficient is -0.030 for 23 objects.

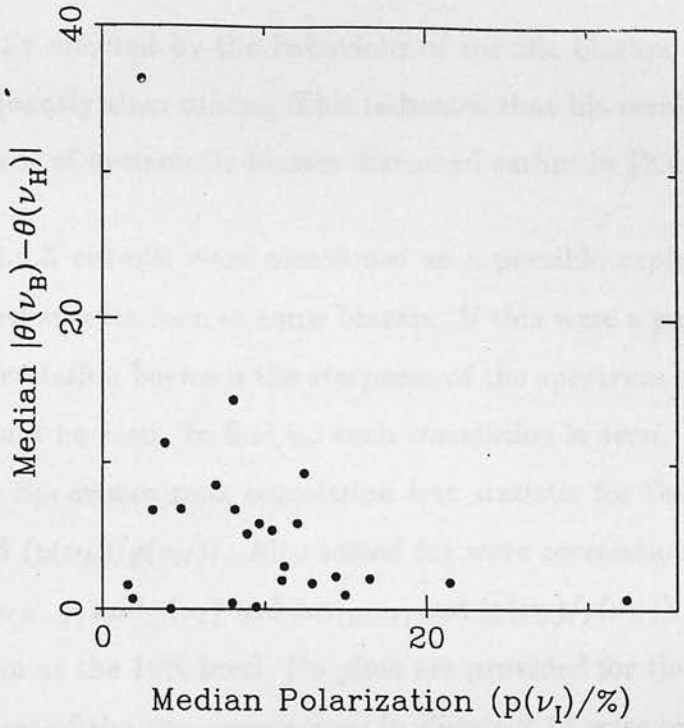

Figure 2.13: *(c)* A plot of $|\theta(\nu_B) - \theta(\nu_H)|$ versus $p(\nu_I)$ is shown. The values shown are the median values for each object. The Spearman rank correlation coefficient is -0.209 for 25 objects.

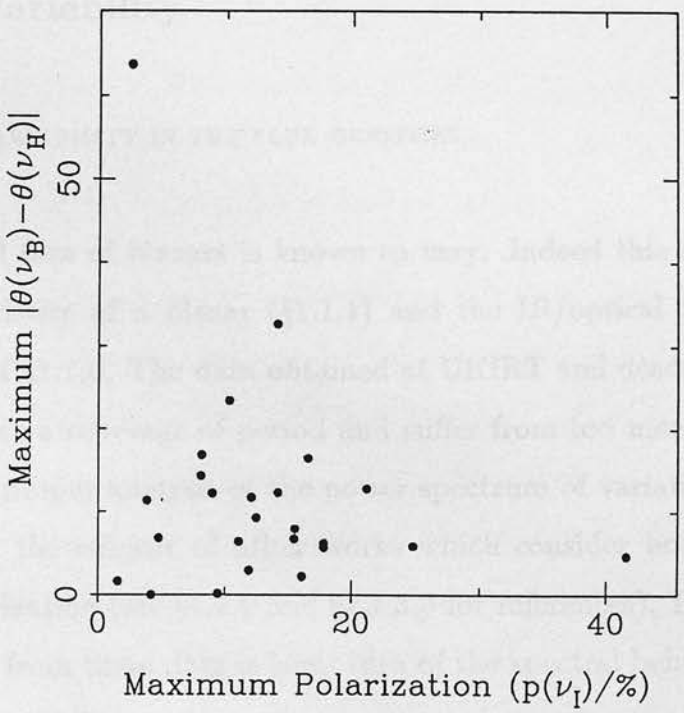

Figure 2.13: *(d)* A plot of $|\theta(\nu_B) - \theta(\nu_H)|$ versus $p(\nu_I)$ is shown. The values shown are the maximum values for each object. The Spearman rank correlation coefficient is -0.124 for 25 objects.

is markedly affected by the behaviour of specific blazars which were observed more frequently than others. This indicates that his result may be susceptible to the kinds of systematic biasses discussed earlier in §2.4.1.

In §2.4.3 cut-offs were mentioned as a possible explanation for the steep and curved spectra seen in some blazars. If this were a general case in blazars, then a correlation between the steepness of the spectrum and the occurrence of FDP should be seen. In fact no such correlation is seen. This has been tested using the Spearman rank correlation test statistic for the correlation between $\alpha(\nu_I)$ and $(p(\nu_B)/p(\nu_H))$. Also tested for were correlations between $\alpha(\nu_I)$ and $p(\nu_I)$, $\Delta\alpha_{(B-H)}$ and $p(\nu_I)$ and $\Delta\alpha_{(B-H)}$ and $(p(\nu_B)/p(\nu_H))$. No correlations were found even at the 10% level. No plots are provided for these comparisons. The illustrations of the non-correlations in Figure 2.13 were only displayed because such correlations had been claimed in the literature.

2.6 Variability

2.6.1 VARIABILITY IN THE FLUX DENSITIES

The total flux of blazars is known to vary. Indeed this is one of the defining characteristics of a blazar (§1.1.1) and the IR/optical fluctuations were the subject of §1.1.6. The data obtained at UKIRT and described in §2.2 have too incomplete a coverage of period and suffer from too many selection biasses to enable a proper analysis of the power spectrum of variations. In any case this has been the subject of other works which consider both the total flux and the polarization (see §1.1.6 and §1.1.3.3 for references). However, what can be obtained from these data is some idea of the spectral behaviour and amplitude of such variability.

Some spectacular short-period variations have been claimed to be seen in the IR/optical behaviour of blazars (e.g. 1 mag on 30s timescales for 0851+202;

Wolstencroft, Gilmore & Williams 1982). The total integration times for the data under discussion here are much longer than 30s. Typical integration times were of the order of 10 minutes. Nevertheless, the UKIRT data does contain some information about such variations. The rotation period of the waveplate was small (3.2s for the Mark II instrument), and sudden changes in flux as found by Wolstencroft, Gilmore & Williams (1982) would have an instantly appreciable effect on both the flux and polarization errors. In fact if such variations were frequent measurement of polarization with this device would be impossible. That the errors on the polarimetry did not indicate that such rapid changes in flux occurred. This indicates that such variations, if real, are extremely rare events.

Variability in the absolute level of total flux is well known in blazars and has been studied elsewhere (examples of such work are referenced in §1.1.6). Another interesting phenomenon is the behaviour of the spectral shape as the flux varies. Gear, Robson & Brown (1986) give an example of blazar variability where the spectral index variations were such that the spectrum flattened as the flux increased. This could potentially be an important diagnostic of any model of the emission region. However these observations (of 0851 + 202) do not characterise all examples of flare evolution.

Before discussing the variability in detail it is necessary to differentiate between the two sets of timescales being tested by these data. Data were taken at three different 'epochs' (1986 July/August, 1987 July and 1987 September). Within these epochs data were taken over several nights. Consequently there are different sorts of timescales to be considered. These are the two inter-epoch timescales of a year and three months and the inter-night timescale. The variations discussed in this and the following section (§2.6.2) were tested using the χ^2-statistic. This was used to test the null hypothesis that there was no difference between the measurements for any particular pair of observations. The critical level of significance used was 1.0%. Any value lower than this was regarded as evidence for variability. As in previous sections, it must be

stressed that this level of significance (unjustifiably) assumes normal errors in the photometry.

Inter-epoch variability in the flux densities was seen in the majority of the observations. The exceptions to this are the observations of $0118-272$, $0138-097$ and $1641+399$. Both $0118-272$ and $0138-097$ exhibited flux variability between the 1986 and 1987 July epochs while remaining constant between 1987 July and September. The variability of $1641+399$ was discussed in §2.3.1.2. Night to night variations were also commonly seen, though exceptions were more common than above. Only two objects ($0109+224$ in 1987 September, and $1253-055$ in 1986 August) showed variability which could be characterised in terms of a constant spectral index. $0109+224$ had shown variability in the spectral index during 1986 August, while $1253-055$ was generally observed at higher-than-average airmass. This may imply that the observed constancy of the spectral index in this latter object was an artefact of the larger photometric errors of these observations. No observations were seen which repeated the pattern of Gear, Robson & Brown (1986), however two objects did show steepening spectral indices with increasing flux ($0048-097$ and $0109+224$) both in 1986 August.

2.6.2 VARIABILITY IN THE POLARIZATION PROPERTIES

Variations in the polarization parameters were tested for in the same manner as the photometric changes described above (i.e. by use of the χ^2 statistic). As with the flux variability inter-epoch variations were seen in the majority of blazars. With the exception of those objects which did not display any significant polarization, the only example of an object which displayed constant inter-epoch polarization degree was $2254+074$.

Inter-night variations of the degree of polarization were also commonly seen. In addition to $2254+074$ only five other objects failed to show any inter-night

variations when repeat observations were performed. These were $0118-272$, $0138-097$, $1418+546$, $1641+399$ and $2223-052$. The remaining objects all showed inter-night changes in the degree of polarization during at least one of the three epochs of observation. These variations did not always coincide with significant changes in the observed flux density of these objects.

The variations in the polarization data were not all of a similar form. For example the changes in polarization of $1253-055$ showed a generally increasing level of polarization with the onset of FDP ($dp/d\nu > 0$). In contrast $0109+224$ showed (during 1986 August) FDP of both senses ($dp/d\nu < 0$ and $dp/d\nu < 0$). A third kind of variability was that shown by $0048-097$ in 1987 July when no evidence for FDP was seen but the overall level of polarization rose and then fell at all the observed frequencies.

There is some evidence for rapid variability in the polarization position angle. This was mentioned above (§2.5.2) as a possible cause of apparent FDθ . This is evident in the data of 1253–055 (3C 279) during 1986 August. All these data were collected with the Mark I instrument (§2.1.1). Consequently the flux and polarization spectrum was built up out of a series of simultaneous measurements at three frequencies. The separate sets of measurements would be of different durations depending on signal-to-noise ratios required. Only on 1986 August 2 did any of the individual sets of three frequencies show strong evidence for FDθ . For the two sets of observations on this night (HIB and JVB) the levels of significance when testing for frequency independence were 10^{-11} and 10^{-9} respectively. This indicates that on this night FDθ was definitely observed. On all other the nights during this period the data were consistent with frequency-independent position angles but with variations over the approximately ten minute timescale of the integrations. These variations were of the order of half a degree over such ten minute timescales. Table 2.13 shows the averaged position angle for each run during this period. Inspection of this table shows that for any pair of runs the evidence for variability is, at best, only marginally significant. Nevertheless this was capable of inducing the artificial FDθ in the summed data.

Table 2.13: The position angle data for 1253 − 055 during 1986 August.

U.T. Date	Wavebands	U.T. Time / hours	Position angle / deg
1986 August 1	HIB	6.165	120.46 (0.35)
	HIB	6.358	120.84 (0.38)
1986 August 2	HIB	6.260	FDθ
	JVB	6.415	FDθ
1986 August 4	HIB	5.825	125.40 (0.20)
	HIB	5.958	125.20 (0.20)
	JVB	6.072	126.06 (0.21)
	JRB	6.166	126.77 (0.16)
	JRU	6.313	128.00 (0.20)
1986 August 5	HIB	5.910	132.57 (0.29)
	HIB	5.999	131.87 (0.23)
	JVU	6.154	132.16 (0.20)
	JRU	6.280	131.45 (0.36)
1986 August 6	HIB	5.798	136.23 (0.32)
	HVB	5.997	136.85 (0.42)
	JRU	6.161	135.66 (0.20)

The data given in Appendix A are these summed values. These are the best estimates of the position angle during the whole series of observations but the errors are underestimated as they do not take into account the variability which may have occurred while observations at other frequencies were being made. There was no evidence for similar rapid changes in the polarization degree nor did any other object show such rapid variability of the position angle.

Longer-period variations in the position angle were seen. One object (0235+164) was observed to have a polarization position angle which was constant over the inter-epoch timescale. Only two high signal-to-noise observations of this object were made (in 1987 July and 1987 September) and the two sets of values were consistent. All other objects exhibited inter-epoch variability of the position angle. Inter-night variations of the position angle were also common. Only three objects failed to show inter-night variations during any of the epochs. These were $0118-272$, $0138-097$ and $1418+546$. Note that these objects also failed to display any inter-night variations of the degree of polarization. However the other objects which similarly failed to show inter-night changes in the polarization degree did show inter-night changes in position angle. These variations are not all characterised by uniform rotations with time. For example $0048-097$ exhibited both clockwise and anti-clockwise rotations during 1986 July/August.

The fact that variability in the position angle is the rule rather then the exception should not be taken as invalidating the results of Rusk & Seaquist (1985) and Impey (1987). These authors showed that the polarization position angles of objects with preferred orientations were generally aligned along the milliarcsecond radio-structure axis. The variations which were detected in the UKIRT data were generally of a few to ten degrees in amplitude. Impey (1987) regarded any object where two-thirds of the position angles were all consistent to within 40° as having a preferred (range of) position angle(s). Six objects exhibited position angle variability around or in excess of this limit. These were $0109+224$, $0118-272$, $0219+428$, $1418+546$, $1749+096$ and $2254+074$.

Three other objects showed FDθ which would itself come close to violating the 40° limit. These were 0138 − 097, 1727 + 502 and 2155 − 304. It should be noted that in some of these latter observations the errors in the observed position angles are high enough that the FDθ may not need to be so extreme as to violate the 40° limit. Since the majority of the detected variations were of much smaller amplitude than this, the incorporation of this data set into his analysis is unlikely to affect his result. Unfortunately Impey (1987) does not publish all of the data from which he draws his conclusions so it is not possible to directly estimate the effect of these data on his result.

Finally the origin of the variation in the observed position angles must be considered. Where FDθ occurs a two-component model such as that proposed by Holmes *et al.* (1985b) could perhaps explain the variability. Discussion of such models will be deferred to the following section. What will be discussed here is the explanation for the rotations of position angle which occur without FDθ (or FDP) and sometimes in the absence of changes in the degree of polarization (e.g. 0219 + 428, 1987 September and 1641 + 399 1986 August). The most naïve explanation is that these apparent rotations in position angle are the result of bulk rotations of the magnetic field in the emission region. However there are alternative explanations. There is the picture advocated by Königl & Choudhuri (1985b) and used by Kikuchi *et al.* (1988) to explain their observations of 0851 + 202. In this case the observed polarization results from emission from a shock which amplifies the magnetic field as it travels down the jet. This is assumed to contain an ordered magnetic field which causes the observed position angle to change with distance along the jet in a non-random way. Another possibility is that changes in the velocity of a relativistically moving source will cause changes in the observed position angle because of relativistic aberration. This explanation was suggested by Blandford & Königl (1979) and then expanded upon by Björnsson (1982). Björnsson (1982) showed that the expected behaviour of a relativistically moving source would mimic that of two-polarized components with varying relative orientation. This would imply

that the most rapid changes in position angle would be associated with minima in the polarization degree. He showed that linear increases in position angle with time would be inconsistent with this picture (e.g. 0236 + 164 at radio frequencies; Ledden & Aller 1978). Another contrary example of behaviour is provided by rotations in excess of 180° (e.g. Altschuler 1980).

In principle there is no problem with the application of the first explanation given above. However the mechanism whereby bulk rotations in the magnetic field would be caused is unknown and will remain a major obstacle to a complete model of the emission region. The second explanation strongly depends on the large-scale ordering of the magnetic field in a jet. This is especially true if periodic variations in the position angle need to be explained (as in the data of Kikuchi *et al.* 1988). No such periodic variations are examined in the data presented here, so applying these models to these data is impossible. This is not to say that these data are inconsistent with these models as the time coverage in the individual epochs is too short to show the distinctive characteristics of the expected variations. For example the Kikuchi *et al.* (1988) data were obtained over a period of several months. No examples either of variations in excess in of 180° or of rapid variability at low levels of polarization were seen. Consequently these data provide no examples which either support or contradict changes in relativistic velocity as the origin of the position angle fluctuations.

2.7 Models of the Frequency Dependence of Polarization

2.7.1 THEORETICAL BACKGROUND

In §1.3.1 a brief introduction was made to the physics of synchrotron radiation. The work of Nordsieck (1976) and Björnsson & Blumenthal (1982) was mentioned, and the latter sets out a formalism whereby the polarization properties can be evaluated for an inhomogeneous source. This will now be gone over in

more detail.

Björnsson & Blumenthal's (1982) result was given in equation 1.8 as;

$$p(\nu) = \Pi(\nu)\,\frac{\alpha(\nu)+1}{\alpha(\nu)+\frac{5}{3}}\,. \tag{2.8}$$

This is essentially the same result as was obtained by Nordsieck (1976) and is applicable in all but the most extreme conditions. $\Pi(\nu)$ is composed of integrals over the magnetic field geometry;

$$\Pi(\nu) = \sqrt{q^2(\nu)+u^2(\nu)}\,, \tag{2.9a}$$

$$q(\nu) = \frac{\int b^2\,H(b,\chi,\gamma)\,\cos(2\chi)\,G(\nu/\nu_c)\,db\,d\chi\,d\gamma}{\int b^2\,H(b,\chi,\gamma)\,G(\nu/\nu_c)\,db\,d\chi\,d\gamma}\,, \tag{2.9b}$$

$$u(\nu) = \frac{\int b^2\,H(b,\chi,\gamma)\,\sin(2\chi)\,G(\nu/\nu_c)\,db\,d\chi\,d\gamma}{\int b^2\,H(b,\chi,\gamma)\,G(\nu/\nu_c)\,db\,d\chi\,d\gamma}\,. \tag{2.9c}$$

Here $G(\nu/\nu_c)$ is the synchrotron function given in §1.3.1 (equation 1.5f), γ is the electron Lorentz factor, b is the magnetic field density projected onto the plane of the sky, χ is the apparent position angle of the field on the sky and $H(b,\chi,\gamma)$ is the trivariate probability density function of these parameters within the source. The observed position angle (θ) is then given by;

$$\tan 2\theta = \frac{u(\nu)}{q(\nu)}\,. \tag{2.10}$$

The functions $q(\nu)$ and $u(\nu)$ can be considered as weighted averages of $\cos(2\chi)$ and $\sin(2\chi)$, where the weighting is provided by the amplitude of the polarized flux.

The exact polarization properties that would result from these equations depend on the form of the probability density function $H(b,\chi,\gamma)$. If this function is separable such that;

$$H(b,\chi,\gamma) = h(b,\gamma)\phi(\chi)\,, \tag{2.11}$$

then the polarization position angle (θ) is independent of frequency and the frequency dependence of the degree of polarization is given by equation 1.8 with $\Pi(\nu)$ independent of frequency. The α-term can adequately represent the frequency dependence for all forms of H which give rise to convex spectra. The maximum deviation from this is 7.5% at $\alpha \approx 0.2$. Since concave spectra are rarely seen in blazars (§2.4), this should not be a problem. The results for other forms of H are more complicated and are discussed at length by Björnsson & Blumenthal (1982). In brief, they found that behaviour with both $dp/d\alpha > 0$ and $dp/d\alpha < 0$ could occur depending on whether the degree of alignment of the magnetic field increases or decreases with b. If the alignment increases with b then the polarization increases with α (which was the result of Nordsieck 1976).

Section 2.4.3 discussed the possible presence of cut-offs in the energy spectrum of the synchrotron radiating electrons. The effect on the observed total flux spectrum was discussed. Such a cut-off would also have a dramatic effect on the observed polarization behaviour. Strong FDP occurs in the region around the cut-off but no FDθ is seen provided equation 2.11 applies. Figure 2.14 shows the expected polarization signature for a two-component model consisting of a polarized cut-off component and an unpolarized power-law component. The cut-off was (as in §2.4) assumed to be a sharp upper limit in the electron energy distribution. The parameters used to generate this diagram are wholly *ad hoc* and used to create an example of the sort of frequency behaviour which may result. The rise in polarization results from the fact that synchrotron emission from an isotropic but monoenergetic electron distribution tends to 100% polarization above the critical frequency. This can be seen in Figure 1.2 in §1.3.1. The fall-off in polarization results from the dominance of the unpolarized emission at high frequencies.

To round off this discussion, the two component model of Holmes *et al.* (1984b) must be mentioned. This is an empirical model which makes little use of the particular qualities of synchrotron radiation. It was proposed to explain the behaviour of 0851 + 202 during 1983 January. It consisted of two

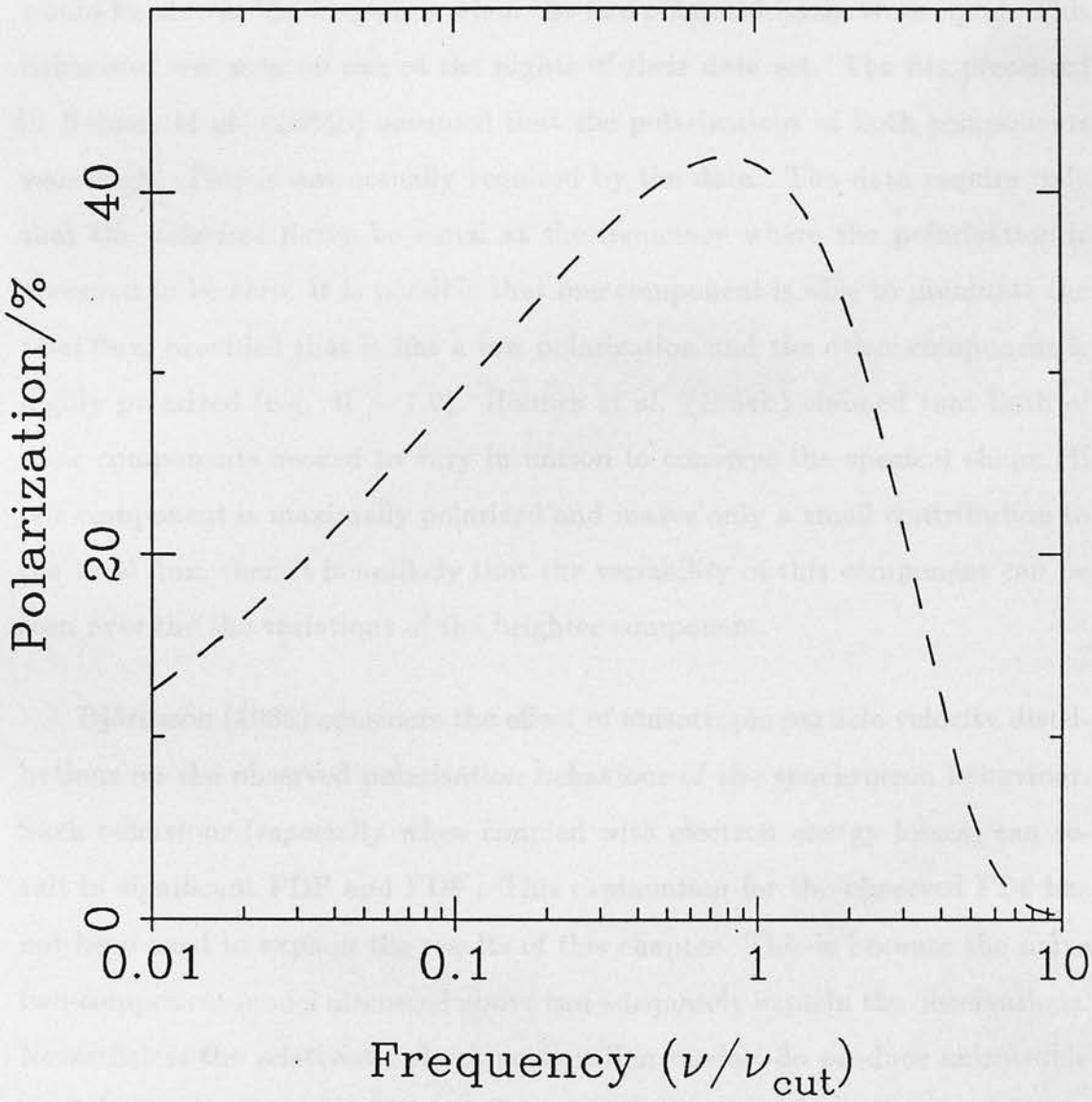

Figure 2.14: An example of the polarization behaviour of a cut-off source. The cut-off component has a low frequency spectral index of 1.0, the unpolarized component has a spectral index of 1.5 and the two components are matched to have the same fluxes at the criticial frequency corresponding to the cut-off. The cut-off component was assumed to have a perfectly ordered magnetic field ($\Pi = 1.0$).

components each of which had a parabolic flux distribution (in the $\log S_\nu(\nu) - \log \nu$ plane). The polarization was given by equation 1.8 for each component with $\Pi(\nu)$ independent of frequency. The position angles for each component were assumed to be different. The motivation for this model was that when the two components were oriented at right angles to each other the polarization would be zero at the frequency when the two polarized fluxes were equal. This behaviour was seen on one of the nights of their data set. The fits presented in Holmes *et al.* (1984b) assumed that the polarizations of both components were high. This is not actually required by the data. The data require only that the *polarized* fluxes be equal at the frequency where the polarization is observed to be zero. It is possible that one component is able to dominate the *total* flux, provided that it has a low polarization and the other component is highly polarized (e.g. $\Pi \sim 1.0$). Holmes *et al.* (1984b) claimed that both of their components needed to vary in unison to conserve the spectral shape. If one component is maximally polarized and makes only a small contribution to the total flux, then it is unlikely that the variability of this component can be seen over the the variations of the brighter component.

Björnsson (1986) considers the effect of anisotropic particle velocity distributions on the observed polarization behaviour of the synchrotron behaviour. Such behaviour (especially when coupled with electron energy losses) can result in significant FDP and FDθ . This explanation for the observed FDθ has not been used to explain the results of this chapter. This is because the naïve two-component model discussed above can adequately explain the observations. Nevertheless the relativistic shock acceleration models do produce anisotropic particle distributions (e.g. Kirk & Schneider 1987, Heavens & Drury 1988). In the cut-off models which are applied in §2.7.2 and §2.7.3 shock acceleration is implicitly assumed. An important piece of future work would be to evaluate the expected frequency dependent properties of synchrotron radiation from the resulting anisotropic particle distributions.

2.7.2 APPLICATION TO THE OBSERVATIONS OF 1253 − 055

The previous section has laid out the basis for interpreting the polarization behaviour of blazars. The best example of this in the UKIRT data set are the 1253 − 055 (3C 279) data. The adjective 'best' is used because these data are extremely polarized and consequently have high signal-to-noise ratios. The main problem with these data is that they were all obtained at moderately high airmass ($\sec z = 1.2 - 2.0$) which has increased the errors on the photometry.

The behaviour of this object will now be qualitatively described. The fluxes were fitted by power-laws on all nights in 1986 August. There was no evidence for variability between 1986 August 1 and 1986 August 4. The fluxes decreased marginally from 1986 August 4 to August 5 (significant at the 5% level). A greater decrease occurred between August 5 and August 6 which was significant at the 6×10^{-5} level. The photometric errors were too large to permit any description of the spectral index behaviour during this variability. This object was also observed a year later on 1987 July 28. On this date the flux could again be expressed as a power-law. In the following discussion the data obtained on the night of 1986 August 1 will be excluded as these consist of only three frequency points which do not allow enough degrees of freedom.

The polarization behaviour was more variable than the flux behaviour, though this may just be a result of the higher signal-to-noise ratios of this information. The polarization degree was initially flat on 1986 August 1. On the following nights FDP developed with $dp/d\nu > 0$ and the polarization degree rose to a maximum on 1986 August 5. The following night's data were not significantly different. The position angle frequency dependence was subject to the systematic errors discussed in §2.5.2 and §2.6.2. The significant FDθ seen on 1986 August 2 appears to be real. Otherwise the data appear to be consistent with variable but frequency-independent position angles. This makes the explanation of the polarization behaviour on these nights much easier. The 1987 July 28 data showed FDP ($dp/d\nu > 0$) but no FDθ .

The Björnsson & Blumenthal (1982) parameterisation (equation 1.8) will be used as a first attempt at an explanation of this behaviour. Hereafter it will be referred to as the α-parameterisation. The lack of any FDθ on most of nights will be used to justify a frequency-independent form of $\Pi(\nu)$ as an initial approximation. This has been used to model all the data of $1253-055$ (including the data of 1986 August 2 for which it is not strictly applicable). Table 2.14 shows the results of these fits. The spectral flux distribution has been fitted using the parabolic form of equation 2.3. Figure 2.15 shows the application of this model to the 1986 August 5 data.

The cut-off polarization behaviour was also fitted to these data. Again it was assumed that the magnetic field distribution in the region was such that no FDθ would result. However it was assumed that the field was only partially ordered so that the region would not necessarily be expected to emit approximately 70% polarized radiation. It was not possible to fit the data using a single such shock component. The cut-off fits presented in Table 2.14 include a second unpolarized component which permits reasonable fits to the data. In this case the observed FDP results from a combination of the intrinsic FDP of the cut-off component and the dilution of the polarized flux by an unpolarized component of different spectral shape. The fits presented in the table are characterised by the following parameters: the 10^{14} Hz flux densities of the cut-off and power-law components (S_1 and S_2 respectively in units of mJy), the two spectral indices (α_1 and α_2), the cut-off frequency (ν_c in units of 10^{14} Hz) and the polarization parameter (Π). This latter is defined such that at low frequencies the cut-off component polarization is $\Pi\,(1+\alpha)/(\frac{5}{3}+\alpha)$ and can take values between 0.0 and 1.0. All the frequencies are measured in the observer's frame. Figure 2.16 shows the best fit to the 1986 August 5 data.

The relative merits of these two explanations must be discussed. Even assuming normal statistics neither can be rejected on the basis of the χ^2 at the 1% level. Any preference between the two must rely on their relative simplicity. The α-parameterisation of equation 1.8 (with equation 2.11) essentially sepa-

Table 2.14: The results of fits to the $1253-055$ data. $P(\chi^2)$ is the probability of obtaining the fitted value of χ^2 or greater if the model is correct and normal statistics are assumed.

α-parameterisation					
	1986 Aug. 2	1986 Aug. 4	1986 Aug. 5	1986 Aug. 6	1987 Jul. 28
$\log S_{14}$	1.57	1.40	1.35	1.25	1.16
a	0.50	−0.17	−0.08	−0.08	−0.28
b	−0.63	−1.21	−1.21	−1.10	−1.93
Π	0.39	0.48	0.54	0.55	0.40
χ^2	2.96	11.7	9.60	12.0	19.5
$P(\chi^2)$	0.81	0.31	0.48	0.28	0.08
Cut-off Model					
$\log S_1$	1.62	1.52	1.51	1.35	1.36
α_1	0.96	0.78	0.93	0.79	0.93
Π	0.42	0.54	0.60	0.64	0.44
ν_c	14.0	12.8	11.6	12.8	3.78
$\log S_2$	0.79	1.10	1.06	0.97	1.07
α_2	1.50	1.72	1.89	1.55	2.49
χ^2	3.92	7.50	7.21	7.27	7.51
$P(\chi^2)$	0.42	0.48	0.51	0.51	0.68

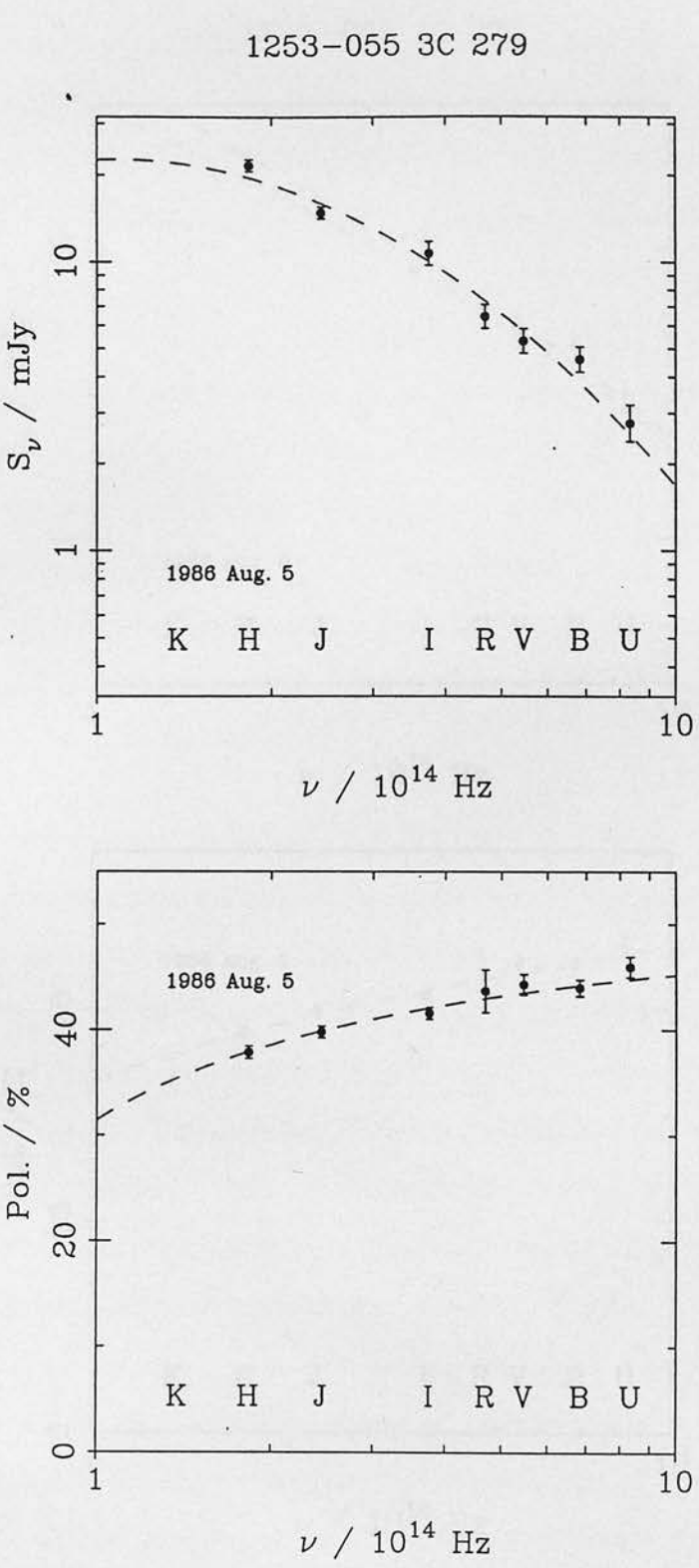

Figure 2.15: The fitted flux density and polarization curves to the data of 1986 August 5 using the α-parameterisation. A parabolic fit to the flux data has been used to predict the polarization via equation 1.8.

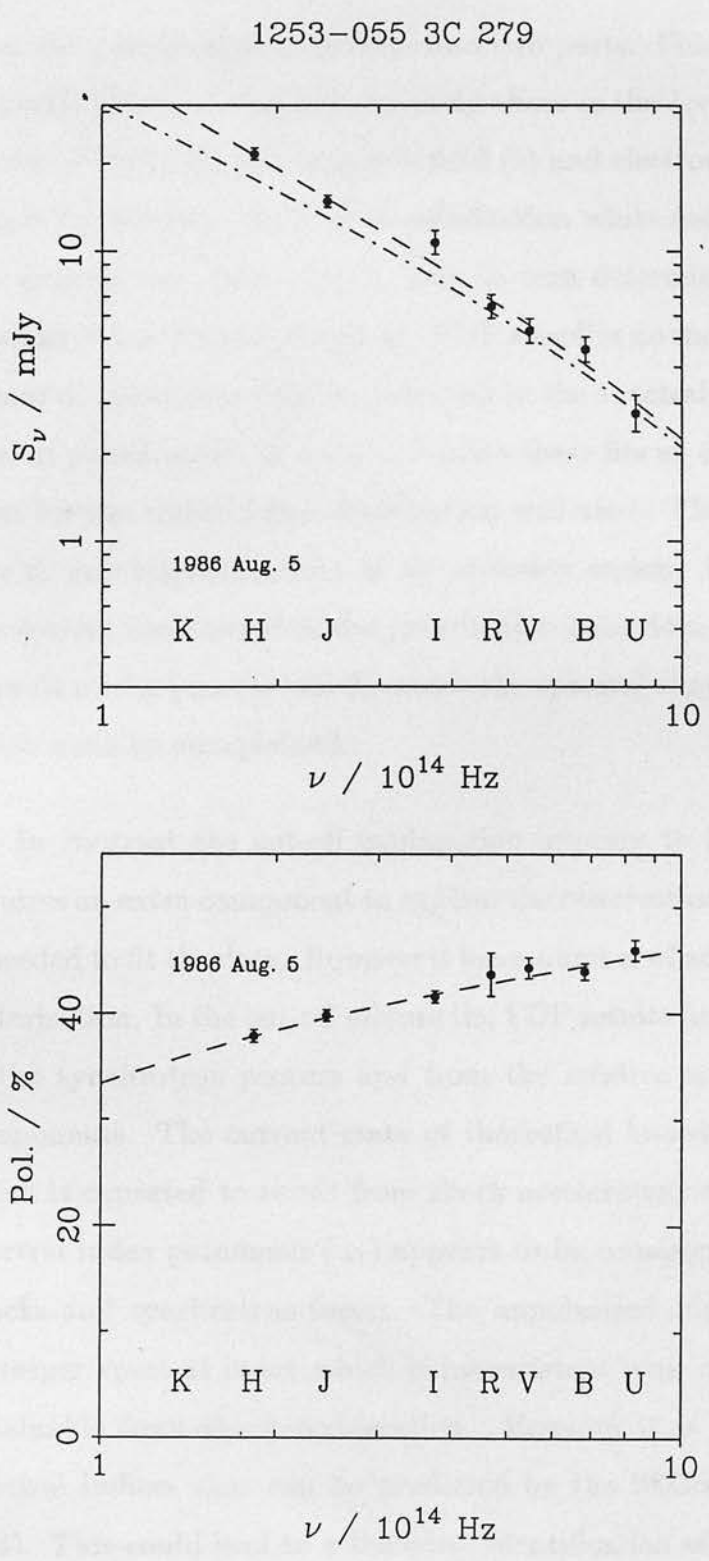

Figure 2.16: A fit to the data of 1986 August 5 using the cut-off model. The dashed lines represent the fits to the total flux density and polarization while the dot-dashed line represents the flux of the cut-off component alone.

rates the polarization behaviour into two parts. Firstly there is the degree of magnetic field ordering and secondly there is the (potentially coupled) distribution of the projected magnetic field (b) and electron Lorentz factor (γ). The former determines the level of polarization while the latter factor determines the spectral flux distribution. This in turn determines the FDP through the spectral index. Consequently the FDP supplies no more information about the nature of the source than is contained in the spectral flux distribution and the level of polarization. In order to obtain these fits an empirical three-parameter form for the spectral flux distribution was used. This has absolutely no relation to any physical model of the emission region. If the α-parameterisation is a correct description of the polarization behaviour then the FDP is entirely a result of the process which causes the spectral shape of the continuum flux, which remains unexplained.

In contrast the cut-off explanation appears to be more complicated. It requires an extra component to explain the observations and an extra parameter is needed to fit the data. However it has a number of advantages over the α-parameterisation. In the cut-off picture the FDP results from the intrinsic properties of the synchrotron process and from the relative spectral indices of the two components. The current state of theoretical knowledge about the spectrum which is expected to result from shock acceleration was reviewed in §2.4. The spectral index parameter (α_1) appears to be consistent with relativistic strong shocks and synchrotron losses. The unpolarized component appears to have a steeper spectral index which is inconsistent with current estimates of those obtainable from shock acceleration. However it is well within the range of spectral indices that can be predicted by the SSC models (also discussed in §2.4). This could lead to a tentative identification of this component with the integrated emission of the quiescent jet, while the cut-off would arise from a shock in this flow. Nevertheless, despite this last ambiguity, the cut-off model contains more information about the physical nature of the source than the α-parameterisation.

Neither of these pictures can account for the FDθ of 1986 August 2. In the α-parameterisation picture FDθ implies that the functions $q(\nu)$ and $u(\nu)$ in equation 2.9 are frequency-dependent. In general this gives rise to a potentially frequency-dependent form for $\Pi(\nu)$. Despite this the α-parameterisation is still able to fit the observed FDP on this night. This could imply that although equation 2.11 is not valid it is a reasonable first approximation. The frequency dependence due to $\Pi(\nu)$ would then be small compared to that arising from the α term which would then be able to fit the observed data to within observational errors. The change in position angle over the observed frequency range is consistent with this hypothesis. Similar considerations could explain the FDθ in the cut-off component which would be necessary if this picture were to be able to explain the observations of 1986 August 2. Alternatively if the second component were not unpolarized but had a small polarization at a slightly different position angle to that of the cut-off component then the observed FDθ could result without requiring intrinsic FDθ in the cut-off polarization behaviour. This is, of course, the explanation used by Holmes *et al.* (1982) to describe their data. However this would introduce a number of extra parameters to the fits to these data which, in themselves, would make more likely a satisfactory fit to the limited number of points available.

An important question is the constancy of some of these parameters as the source varies. Can the observed variations be characterised as simple changes in a small subset of parameters in either of these pictures? In the α-parameterisation the fitted flux parameters appear to change markedly from 1986 August 2 to 1986 August 6. However it was stated above that the spectral index did not change significantly during the observing period. If the parameters in Table 2.14 are used to calculate the spectral index at I (which is the best constrained part of the fit) then the calculated spectral indices remain essentially constant over the period of the 1986 August observations. The variability arises from changes in $\log S_{14}$ and Π. In the cut-off picture the situation is more complicated. The variations in ν_c, α_1 and α_2 are within the uncertainties in these parameters. The

observed variations, in this picture, result from a complicated mix of variations in $\log S_1$,'$\log S_2$ and in Π.

2.7.3 APPLICATION TO OTHER DATA

It is important to see whether either of the explanations, advanced above, are able to explain the majority of the remaining observations of blazars. The α-parameterisation was fitted to all the polarized observations with four or more flux points. There were fifty sets of observations satisfying this criterion (excluding the observations of 1641+399 for which an alternative explanation was advanced in §2.3.1). No allowance was made for the presence of FDθ . The validity of the α-parameterisation when FDθ occurs was discussed above (§2.7.2). Of the fifty sets of observations thirty-three were successfully fitted at the 5% level of significance. The fitted values of the B-field ordering parameter are shown in Figure 2.17. The rejected fits are summarised in Table 2.15.

Four of the rejected fits were not significant at the 1% level. It is probably unreasonable to consider these data as inconsistent with the α-parameterisation given the likely non-normal errors in the photometry. The remaining observations in Table 2.15 are worthy of of discussion. There was no *a priori* reason to expect that the α-parameterisation would not have been able to fit the data of $0048-097$ (1986 Aug. 3). The observations of $0109+224$ and $1418+546$ were characterised by sharp rises in the degree of polarization with frequency. (a factor of ~ 6 for the 0109+224 data). Extrapolating from the observed frequencies the polarization would have fallen to zero above 10^{14} Hz in both cases. There was some apparent FDθ but this was not very significant given the tendency to underestimate the errors at low signal-to-noise ratios (§2.1.4). The observation of $1418+546$ was an isolated measurement but those of $0109+224$ were preceded by a number of three-frequency measurements which exhibited FDP with both $dp/d\nu > 0$ and $dp/d\nu < 0$. It is possible that a multicomponent model can explain these data but without observations at lower frequencies than K such an

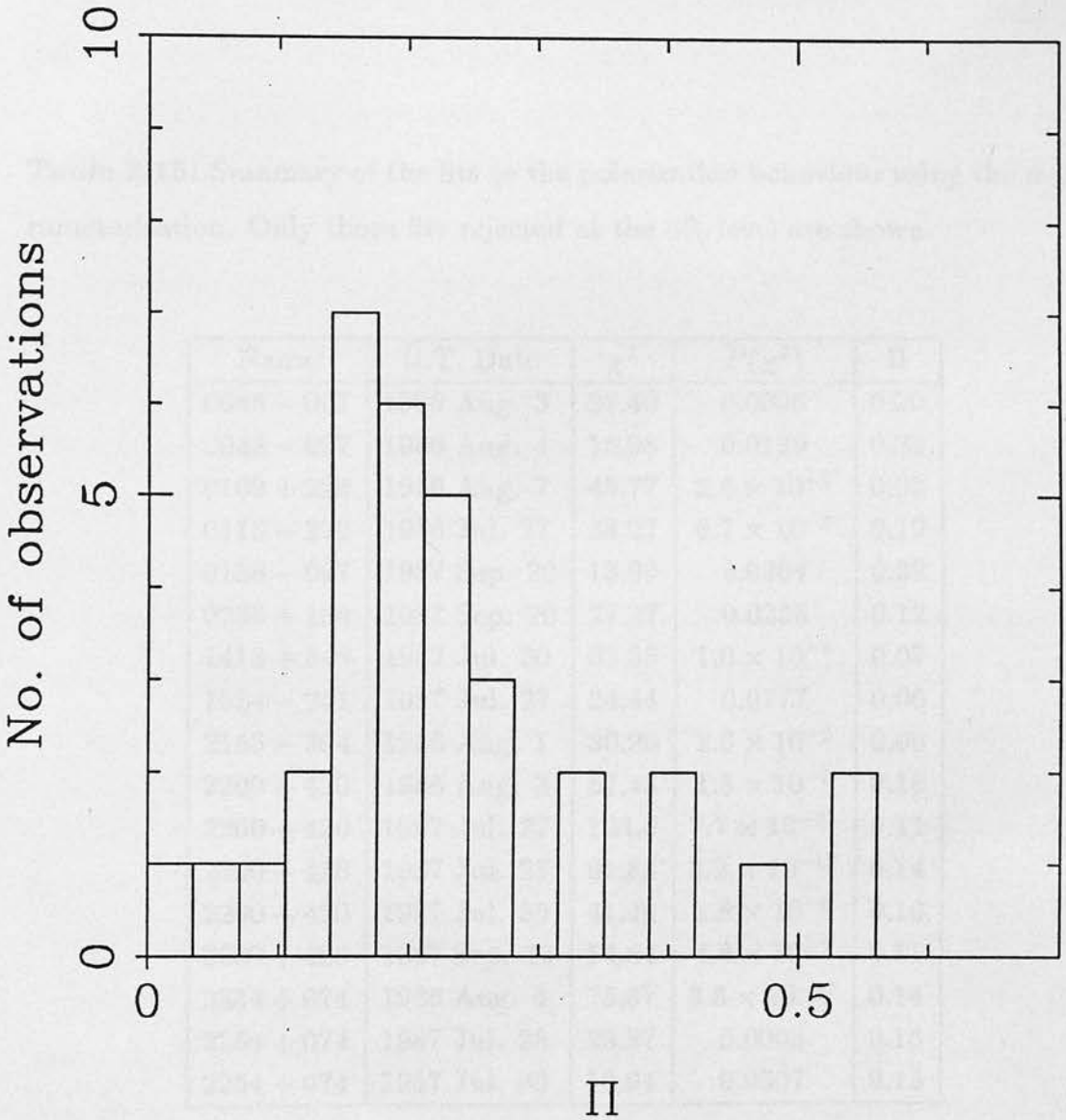

Figure 2.17: The distribution of the fitted values of Π (the B-field ordering parameter) using the α-parameterisation.

Table 2.15: Summary of the fits to the polarization behaviour using the α-parameterisation. Only those fits rejected at the 5% level are shown.

Name	U.T. Date	χ^2	$P(\chi^2)$	Π
$0048-097$	1986 Aug. 3	27.40	0.0006	0.20
$0048-097$	1986 Aug. 4	15.98	0.0139	0.22
$0109+224$	1986 Aug. 7	45.77	2.6×10^{-7}	0.09
$0118-272$	1986 Jul. 27	38.27	6.7×10^{-6}	0.19
$0138-097$	1987 Sep. 20	13.93	0.0304	0.32
$0235+164$	1987 Sep. 20	27.27	0.0236	0.12
$1418+546$	1987 Jul. 30	62.93	1.0×10^{-8}	0.07
$1514-241$	1987 Jul. 27	24.44	0.0177	0.06
$2155-304$	1986 Aug. 1	30.96	2.6×10^{-5}	0.05
$2200+420$	1986 Aug. 3	57.43	1.5×10^{-9}	0.16
$2200+420$	1987 Jul. 27	124.5	7.7×10^{-21}	0.11
$2200+420$	1987 Jul. 28	91.85	2.2×10^{-13}	0.14
$2200+420$	1987 Jul. 30	41.40	1.8×10^{-6}	0.16
$2200+420$	1987 Sep. 19	54.84	4.8×10^{-9}	0.11
$2254+074$	1986 Aug. 4	75.67	3.5×10^{-12}	0.14
$2254+074$	1987 Jul. 28	28.87	0.0003	0.15
$2254+074$	1987 Jul. 30	16.94	0.0307	0.15

explanation cannot be strongly tested. The observation of $0118-272$ was mentioned in §2.3.2 as having a peculiar spectrum due to an anomalous H flux point. The photometric calibration of this point was rechecked and no obvious error found. $1514-241$ is located in a nearby galaxy giving an explanation as to why this object was inconsistent with the α-parameterisation as the observed fluxes are expected to be contaminated by starlight. The observation of $2155-304$ showed FDθ as well as FDP so the α-parameterisation would not strictly be applicable (as was discussed in §2.7.2). None of the observations of $2200+420$ (BL Lac) were able to be fitted by the α-parameterisation. These were generally characterised by spectral curvature and FDθ as well as FDP. It is not surprising that the FDP was not reasonably fitted by the α-parameterisation as this object is located in a nearby galaxy and the fluxes contain an unquantifiable amount of contaminating starlight. A likely explanation for the observed FDθ is a multi-component picture such as that of Holmes *et al.* (1984b). However the fitting of such a model would require accurate photometry of the blazar component which is not achievable with these data. The observation of $2254+074$ (1986 Aug. 4) showed an essentially frequency-independent degree of polarization from H to B. The U polarization was significantly higher than that measured at the lower frequencies. This behaviour was inconsistent with the α-parameterisation. The observations of 1987 July also showed a tendency for the FDP to be more marked at the higher optical frequencies.

The cut-off model described in §2.7.2 was also fitted to a number of other objects. These were selected as showing FDP with $dp/d\nu > 0$, no evidence for either FDθ and convex spectra. Also excluded were those objects which the α-parameterisation failed to explain because of the reasons given above. One exception to this was the data of $0048-097$ (1986 Aug.3) where there was no *a posteriori* justification for the failure of the α-parameterisation to work. The results of these fits are shown in Table 2.16. Note that the fits to the $1253-055$ data have already been given in Table 2.14. Of the fits which were attempted only four were rejectable at the 5% level. The observation of $0048-097$ (1986

Table 2.16: A summary of the fits to the FDP of blazars, using the cut-off model outlined in §1.7.2 for fits to the data of 1253 − 055.

Name	U.T. Date	χ^2	$P(\chi^2)$	$\log S_1$	α_1	Π	ν_c	$\log S_2$	α_2
0048 − 097	1986 Aug. 3	16.7	0.01	0.48	1.06	0.95	11.5	1.24	1.48
0048 − 097	1986 Aug. 4	4.79	0.31	0.39	0.87	0.85	119.	1.00	1.12
0048 − 097	1986 Aug. 6	8.47	0.21	0.85	0.50	0.25	14.1	1.13	3.24
0109 + 224	1986 Aug. 7	7.19	0.30	−0.38	0.50	1.00	6.8×10^6	1.16	1.33
0118 − 272	1986 Aug. 5	7.88	0.25	0.50	0.93	1.00	12.9	1.13	1.18
0118 − 272	1987 Jul. 30	4.44	0.82	0.99	1.01	0.27	26.9	0.86	1.38
0118 − 272	1987 Sep. 21	6.53	0.16	0.99	1.04	0.28	21.9	0.76	1.51
0138 − 097	1987 Jul. 28	1.71	0.94	0.68	0.98	0.27	32.4	0.89	3.67
0138 − 097	1987 Sep. 19	10.6	0.23	0.50	0.95	0.52	15.3	0.58	1.56
0138 − 097	1987 Sep. 21	3.01	0.56	0.69	0.72	0.32	9.96	−0.62	2.01
0138 − 097	1987 Sep. 20	10.2	0.04	0.29	0.74	0.69	50.0	0.56	1.14
0235 + 164	1987 Sep. 20	23.2	0.003	0.74	0.69	0.13	2.42	0.92	3.28
1418 + 546	1987 Jul. 30	13.3	0.10	−0.38	0.56	1.00	20.0	1.38	1.65
1749 + 096	1987 Jul. 27	29.2	5.7×10^{-5}	0.80	1.32	0.12	1.95	−4.66	−3.18
2155 − 304	1987 Jul. 27	9.40	0.40	1.72	0.50	0.21	33.3	1.56	0.86
2254 + 074	1987 Aug. 3	41.8	2.0×10^{-7}	0.68	0.84	0.17	2.87	0.46	3.25

Aug. 3) was acceptable at the more correct 1% level. The fit to the data of 0109 + 224 (1986 Aug. 7) was achieved with a very high value of ν_c which means that the fit was essentially a result of the FDP due to the effect of the unpolarized component on the apparent behaviour. Only a limited number of fits were attempted to the UKIRT data set since the amount of computer time required to achieve these was significant. Nevertheless this does show that the cut-off picture can explain many of the examples of FDP which occur including some that the α-parameterisation cannot.

2.7.4 DISCUSSION

In this section the aim is to discuss the extent to which a common explanation can be found for all the flux and polarization behaviour seen in blazars. The discussion will be limited mainly to the observations presented here and their implications for models of the IR/optical continuum.

Two pictures have been presented in the previous two sections which can explain the salient features of the observations. In most cases the data is unable to distinguish between the two alternatives.

The problem with the α-parameterisation was mentioned in §2.7.1. To repeat, this is that the form of the spectral flux distribution is entirely empirical with no physical justification. All of the information contained in the observations has been removed to this parameterisation of the observed spectra. Without a theory which can explain these spectra no further insights into the physics of the emission region can be obtained beyond the conclusion that, to first order, equation 2.11 applies in the emission region. The SSC pictures do provide a parameterisation whereby the spectrum expected from an inhomogeneous relativistic jet can be be evaluated. These fits have had some success in fitting the observed spectral characteristics of blazars (e.g. Madau, Ghisellini & Persic 1987) but rely on observations over many decades of frequency to

constrain their parameters.

The cut-off model is attractive because it can be interpreted in terms of particle acceleration at shocks. This link can be made because an upper energy cut-off in the electron energy distribution is an expected feature of shock acceleration. This occurs because above certain energies the acceleration timescale is longer then the energy loss timescale. Biermann & Strittmatter (1987) consider energy losses due to synchrotron emission and photon interactions and derive a cut-off frequency between 3×10^{14} Hz and 2×10^{15} Hz. However this result is critically dependent on the many assumptions made in its derivation. Examples of these are the fact that a Kolmogorov spectrum ($\propto k^{-5/3}$) was used to model the spectrum of the turbulent magnetic energy density which is responsible for the scattering, and that an incorrect upper limit to the shock speed was used. Both assumptions may be critical. The cut-off frequency depends very sensitively on the spectral index of turbulence. Heavens (1984) showed that a k^{-1} spectrum can give rise to a cut-off at X-ray frequencies or higher for shocks speeds greater than 3000 km s^{-1}. The cut-off frequency also depends on the square of the shock speed. Biermann & Strittmatter (1987) apply an incorrect upper limit to this speed (Heavens, personal communication). Nevertheless it is worth briefly comparing these results with the fitted values of ν_c given in §2.7.2 and §2.7.3. For $1253-055$ the Biermann & Strittmatter (1987) upper limit corresponds to an observer's frame frequency of 1.3×10^{15} Hz. The 1986 August fits are broadly consistent with being around this upper limit while the 1987 July fit is at a much lower frequency. Interpretation of ν_c for the objects in Table 2.16 is harder as not all the objects have measured redshifts. Nevertheless most of the fits have best-fit cut-off frequencies which are either close to Biermann & Strittmatter's (1987) upper limit or are higher. This is consistent with the fact that polarization 'hump' seen in Figure 2.14 is not observed. This would only be observed at high frequencies relative to ν_c. The origin of this feature is that at frequencies well above the cut-off the flux from this component is decreasing exponentially. Therefore at high frequencies any unpolarized components must

dominate the observed flux. In fact the only instances of $dp/d\nu < 0$ were discussed in §2.3. These either are transient phenomena (e.g. $0109+224$ in 1986 August) or have an explanation in terms of the line emission and 'blue bump' (see §2.3.1). No significant cases showing $d^2\alpha/d^2\nu = 0$ were seen. This is a problem for the interpretation of the observed FDP in terms of cut-offs unless the Biermann & Strittmatter (1987) result is genuinely indicative of a general result that the physical processes in shock acceleration (of all types) produce cut-offs over relatively restricted range of frequency.

The expected emission parameters of relativistic particles which have been accelerated by shocks in relativistic flows are just now becoming calculable (e.g. Kirk & Schneider 1987, Heavens & Drury 1988). However there remain a number of problems to be solved before a complete description of the physics of such shock acceleration mechanisms becomes available. An example of an outstanding problem is that the problem of the relativistic shock has only been solved for the case where the magnetic field is parallel to the shock normal. However substantial amplification of the perpendicular component is expected (e.g. de Hoffman & Teller 1950). This would imply that, in general, shocks would be dominated by such perpendicular fields. Consequently it is probably unreasonable to base interpretations of blazars on the predicted spectral indices from a family of shock models which are perhaps unlikely to be common in relativistic flows.

How can the cut-off picture be placed in a framework which explains all the observed features of blazar emission? It has been shown how the cut-off picture can explain FDP where it occurs without significant FDθ . The α-parameterisation can also do this. However whenever FDθ occurs these models fail to explain the observations. Holmes *et al.* (1984b) and Brindle *et al.* (1986) have shown that even some extreme cases of FDθ can be explained by a two-component picture. In this framework the observed FDθ is a result of two regions emitting polarized radiation at different position angles with different spectral shapes.

Unfortunately many of the best-defined examples of FDθ in the data presented here were unable to test the two-component picture. This was either because the FDθ occurred in an object known to be contaminated by starlight (e.g. $2200+420$) or because the object only showed FDθ in three-frequency Mark I instrument data which provides insufficient information to allow a model to be fitted. However it can be stated that no instances of the most characteristic two-component behaviour were seen. That is there were no observations similar to those of $0851+202$ in 1983 January (Holmes *et al.* 1984b) which displayed minima in their polarization curves and 90° shifts in the position angles.

The motivation for advancing the cut-off model as an explanation of the polarization behaviour were those observations which showed FDP. However it was seen in §2.5 that many of the observations of blazars were characterised by power-law spectra, frequency-independent degrees of polarization and frequency independent position angles of polarization. These observations can be placed in the same framework as the cut-off model in two ways. Either they could be shock components observed at frequencies much lower than ν_c or they could be the integrated emission of the quiescent jet which may be polarized. This latter possibility was raised in §2.7.2 as an explanation for the FDθ seen in the observations of $1253-055$.

If the 'best guess' model of the polarization behaviour is taken to be a cut-off component representing a shock with a steeper spectrum component representing the underlying jet, how would this relate to observations outside of the IR/optical spectral region? As was mentioned in Chapter 1, Rusk & Seaquist (1985) and Impey (1987) have shown that there is a definite tendency for those objects with preferred optical polarization position angles to have these oriented along the same axis as the VLBI structure axis. Assuming synchrotron emission implies that the magnetic fields in these emission regions are oriented perpendicular to the jet axis. Such quiescent position angles could be speculatively assigned to the hypothetical jet component. The other component would then be the shock or cut-off component which may in principle have a different

position angle.

The consistency of the above speculation can be checked by reference to the observations of 0851 + 202. In their two-component decomposition Holmes *et al.* (1984b) identified two distinct orientations. One appeared constant (at about 100°) and the other rotated during the observations of 1983 January. Roberts & Wardle (1987) report VLBI flux and polarization observations of this object at two epochs (1981.9 and 1982.9). Both of these show south-westerly highly polarized extensions from the moderately polarized core. If these are interpreted as jets then the position angle is of the order of −100°. Polarization perpendicular to this axis would be at 170°. The polarization of the constant component is closer to being oriented along the supposed jet axis, but is not quite close enough to be definitely linked with the quiescent components described above.

Unfortunately the variability of the spectral index cannot test this picture. The observations of 0851 + 202 (Gear, Robson & Brown 1986) where the spectral index appears to flatten as the flux increases can be interpreted as the low-frequency power-law regime of the cut-off component dominating the steeper spectrum jet as the source evolves. However the converse behaviour, a steepening spectrum with increasing flux can be achieved by suitable evolution of the cut-off frequency.

2.8 Concluding Remarks

This chapter has presented the results of a programme of multi-frequency polarimetric observations of blazars. Over 100 observations of 37 blazars were obtained during three separate observing trips in 1986 July/August, 1987 July and 1987 September. The data consist of simultaneous observations using up to 8 different filters at infrared to optical frequencies. The major results of the previous sections will now be summarised.

- The effect of unpolarized non-synchrotron components on the observed emission of blazars was discussed in §2.3. In particular the observations of 1641 + 399 (3C 345) were discussed in terms of an unpolarized 'blue bump' component being responsible for the fall-off in the polarization at optical frequencies. This has been interpreted as the emission from an accretion disc. However, it is not possible to determine accurately the parameters of such a component from polarimetric data at such a limited number of frequencies.

- The spectral flux distributions of the observations were examined in §2.4. In many cases the spectrum could be represented as a power-law over the full range of observed frequencies, but significant spectral curvature was not uncommon. The behaviour of the polarized flux density was similar to that of the total flux density whose properties could then be assumed to be representative of the blazar component. The spectral behaviour was seen to be inconsistent with that expected from particle acceleration at relativistic shocks unless the observations were made in the region of a high-frequency cut-off. Inhomogeneous source models can also explain the observed behaviour.

- The polarization behaviour was discussed in §2.5. One object (1253 − 055 3C 279) was seen to have a polarization of $45.5 \pm 0.9\%$. This is the highest optical/IR polarization that has been observed in a blazar. Frequency dependence of the degree of polarization was often seen. Almost all examples were seen to have $dp/d\nu > 0$. The counter examples were often associated with the 'blue bumps' discussed in §2.3. Frequency dependence of the polarization position angle was found to be a rare feature of blazar behaviour. No evidence was found to support claims that frequency dependence is associated with high levels of polarization.

- Variability was confirmed to be a common feature of blazar behaviour. No striking common characteristics were found to describe all the variations which were observed.

- The possible explanations of the observed frequency dependence in the polarization properties were discussed in §2.7. Two explanations were found which can explain most of the observed behaviour of blazars. The first explanation is that the observed frequency dependence is linked to the intrinsic curvature in the blazar flux spectrum. However no explanation for this curvature is available. A second explanation is provided by a polarized component with a high-frequency cut-off and a second component with a steeper spectral index and no significant polarization. Neither of these pictures can simply explain the observed frequency dependence of the position angles. The relationship of the second picture to possible jet models of blazars is also discussed.

To conclude this chapter the prospects for future observations must be mentioned. In some ways the results presented in this chapter are discouraging as no single model of the emission region in blazars is advanced. It is not easy to see how to distinguish between the α-parameterisation and the cut-off model as an explanation of the observed behaviour. If a theoretical prediction of the observed spectral shape of a blazar is not available, then the validity of the α-parameterisation must be tested using an empirical fit to the observed flux data. The fits presented in the previous section could be better constrained if flux information were available from higher and lower frequencies than those observed. This would make the empirical determination of the observed spectral index more secure at K, H & J and B & U. This in turn would more severely test the observed polarization behaviour at these frequencies. Testing the cut-off model would also benefit from a wider frequency coverage. Polarization information at lower frequencies would be particularly important. This is because the hypothetical unpolarized (or low polarization) component will dominate the observed behaviour at low frequencies if it has a steeper spectrum (as for the fits to the $1253-055$ data).

Chapter 3

The Cluster Environments of Blazars

3.1 Introduction

This chapter presents a study of the cluster environments of blazars in relation to those of other radio-loud quasars. The motivation for this was originally to test whether blazars can be a subset of the radio quasars distinguished solely by their orientation under the relativistic beaming hypothesis or unified scheme. The reasons for considering blazars in terms of the unified scheme are set out in Sect. 1.2. In their original paper, Orr & Browne (1982) concluded that the relative numbers of core-dominated radio quasars versus extended radio-quasars were consistent with the former being an aligned subset of the latter. This assumed the beaming parameters derived from superluminal motion studies and the simplest jet model. This is the basic unified scheme. It is now clear that relatively naïve extensions to the simplest picture of beamed jet emission can greatly alter the boosting factor and width of the beaming cone (Lind & Blandford 1985). Consequently it becomes very difficult to test the unified scheme on the basis of the relative numbers of the supposed aligned and misaligned sources. More stringent tests are provided by those methods which involve comparison of the unbeamed parameters of the two source populations. Heckman (1983), Miller (1984), Fabbiano *et al.* (1984) and Browne & Murphy (1986) have all attempted to test the unified scheme by comparing the optical and X-ray properties. However, their results are complicated by the uncertainties in the amount of beamed emission present in these two wavebands. The cluster environment of blazars is one observational parameter which is hard to imagine

being, in any way, orientation dependent.

The cluster environments of radio sources have been investigated by a number of authors. Longair & Seldner (1978; hereafter LS) investigated the environments of radio galaxies and derived the formalism that will be used in this chapter (see Sect. 3.2). Their work was extended to $z \sim 0.15$ by Peacock & Prestage (1988; hereafter PP) and then to $z \sim 0.8$, by Yates, Miller & Peacock (1988). Their results will be broadly summarised here, and discussed more fully in Sect 3.4. LS and PP found that compact radio sources are found in sparsely populated environments. Their results for the extended radio galaxies were expressed in terms of the Fanaroff and Riley (1974) classes. The less luminous FR I sources were found to lie in fairly dense environments, approximately corresponding to richness 0 or 1 in the cluster catalogue of Abell (1958). The more luminous FR II sources were generally found in less dense environments than the FR I sources. PP found marginal evidence that the FR II sources were nevertheless in denser environments than the compact radio galaxies. PP noted that these trends could present problems for the unified scheme, which would imply that the compact radio sources should lie in similar environments to their more extended counterparts. However, PP also noted that to test this rigorously it would be necessary to compare the environments of the compact radio sources with supposed misaligned counterparts of *similar extended radio power*.

Yee & Green (1984) and Yee & Green (1987; hereafter YG) have studied the environments of quasars using the same techniques as LS etc. Their results show that the environment of quasars appears to be correlated with redshift. They find an increase of the order of ~ 3 in the amplitude of the galaxy-quasar correlation function,B_{gq}, from $z \approx 0.4$ to $z \approx 0.6$. They also find that the richness of the clusters they find are of the order of Abell richness 1. The data presented here will be used to test the nature of the redshift correlation found by YG. The dependence of YG's results on the LF will also be discussed.

This work was carried out in collaboration with Lance Miller and Peter Brand.

3.2 Measurement of Clustering around Quasars

The techniques described in this section are those derived by LS to measure the strength of the cluster environments of extragalactic objects.

3.2.1 THE ANGULAR CORRELATION FUNCTION AND A_{gq}

It is assumed that the galaxies belonging to any cluster associated with a quasar are distributed isotropically around it. The standard form of the angular correlation function can then be used to describe the apparent distribution (e.g. Peebles 1980).

$$N(\theta) = n_g[1 + \omega(\theta)]\, d\Omega \tag{3.1}$$

Here n_g is the mean background density of galaxies (per unit solid angle) and $\omega(\theta)$ is the angular correlation function. It is well known that galaxies are clustered together on the sky and that for $\theta < 1°$ the corelation function can be expressed as;

$$\omega(\theta) = A\theta^{1-\gamma}, \tag{3.2}$$

(e.g. Groth & Peebles 1977). This function is used to describe the excess number of galaxies above a magnitude limit which are seen around the quasar (or radio galaxy). In principle it should be possible to determine both the parameters A and γ from the observed counts. However, in practice, the number of galaxies counted around these objects is too small for this to be feasible. LS,YG and PP all adopt a γ of 1.77, this value is that found by Peebles (1975) for the galaxy-galaxy correlation function. More recent and deeper determinations of

$\omega(\theta)$ have found slightly different values of γ (for example Maddox *et al.* (1988) find a γ of 1.66). YG attempted to check the value of γ for their galaxy counts around quasars and found no significant difference from 1.77, and PP analysed the effects of an erroneous value of γ and decided that, for $\gamma \sim 2$, the errors would not be large. The value of 1.77 is used here.

The value of A_{gq} (denoting the galaxy-quasar correlation amplitude (YG)) is then given by;

$$A_{gq} = \frac{N - n_g \Omega}{n_g J} \tag{3.3}$$

where,

$$J = \int_{\Omega} \theta^{1-\gamma} \, d\Omega, \tag{3.4}$$

where N is the number of galaxies counted in a solid angle, Ω, about the quasar. This quantity is only useful in comparing counts of galaxies at similar limiting magnitudes and at similar distances. So, the value of A_{gq} must be related to the *space* density of galaxies at the redshift of the quasar.

3.2.2 THE SPATIAL CORRELATION FUNCTION AND B_{gq}

With the assumption that the galaxies are distributed isotropically about the quasar, the space distribution of galaxies may be described by a spatial correlation function, $\xi(r)$.

$$N(r)dV = \rho_g[1 + \xi(r)]dV \tag{3.5}$$

If $\omega(\theta)$ is given by eqn. 3.2 then $\xi(r)$ is given by;

$$\xi(r) = B_{gq} r^{-\gamma}. \tag{3.6}$$

LS derive the relationship between $\xi(r)$ and $\omega(\theta)$, which they write as;

$$A_{gq} = H(z,m)B_{gq}. \tag{3.7}$$

$H(z,m)$ is a function of z, the redshift of the quasar and m the limiting magnitude of the galaxy counts.

$$H(z,m) = \frac{I_\gamma}{n_g} D_L^{3-\gamma} \Phi(m,z) \tag{3.8}$$

I_γ is an integration constant ($I_{1.77} = 3.78$), D_L is the luminosity distance to the quasar, and $\Phi(m,z)$ is the normalised integral luminosity function (LF) up to the absolute magnitude corresponding to m at the redshift, z. In order to obtain this result, LS assumed that the cluster described by $\xi(r)$ preserves its size and amplitude. This implies that the galaxies in the cluster do *not* take part in the Hubble flow.

3.2.3 THE GALAXY LF'S AND EVOLUTION

The integral LF, $\Phi(m,z)$, can be expressed as,

$$\Phi(m,z) = \sum_{i=1}^{n} \int_{-\infty}^{M_i} \phi_i(M)\, dM, \tag{3.9}$$

where the summation is performed over n morphological types of galaxy, each having a different absolute magnitude limit M_i. These M_i are related to the observed magnitude limit m by,

$$M_i = m - 5\log(D_L/10) - K_i(z), \tag{3.10}$$

where $K_i(z) = k_i(z) + e_i(z)$ contains the K-corrections and the galaxy evolution corrections. M_i is not strictly the absolute magnitude, as it includes an evolution correction.

The LF used in this chapter is the Schechter (1976) LF,

$$\phi(M) = 0.4 \ln 10\, \phi^\star\, 10^{0.4(\alpha+1)(M^\star - M)}\, e^{10^{0.4(M^\star - M)}}. \tag{3.11}$$

King & Ellis (1985) and Sebok (1986) have determined the local LF in the B_j and Gunn r wavebands respectively. The values of $M_i^\star$ were transformed to the R waveband, using the galaxy colours from Sebok (1986) and the colour transformations from Shanks *et al.* (1984) (B_j to B) and Bessel (1986) ($(V-R)$ to $(g-r)$). The function, $K_i(z)$, is derived from the galaxy evolution model of Guiderdoni & Rocca-Volmerange (1987), as formulated by Dunlop (1988). These calculations are performed for a cosmology with $H_0 = 50$ km s^{-1} Mpc^{-1} and $q_0 = 0.0$, and for galaxies formed at $z_f \sim 5$. The calculations are restricted to these cosmological parameters because of limitations in the computer code used to evaluate the models. These values of the constants will be used in all the following results. This choice of parameters is the same as that used by Sebok (1986). King & Ellis (1985) differ in that they use $q_0 = 0.1$. This difference should not be important, as the $M_i^\star$ are evaluated at low redshift. Nevertheless, an erroneous value of q_0 can result in significant errors in Φ. A q_0 of 0.5 as opposed to 0.0 will result in values of the limiting absolute magnitude being 0.3 mag fainter at a redshift of 0.5. Added to this is the change in the $K_i(z)$. The models of Guiderdoni & Rocca-Volmerange (1987) use the look-back time (a function of q_0) to make their evolutionary calculations. If the limiting magnitude is brighter than $M^\star$, it falls in the exponentially varying portion of the Schechter LF. Small changes in the limiting magnitude can then result in large variations in the results of the LF integrations. The effects of changing q_0 have not been investigated further, because these effects may well be masked by systematic uncertainties in the LF (§3.4.1.). It should be noted that an erroneous value of q_0 will introduce a spurious correlation of the calculated values of B_{gq} with z. The calculated functions, $K_i(z)$, are shown in Figure 3.1. Table 3.1 shows the transformed LF parameters, $\phi_i^\star, M_i^\star$ and α. The morphological types listed by King & Ellis (1985) and Sebok (1986) do not correspond exactly to those for which $K_i(z)$ is calculated. Simple interpolation has been used to obtain the LF parameters for the morphological types given in the table. The $K(z)$ for the Irr galaxies is rather uncertain, as the star-formation history of these objects is unknown. Consequently, if would be worrying if the

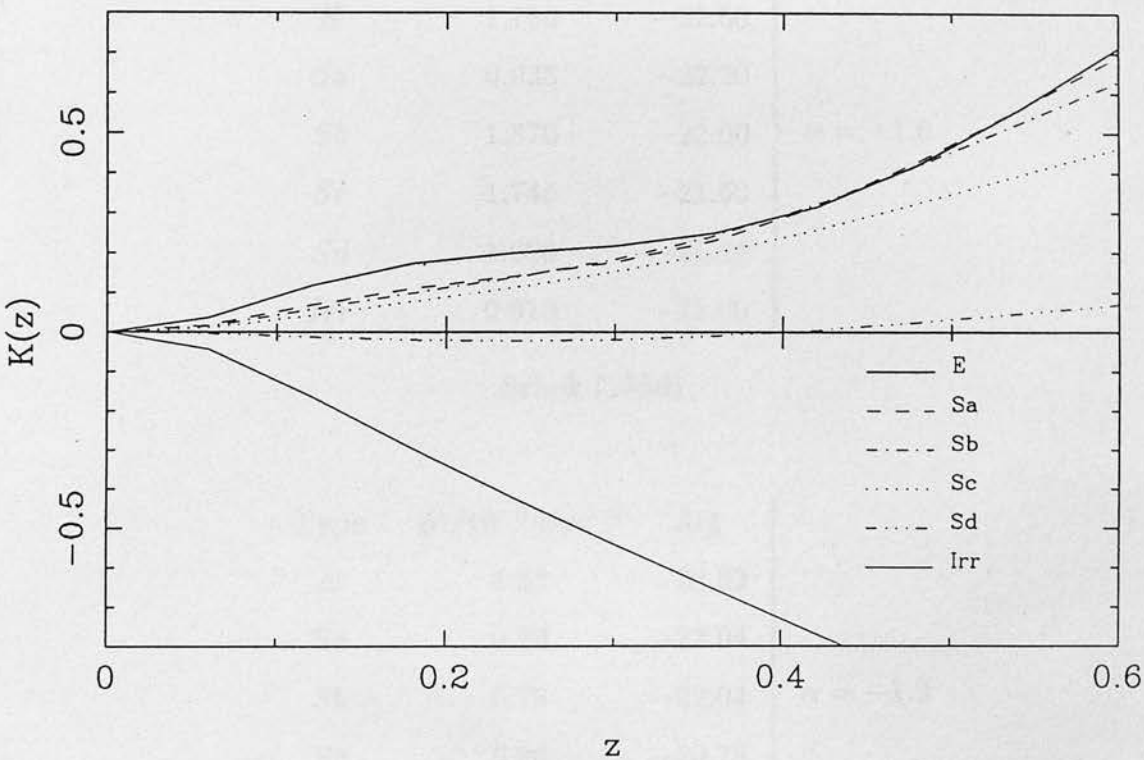

Figure 3.1: The functions $K_i(z)$ for each morphological type.

Table 3.1: The LF parameters.

King and Ellis (1985)

Type	$\phi^\star/10^{-3}Mpc^{-3}$	$M_R^\star$	
E	1.786	-22.50	
Sa	0.935	-22.20	
Sb	1.870	-22.00	$\alpha = -1.0$
Sc	1.745	-21.60	
Sd	1.620	-21.20	
Irr	0.810	-21.00	

Sebok (1986)

Type	$\phi^\star/10^{-3}Mpc^{-3}$	$M_R^\star$	
E	1.53	-22.32	
Sa	0.73	-22.04	
Sb	0.73	-22.04	$\alpha = -1.2$
Sc	5.26	-20.78	
Sd	2.50	-19.70	
Irr	2.50	-19.70	

LF for this class of galaxy were to dominate the value of Φ. This was checked for the deep CCD observations described in §3.3, and it was found that the largest contribution was made by Sc galaxies, even in the deepest images.

3.2.4 THE ERRORS ON A_{gq} AND B_{gq}

The values of A_{gq} and B_{gq} can be subject to large errors. Random errors are introduced by the measurement of excess numbers of galaxies in the presence of a number of background galaxies which is subject to statistical variations. PP point out that the total number of galaxies in the quasar frame, N, is not subject to any statistical error, it is the quantity $n_g\Omega$ in eqn. 3.3 which may differ from the true number of background galaxies in the area of sky Ω. These same random errors also occur in the counts of galaxies used to estimate n_g. The distribution of background galaxies will be expressed as eqn. 3.1. Peebles (1980) derives the variance of volume galaxy counts, where these are distributed according to the three-dimensional analogy of this equation (eqn. 3.5). The analogous result for the variance of angular galaxy counts is,

$$\sigma^2 = n_g\Omega + n_g^2 \iint \omega(\theta_{12})\, d\Omega_1\, d\Omega_2. \tag{3.12}$$

This can be written as,

$$\sigma^2 = n_g\Omega + n_g^2\Omega \int \omega(\theta)\, d\Omega, \tag{3.13}$$

in the limit of large areas of sky relative to the scale of the angular correlation function. This equation is used to estimate the error in both the number of field galaxies in the region containing the quasar and in the estimate of n_g. The value of A_{gg} used is that of Maddox *et al.* (1988) scaled to the effective depth of the number counts used. This scaling uses the relativistic analogy of Peebles' (1980) eqn. 50.13;

$$\omega(\theta) = \left(\frac{1}{(1+z)^2}\frac{dr}{dz}\right)^{-1} W\left(\frac{\theta D_L}{(1+z)^2}\right), \tag{3.14}$$

where r is the proper radial distance. The effective luminosity distance and corresponding redshift are chosen such that M^* corresponds to the magnitude limit of the galaxy counts. Using this expression for the variance in the galaxy counts can increase the value of σ by a factor ~ 1.5 over the use of Poissonian statistics.

3.3 The Experiment

3.3.1 THE SAMPLE

The full samples, that were intended to be observed, are presented here. This is to aid any observers who wish to further this study. Unfortunately, weather conditions prevented completion of the experiment as originally planned. Table 3.2 lists all the blazars (confirmed and candidate) with redshifts in the range 0.1 to 0.6 (see Table 1.1). The redshift range is chosen to exclude low-redshift objects, whose cluster environments are measurable using photographic plate material. The high-redshift limit was chosen to be the expected redshift at which a cluster would not be detectable in a reasonable time by a CCD imaging technique. YG published their results after this experiment was formulated. Their results show that it is possible to measure the cluster environment of quasars out to redshifts of $z \sim 0.65$, so the samples could be extended to higher redshift. The primary aim of this experiment is to test the unified scheme, so the comparison sample has been chosen to consist of quasars whose radio power is dominated by extended radio emission of comparable power to that of the blazars. This is because the large-scale structure is supposed to be dominated by unbeamed material and hence forms a suitable characteristic by which selection of the comparison sample can be performed. These objects present the most likely misaligned counterparts of the blazars under this hypothesis. Table 3.3 lists quasars satisfying this requirement in the required redshift range. The main source of the radio data needed to compile this list is the catalogue of Hintzen,

Table 3.2: Blazars in the redshift range $0.1 < z < 0.6$.

Name	z	$\log P_{ext}$ [1]
$0219+428$	0.444	25.82
$0317+186$	0.190	
$0323+022$	0.147	< 22.38
$0403-132$	0.571	26.03
$0735+178$	≤ 0.424	< 23.04
$0736+017$	0.191	23.63
$0752+258$	0.446	25.58
$0851+202$	0.306	< 22.74
$1150+497$	0.334	25.60
$1218+304$	0.130	
$1219+285$	0.102	< 21.89
$1235+632$	0.297	
$1253-055$	0.538	26.41
$1400+162$	0.244	25.03
$1408+020$	0.199	
$1413+135$	0.260	
$1510-089$	0.361	
$1546+027$	0.413	
$1641+399$	0.595	25.95
$1749+096$	0.320	< 22.56
$1921-293$	0.353	
$2032+107$	0.601	24.65
$2131-021$	0.557	
$2155-304$	0.117	23.78
$2208-137$	0.392	25.61
$2254+074$	0.190	24.73
$2345-167$	0.600	25.39

(1) Extended radio powers are given in W Hz^{-1} sr^{-1} at a rest frame frequency of 1490 MHz. All powers obtained from fluxes given by Antonucci & Ulvestad (1985), except for $0323+022$ (Feigelson *et. al.* (1986)) and $2131-021$ (Wills (1979)).

Table 3.3: Quasars dominated by extended radio emission in the redshift range $0.1 < z < 0.6$.

Name	z	$\log P_{ext}$ [1]
$0003+158$	0.450	25.58 [a]
$0041+119$	0.228	24.98 [b]
$0110+297$	0.363	25.32 [c]
$0133+207$	0.425	26.23 [a]
$0214+108$	0.408	25.70 [a]
$0340+048$	0.357	25.78 [d]
$0805+578$	0.438	25.75 [b]
$0837-120$	0.200	25.24 [a]
$0846+100$	0.366	25.34 [a]
$0903+169$	0.411	25.70 [b]
$1004+130$	0.240	25.31 [a]
$1012+488$	0.385	24.83 [b]
$1048-090$	0.344	25.80 [a]
$1058+110$	0.420	25.36 [a]
$1100+772$	0.311	25.85 [e]
$1223+252$	0.268	24.88 [a]
$1232-249$	0.355	25.76 [a]
$1512+370$	0.371	25.47 [c]
$1545+210$	0.264	25.56 [e]
$1606+180$	0.346	25.27 [b]
$1623+173$	0.552	25.48 [b]
$1634+269$	0.561	25.95 [a]
$1739+184$	0.186	24.38 [b]
$2135-147$	0.200	25.59 [a]
$2217+087$	0.228	24.51 [f]
$2251+113$	0.323	25.67 [b]

(1) Extended radio powers are given in W Hz^{-1} sr^{-1} at a rest frame frequency of 1490 MHz.

Radio references

(*a*) Miley & Hartsuijker (1977) (*b*) Hintzen, Ulvestad & Owen (1983) (*c*) Potash & Wardle (1979) (*d*) Wills (1979) (*e*) Pooley & Henbest (1974) (*f*) Harris *et. al.* (1983).

Ulvestad & Owen (1983), who give references to the radio structures of a large sample of quasars from the 4C and Parkes radio surveys. Also shown in Tables 3.2 and 3.3 are the 1490 MHz rest-frame extended radio powers. A spectral index of $\alpha = 0.8$ has been assumed for these calculations. These powers, and those presented later in Table 3.6, have been obtained from a heterogenous set of radio observations at different frequencies and resolutions. This may imply that they are quite uncertain, but they will be mainly employed as variables for the ranking statistics in Sect. 3.4.2 and Sect. 3.4.3. Consequently this uncertainty should not be too important. The frequency of 1490 MHz and spectral index are chosen to correspond to those used by Antonucci & Ulvestad (1985).

3.3.2 THE OBSERVATIONS

The observational technique used to measure the quantities N and n_g in eqn. 3.3 was to take two deep CCD images for each quasar. The first field would be centred on the quasar (or slightly offset to avoid bright stars). The second field was be offset about 30 arcminutes away from the quasar. This corresponds to 4.5 Mpc at $z = 0.1$ for the cosmological parameters chosen in §3.2.3. The direction of this offset was chosen to avoid groups of bright stars visible on copies of the Palomar Observatory sky survey and SERC/ESO southern sky survey. The galaxy counts in the second field were used to estimate the background galaxy density n_g. All the observations were made using the Kitt Peak R filter. This waveband offers the best compromise between the rise in the spectral energy distribution of galaxies (towards $1\,\mu$m), and the decreasing sensitivity of the CCD detector above its peak at $\sim 0.5\,\mu$m.

The observations were made at the 2.5m Isaac Newton Telescope (INT) on La Palma in the Canary Islands. The instrument used was the prime focus CCD camera. This uses an RCA SID501 chip which has 320×512 30 μm pixels. At the INT prime focus, each pixel is 0.74 arcsec in angular size. This chip was preferred over the GEC chip , which has the lower read-out noise (3

e^-versus 55 e^-), because of the RCA chip's higher quantum efficiency. The ideal mode of observation was to take three 500s exposures for each field. This balanced the effects of saturation against the increased dominance of read-out noise in the shorter exposures. This procedure demanded that the telescope guiding accuracy over the 500s exposures was less than 1 arcsec. The INT has an autoguider which can easily achieve the guiding accuracy necessary. Unfortunately the autoguider was not functioning during about half the observations described here. When the telescope was unguided, the poor tracking of the INT forced shorter integrations than would have been preferred. The images appeared sufficiently elongated after 500s exposures for the exposure time to be reduced to 300s, and five separate exposures were needed for each field, and a consequent loss in signal-to-noise ensued.

Initial reduction was performed using the FIGARO data reduction package available on STARLINK. A problem was caused by the fact that all the images showed strong (3%) fringing. Unfortunately, a lineless light source for dome flats was not available. Consequently, it was necessary to flat-field the data by treating these (additive) intensity variations as (multiplicative) sensitivity variations. This ensures a systematic uncertainty in the photometry of a few percent. The flat fields were created by taking the median value for each pixel on the chip, which was found by comparing all sky-limited images scaled to have the same background level. These flat fields proved efficient at cosmetically flattening the images.

3.3.3 PHOTOMETRY

Detection of galaxies and the photometry was performed using a modification of the PPP algorithms of Howard Yee. Yee, Green & Stockman (1986) (hereafter YGS) describe the general principles behind these routines, so they will only be briefly outlined here. First all images with total intensity above a particular value were detected. This threshold value is specified as a certain percentage of

the sky background which is determined locally about each point on the chip. The percentage threshold was found by experiment for each frame. Un-weighted aperture photometry is then performed about each object. The algorithms use partial pixel weighting to include flux from pixels which do not lie wholly within the aperture. Where apertures for nearby objects overlap, the minimum point in the flux profile between the two centres is used to determine the object to which the pixels' flux is assigned. These fluxes were calculated for apertures from 2 pixels to 25 pixels in diameter. The sky value is estimated from a 10-pixel wide ring around the largest diameter. The algorithms described in YGS are then used to check the growth-curve and choose the largest aperture with a consistent value. Star-galaxy classification is determined by comparison with the growth-curve of a chosen star (or stars). The parameter used is that designated C by YGS.

$$C = \frac{1}{N-2}\sum_{i=3}^{N}(m_i - m_i^{\star}) - C_0, \tag{3.15}$$

where N is the highest accepted aperture for the object and $m_i^{\star}$ and m_i are the instrumental magnitudes for the reference star and object respectively. The parameter C_0 is the mean difference between the object and reference star magnitudes for the inner two apertures. An example of the distribution of this parameter is shown in Figure 3.2. The classes shown on this plot are those used by YGS to classify their images. Images classed as 1 or 2 are assumed to be galaxies, while images classified as 3 are stars and images classified as 0 are more tightly peaked than stellar images and hence are presumably cosmic rays. For this chapter, all images classified as 0 or 3 (i.e. spurious images or stars) are rejected for $R < 21.5$. However the poor signal-to-noise of the fainter objects could conceivably move galaxies into the stellar locus at faint magnitudes. The number of galaxies should greatly exceed the number of stars at these magnitudes (e.g. Tyson & Jarvis 1979). For these reasons, it was decided to include all class 1 objects fainter than $R = 21.5$ in the galaxy counts. The remaining two classes are assumed to contain all the detectable galaxies on the image. Finally all the magnitudes are extrapolated to a common aperture of

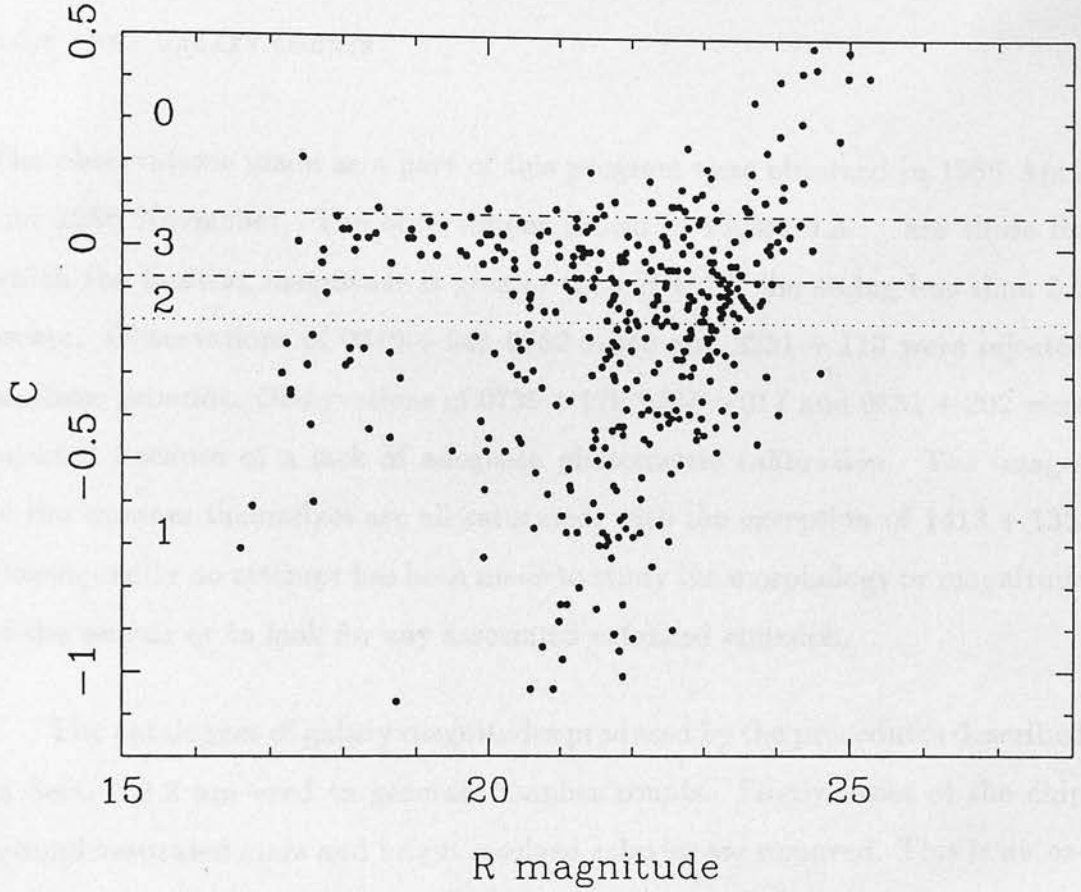

Figure 3.2: A plot of the star-galaxy separation parameter, C, versus R magnitude for field containing the quasar $1545+210$. The dashed lines show the image classes (0) cosmic rays (1) galaxies (2) possible galaxies and (3) stars.

diameter 17 pixels or 12.58 arcsec (corresponding to a metric diameter of 90 h^{-1} kpc at $z = 0.4$). The curve-of-growth used to extrapolate these magnitudes is that of the reference star, which is not strictly the correct one to use for the galaxies. This is the procedure adopted by YGS and the errors so introduced should be small.

3.3.4 THE GALAXY COUNTS

The observations made as a part of this program were obtained in 1986 April and 1986 November. The observations shown in Figure 3.3 are those for which the limiting magnitude is greater than $R = 22$, the seeing less than 3.5 arcsec. Observations of $0340 + 048, 0752 + 258$ and $2251 + 113$ were rejected on these grounds. Observations of $0735 + 178, 0736 + 017$ and $0851 + 202$ were rejected because of a lack of adequate photometric calibration. The images of the quasars themselves are all saturated, with the exception of $1413 + 135$. Consequently no attempt has been made to study the morphology or magnitude of the quasar or to look for any associated extended emission.

The catalogues of galaxy magnitudes produced by the procedures described in Sect. 3.3.2 are used to generate number counts. Firstly areas of the chip around saturated stars and bright resolved galaxies are removed. This is necessary as the object finding routine has a tendency to resolve these objects into spurious 'galaxies'. This is a particular problem with the diffraction spikes of bright stellar images. The differential number-magnitude relation is then plotted and the modal magnitude value is estimated. The limiting magnitude is assumed to be 0.20 mag less than this value. The limiting magnitude is then corrected for the effects of interstellar extinction using the $E(B - V)$ values of Burstein & Heiles (1982) and the extinction curve of Rieke & Lebofsky (1985). The resulting number counts are shown in Table 3.4. Catalogues of the objects found in these frames are not presented here, because of the number of galaxies detected. The values of B_{gq} have been calculated using the LF models described

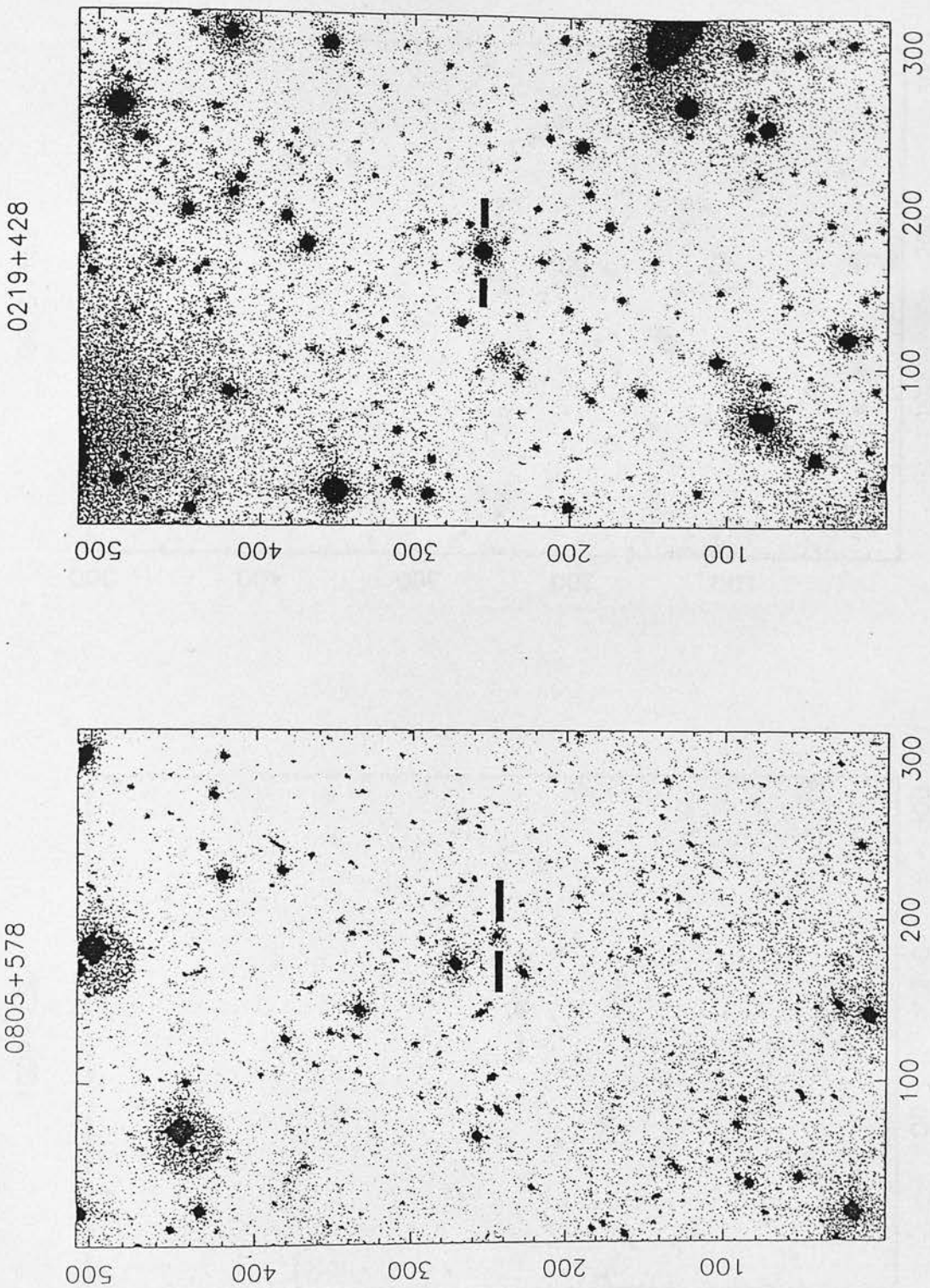

Figure 3.3: (*a*,*b*) Grey-scale representations of the CCD data. In each case the quasar is marked. The frames are oriented such that North is to the right and East is to the top.

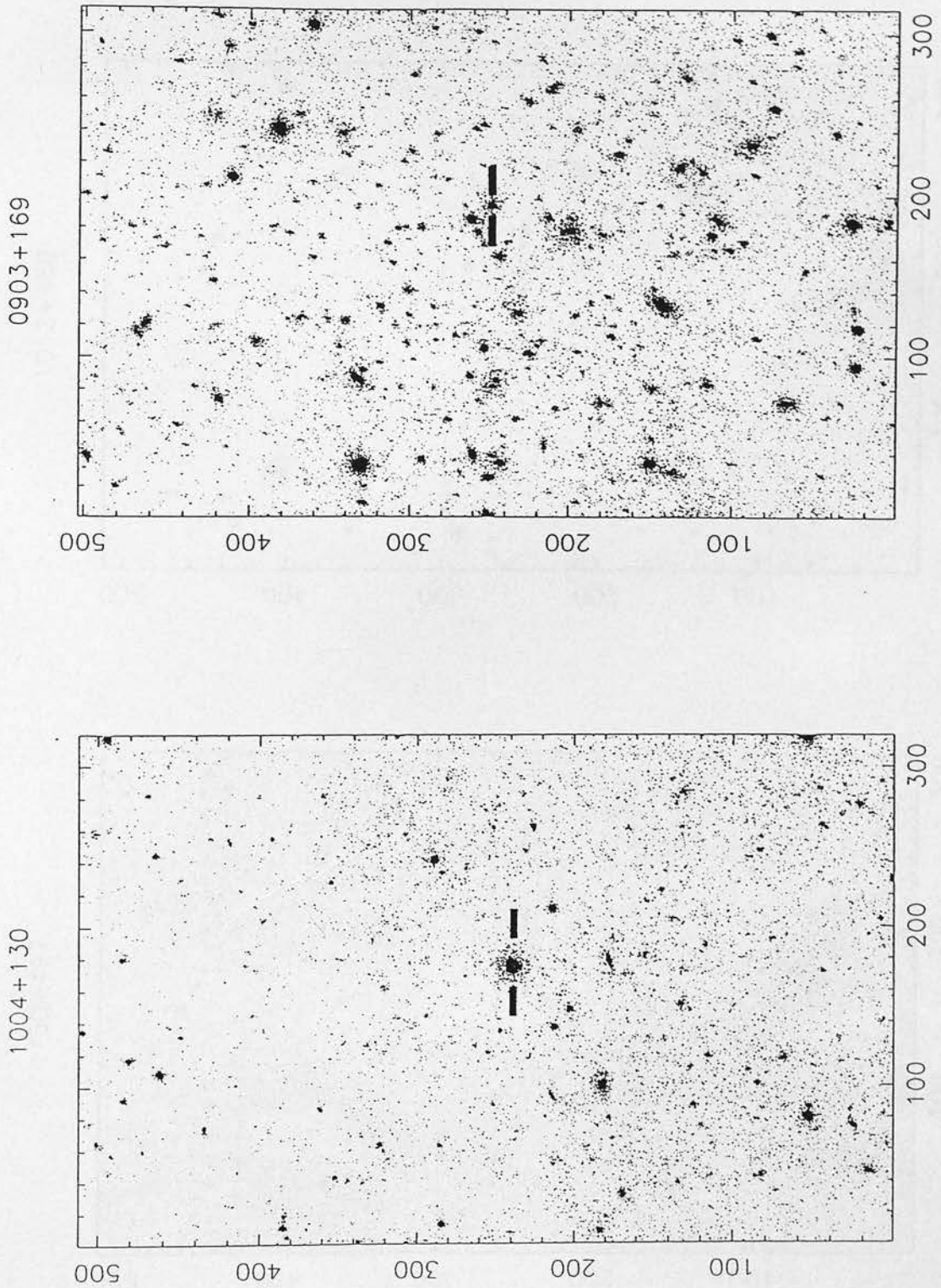

Figure 3.3: (*c,d*) Grey-scale representations of the CCD data.

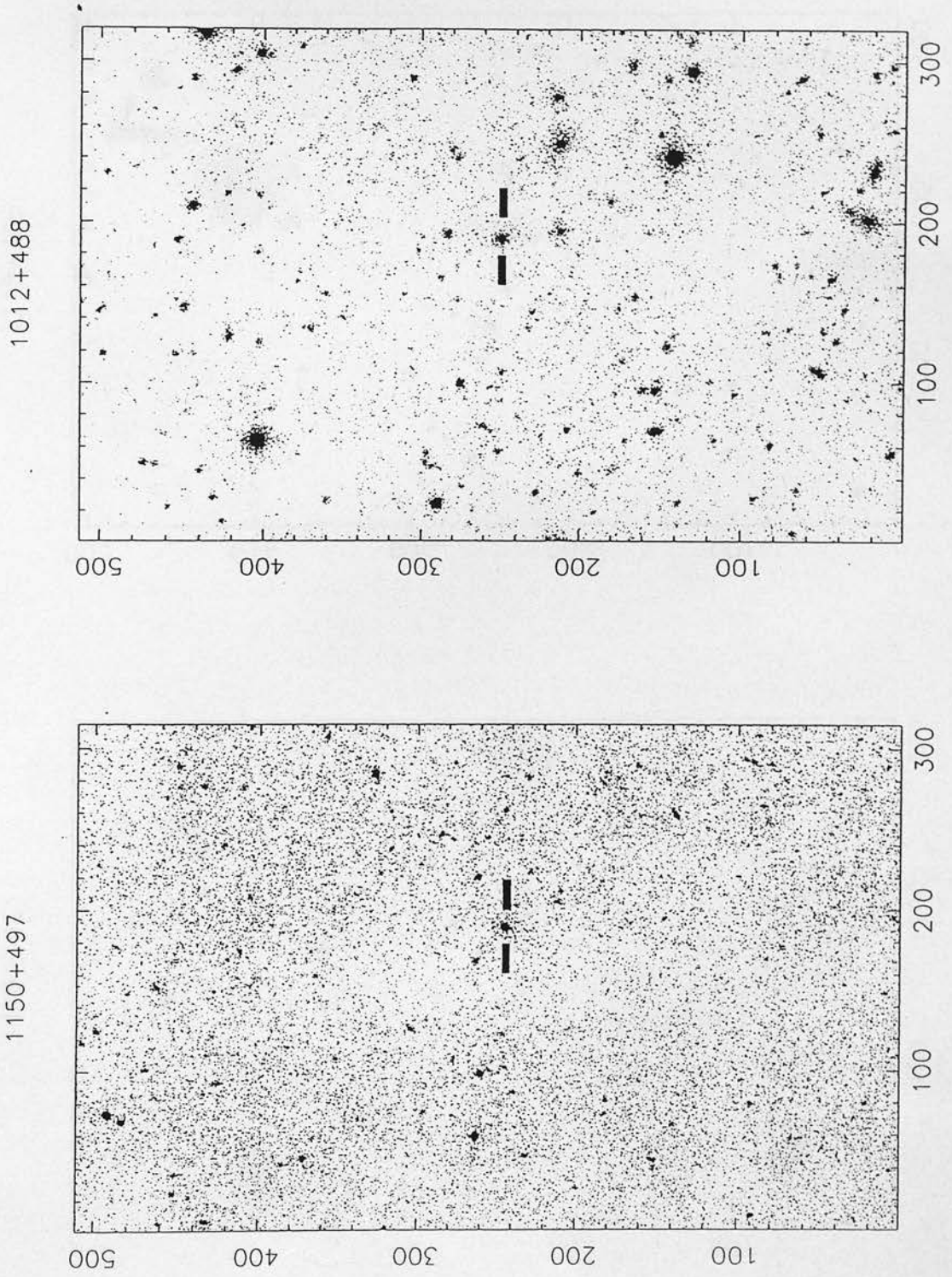

Figure 3.3: (*e,f*) Grey-scale representations of the CCD data.

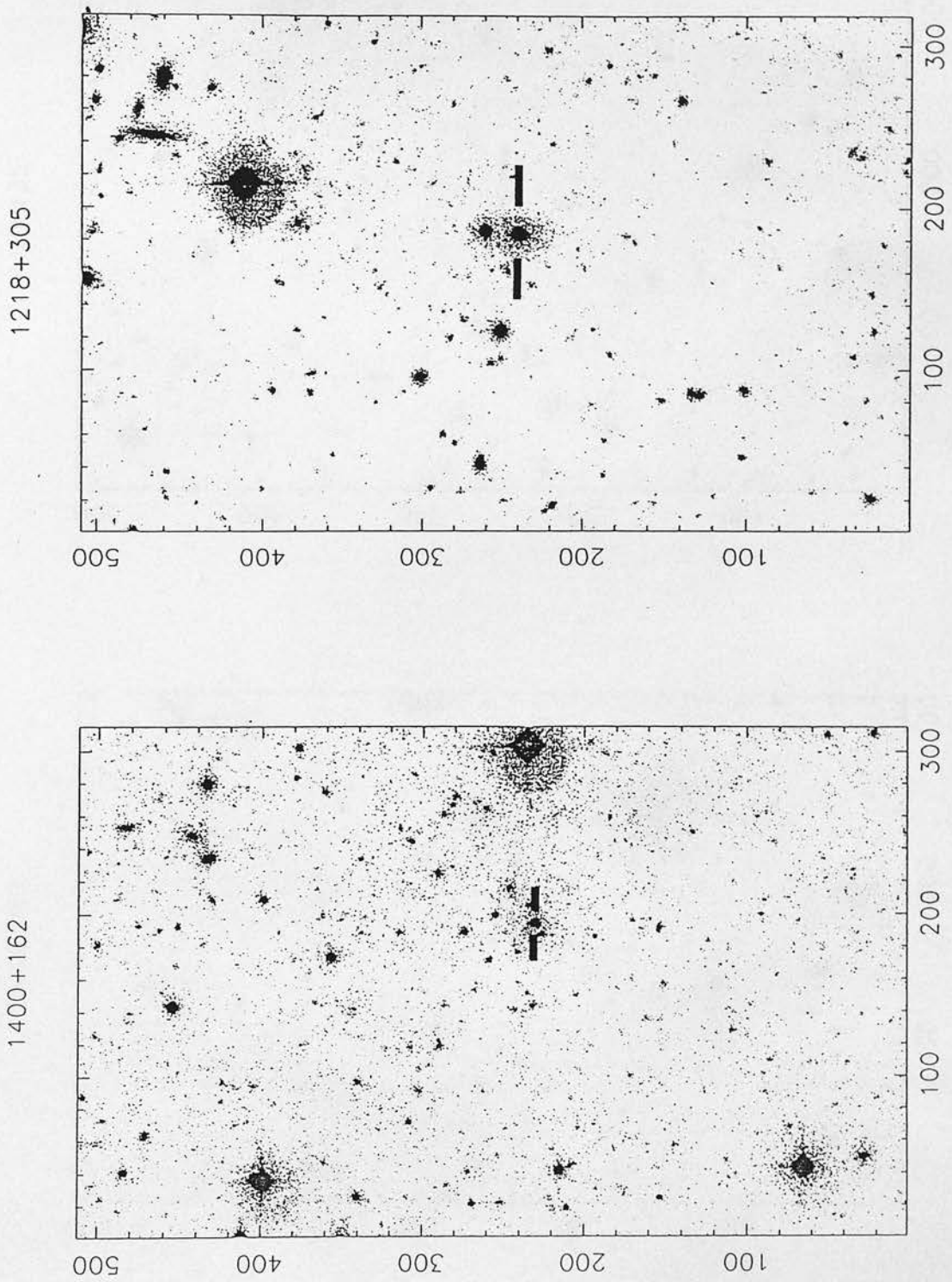

Figure 3.3: (g,h) Grey-scale representations of the CCD data.

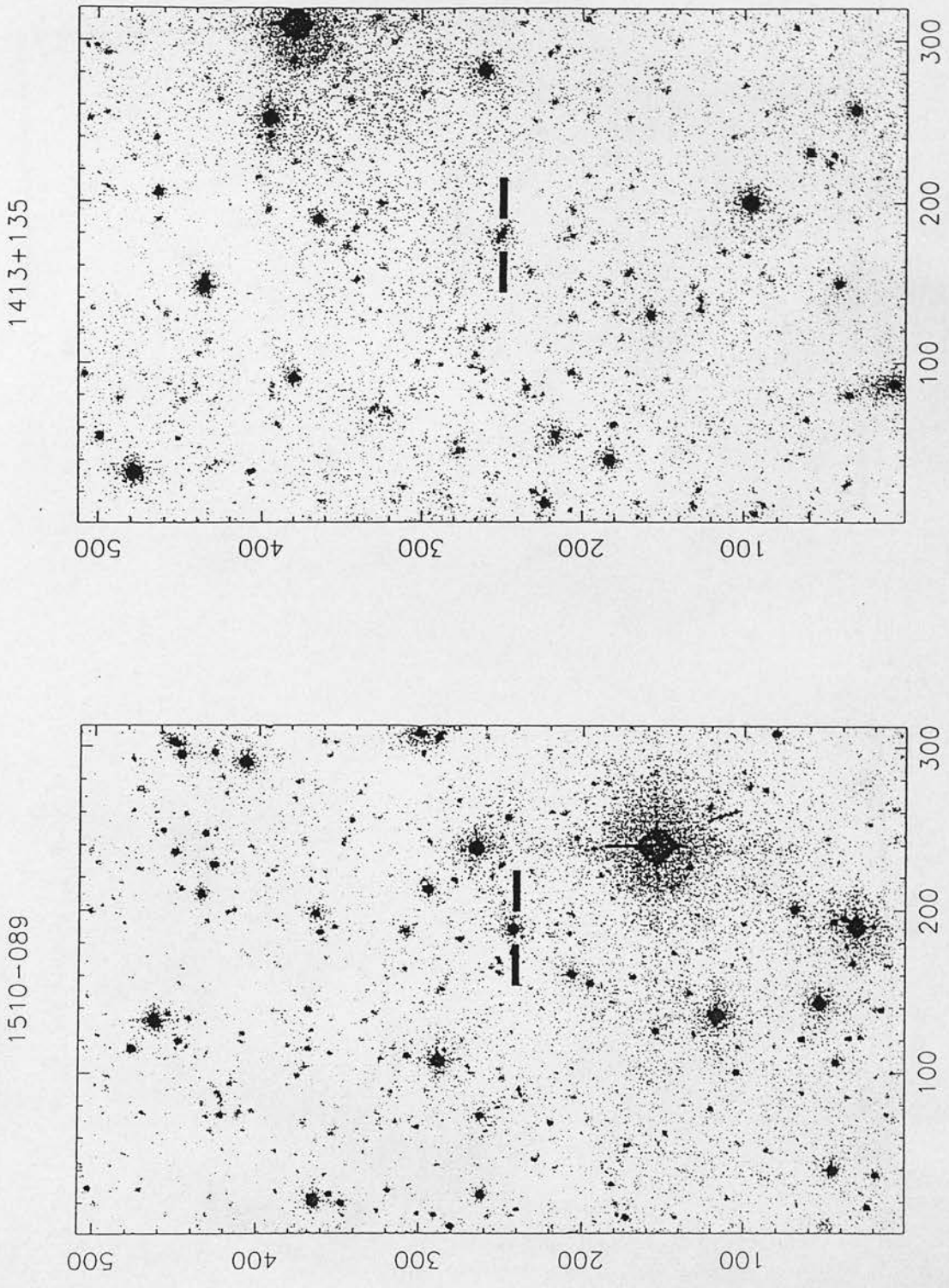

Figure 3.3: (i,j) Grey-scale representations of the CCD data.

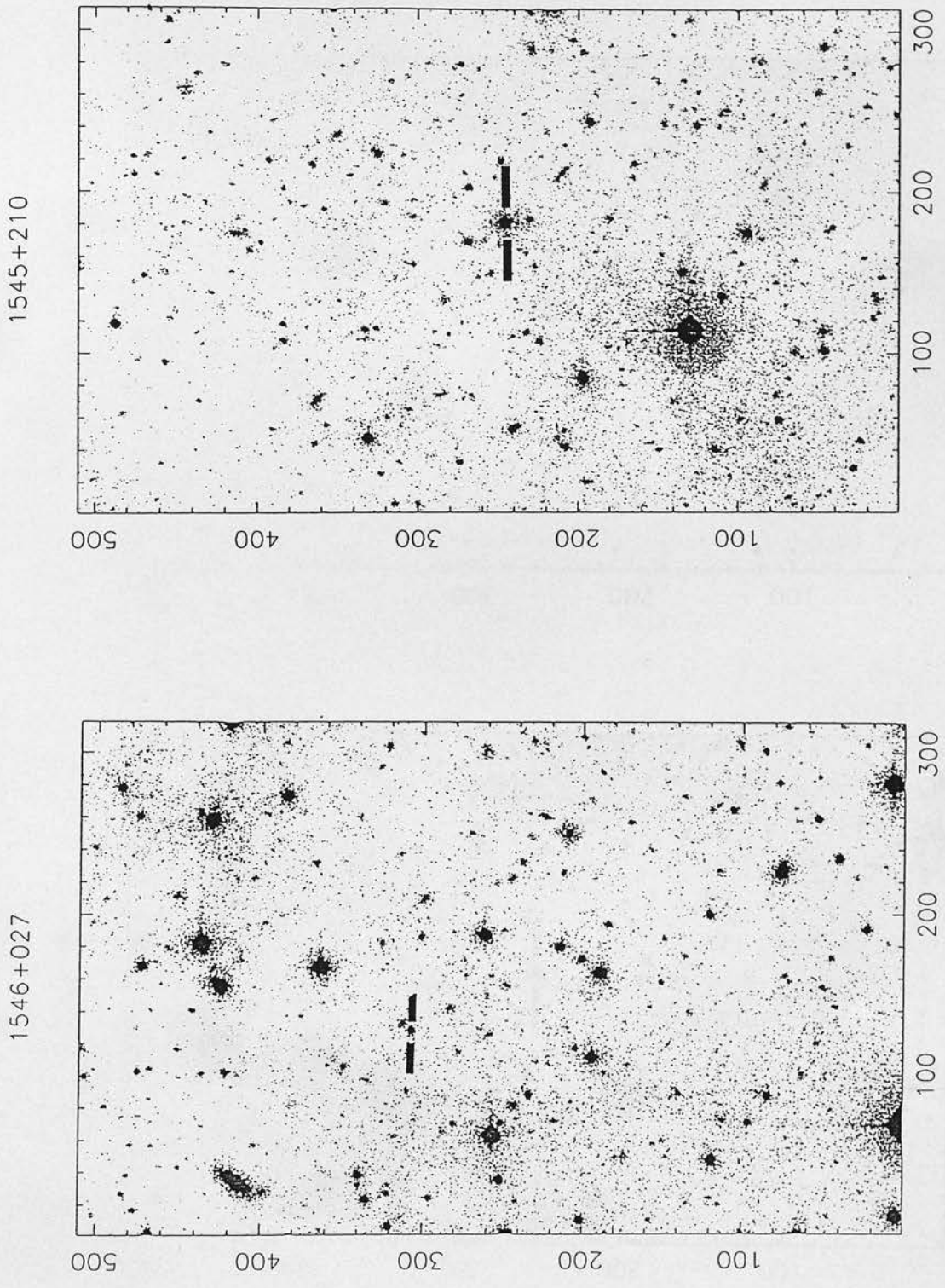

Figure 3.3: (k,l) Grey-scale representations of the CCD data.

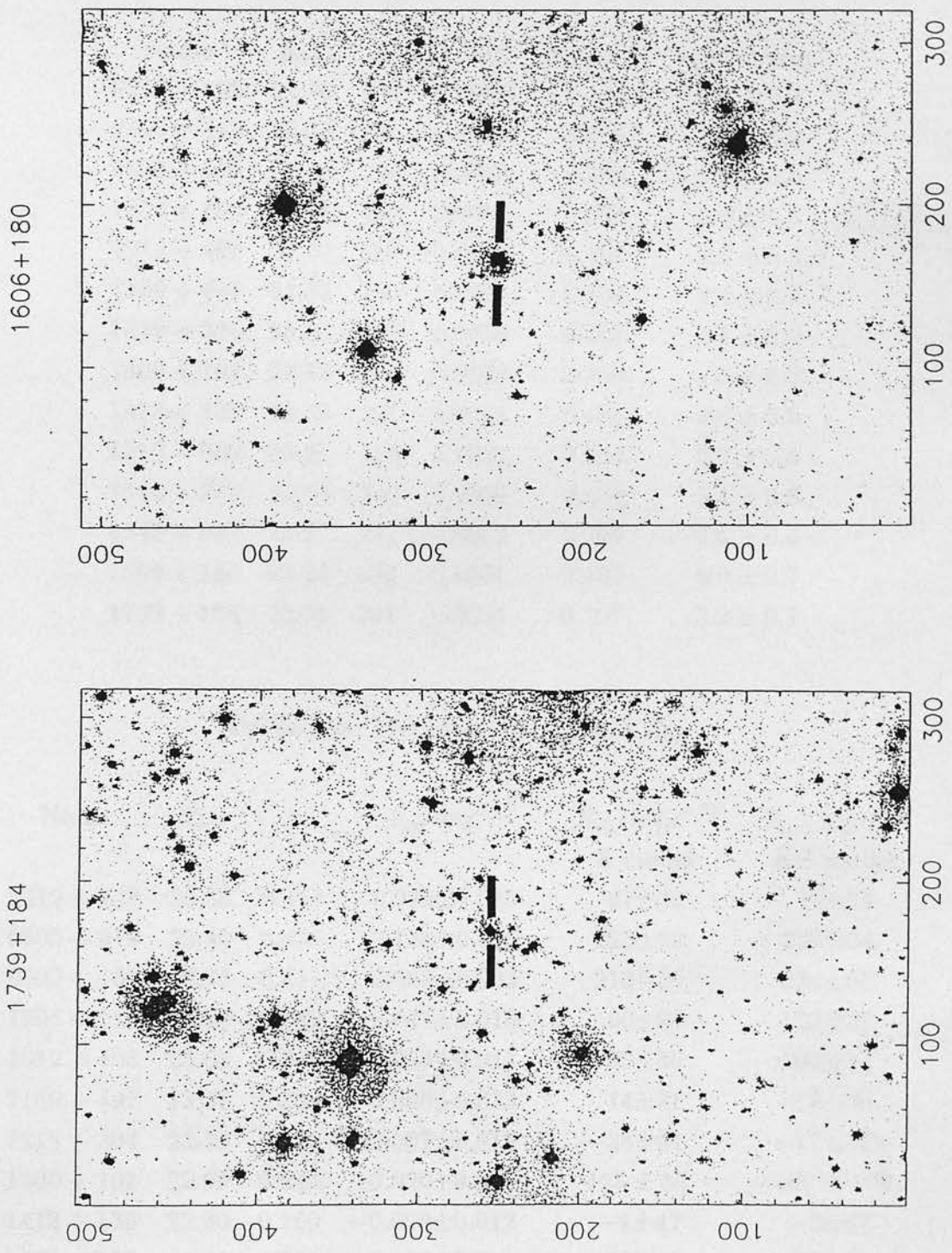

Figure 3.3: (m,n) Grey-scale representations of the CCD data.

Table 3.4: The galaxy counts.

Name	R_{lim}	N	Ω/deg^2	$J/\mathrm{deg}^{1.23}$	$n_g/10^4/\mathrm{deg}^2$
$0219+428$	23.56	223	0.0063	0.109	2.4 ± 0.4
$0805+578$	23.40	301	0.0059	0.106	1.5 ± 0.2
$0903+169$	22.75	236	0.0060	0.105	1.6 ± 0.5
$1004+180$	23.18	180	0.0062	0.108	1.6 ± 0.3
$1012+488$	23.64	267	0.0061	0.107	2.7 ± 0.4
$1150+497$	23.37	159	0.0061	0.106	2.4 ± 0.3
$1218+304$	23.30	207	0.0058	0.107	4.1 ± 0.5
$1400+162$	22.69	166	0.0059	0.106	4.3 ± 0.2
$1413+135$	23.30	221	0.0061	0.108	3.6 ± 0.5
$1510-089$	23.31	223	0.0054	0.104	3.7 ± 0.5
$1545+210$	23.86	340	0.0060	0.104	5.1 ± 0.6
$1546+027$	23.07	177	0.0059	0.105	2.6 ± 0.4
$1606+180$	23.23	311	0.0061	0.102	5.9 ± 0.7
$1739+184$	22.65	211	0.0055	0.107	5.2 ± 0.7

Table 3.5: The values of A_{gq} and B_{gq}.

Name	R_{lim}	z	$A_{gq}/\mathrm{deg}^{0.77}$	$B_{gq}/\mathrm{Mpc}^{1.77}$ S model	$B_{gq}/\mathrm{Mpc}^{1.77}$ KE model
$0219+428$	23.56	0.444	0.029 ± 0.015	67 ± 33	73 ± 84
$0805+578$	23.40	0.438	0.138 ± 0.025	223 ± 22	236 ± 24
$0903+169$	22.75	0.411	0.083 ± 0.033	213 ± 59	234 ± 58
$1004+180$	23.18	0.240	0.047 ± 0.016	86 ± 26	123 ± 37
$1012+488$	23.64	0.385	0.034 ± 0.013	83 ± 30	102 ± 37
$1150+497$	23.37	0.334	0.006 ± 0.013	14 ± 31	18 ± 39
$1218+304$	23.30	0.130	-0.007 ± 0.012	-38 ± 64	-77 ± 122
$1400+162$	22.69	0.244	-0.020 ± 0.014	-125 ± 84	-160 ± 108
$1413+135$	23.30	0.260	-0.000 ± 0.012	-1 ± 47	-2 ± 67
$1510-089$	23.31	0.361	0.006 ± 0.011	24 ± 45	28 ± 53
$1545+210$	23.86	0.264	0.006 ± 0.011	26 ± 47	41 ± 73
$1546+027$	23.07	0.413	0.009 ± 0.013	31 ± 46	32 ± 46
$1606+180$	23.23	0.346	-0.008 ± 0.012	-52 ± 80	-62 ± 95
$1739+184$	22.65	0.186	-0.013 ± 0.012	-108 ± 97	-156 ± 142

in Sect. 3.2.3 and are shown in Table 3.5. There are two problem objects. As a result of technical malfunction, no comparison frame for $0903+169$ was obtained. In order to estimate n_g the background counts of all the comparison frames at $R = 23$ were compared. The value of $2.0 \times 10^4\,\mathrm{deg}^{-2}$ was used as the median value. This was scaled to the appropriate limiting magnitude, using a slope of 0.4 for the $\log N - \mathrm{mag}$ relation. This slope was estimated from the data of Shanks *et al.* (1984). The resulting n_g was used to calculate the values of A_{gq} and B_{gq} given in Table 3.5. An error in n_g of $5.0 \times 10^3\,\mathrm{deg}^{-2}$ was assumed in order to estimate the errors. The comparison frame for $1400+162$ contains a low-redshift galaxy cluster. This cluster causes a high value of n_g to be estimated. Consequently the values of A_{gq} and B_{gq} are negative. However, adopting the procedure, described above, for estimating n_g, produces high values. This could possibly be a result of the cluster being of low enough redshift to extend onto the quasar frame. In order to avoid biassing of the results, it was decided that it would be safer to ignore this object in the following discussions.

3.4 Discussion

3.4.1 THE PROBLEM OF Φ

All the values of B_{gq}, given in Table 3.5, have been calculated using the method described in Section 3.2.3 to evaluate the LF integral, $\Phi(m,z)$ in eqn. 3.8. Two determinations of the local LF have been used. These are those of Sebok(1986) and King & Ellis (1985) (see Table 3.1). The combination of these LFs and the $K_i(z)$ obtained from the model of Guiderdoni & Rocca-Volmerange (1987), are referred to as the S and KE models respectively. Table 3.5 shows that there is no significant difference between the values of B_{gq} obtained using the two models. From here on the KE model values will be neglected. This should not be taken as implying that these values are thought to be less accurate than those obtained using the S model.

A problem does arise when comparing the values of B_{gq} calculated using either the S or KE models with those of YG. Table 3.6 shows YG's calculated values of B_{gq} and those evaluated using the S model and YG's galaxy counts. The disparity is large. The S model value for 1137+66 is a factor of 2.86 smaller than YG's value. YG used a very different method to estimate Φ. The model (S2 in their notation) used to obtain their tabulated B_{gq} values was based on an un-normalised Sebok (1986) LF (their model S2) in an H_0= 50 km s^{-1} Mpc^{-1}, q_0=0.5 cosmology. Their K-correction was obtained from Sebok (1986), while their evolution correction was estimated from the values of $M^\star$ obtained from fits of the Schechter (1976) LF to the observed distribution of excess galaxies in their quasar frames. YG calculated these values of $M^\star$ for three redshift bins, and then parameterised their evolution according to the form adopted by Shanks *et al.* (1984). The values of the volume normalisation constants, $\phi^\star$, were assumed to have the morphological mix of Sebok (1986), while the absolute scaling was provided by fits to their galaxy counts in the comparison frames. This absolute scaling results in their values of Φ being systematically smaller by a factor of 2.27 than the S model. The remaining difference between the the YG model and the S model is a result of both the different cosmological model and the $K_i(z)$. The latter function is very different for the YG model. YG's Table 3 gives $e_i(z)$ for their model as 0.93 ± 0.52 for $z = 0.42$. The appropriate K-correction from Sebok(1986) is $k_i(0.42) \approx 0.44$ for Sa and Sb galaxies. The corresponding $K_i(z)$ from the Guiderdoni & Rocca-Volmerange (1987) model is ~ 0.3. Differences in the $K_i(z)$ and the cosmology will together change the limits in the integrals over the Schechter function in eqn. 3.9. For magnitude limits fainter than $M^\star$ small changes in these limits can cause large changes in the values of these integrals, and hence large changes in Φ.

These differences in the two estimates of Φ make determining the absolute value of B_{gq} difficult. The uncertainty in $K_i(z)$ introduces potential redshift-dependent systematic uncertainties which may result in spurious correlations of B_{gq} with redshift (see Sect. 3.4.3). Furthermore, comparison with the results of

Table 3.6: The YG sample of quasars.

IAU Desig.	z	$\log P_{ext}$ [1]	B_{gq} [2]	B'_{gq} [3]
$0003+15$	0.450	25.58 [a]	473 ± 174	123 ± 56
$0044+03$	0.624		26 ± 291	9 ± 161
$0130+24$	0.457	25.54 [b]	-90 ± 97	-23 ± 51
$0134+32$	0.367		108 ± 118	37 ± 44
$0349-14$	0.614	26.27 [a]	731 ± 337	204 ± 131
$0742+31$	0.462	25.61 [c]	145 ± 181	40 ± 72
$1007+41$	(0.611)	26.14 [d]	-210 ± 212	-62 ± 135
$1048-09$	0.344	25.71 [a]	286 ± 160	88 ± 57
$1049+61$	0.422	25.71 [e]	-165 ± 80	-47 ± 58
$1058+11$	0.420	25.35 [a]	160 ± 131	28 ± 51
$1103-00$	0.422	25.65 [f]	-46 ± 98	-20 ± 53
$1104+16$	0.634	25.65 [f]	943 ± 381	279 ± 167
$1137+66$	0.652	26.53 [d]	993 ± 550	347 ± 235
$1156+63$	0.594		653 ± 388	230 ± 175
$1305+06$	0.599		792 ± 364	245 ± 144
$1510-08$	0.361		278 ± 141	52 ± 45
$1548+11$	0.436	25.08 [f]	304 ± 157	80 ± 54
$1618+17$	0.555	26.23 [f]	187 ± 220	52 ± 95
$1641+39$	0.595	25.95 [g]	773 ± 297	201 ± 100
$0931+43$	0.457		250 ± 152	92 ± 83
$0936+39$	0.458		186 ± 168	53 ± 70
$1216+06$	0.332		-44 ± 76	-12 ± 43
$1259+59$	0.473		-78 ± 121	-23 ± 69
$1333+17$	0.555		111 ± 251	38 ± 134
$1358+04$	0.427		24 ± 111	7 ± 55
$1543+48$	0.399		62 ± 101	17 ± 46

(1) Powers given in W Hz^{-1} sr^{-1} at a rest frame frequency of 1490 MHz.

(2) YG's values of B_{gq}. The units are $Mpc^{1.77}$.

(3) Recalculated values of B_{gq}, using the S model.

Radio references

(*a*) Miley & Hartsuijker (1977) (*b*) Potash & Wardle (1979) (*c*) Fanti *et al.* (1977) (*d*) Saikia, Kulkarni & Porcas (1986) (*e*) Owen, Porcas & Neff (1978) (*f*) Hintzen, Ulvestad & Owen (1983) (*g*) Antonucci & Ulvestad (1985).

Longair & Seldner (1979) and Prestage and Peacock (1988) or the Abell (1958) cluster richness classes are impossible if there are gross systematic uncertainties in the models used to calculate Φ. The YG model has the advantage that it is derived self-consistently from the observed galaxy-counts. However, the errors on the evolution correction are large, and this may have affected the fitted values of ϕ^*. In contrast, the S model represents the best guess at the way the locally determined LF evolves according to current models of galaxy evolution, but the discrepancy with the YG model is extreme. Consequently great care should be taken when comparing the results presented here with those of other authors. A further complication is introduced by the fact that both PP and YG quote B_{gq} relative to the mean correlation amplitude for galaxies, $\langle B_{gg} \rangle$. However, they choose different values for this. PP use $\langle B_{gg} \rangle = 40$ from Groth & Peebles (1978), while YG use $\langle B_{gg} \rangle = 67.5$ from Davis & Peebles (1983). YG note that this latter value lies at the upper end of a large distribution of values reported in the literature. The unnormalised B_{gq} values given in Tables 3.5 and 3.6 will be used in the remainder of this chapter.

3.4.2 THE ENVIRONMENTS OF BLAZARS AND THE UNIFIED SCHEME

The observations presented in Sect. 3.3.4 present data on six blazars and seven extended radio quasars (excluding 1400+162). YG observed two blazars, 1510−089 and 1641 + 399, and two of the sources from Table 3.3, 0003 + 158 and 1048 − 090. The two observations of 1510 − 089 have been combined to give an estimate of B_{gq} of 38 ± 32. The weighted mean and error of the seven blazar B_{gq}'s is 33 ± 15. For the nine extended radio quasars the mean B_{gq} is 127 ± 13. There is a thus a tendency in these data for the quasars to be in denser environments. However estimating the significance of this result is impossible unless the distributions of the B_{gq} in the two populations are known. A non-parametric statistical test is required. Conover (1980) describes the Mann-Whitney test for determining if two random samples are drawn from identical distributions. The null hypothesis is that the B_{gq} distributions are

identical for both the blazar sample and the quasar sample. Using the Mann-Whitney test, this hypothesis cannot be rejected, even for the $\alpha = 0.2$ level of significance. There is thus no convincing evidence that the environments of blazars are different from those of the extended radio quasars. This is entirely consistent with the results of the unified scheme. However, without the highly uncertain, YG measurement of the environment of $1641 + 399$, the difference is significant at the 10% level. So the result may be suggestive enough to merit further study.

Although the result achieved by this experiment is a null result, it is worthwhile to briefly discuss the validity of this experiment as a test of the unified scheme. The sample of blazars listed in Table 3.2 is by no means a homogeneous sample of objects with similar properties. Some of the blazars listed have been selected as a result of X-ray surveys. There is some indication that these objects may have quite distinct properties from the other blazars (Ledden & O'Dell 1985). One of these, $1218 + 304$, has been observed as part of this program and the measured B_{gq} is the lowest of all the blazars, though the errors are large enough for this not to be significant. Another problem is the extended radio powers. Of the blazars that we observed, only three have measured powers. These are consistent with the powers of the comparison quasar sample, so the test of the unified scheme has been formulated correctly if the unknown blazar powers are similar. However, some of the blazar radio powers from Table 3.2 are much smaller than those of the extended radio quasars. These quasars cannot be the candidate misaligned counterparts of the blazars with weak radio powers ($0735 + 178, 0851 + 202, 1749 + 096$ etc.). To complete this experiment properly it is thus important to obtain extended radio powers for all the blazars in the sample.

3.4.3 THE CORRELATION OF B_{gq} WITH REDSHIFT

The main result of YG was that the strength of the cluster environments of quasars appeared to correlate with redshift. In Sect. 3.4.1 the differences between their values of B_{gq} and those found using the S model for Φ were discussed. The uncertainties in the $K_i(z)$ could potentially cause spurious redshift dependencies in the B_{gq}. Figure 3.4 shows the plot of B_{gq} versus z for the YG sample (including the optically-selected quasars), using both the YG and S models for Φ. The significance of this correlation and the others discussed in this section are estimated using the Spearman rank correlation statistic (e.g. Conover 1980). The values and levels of significance of these correlations are given in Table 3.7. The correlation of B_{gq} with z is marginally more significant for the S model than for the YG model. This confirms that the different forms of $K_i(z)$ can indeed affect the redshift dependence of B_{gq} but shows that this effect is not large.

Figure 3.5 [p] shows the plot of B_{gq} versus z for the combined sample of YG's radio-loud quasars and the blazars and quasars observed as part of the test of the unified scheme. This sample consists of 31 quasars and confirms the significance of the $B_{gq}-z$ correlation. No distinction has been made between the blazars and other quasars in this plot. YG considered whether the correlation they saw in their data was a real example of evolution with redshift or a selection effect. Specifically they looked for a correlation with the absolute magnitude of the quasars and found no evidence that B_{gq} depends on the quasar's luminosity. However the correlation with redshift arises almost entirely amongst the radio-loud members of YG's sample. There is no evidence for the correlation amongst the 7 radio-quiet quasars. Consequently the possibility that the correlation might be a result of a radio selection effect must also be examined.

There are 23 members of the combined sample for which extended radio powers are available (see Tables 3.2, 3.3 and 3.6). Extended radio powers are used in the examination of radio-selection effects as these should be unbeamed

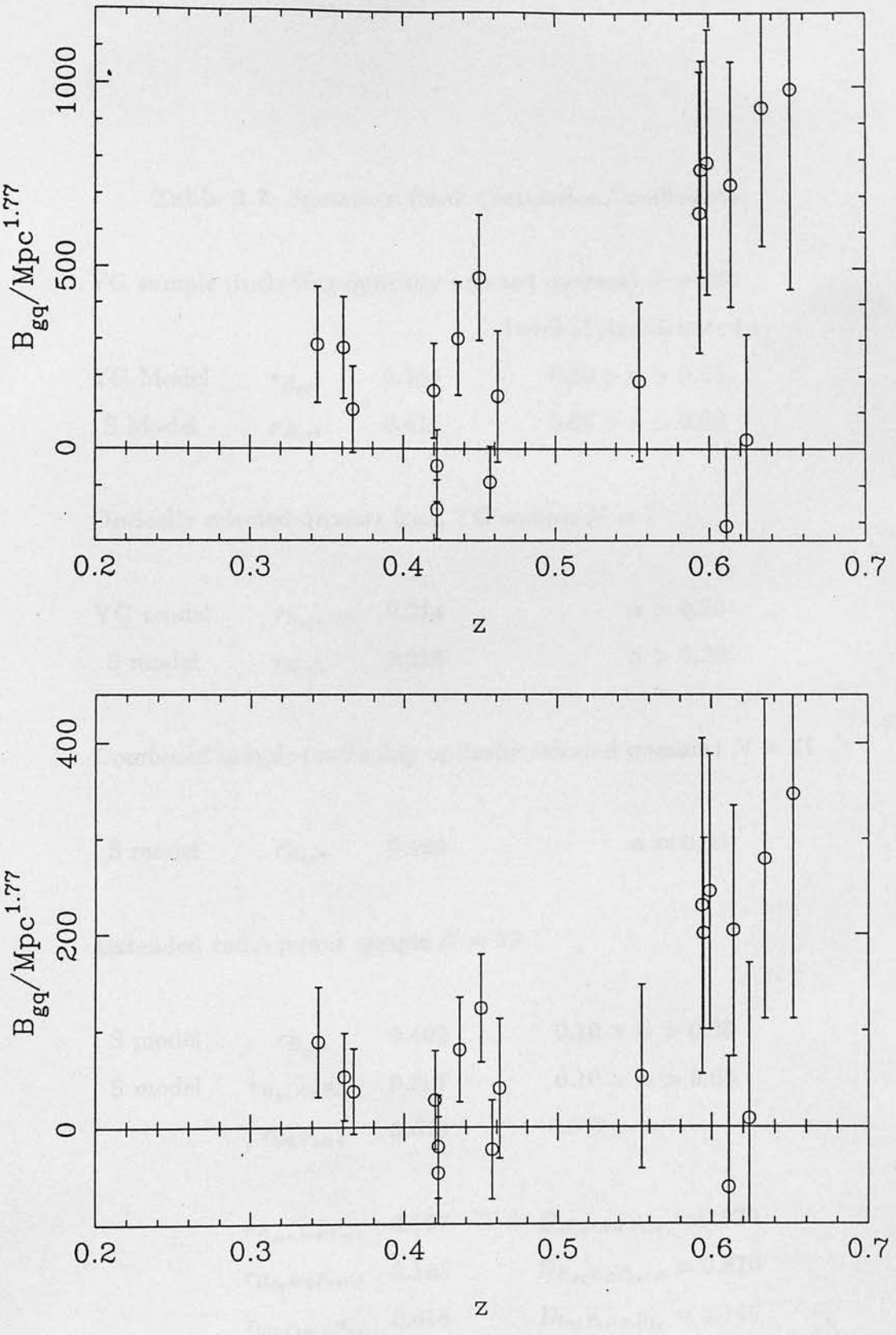

Figure 3.4: Plots of B_{gq} versus z for the YG sample using (a) the YG LF and (b) the Sebok LF.

Table 3.7: Spearman Rank Correlation Coefficients.

YG sample (including optically selected quasars) $N = 26$

			Level of significance (α)
YG Model	$r_{B_{gq}z}$	0.383	$0.10 > \alpha > 0.05$
S Model	$r_{B_{gq}z}$	0.413	$0.05 > \alpha > 0.02$

Optically selected quasars from YG sample $N = 7$

YG model	$r_{B_{gq}z}$	0.214	$\alpha > 0.20$
S model	$r_{B_{gq}z}$	0.214	$\alpha > 0.20$

Combined sample (excluding optically selected quasars) $N = 31$

S model	$r_{B_{gq}z}$	0.466	$\alpha \approx 0.03$

Extended radio power sample $N = 23$

S model	$r_{B_{gq}z}$	0.402	$0.10 > \alpha > 0.05$
S model	$r_{B_{gq}\log P_{ext}}$	0.397	$0.10 > \alpha > 0.05$
	$r_{\log P_{ext}z}$	0.679	$0.002 > \alpha$
	$r_{B_{gq}z,\log P_{ext}}$	0.197	$D_{B_{gq}z,\log P_{ext}} = 0.870$
	$r_{B_{gq}\log P_{ext},z}$	0.185	$D_{B_{gq}\log P_{ext},z} = 0.816$
	$r_{\log P_{ext}z,B_{gq}}$	0.618	$D_{\log P_{ext}z,B_{gq}} = 3.146$

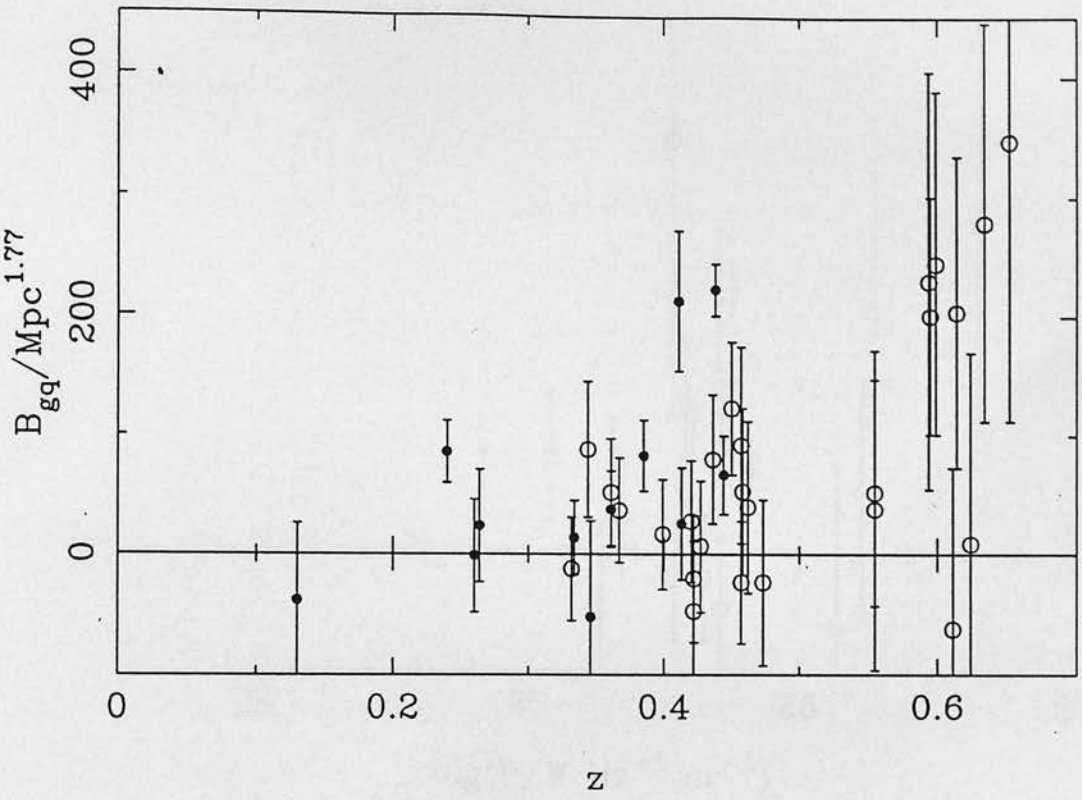

Figure 3.5: B_{gq} versus z for the combined sample using the Sebok LF.

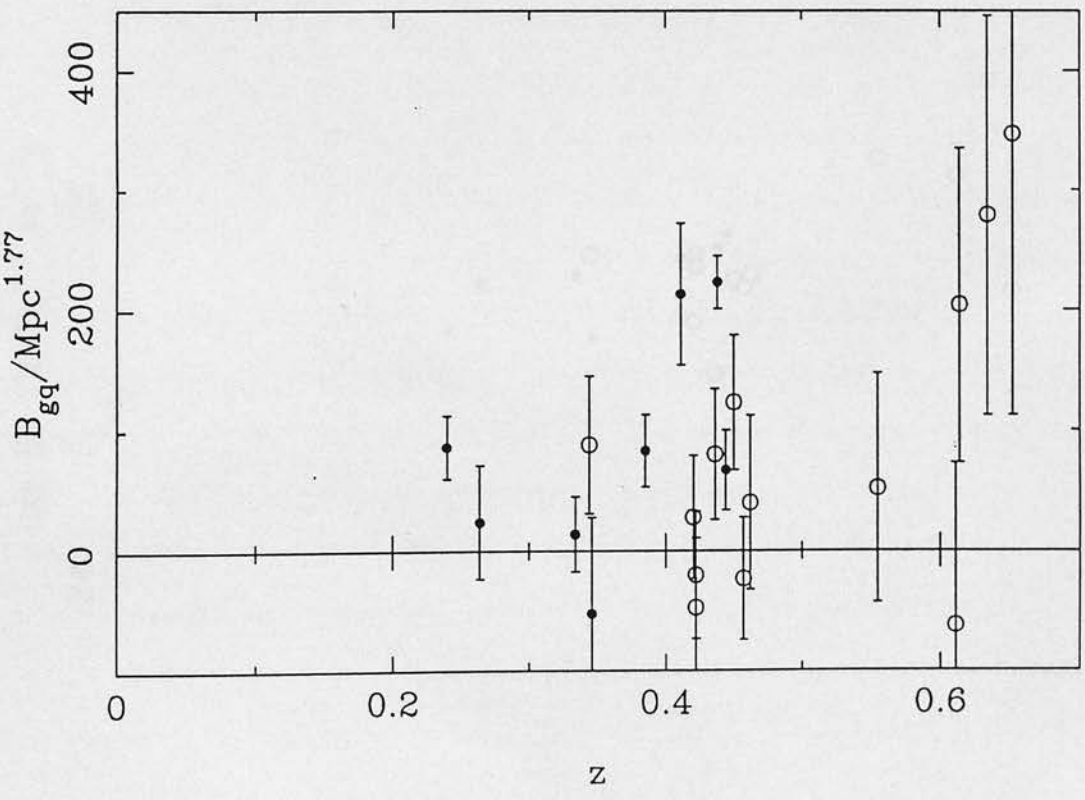

Figure 3.6: (*a*) B_{gq} versus z for the $\log P_{ext}$ sample; Sebok LF.

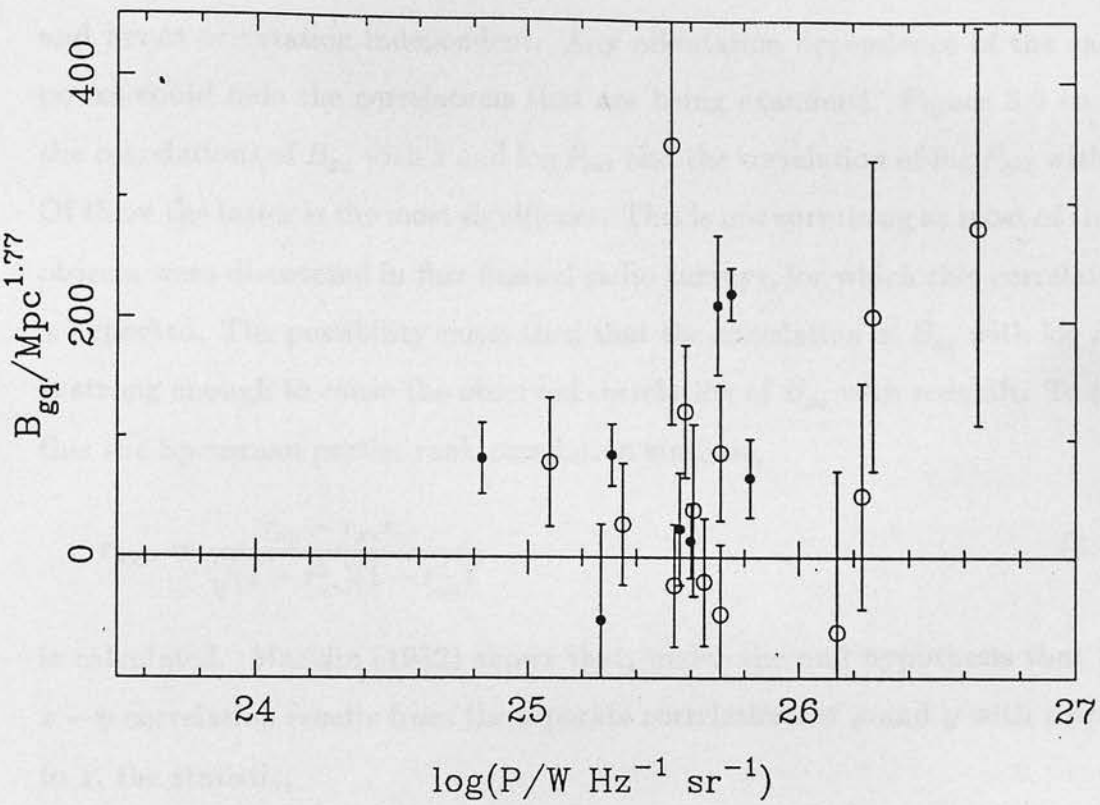

Figure 3.6: (*b*) B_{gq} versus $\log P_{ext}$ for the $\log P_{ext}$ sample; Sebok LF.

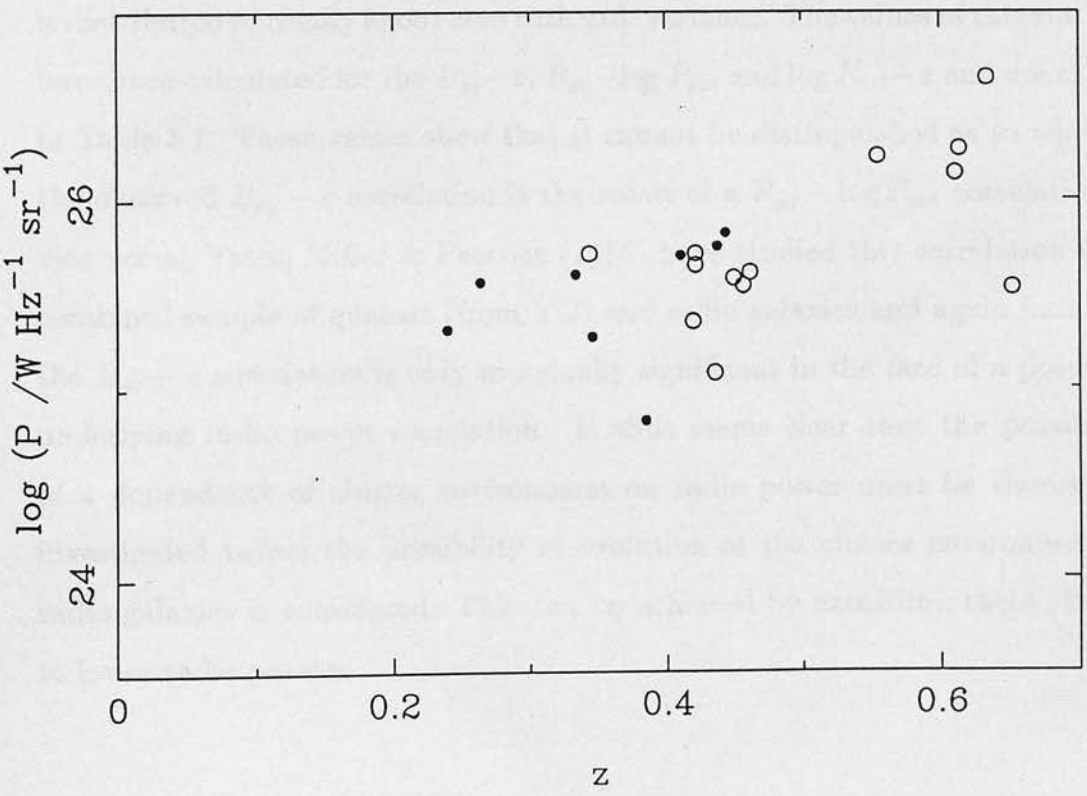

Figure 3.6: (*c*) $\log P_{ext}$ versus z for the $\log P_{ext}$ sample.

and hence orientation independent. Any orientation dependence of the radio power could hide the correlations that are being examined. Figure 3.6 shows the correlations of B_{gq} with z and $\log P_{ext}$ and the correlation of $\log P_{ext}$ with z. Of these the latter is the most significant. This is not surprising as most of these objects were discovered in flux limited radio surveys, for which this correlation is expected. The possibility exists then that the correlation of B_{gq} with $\log P_{ext}$ is strong enough to cause the observed correlation of B_{gq} with redshift. To test this the Spearman partial rank correlation statistic,

$$r_{xy,z} = \frac{r_{xy} - r_{xz}r_{yz}}{\sqrt{(1 - r_{xz}^2)(1 - r_{yz}^2)}}, \tag{3.16}$$

is calculated. Macklin (1982) shows that, under the null hypothesis that the $x - y$ correlation results from the separate correlations of x and y with respect to z, the statistic,

$$D_{xy,z} = \frac{1}{2}(N - 4)^{\frac{1}{2}} \ln\left(\frac{1 + r_{xy,z}}{1 - r_{xy,z}}\right), \tag{3.17}$$

is distributed normally about zero with unit variance. The values of this statistic have been calculated for the $B_{gq} - z$, $B_{gq} - \log P_{ext}$ and $\log P_{ext} - z$ and are shown in Table 3.7. These values show that it cannot be distinguished as to whether the observed $B_{gq} - z$ correlation is the result of a $B_{gq} - \log P_{ext}$ correlation or vice versa. Yates, Miller & Peacock (1988) have studied this correlation for a combined sample of quasars (from YG) and radio galaxies and again find that the $B_{gq} - z$ correlation is only marginally significant in the face of a potential underlying radio power correlation. It thus seems clear that the possibility of a dependence of cluster environment on radio power must be thoroughly investigated before the possibility of evolution of the cluster environment of radio galaxies is considered. This can be achieved by extending these studies to lower radio powers.

3.5 Concluding Remarks

This chapter has presented a study of the cluster environment of blazars in relation to a study of the cluster environment of quasars in general. The conclusions can be summarised as follows;

(a) The measurement of the galaxy-quasar covariance amplitude, B_{gq}, is fraught with systematic errors. These mainly involve the choice of luminosity function, K-correction and galaxy evolution. When measuring the environment of quasars at intermediate redshift ($z \approx 0.5$), different models can cause very different estimations of B_{gq}. This makes comparison of results of different such studies very difficult unless either the raw data (Table 3.4) or a complete specification of the LF are provided. Nevertheless provided a consistent prescription for the LF is used, studies such as those presented in this chapter are possible. However, this is always with the proviso that the form of the LF used may introduce systematic errors which mimic evolution with redshift.

(b) No significant difference can be detected between the environments of seven blazars and nine extended radio quasars. This result is consistent with the prediction of 'unified schemes' where core radio and optical emission from quasars is beamed and the two samples represent aligned and misaligned sources respectively. However, this result is based on a relatively small number of objects, consequently the significance of the differences that are seen is low. In order to extend the study, it is necessary to include more blazars. The possibility of a correlation of B_{gq} with radio power confirms that it is essential that the two samples be selected so as to have the same distribution of radio powers.

(c) The apparent correlation of B_{gq} with redshift found by YG is confirmed. However a marginal correlation of B_{gq} with extended radio power is also seen. It cannot be distinguished whether the redshift correlation is intrinsic and the apparent correlation of B_{gq} with radio power is a result of this correlation and the expected correlation of radio power with redshift, or vice versa. In order to investigate this it is necessary to observe quasars of a narrow range of radio power over a wide redshift range or of a narrow range of redshift over a wide

range of radio power. Given the uncertainties in $K(Z)$, expressed above, it is expected that the latter would provide a more conclusive test as to whether the radio power effect is truly an intrinsic correlation with redshift. However, if this is not sufficient to explain the $B_{gq} - z$ correlation, this does not necessarily prove that this is intrinsic. The effects of the systematic uncertainties in the LF (and of course the effect of q_0) could induce some redshift effects.

References

Abell, G.O., 1958. *Astrophys. J. Suppl.*, **3**, 211.

Abramowicz, M.A., Calvani, M. & Nobili, L., 1980. *Astrophys. J.*, **242**, 772.

Allen, D.A., Ward, M.J. & Hyland, A.R., 1982. *Mon. Not. R. astr. Soc.*, **199**, 969.

Aller, H.D., Aller, M.F. & Hughes, P.A., 1985. *Astrophys. J.*, **298**, 296.

Aller, H.D., Aller, M.F., Latimer, G.E. & Hodge, P.E., 1985. *Astrophys. J. Suppl.*, **59**, 513.

Altschuler, D.R., 1980. *Astr. J.*,**85**, 1559.

Angel, J.R.P. & Stockman, H.S. (AS80), 1980. *Ann. Rev. Astron. Astrophys.*, **18**, 321.

Antonucci, R.R.J., 1986. *Astrophys. J.*, **304**, 634.

Antonucci, R.R.J., 1988. In: *Supermassive Black Holes*, Ed. Kafatos, M., C.U.P., p.26.

Antonucci, R.R.J. & Barvainis, R., 1988. *Astrophys. J.*, **325**, L121.

Antonucci, R.R.J., Hickson, P., Miller, J.S. & Olszewski, E.W., 1987. *Astr. J.*, **93**, 785.

Antonucci, R.R.J., Hickson, P., Olszewski, E.W. & Miller, J.S., 1986. *Astr. J.*, **92**, 1.

Antonucci, R.R.J. & Ulvestad, J.S., 1984. *Nature*, **308**, 617.

Antonucci, R.R.J. & Ulvestad, J.S. (AU85), 1985. *Astrophys. J.*, **294**, 158.

Arp, H.C., Sargent, W.L.W., Willis, A.G. & Oosterbaan, C.E., 1979. *Astrophys. J.*, **230**, 68.

Babandzhanyants, M.K., Belokon,E.T., Denisenko, N.S., & Semënova, E.V., 1985. *Sov. Astron.*, **29**, 394.

Bailey, J.A. & Hough, J.H., 1982. *Publs. astr. Soc. Pacif.*, **94**, 618.

Bailey, J.A., Hough, J.H. & Axon, D.J., 1983. *Mon. Not. R. astr. Soc.*, **203**, 339.

Bailey, J.A., Sparks, W.B., Hough, J.H. & Axon, D.J., 1986. *Nature*, **322**, 150.

Baldwin, J.A., Wampler, E., Burbidge, E.M., O'Dell, S., Smith, H., Hazard, C., Nordsieck, K., Pooley, G., & Stein, W., 1977. *Astrophys. J.*, **215**, 408.

Barbieri, C., Cristiani, S., Omizzolo, S. & Romano, G., 1985. *Astron. Astrophys.*, **142**, 316.

Bartel, N., Herring, T.A., Ratner, M.I., Shapiro, I.I. & Corey, B.E., 1986. *Nature*, **319**, 733.

Barvainis, R. & Predmore, C.R., 1984. *Astrophys. J.*, **282**, 402.

Begelman, M.C., Blandford, R.D. & Rees, M.J., 1984. *Rev. Mod. Phys.*, **56**, 255.

Begelman, M.C. & Sikora, M., 1987. *Astrophys. J.*, **322**, 650.

Beichman, C.A., Neugebauer, G., Soifer, B.T., Wootten, H.A., Roellig, T. & Harvey, P.M., 1981. *Nature*, **293**, 711.

Bessel, M.S., 1979. *Publs. astr. Soc. Pacif.*, **91**, 589.

Bessel, M.S., 1986. *Publs. astr. Soc. Pacif.*, **98**, 1303.

Biermann, P.L. & Strittmatter, P.A., 1987. *Astrophys. J.*, **322**, 643.

Biermann, P., Duerbeck, H., Eckart, A., Fricke, K., Johnston, K.J., Kühr, H., Liebert, J., Pauliny–Toth, I.I.K., Schleicher, H., Stockman, H., Strittmatter, P.A. & Witzel, A., 1981. *Astrophys. J.*, **247**, L53.

Biretta, J.A., Moore, R.L. & Cohen, M.H., 1986. *Astrophys. J.*, **308**, 93.

Björnsson, C.-I., 1982. *Astrophys. J.*, **260**, 855.

Björnsson, C.-I., 1986. *Mon. Not. R. astr. Soc.*, **216**, 241.

Björnsson, C.-I. & Blumenthal, G.R., 1982. *Astrophys. J.*, **259**, 805.

Blandford, R.D., 1987. In: *Superluminal Radio Sources*, Eds. Zensus, J.A. & Pearson, T.J., C.U.P., p.310.

Blandford, R.D. & Königl, A., 1979. *Astrophys. J.*, **232**, 34.

Blandford, R.D. & Rees, M.J., 1974. *Mon. Not. R. astr. Soc.*, **169**, 395.

Blandford, R.D. & Rees, M.J., 1978. In: Pittsburgh Conference on BL Lac Objects, Ed. Wolfe, A.M., Univ. of PIttsburgh, p. 328.

Boissé, P. & Bergeron, J., 1988. *Astron. Astrophys.*, **192**, 1.

Boksenberg, A., Carswell, R.F. & Oke, J.B., 1976. *Astrophys. J.*, **206**, L121.

Bolton, J.G. & Wall, J.V., 1970. *Aust. J. Phys.*, **23**, 789.

Borra, E.F. & Corriveau, G., 1984. *Astrophys. J.*, **276**, 499.

Bowyer, S., Brodie, J., Clarke, J.T. & Henry, J.P., 1984. *Astrophys. J.*, **278**, L103.

Bregman, J.N., Glassgold, A.E., Huggins, P.J., Aller, H.D., Aller, M.F., Hodge, P.E., Rieke, G.H., Lebofsky, M.J., Pollock, J.T., Pica, A.J., Leacock, A.J., Smith, A.G., Webb, J., Balonek, T.J., Dent, W.A., O'Dea, C.P., Ku, W.H–M., Schwartz, D.A., Miller, J.S., Rudy, R.J. & LeVan, P.D., 1984. *Astrophys. J.*, *276*, 454.

Bregman, J.N., Glassgold, A.E., Huggins, P.J., Kinney, A.L., McHardy, I., Webb, J.R., Pollock, J.T., Leacock, R.J., Smith, A.G., Pica, A.J., Aller, H.D., Aller, M.F., Hodge, P.E., Miller, J.S., Stephens, S.A., Dent, W.A., Balonek, T.J., Barvainis, R., Neugebauer, G., Impey, C.D., Soifer, B.T., Matthews, K., Elias, J.H. & Wiśniewski, W.Z., 1988. *Astrophys. J.*, (in press).

Bregman, J.N., Glassgold, A.E., Huggins, P.J., Neugebauer, G., Soifer, B.T., Matthews, K., Elias, J., Webb, J., Pollock, J.T., Pica, A.J., Leacock, R.J., Smith, A.G., Aller, H.D., Aller, M.F., Hodge, P.E., Dent, W.A., Balonek, T.J., Barvainis, R.E., Roellig, T.P.L., Wisniewski, W.Z., Rieke, G.H., Lebofsky, M.J., Wills, B.J., Wills, D., Ku, W.H.–M., Bregman, J.D., Witteborn, F.C., Lester, D.F., Impey, C.D. & Hackwell, J.A., 1986. *Astrophys. J.*, **301**, 708.

Bregman, J.N., Glassgold, A.E., Huggins, P.J., Pollock, J.T., Pica, A.J., Smith, A.G., Webb, J.R., Ku, W.H.–M., Rudy, R.J., LeVan, P.D., Williams, P.M., Brand, P.W.J.L., Neugebauer, G., Balonek, T.J., Dent, W.A., Aller, H.D., Aller, M.F. & Hodge, P.E., 1982. *Astrophys. J.*, **253**, 19.

Bregman, J.N., Lebofsky, M.J., Aller, M.F., Rieke, G.H., Aller, H.D., Hodge, P.E., Glassgold, A.E. & Huggins, P.J., 1981. *Nature*, **293**, 714.

Bridle, A.H., 1988. In: *Active Galactic Nuclei*, Eds. Miller, H.R. & Wiita, P.J., Springer–Verlag (in press).

Bridle, A.H. & Perley, R.A., (BP84) 1984. *Ann. Rev. Astron. Astrophys.*, **22**, 319.

Brindle, C., 1986. *Ph.D. thesis*, Hatfield Polytechnic.

Brindle, C., Hough, J.H., Bailey, J.A., Axon, D.J. & Hyland, A.R., 1986. *Mon. Not. R. astr. Soc.*, **221**, 739.

Brindle, C., Hough, J.H., Bailey, J.A., Axon, D.J., Schulz, H., Kikuchi, S., McGraw, J.T., Wisniewski, W.J., Fontaine, G., Nadesu, D., Clayton, G., Anderson, E., Jameson, R.F., Smith, R. & Wallis, R.E., 1985. *Mon. Not. R. astr. Soc.*, **214**, 619.

Brodie, J., Bowyer, S. & Tennant, A., 1987. *Astrophys. J.*, **318**, 175.

Brown, L.M.J., Robson, E.I., Gear, W.K., Crosthwaite, R.P., McHardy, I.M., Hanson, C.G., Geldzahler, B.J. & Webb, J.R., 1986. *Mon. Not. R. astr. Soc.*, **219**, 671.

Browne, I.W.A., 1987. In: *Superluminal Radio Sources*, Eds. Zensus, J.A. & Pearson, T.J., C.U.P., p. 129.

Browne, I.W.A. & Murphy, D.W., 1987. *Mon. Not. R. astr. Soc.*, **226**, 601.

Browne, I.W.A., Savage, A.S. & Bolton, J.G., 1975. *Mon. Not. R. astr. Soc.*, **173**, 87P.

Bruzual A., G., 1983. *Rev. Mex. Astr. Astrofis.*, **8**, 63.

Buckley, D.A.H., Tuohy, I.R. & Remillard, R.A., 1985. *Proc. Astr. Soc. Austr.*, **6**, 147.

Burbidge, E.M., 1965. *Astrophys. J.*, **142**, 1674.

Burbidge, E.M. & Kinman, T.D., 1966. *Astrophys. J.*, **145**, 654.

Burbidge, E.M. & Strittmatter, P.A., 1972. *Astrophys. J.*, **174**, L57.

Burbidge, E.M. & Rosenberg, F.D., 1965. *Astrophys. J.*, **142**, 1673.

Burbidge, G.R., Crowne, A.H. & Smith, H.E., 1977. *Astrophys. J. Suppl.*, **33**, 113.

Burstein, D. & Heiles, C., 1982. *Astr. J.*, **87**, 1165.

Campins, H. Rieke, G.H. & Lebofsky, M.J., 1985. *Astr. J.*, **90**, 896.

Carrasco, L., Dultzin–Hacyan, D. & Cruz–Gonzalez, I., 1985. *Nature*, 146.

Cawthorne, T.V. & Rickett, B.J., 1985. *Nature*, **315**, 40.

Chan, K.L. & Henriksen, R.N., 1980, *Astrophys. J.*, **241**, 534.

Chanan, G.A., Margon, B., Helfand, D.J., Downes, R.A. & Chance,D., 1982. *Astrophys. J.*, **261**, L31.

Cohen, R.D., Smith, H.E., Junkkarinen, V.T. & Burbidge, E.M., 1987. *Astrophys. J.*, **318**, 577.

Condon, J.J., Condon, M.A., Jauncey, D.L., Smith, M.G., Turtle, A.J. & Wright, A.E., 1981. *Astrophys. J.*, **244**, 5.

Corso, G.J., Ringwald, F.A. & Harris, R.W., 1988. *Astrophys. J.*, **195**, 25.

Conover, W.J., 1980. *Practical Nonparametric Statistics*, Wiley 2nd. Ed., New York.

Cotton, W.D., Wittels, J.J., Shapiro, I.I., Marcaide, J., Owen, F.N., Spangler, S.R., Rius, A., Angulo, C., Clark, T.A. & Knight, C.A., 1980. *Astrophys. J.*, **238**, L123.

Cruz–Gonzalez, I. & Huchra, J.P., 1984. *Astr. J.*, **89**, 441.

Danziger, I.J., Fosbury, R.A.E., Goss, W.M. & Ekers, R.D., 1979. *Mon. Not. R. astr. Soc.*, **188**, 415.

Davis, M. & Peebles, P.J.E., 1983. *Astrophys. J.*, **267**, 465.

Davis, R.J., 1986. In: *IAU Symposium 119 Quasars*, Eds. Swarup, G. & Kapahi, V.K., p211.

de Hoffman, F. & Teller, E., 1950. *Phys. Rev.*, **80**, 692.

Dreher, J.W., Roberts, D.H. & Lehár, 1986. *Nature*, **320**, 239.

Drury, L.O'C., 1983. *Rep. Prog. Phys.*, **46**, 973.

Dunlop, J.S., 1988 *Ph.D. Thesis*, University of Edinburgh.

Eachus, L. & Liller, W., 1975. *Astrophys. J.*, **200**, L61.

Edelson, R.A. & Malkan, M.A., 1986. *Astrophys. J.*, **308**, 59.

Elliott, J.L. & Shapiro, S.L., 1974. *Astrophys. J.*, **192**, L3.

Fabbiano, G., Miller, L., Trinchieri, G., Longair, M.S. & Elvis, M., 1984. *Astrophys. J.*, **277**, 115.

Falomo, R., Maraschi, L., Tanzi, E.G. & Treves, A., 1987. *Astrophys. J.*, **318**, L39.

Fanaroff, B.L. & Riley, J.M., *Mon. Not. R. astr. Soc.*, **167**, 31P.

Fanti, C., Fanti, R., Formiggini, L., Lari, C., & Padrielli, L., 1977. *Astron. Astrophys. Suppl.*, **28**, 351.

Feigelson, E.D., Bradt, H., McClintock, J., Remillard, R., Urry, C.M., Tapia, S., Geldzahler, B., Johnston, K., Romanishin, W., Wehinger, P.A., Wyckoff, S., Madejski, G., Schwartz, D.A., Thorstensen, J. & Schaefer, B.E., 1986. *Astrophys. J.*, **302**, 337.

Filippenko, A.V., Djorgovski, S., Spinrad, H. & Sargent, W.L.W., 1986. *Astr. J.*, **91**, 49.

Foltz, C.B., & Chaffee, F.H., Jr., 1987., *Astr. J.*, **93**, 529.

Folsom, G., Smith, A.G. & Hackney, R.L., 1970. *Astrophys. Lett.*, **7**, 15.

Fosbury, R.A.E. & Disney, M.J., 1976. *Astrophys. J.*, **207**, L75.

Fricke, K.J., Kollatschny, W. & Witzel, A., 1983. *Astron. Astrophys.*,**117**, 60.

Garrington, S.T., Leahy, J.P., Conway, R.G. & Laing, R.A., 1988. *Nature*, **331**, 147.

Gear, W.K., Brown, L.M.J., Robson, E.I., Ade, P.A.R., Griffin, M.J., Smith, M.G., Nolt, I.G., Radostitz, J.V., Veeder, G., & Lebofsky, L., 1986. *Astrophys. J.*, **304**, 295.

Gear, W.K., Robson, E.I., Ade, P.A.R., Griffin, M.J., Brown, L.M.J., Smith, M.G., Nolt, I.G., Radostitz, J.V., Veeder, G., & Lebofsky, L., 1985. *Astrophys. J.*, **291**, 511.

Gear, W.K., Robson, E.I. & Brown, L.M.J., 1986. *Nature*, **324**, 546.

Ghisellini, G., Maraschi, L., Tanzi, E.G. & Treves, A., 1986. *Astrophys. J.*, **310**, 317.

Ghisellini, G., Maraschi, L. & Treves, A., 1985. *Astron. Astrophys.*, **146**, 204.

Glassgold, A.E., Bregman, J.N., Huggins, P.J., Kinney, A.L., Pica, A.J., Pollock, J.T., Leacock, R.J., Smith, A.G., Webb, J.R., Wiśniewski, W.Z., Jeske, N., Spinrad, H., Henry, R.B.C., Miller, J.S., Impey, C.D., Neugebauer, G., Aller, M.F., Aller, H.D., Hodge, P.E., Balonek, T.J., Dent, W.A. & O'Dea, C.P., 1983. *Astrophys. J.*, **274**, 101.

Gould, R.J., 1979. *Astron. Astrophys.*, **76**, 306.

Grandi, S.A., 1981. *Astrophys. J.*, **251**, 451.

Grandi, S.A., 1982. *Astrophys. J.*, **255**, 25.

Green, R.F. & Yee, H.K.C., 1984. *Astrophys. J. Suppl.* , **54**, 495.

Groth, E.J. & Peebles, P.J.E., 1977. *Astrophys. J.*, **217**, 385.

Guiderdoni, B. & Rocca–Volmerange, B., 1987. *Astron. Astrophys.*, **186**, 1.

Guilbert, P.W., Fabian, A.C. & McCray, R., 1983. *Astrophys. J.*, **266**, 466.

Hanson, C.G. & Coe, M.J.,1985. *Mon. Not. R. astr. Soc.*, **217**, 831.

Harris, D.E., Dewdney, P.E., Costain, C.H., Butcher, H. & Willis, A.G, 1983. *Astrophys. J.*, **270**, 39.

Heavens, A.F., 1984. *Mon. Not. R. astr. Soc.*, **207**, 1P.

Heavens, A.F., 1988. In: *Workshop on Hotspots in Extragalactic Radio Sources*, Ed. Meisenheimer, K. & Röser, H.–J., (in press).

Heavens, A.F. & Drury, L.O'C., 1988. *Mon. Not. R. astr. Soc.*, (in press).

Heavens, A.F. & Meisenheimer, K., 1987. *Mon. Not. R. astr. Soc.*, **225**, 335.

Heckman, T.M., 1983. *Astrophys. J.*, **271**, L5.

Hintzen, P. & Owen, F., 1981. *Astr. J.*, **86**, 1577.

Hintzen, P. Ulvestad, J.S. & Owen, F., 1983. *Astr. J.*, **88**, 709.

Holmes, P.A., 1985. *Ph.D. Thesis*, University of Edinburgh.

Holmes, P.A., Brand, P.W.J.L., Impey, C.D. & Williams, P.M., 1984a. *Mon. Not. R. astr. Soc.*, **210**, 961.

Holmes, P.A., Brand, P.W.J.L., Impey, C.D., Williams, P.M., Smith, P., Elston, R., Balonek, T., Zeilik, M., Burns, J., Heckert, P., Barvainis, R., Kenny, J., Schmidt, G. & Puschell, J., 1984b. *Mon. Not. R. astr. Soc.*, **211**, 497.

Hough, J.H., Brindle, C., Axon, D.J., Bailey, J.A. & Sparks, W.B., 1987. *Mon. Not. R. astr. Soc.*, **224**, 1013.

Hughes, P.A., Aller, H.D. & Aller, M.F., 1985. *Astrophys. J.*, **298**, 301.

Hutchings, J.B., Crampton,D. & Campbell,B., 1984. *Astrophys. J.*, **280**, 41.

Impey, C.D., 1987. In : *Superluminal Radio Sources*, p. 233, eds. Zensus, J.A. & Pearson, T.J., C.U.P.

Impey, C.D. & Brand, P.W.J.L., 1982. *Mon. Not. R. astr. Soc.*, **201**, 849.

Impey, C.D., Brand., P.W.J.L., Wolstencroft, R.D. & Williams, P.M., 1982. *Mon. Not. R. astr. Soc.*, **200**, 19.

Impey, C.D., Brand., P.W.J.L., Wolstencroft, R.D. & Williams, P.M., 1984. *Mon. Not. R. astr. Soc.*, **209**, 245.

Impey, C.D. & Neugebauer, G., 1988. *Astr. J.*, **95**, 307.

Impey, C.D. & Tapia, S., 1988. *Astrophys. J.*, (in press).

Jauncey, D.L., Wright, A.E., Peterson, B.A. & Condon, J.J., 1978. *Astrophys. J.*, **219**, L1.

Kardashev, N.S., 1962. *Sov. Astron. - A.J.*, **6**, 317.

Kidger, M.R. & Beckman, J.E., 1986. *Astron. Astrophys.*, **154**, 288.

Kikuchi, S., Inoue, M., Mikami, Y., Tabara, H. & Kato, T., 1988. *Astron. Astrophys.*, **190**, L8.

Kikuchi, S. & Mikami, Y., 1987. *Publs. astr. Soc. Japan*, **39**, 237.

King, C.R. & Ellis, R.S., 1985. *Astrophys. J.*, **288**, 456.

Kirk, J.G. & Schneider, P., 1987 *Astrophys. J.*, **315**, 425.

Komesaroff, M.M., Roberts, J.A. & Murray, J.D., 1988. *Observatory*, **108**, 9.

Königl, A., 1981. *Astrophys. J.*, **243**, 700.

Königl, A. & Choudhuri, A.R., 1985a. *Astrophys. J.*, **289**, 173.

Königl, A. & Choudhuri, A.R., 1985b. *Astrophys. J.*, **289**, 188.

Laing, R.A., 1980. *Mon. Not. R. astr. Soc.*, **193**, 439.

Laing, R.A., 1988. *Nature*, **331**, 149.

Landau, R., Grolsch, B., Jones, T.J., Jones, T.W., Pedelty, J., Rudnick, L., Sitko, M.L., Kenney, J., Roellig, T., Salonen, E., Urpo, S., Schmidt, G., Neugebauer, G., Matthews, K., Elias, J.H., Impey, C.D., Clegg, P. & Harris, S., 1986. *Astrophys. J.*, **308**, 78.

Landolt, A.U., 1983. *Astr. J.*, **88**, 439.

Lawrence, C.R., Pearson, T.J., Readhead, A.C.S. & Unwin, S.C., 1986. *Astr. J.*, **91**, 494.

Ledden, J.E. & Aller, H.D., 1978. In:*Pittsburgh Conference on BL Lac Objects*, Ed. Wolfe, A.M., Univ. of Pittsburgh, p. 60.

Ledden, J.E., & O'Dell, S.L., 1985. *Astrophys. J.*, **298**, 630.

Liller, M.H. & Liller, W., 1975. *Astrophys. J.*, **199**, L133.

Lind, K.R. & Blandford, R.D., 1985. *Astrophys. J.*, **295**, 358.

Longair, M.S., 1981. *High Energy Astrophysics*, C.U.P.

Longair, M.S. & Seldner, M., 1979. *Mon. Not. R. astr. Soc.*, **189**, 433.

Lynds, C.R., 1967. *Astrophys. J.*, **147**, 837.

Lynds, C.R., Hill, S.J., Heere, K. & Stockton, A.N., 1966. *Astrophys. J.*, **144**, 1244.

Macklin, J.T., 1982. *Mon. Not. R. astr. Soc.*, **199**, 1119.

Madau, P., Ghisellini, G. & Persic, M., 1987. *Mon. Not. R. astr. Soc.*, **224**, 257.

Maddox, S.J., Efstathiou, G. & Loveday, J., 1988. In:*Evolution of Large Scale Structure in the Universe, IAU Symp. No. 130*, Eds. Audouze, J., Pelletan, M.–C. & Szalay, A., Kluwer, Dordrecht, p. 151.

Makino, F., Tanaka, Y., Matsuoka, M., Koyama, K., Inoue, H., Makishima, K., Hoshi, R., Hayakawa, S., Kondo, Y., Urry, C.M., Mufson, S.L., Hackney, K.R., Hackney, R.L., Kikuchi, S., Mikami, Y., Wiśniewski, W.Z., Hiromoto, N., Nishida, M., Burnell, J., Brand, P.W.J.L., Williams, P.M., Smith, M.G., Takahara, F., Inoue, M., Tsuboi, M., Tabara, H., Kato, T., Aller, M.F. & Aller, H.D., 1987. *Astrophys. J.*, **313**, 662.

Malkan, M.A., 1983. *Astrophys. J.*, **268**, 582.

Malkan, M.A. & Moore, R.L., 1986. *Astrophys. J.*, **300**, 216.

Malkan, M.A. & Sargent, W.L.W., 1982. *Astrophys. J.*, **254**, 22.

Marscher, A.P., 1980. *Astrophys. J.*, **235**, 386.

Marscher, A.P., 1983. *Astrophys. J.*, **264**, 296.

Marscher, A.P., 1987. In *Superluminal Radio Sources*, Eds. Zensus, J.A. & Pearson, T.J., C.U.P., p.280.

Marscher, A.P. & Gear, W.K., 1985. *Astrophys. J.*, **298**, 114.

Marscher, A.P., Shaffer, D.B., Booth, R.S. & Geldzahler, B.J., 1987. *Astrophys. J.*, **319**, L69.

Marscher, A.P. & Scott, J.S., 1980. *Publs. astr. Soc. Pacif.*, **92**, 127.

Mathews, J. & Walker, R.L., 1970. *Mathematical Methods of Physics*, Benjamin, 2nd. Ed.

Mead, A.R.G., Brand, P.W.J.L., Hough, J.H. & Bailey, J.A., 1988. *Mon. Not. R. astr. Soc.*, **233**, 503.

Meisenheimer, K. & Heavens, A.F., 1986. *Nature*, **323**, 419.

Meisenheimer, K. & Röser, H.–J., 1984. *Astrophys. J.*, **279**, L39.

Miley, G.K., 1980. *Ann. Rev. Astron. Astrophys.*, **18**, 165.

Miller, J.S., French, H.B. & Hawley, S.A., 1978. In: *Pittsburgh Conference on BL Lac Objects*, Ed. Wolfe, A.M., Univ. of Pittsburgh, p. 176.

Miller, L., 1984. *VLBI and Compact Radio Sources, IAU Symposium 110*, p. 189, eds. Fanti, R. *et. al.*, Reidel, Dordrecht,Netherlands.

Moles, M., García–Pelayo, J.M., Masegosa, J. & Aparicio, A., 1985. *Astrophys. J.*, **58**, 255.

Moore, R.L., McGraw, J.T., Angel, J.R.P., Duerr, R., Lebofsky, M.J., Rieke, G.H., Wiśniewski, W.Z., Axon, D.J., Bailey, J.A., Hough, J.H., Thompson, I., Breger, M., Schulz, H., Clayton, G.C., Martin, P.G., Miller, J.S., Schmidt, G.D., Africano, J. & Miller, H.R., 1982. *Astrophys. J.*, **260**, 415.

Moore, R.L., Schmidt, G.D. & West, S.C., 1987. *Mon. Not. R. astr. Soc.*, **314**, 176.

Moore, R.L. & Stockman, H.S., 1981. *Astrophys. J.*, **243**, 60.

Moore, R.L. & Stockman, H.S., 1984. *Astrophys. J.*, **279**, 465.

Netzer, H. & Wills, B.J., 1983. *Astrophys. J.*, **275**, 445.

Neugebauer, G., Green, R.F., Matthews, K., Schmidt, M., Soifer, B.T. & Bennett, J., 1987. *Astrophys. J. Suppl.*, **63**, 615.

Nordsieck, K.H., 1976. *Astrophys. J.*, **209**, 653.

O'Dell, S.L., Scott, H.A. & Stein, W.A., 1987. *Astrophys. J.*, **313**, 164.

Oke, J.B., Shields, G.A. & Korycansky, D.G., 1984. *Astrophys. J.*, **277**, 64.

Orr, M.J.L. & Browne, I.W.A., 1982. *Mon. Not. R. astr. Soc.*, **200**, 1067.

Ostriker, J.P. & Vietri, M., 1985. *Nature*, **318**, 446.

Owen, F.N., Porcas, R.W. & Neff, S.G., 1978. *Astr. J.*, **83**, 1009.

Pacholczyk, A.G., 1970. *Radio Astrophysics*, Freeman, San Francisco.

Pacholczyk, A.G., 1977. *Radio Galaxies*, Pergamon.

Peacock, J.A., 1986. In: *Astrophysical Jets and their Engines*, Ed. Kundt, W., Reidel, Dordrecht, p.185.

Peacock, J.A. & Prestage, R.M. (PP), 1988. *Mon. Not. R. astr. Soc.*, **230**, 131.

Pearson, T.J. & Zensus, J.A., 1987. In: *Superluminal Radio Sources*, Eds. Zensus, J.A. & Pearson, T.J., C.U.P., p.1.

Peebles, P.J.E., 1975. *Astrophys. J.*, **196**, 647.

Peebles, P.J.E., 1980. *The Large-Scale Structure of the Universe*, Princeton University Press.

Perley, R.A., Fomalont, E.B. & Johnston, K.J., 1980. *Astr. J.*, **85**, 649.

Peterson, B.A., Jauncey, D.L., Wright, A.E. & Condon, J.J., 1976. *Astrophys. J.*, **207**, L5.

Phillips, K.C. & Mészáros, P., 1986. *Astrophys J.*, **310**, 284.

Pineault, S., 1981. *Astrophys. J.*, **246**, 612.

Pooley, G.G. & Henbest, S.N., 1974. *Mon. Not. R. astr. Soc.*, **169**, 477.

Porcas, R.W., 1987. In: *Superluminal Radio Sources*, Eds. Zensus, J.A. & Pearson, T.J., C.U.P., p.12.

Potash, R.I. & Wardle, J.F.C., 1979. *Astr. J.*, **84**, 707.

Puschell, J.J. & Stein, W.A., 1980. *Astrophys. J.*, **237**, 331.

Puschell, J.J., Jones, T.W., Phillips, A.C., Rudnick, L., Simpson, E., Sitko, M., Stein, W.A. & Moneti, A., 1983. *Astrophys. J.*, **265**, 625.

Rees, M.J., 1966. *Nature*, **211**, 468.

Rees, M.J., 1984. *Ann. Rev. Astron. Astrophys.*, **22**, 471.

Reynolds, S.P., 1982a. *Astrophys. J.*, **256**, 13.

Reynolds, S.P., 1982b. *Astrophys. J.*, **256**, 38.

Rieke, G.H. & Lebofsky, M.J., 1985. *Astrophys. J.*, **288**, 618.

Rieke, G.H., Lebofsky, M.J. & Kinman, T.D., 1979. *Astrophys. J.*, **232**, L151.

Roberts, D.H. & Wardle, J.F.C., 1987. In: *Superluminal radio Sources*, Eds. Zensus, J.A. & Pearson, T.J., p. 193.

Röser, H.–J. & Meisenheimer, K., 1986. *Astron. Astrophys.*, **154**, 15.

Romanishin, W., 1987. *Astrophys. J.*, **320**, 586.

Rusk, R. & Seaquist, E.R., 1985. *Astr. J.*, **90**, 30.

Rybicki, G.B. & Lightman, A.P., 1979. *Radiative Processes in Astrophysics*, Wiley, New York.

Saikia, D.J., Kulkarni, V.K. & Porcas, R.W., *Mon. Not. R. astr. Soc.*, **219**, 719.

Schechter, P.L., 1976. *Astrophys. J.*, **203**, 297.

Scheuer, P.A.G., 1984. In: *IAU Symposium 110, VLBI and Compact Radio Sources*, eds. Fanti, R., Kellerman, K. & Setti, G., Reidel, Dordrecht, p197.

Scheuer, P.A.G. & Readhead, A.C.S, 1979. *Nature*, **277**, 182.

Schilizzi, R.T. & de Bruyn, A.G., 1983. *Nature*, **303**, 26.

Schmidt, M., 1965. *Astrophys. J.*, **141**, 1295.

Sebok, W.L., 1986. *Astrophys. J. Suppl.* , **62**, 301.

Serkowski, K., 1974. *Methods of Experimental Physics*, **12 A**, 361, Academic Press, New York.

Sillanpää, A., Haarala, S., Valtonen, M.J., Sundelius, B., & Byrd, G.G., 1988. *Astrophys. J.*, **325**, 628.

Shanks, T., Stevenson, P.R.F., Fong, R. & MacGillivray, H.T., 1984. *Mon. Not. R. astr. Soc.*, **206**, 767.

Simon, R.S., Johnston, K.J., Hall, J., Spencer, J.H. & Waak, J.A., 1987. In: *Superluminal Radio Source*, Eds. Zensus, J.A. & Pearson, T.J., C.U.P., p72.

Sitko, M.L. & Junkkarinen, V.T., 1985. *Publs. astr. Soc. Pacif.*, **97**, 1158.

Sitko, M.L., Rudnick, L., Jones, T.W. & Schmidt, G.D., 1984. *Publs. astr. Soc. Pacif.*, **96**, 402.

Sitko, M.L., Schmidt, G.D. & Stein, W.A., 1985. *Astrophys. J. Suppl.*, **59**, 323.

Smith, H.E, Burbidge, E.M., Baldwin, J.A., Tohline, J.E., Wampler, E.J., Hazard, C. & Murdoch, H.S., 1977. *Astrophys. J.*, **215**, 427.

Smith, H.E. & Spinrad, H., 1980. *Astrophys. J.*, **236**, 419.

Smith, P.S., Balonek, T.J., Elston, R. & Heckert, P.A., 1987. *Astrophys. J. Suppl.* , **64**, 459.

Smith, P.S., Balonek, T.J., Heckert, P.A. & Elston, R. (SBHE), 1986. *Astrophys. J.*, **305**, 484.

Smith, P.S., Elston, R., Berriman, G., Allen, R.G. & Balonek, T.J., 1988. *Astrophys. J.*, (in press).

Stein, W.A., O'Dell, S.L. & Strittmatter, P.A., 1976. *Ann. Rev. Astron. Astrophys.*, **14**, 173.

Stickel, M., Fried, J.W. & Kühr, H., 1988a. *Astron. Astrophys.*, **191**, L16.

Stickel, M., Fried, J.W. & Kühr, H., 1988b. *Astron. Astrophys.*, **198**, L13.

Stocke, J.T., Liebert, J., Schmidt, G., Gioia, I.M., Maccacaro, T., Schild, R.E., Maccagni, D. & Arp, H.C., 1985. *Astrophys. J.*, **298**, 619.

Stockman, H.S., 1978. in *Pittsburgh Conference on BL Lac Objects*, ed. Wolfe, A.M., Univ. of Pittsburgh.

Stockman, H.S., Moore, R.L. & Angel, J.R.P., 1984. *Astrophys. J.*, **279**, 485.

Strittmatter, P.A., Carswell, R.F., Gilbert, G. & Burbidge, E.M., 1974. *Astrophys. J.*, **190**, 509.

Tanzi, E.G., Barr, P., Bouchet, P., Chiapetti, L., Cristiani, S., Falomo, R., Giommi, P., Maraschi, L. & Treves, A., 1986. *Astrophys. J.*, **311**, L13.

Turnshek, D.A., 1984. *Astrophys. J.*, **280**, 51.

Tyson, J.A. & Jarvis, J.F., 1979. *Astrophys. J.*, **230**, L153.

Ulmer, M.P., Brown, R.L., Schwartz, D.A., Patterson, J. & Cruddace, R.G., 1983. *Astrophys. J.*, **270**, L1.

Ulvestad, J.S. & Antonucci, R.R.J., 1986., *Astr. J.*, **92**, 6.

Ulvestad, J.S. & Antonucci, R.R.J., 1988. *Astrophys. J.*, **328**, 569.

Ulvestad, J.S. & Johnston, K.J., 1984. *Astr. J.*, **89**, 189.

Ulvestad, J.S., Johnston, K.J. & Weiler, K.W., 1983. *Astrophys. J.*, **266**, 18.

Valtaoja, E., Lehto, H., Teerikorpi, P., Korhonen, T., Valtonen, M., Teräsranta, H., Salonen, E., Urpo, S., Tiuri, M., Piirola,, V. & Saslaw, W.C., 1985. *Nature*, **314**, 148.

Vinokur, M., 1965. *Annales d'Astrophysique*, **28**, 412.

Wall, J.V., Danziger, I.J., Pettini, M., Warwick, R.S. & Wamsteker, W., 1986. *Mon. Not. R. astr. Soc.*, **219**, 23P.

Wardle, J.F.C. & Kronberg, P.P., 1974. *Astrophys. J.*, **194**, 249.

Wardle, J.F.C., Moore, R.L. & Angel, J.R.P., 1984. *Astrophys. J.*, **279**, 93.

Wardle, J.F.C., Roberts, D.H., Potash, R.I. & Rogers, A.E.E., 1986. *Astrophys. J.*, L1.

Webb, W. & Malkan, M.A., 1986. In: *Continuum Emission in Active Galactic Nuclei*, Ed. Sitko, M.L., K.P.N.O., P. 71.

Wilkes, B.J., Wright, A.E., Jauncey, D.L. & Peterson, B.A., 1983. *Proc. astr. Soc. Austr.*, **5**, 2.

Wills, B.J., 1988. In: *Physics of the Formation of FeII Lines Outside LTE, IAU Colloq. 94*, Eds. Viotti, R., Vittone, A. & Friedjung, M., Reidel, Dordrecht, p. 161.

Wills, B.J. & Browne, I.W.A., 1986. *Astrophys. J.*, **302**, 56.

Wills, B.J., Netzer, H. & Wills, D., 1985. *Astrophys. J.*, **288**, 94.

Wills, B.J., Pollock, J.T., Aller, H.D., Aller, M.F., Balonek, T.J., Barvainis, R.E., Binzel, R.P., Chaffee ,Jr., F.H., Dent, W.A., Douglas, J.N., Fanti, C., Garrett, D.B., Gregorini, L., Henry, R.B.C., Hill, R.E., Howard, R., Jeske, N., Kepler, S.O., Leacock, R.J., Mantovani, F., O'Dea, C.P., Padrielli, L., Perley, P., Pica, A.J., Puschell, J.J., Sanduleak, N., Shields, G.A., Smith, A.G., Thuan, T.X., Wade, C.M., Wasilewski, A.J., Webb, J.R., Wills, D. & Wiśniewski, W.Z., 1983. *Astrophys. J.*, **274**, 62.

Wills, B.J. & Wills, D., 1979. *Astrophys J. Suppl.*, **41**, 689.

Wills, D., 1979. *Astrophys. J. Suppl.*, **39**, 291.

Wills, D. & Lynds, R., 1978. *Astrophys. J. Suppl.*, **36**, 317.

Wills, D. & Wills, B.J., 1976. *Astrophys. J. Suppl.*, **31**, 143.

Wills, D. & Wills, B.J., 1981. *Nature*, **289**, 384.

Wills, D., Wills, B.J., Barvainis, R., Antonucci, R.R.J. & Breger, M., 1987. *Bull. Amer. astr. Soc.*, **19**, 1083.

Wills, D., Wills, B.J., Breger, M. & Hsu, J.C., 1980. *Astr. J.*, **85**, 1555.

Wisniewski, W.Z., Sitko, M.L. & Sitko, A.K., 1986. *Mon. Not. R. astr. Soc.*, **219**, 299.

Wolstencroft, R.D., Gilmore, G. & Williams, P.M., 1982. *Mon. Not. R. astr. Soc.*, **201**, 479.

Worrall, D.M., Puschell, J.J., Bruhweiler, F.C., Sitko, M.L., Stein, W.A., Aller, M.F., Aller, H.D., Hodge, P.E., Rudy, R.J., Miller, H.R., Wiśniewski, W.Z., Córdova, F.A & Mason, K.O., 1984. *Astrophys. J.*, **284**, 512.

Worrall, D.M., Puschell, J.J., Jones, B., Bruhweiler, F.C., Aller, M.F., Aller, H.D., Hodge, P.E., Sitko, M.L., Stein, W.A., Zhang, Y.X. & Ku, W.H.–M., 1982. *Astrophys. J.*, **261**, 403.

Worrall, D.M., Rodríguez–Espinosa, J.M., Wiśniewski, W.Z., Miller, H.R., Bruhweiler, F.C., Aller, M.F. & Aller, H.D., 1986. *Astrophys. J.*, **303**, 589.

Yates, M.G., Miller,L. & Peacock, J.A., (1988). *Mon. Not. R. astr. Soc.*, (submitted).

Yee, H.K.C. & Green, R.F., 1984. *Astrophys. J.*, **280**, 79.

Yee, H.K.C. & Green, R.F. (YG), 1987. *Astrophys. J.*, **319**, 28.

Yee, H.K.C., Green, R.F. & Stockman, H.S. (YGS), 1986. *Astrophys. J. Suppl.*, **62**, 681.

Zotov, N.V. & Tapia, S., 1979. *Astrophys. J.*, **229**, L5.

Appendix

The Polarimeter Data

Because of their excessive bulk, it has been decided to present the data for Chapter 2 in an appendix. The data for 1986 July/August are presented in Table A1, 1987 July in Table A2 and 1987 September in Table A3. Listed in these tables are the measured fluxes, percentage polarizations and position angles. Also given are the values of $E(B-V)$ which were estimated from the extinction maps of Burstein & Heiles (1982) (see §2.1.6).

Figure A1 shows flux density (S_ν), polarization ($p(\nu)$), polarized flux density (P_ν) and position angle (θ) versus frequency for each set of observations where at least two of the measured polarizations were significant at the 3σ level. Care must be taken with the interpretation of the polarized flux plots. These are simply the product of the polarization and the flux density ($P_\nu(\nu) = p(\nu)\, S_\nu(\nu)$). Consequently the plots do not take into account any rotation of the plane of polarization over the frequency range observed. Figure A2 shows the flux density versus frequency for those observations where no significant polarization was observed.

Table A1 : The Observations of 1986 July 31 – 1986 August 7

Filter	Flux density (mJy)		Polarization (%)		Position angle (deg)	
0048-097 OB-081						
E(B-V) = 0.00						
1986 Jul. 31						
H	6.78	(0.63)	11.50	(1.80)	112.29	(4.85)
I	3.69	(0.34)	12.05	(0.52)	118.09	(1.28)
B	1.70	(0.24)	13.91	(0.44)	117.15	(0.83)
1986 Aug. 3						
H	9.63	(0.45)	13.17	(0.78)	116.34	(1.70)
J	5.26	(0.25)	15.09	(1.00)	117.58	(1.68)
I	3.01	(0.23)	14.55	(0.61)	118.13	(1.33)
R	2.34	(0.22)	16.02	(0.52)	116.38	(1.07)
V	1.74	(0.17)	16.59	(0.64)	118.54	(1.34)
B	1.62	(0.16)	16.90	(0.32)	116.45	(0.60)
1986 Aug 4						
H	6.54	(0.18)	14.80	(0.79)	111.71	(1.26)
J	4.71	(0.22)	14.31	(0.74)	112.37	(1.73)
I	3.12	(0.15)	15.67	(0.60)	111.29	(1.13)
V	1.86	(0.15)	17.42	(0.52)	113.68	(1.28)
B	1.73	(0.14)	17.85	(0.35)	111.50	(0.73)
1986 Aug. 6						
H	6.48	(0.30)	12.08	(0.88)	103.04	(1.75)
J	4.84	(0.23)	16.24	(0.68)	102.62	(1.39)
I	3.69	(0.34)	17.98	(0.60)	104.89	(1.02)
R	2.40	(0.23)	18.76	(0.49)	105.90	(0.78)
V	1.95	(0.15)	18.75	(0.57)	107.14	(1.32)
B	1.62	(0.16)	19.39	(0.38)	106.02	(0.57)
1986 Aug. 7						
H	6.60	(0.31)	12.89	(1.15)	106.69	(2.85)
I	3.15	(0.15)	15.79	(0.81)	107.36	(1.31)
B	1.66	(0.10)	18.12	(0.51)	108.82	(0.85)
PKS 0106+013						
E(B-V) = 0.00						
1986 Aug. 4						
H	0.43	(0.06)	33.15	(18.62)	127.96	(15.16)
I	0.23	(0.02)	0.00	(7.84)		
B	0.20	(0.02)	12.28	(5.26)	122.37	(8.54)

Table A1 : Continued.

Filter	Flux density (mJy)		Polarization (%)		Position angle (deg)	
GC 0109+224						
E(B-V) = 0.06						
1986 Aug. 1						
H	7.09	(0.33)	9.06	(1.20)	40.95	(3.55)
I	3.10	(0.29)	10.05	(0.43)	35.64	(1.30)
B	2.14	(0.21)	10.88	(0.34)	34.36	(1.04)
1986 Aug. 4						
H	7.02	(0.26)	5.66	(0.51)	54.70	(4.63)
I	3.07	(0.15)	3.81	(0.50)	42.74	(5.81)
B	1.26	(0.13)	4.13	(0.37)	31.15	(3.22)
1986 Aug. 5						
H	6.96	(0.32)	4.80	(1.90)	61.81	(7.07)
I	3.07	(0.15)	2.70	(0.45)	48.36	(4.71)
B	1.13	(0.07)	1.64	(0.49)	29.07	(7.95)
1986 Aug. 6						
H	6.58	(0.31)	0.00	(1.17)		
I	3.18	(0.15)	0.96	(0.63)	24.63	(3.43)
B	1.35	(0.08)	3.74	(0.47)	13.16	(3.96)
1986 Aug. 7						
H	6.58	(0.31)	1.58	(0.87)	4.06	(8.23)
J	4.70	(0.22)	3.41	(1.06)	22.18	(8.68)
I	2.90	(0.14)	4.95	(0.64)	17.54	(3.90)
R	2.13	(0.16)	6.35	(0.58)	20.31	(2.50)
V	1.61	(0.16)	7.53	(0.59)	21.90	(2.14)
B	1.29	(0.08)	8.63	(0.30)	17.20	(1.03)
0118-272						
E(B-V) = 0.00						
1986 Aug. 5						
H	8.15	(0.38)	15.37	(0.77)	147.79	(1.46)
J	5.98	(0.28)	16.26	(0.91)	148.01	(1.75)
I	4.00	(0.19)	17.82	(0.58)	147.24	(0.97)
R	2.81	(0.14)	17.87	(0.47)	149.97	(0.81)
V	2.19	(0.12)	17.33	(0.63)	149.19	(1.49)
B	1.86	(0.19)	17.21	(0.35)	149.90	(0.59)

Table A1 : Continued.

Filter	Flux density (mJy)		Polarization (%)		Position angle (deg)	
1986 Aug. 6						
H	8.08	(0.37)	16.63	(1.02)	148.71	(1.85)
I	3.97	(0.19)	17.50	(0.53)	148.14	(0.89)
B	1.49	(0.09)	17.56	(0.76)	154.44	(1.33)
1986 Aug. 7						
H	8.38	(0.39)	15.96	(1.42)	149.48	(1.89)
I	3.90	(0.19)	16.49	(0.68)	148.94	(1.20)
B	2.06	(0.12)	17.74	(0.65)	151.60	(1.01)
0138-097						
E(B-V) = 0.00						
1986 Aug. 5						
H	2.96	(0.22)	10.06	(2.02)	66.88	(6.31)
I	1.18	(0.06)	6.00	(1.08)	63.95	(4.93)
B	0.45	(0.04)	4.24	(1.02)	72.79	(6.52)
1986 Aug. 6						
H	2.82	(0.16)	7.68	(2.25)	64.73	(7.67)
I	1.16	(0.06)	7.63	(3.62)	73.96	(3.67)
B	0.30	(0.02)	5.31	(1.21)	76.10	(6.29)
1986 Aug. 7						
H	3.13	(0.14)	10.35	(2.65)	61.06	(5.41)
I	1.14	(0.05)	3.67	(1.38)	70.41	(8.77)
B	0.46	(0.03)	4.45	(1.24)	92.49	(7.18)
0219+428 3C 66A						
E(B-V) = 0.09						
1986 Aug. 1						
H	12.13	(0.56)	8.29	(0.71)	41.07	(2.60)
I	5.66	(0.53)	9.59	(0.24)	43.29	(0.69)
B	1.75	(0.17)	10.05	(0.31)	47.83	(0.78)
1986 Aug 4						
H	9.91	(0.37)	9.57	(0.60)	33.03	(1.75)
I	4.29	(0.21)	10.86	(0.38)	35.17	(0.84)
B	1.51	(0.12)	12.32	(0.53)	35.26	(1.13)

Table A1 : Continued.

Filter	Flux density (mJy)		Polarization (%)		Position angle (deg)	
1986 Aug. 6						
H	9.91	(0.46)	9.41	(1.01)	30.80	(3.16)
I	4.80	(0.23)	9.24	(0.43)	34.25	(1.18)
B	1.95	(0.12)	10.85	(0.64)	35.60	(1.45)
1986 Aug. 7						
H	10.47	(0.49)	11.08	(0.74)	30.28	(1.90)
I	4.54	(0.22)	10.19	(0.34)	32.79	(1.05)
B	1.80	(0.11)	10.51	(0.33)	34.41	(1.07)
0323+022						
E(B-V) = 0.06						
1986 Aug. 1						
H	2.16	(0.14)	0.00	(7.42)		
I	1.03	(0.10)	0.00	(2.09)		
B	0.31	(0.03)	0.00	(2.25)		
0336-019						
E(B-V) = 0.06						
1986 Aug. 5						
H	0.76	(0.13)				
I	0.32	(0.02)				
B	0.10	(0.01)				
0338-214						
E(B-V) = 0.00						
1986 Aug. 6						
H	4.01	(0.22)	11.39	(1.92)	31.92	(4.61)
I	1.47	(0.07)	10.45	(1.40)	29.31	(3.75)
B	0.29	(0.03)	10.60	(1.47)	37.32	(7.71)
1253-055 3C 279						
E(B-V) = 0.03						
1986 Aug. 1						
H	25.17	(1.17)	28.19	(0.55)	120.52	(0.72)
I	11.71	(1.09)	29.17	(0.76)	120.62	(0.37)
B	6.03	(0.60)	30.03	(0.96)	119.88	(0.76)

Table A1 : Continued.

Filter	Flux density (mJy)		Polarization (%)		Position angle (deg)	
1986 Aug. 2						
H	25.64	(1.42)	28.71	(0.59)	121.63	(0.60)
J	17.32	(1.28)	28.18	(1.06)	120.15	(0.39)
I	12.84	(1.20)	29.88	(0.36)	118.44	(0.47)
V	6.67	(0.64)	30.46	(0.79)	117.47	(0.55)
B	5.50	(0.55)	30.91	(0.28)	116.94	(0.28)
1986 Aug. 4						
H	23.82	(0.67)	33.22	(0.26)	125.35	(0.25)
J	17.64	(1.31)	34.66	(0.33)	126.97	(0.28)
I	12.15	(0.58)	36.57	(0.30)	125.01	(0.26)
R	8.49	(0.65)	37.70	(0.29)	127.32	(0.19)
V	7.38	(0.71)	38.17	(0.44)	126.12	(1.05)
B	5.55	(0.41)	39.24	(0.18)	126.09	(0.18)
U	3.64	(0.37)	41.30	(1.09)	127.66	(0.51)
1986 Aug. 5						
H	21.52	(1.00)	37.87	(0.60)	133.34	(0.40)
J	14.81	(0.69)	39.80	(0.54)	132.65	(0.28)
I	10.68	(1.00)	41.58	(0.55)	131.92	(0.30)
R	6.44	(0.61)	43.67	(2.02)	130.75	(0.52)
V	5.30	(0.51)	44.28	(0.97)	131.99	(1.05)
B	4.57	(0.46)	43.95	(0.78)	131.63	(0.31)
U	2.76	(0.40)	45.92	(0.98)	131.77	(0.62)
1986 Aug. 6						
H	17.10	(0.64)	38.13	(0.60)	136.70	(0.47)
J	12.09	(0.57)	38.53	(0.77)	136.30	(0.45)
I	8.10	(0.61)	40.51	(0.89)	136.29	(0.74)
R	6.15	(0.47)	43.07	(0.48)	135.52	(0.31)
V	5.75	(0.56)	43.31	(0.64)	136.14	(0.80)
B	3.70	(0.37)	44.36	(0.64)	134.73	(0.32)
U	2.68	(0.27)	45.47	(0.89)	135.51	(0.48)
1413+135						
E(B-V) = 0.03						
1986 Aug. 6						
H	0.75	(0.11)				
I	0.06	(0.01)				
B	0.00	(0.01)				

Table A1 : Continued.

Filter	Flux density (mJy)		Polarization (%)		Position angle (deg)	
1418+546 OQ 530						
E(B-V) = 0.03						
1986 Aug. 4						
H	9.40	(0.26)	3.56	(0.64)	138.41	(3.62)
I	4.02	(0.19)	4.62	(0.31)	142.15	(2.03)
B	1.18	(0.10)	5.82	(0.46)	138.46	(2.28)
1986 Aug. 5						
H	9.48	(0.44)	4.55	(0.60)	140.42	(3.95)
I	3.23	(0.30)	4.83	(0.52)	149.43	(3.03)
B	2.89	(0.29)	6.41	(0.39)	138.75	(2.24)
1986 Aug. 6						
H	8.65	(0.40)	1.73	(0.78)	122.26	(11.51)
I	3.29	(0.16)	4.94	(0.64)	134.68	(3.63)
B	0.91	(0.05)	5.09	(0.70)	134.51	(3.88)
PKS 1510-089						
E(B-V) = 0.06						
1986 Aug. 1						
H	2.26	(0.13)	9.07	(5.34)	177.65	(7.87)
I	1.23	(0.11)	1.65	(2.09)		
B	0.71	(0.03)	0.00	(2.32)		
1514-241 AP Libra						
E(B-V) = 0.15						
1986 Aug. 1						
H	15.96	(0.74)	1.70	(0.44)	177.65	(7.87)
I	6.87	(0.64)	1.86	(0.28)	3.27	(3.94)
B	1.16	(0.12)	2.38	(0.37)	170.79	(4.07)
1538+149 4C 14.60						
E(B-V) = 0.00						
1986 Aug. 1						
H	0.90	(0.14)	0.00	(16.62)		
I	0.34	(0.03)	10.99	(9.54)		
B	0.13	(0.01)	4.97	(7.54)		

Table A1 : Continued.

Filter	Flux density (mJy)		Polarization (%)		Position angle (deg)	
1641+399 3C 345						
E(B-V) = 0.00						
1986 Aug. 1						
H	4.40	(0.20)	16.37	(1.24)	51.41	(1.82)
J	2.43	(0.20)	14.52	(2.64)	43.60	(5.34)
I	1.45	(0.11)	13.85	(0.73)	54.84	(1.60)
R			12.80	(0.98)	55.96	(2.17)
V	0.91	(0.09)	11.32	(0.79)	52.63	(2.02)
B	0.98	(0.10)	7.85	(0.30)	52.76	(1.04)
1986 Aug. 2						
H	4.16	(0.23)	17.23	(0.95)	52.15	(1.35)
J	2.56	(0.14)	17.24	(1.02)	55.10	(1.39)
I	1.49	(0.11)	15.83	(0.82)	53.83	(1.46)
R	1.06	(0.08)	14.96	(0.66)	51.63	(1.40)
V	0.92	(0.07)	12.57	(0.79)	55.55	(1.72)
B	0.90	(0.05)	8.70	(0.29)	52.48	(0.90)
1986 Aug 4						
H	4.12	(0.19)	17.87	(0.78)	55.65	(0.99)
J	2.59	(0.12)	16.27	(0.79)	53.01	(1.35)
I	1.43	(0.07)	15.01	(0.68)	55.18	(1.34)
R	1.07	(0.04)	12.87	(0.51)	56.74	(1.13)
V	0.97	(0.09)	11.83	(0.46)	53.85	(1.36)
B	0.85	(0.07)	8.61	(0.57)	56.64	(1.67)
U	0.60	(0.06)	7.92	(0.67)	58.14	(1.13)
1986 Aug. 5						
K	8.02	(0.74)	17.93	(1.57)	63.05	(2.51)
H	4.16	(0.19)	19.56	(1.91)	55.29	(2.64)
I	1.39	(0.13)	16.09	(1.14)	59.64	(2.03)
B	0.89	(0.09)	7.73	(0.68)	57.20	(2.57)
1986 Aug. 6						
H	3.98	(0.18)	20.27	(1.30)	57.17	(1.96)
J	2.52	(0.12)	20.03	(1.23)	62.31	(1.75)
I	1.44	(0.07)	14.98	(0.72)	57.00	(1.39)
V	0.87	(0.03)	11.14	(0.81)	60.17	(2.30)
B	0.90	(0.04)	8.65	(0.38)	57.24	(1.22)

Table A1 : Continued.

Filter	Flux density (mJy)		Polarization (%)		Position angle (deg)	
1986 Aug. 7						
H	4.05	(0.19)	18.59	(1.55)	60.72	(2.06)
I	1.45	(0.07)	14.39	(0.81)	58.34	(1.61)
B	0.91	(0.05)	9.60	(0.71)	58.48	(2.48)
1717+178 OT 129						
E(B-V) = 0.06						
1986 Aug. 6						
H	1.34	(0.06)	15.55	(3.97)	39.16	(8.07)
I	0.39	(0.02)	17.82	(3.62)	45.33	(5.08)
B	0.12	(0.01)	20.92	(3.67)	45.37	(4.54)
1986 Aug. 7						
H	1.13	(0.05)	18.59	(1.55)	60.72	(2.06)
I	0.37	(0.02)	14.39	(0.81)	58.34	(1.61)
B	0.10	(0.01)	9.60	(0.71)	58.48	(2.48)
1727+502 I Zw 186						
E(B-V) = 0.00						
1986 Aug. 6						
H	4.16	(0.19)	2.36	(1.55)	142.17	(15.26)
I	1.80	(0.09)	2.51	(0.82)	91.15	(7.55)
B	0.23	(0.01)	4.16	(0.88)	78.49	(6.95)
1986 Aug. 7						
H	4.20	(0.19)	0.43	(0.98)	56.35	(31.99)
I	2.08	(0.10)	2.44	(0.54)	91.88	(6.24)
B	0.65	(0.04)	4.67	(0.59)	92.73	(3.94)
1749+096 OT 081						
E(B-V) = 0.15						
1986 Jul. 31						
H	4.35	(0.40)	16.70	(1.49)	153.42	(2.43)
I	1.44	(0.13)	16.53	(0.95)	165.69	(1.31)
B	0.32	(0.03)	18.41	(0.88)	169.93	(1.39)
1986 Aug. 5						
H	4.64	(0.22)	5.66	(1.85)	16.41	(8.04)
I	1.31	(0.06)	6.64	(1.13)	5.80	(4.53)
B	0.71	(0.04)	7.42	(1.18)	6.29	(4.29)

Table A1 : Continued.

Filter	Flux density (mJy)		Polarization (%)		Position angle (deg)	
1986 Aug. 6						
H	5.00	(0.23)	10.92	(1.35)	27.54	(6.42)
I	1.48	(0.07)	9.62	(0.72)	35.81	(1.89)
B	0.38	(0.04)	9.76	(0.85)	34.36	(2.87)
1986 Aug. 7						
H	4.16	(0.19)	7.80	(1.15)		
I	1.27	(0.06)	8.16	(0.90)	3.99	(2.90)
B	0.30	(0.02)	10.87	(0.89)	1.85	(2.69)
1921-293 OV-236						
E(B-V) = 0.12						
1986 Aug. 3						
H	1.33	(0.12)	9.78	(3.71)	104.12	(12.02)
I	0.57	(0.05)	6.34	(4.13)	100.10	(17.85)
B	0.11	(0.02)	16.89	(4.53)	160.42	(7.29)
6th. Aug 1986						
H	5.08	(0.24)	13.94	(1.91)	126.06	(4.92)
I	1.54	(0.07)	6.98	(1.82)	117.72	(6.59)
B	0.43	(0.04)	5.76	(1.85)	109.18	(8.79)
1986 Aug. 7						
H	2.52	(0.12)	7.10	(2.03)	119.56	(7.91)
I	0.54	(0.03)	8.13	(1.65)	135.93	(6.78)
B	0.08	(0.01)	5.97	(3.04)	111.08	(13.03)
PKS 2155-304						
E(B-V) = 0.00						
1986 Aug. 1						
H	27.76	(1.29)	2.03	(0.30)	148.06	(3.24)
J	21.72	(1.02)	3.11	(0.36)	149.47	(4.93)
I	21.02	(1.58)	3.10	(0.12)	141.54	(1.18)
R	14.74	(1.40)	3.62	(0.08)	137.15	(0.76)
B	14.11	(1.41)	4.03	(0.07)	138.80	(0.53)
1986 Aug. 5						
H	30.44	(1.41)	1.24	(0.35)		
I	20.63	(0.99)	0.72	(0.19)	3.60	(8.10)
B	13.23	(0.79)	0.80	(0.19)	13.33	(7.97)

Table A1 : Continued.

Filter	Flux density (mJy)		Polarization (%)		Position angle (deg)	
1986 Aug. 6						
H	28.02	(1.30)	0.73	(0.21)		
I	26.70	(2.49)	0.45	(0.16)	21.52	(9.23)
B	14.11	(1.41)	0.69	(0.21)	75.08	(7.70)
1986 Aug. 7						
H	29.88	(1.38)	1.85	(0.19)	147.57	(1.89)
J	26.12	(1.22)	1.67	(0.17)	149.75	(3.11)
I	20.82	(1.00)	1.94	(0.16)	149.14	(2.42)
R	18.90	(1.45)	2.03	(0.18)	145.32	(2.46)
V	15.60	(1.51)	2.06	(0.18)	146.78	(2.63)
B	13.47	(1.12)	2.11	(0.12)	142.71	(1.36)
2200+420 BL Lacertae E(B-V) = 0.15						
1986 Jul. 31						
H	19.01	(1.76)	11.83	(0.48)	30.74	(1.17)
I	5.21	(0.49)	12.02	(0.50)	33.50	(0.76)
B	0.73	(0.07)	14.03	(0.65)	35.33	(1.14)
1986 Aug. 1						
H	21.04	(0.97)	12.52	(0.73)	26.56	(1.37)
I	3.96	(0.37)	11.36	(0.43)	27.93	(1.03)
B	0.61	(0.06)	12.57	(0.53)	30.78	(1.24)
1986 Aug. 3						
H	19.54	(0.91)	12.36	(0.24)	20.87	(0.81)
J	11.93	(0.56)	12.49	(0.24)	21.63	(0.57)
I	4.46	(0.33)	12.93	(0.34)	22.46	(0.72)
R	2.04	(0.19)	12.80	(0.42)	25.87	(1.06)
V	1.37	(0.13)	14.24	(0.45)	24.56	(1.32)
B	0.55	(0.06)	16.70	(0.39)	26.09	(0.71)
1986 Aug. 4						
H	18.32	(0.51)	12.24	(0.44)	17.50	(1.09)
I	4.54	(0.22)	13.34	(0.40)	19.62	(0.85)
B	0.61	(0.05)	17.17	(0.71)	22.74	(1.19)

Table A1 : Continued.

Filter	Flux density (mJy)		Polarization (%)		Position angle (deg)	
1986 Aug. 5						
H	19.01	(0.88)	14.33	(0.36)	15.36	(0.58)
I	4.42	(0.21)	14.00	(0.43)	18.43	(0.94)
B	0.54	(0.03)	17.52	(0.74)	23.13	(1.22)
1986 Aug. 6						
H	15.96	(0.74)	14.92	(0.72)	19.39	(1.29)
I	5.21	(0.49)	14.15	(0.37)	22.31	(0.85)
B	0.63	(0.06)	17.24	(0.71)	23.17	(1.22)
1986 Aug. 7						
H	18.83	(0.87)	13.95	(0.38)	22.59	(0.83)
I	4.63	(0.22)	13.81	(0.40)	22.51	(0.89)
B	0.60	(0.04)	16.88	(0.68)	25.91	(1.12)
PKS 2208-137 E(B-V) = 0.00						
1986 Aug. 3						
H	1.87	(0.09)	4.11	(4.16)	152.96	(15.06)
I	0.89	(0.07)	1.40	(1.55)	51.88	(20.48)
B	1.07	(0.11)	0.00	(0.74)		
1986 Aug. 4						
H	1.82	(0.08)	0.00	(3.20)		
I	0.97	(0.05)	1.95	(1.00)	114.07	(15.56)
B	1.10	(0.09)	0.39	(0.56)	66.94	(23.78)
1986 Aug. 6						
H	1.70	(0.13)	9.32	(4.21)	157.41	(12.16)
I	1.19	(0.11)	0.00	(2.28)	109.04	(30.02)
B	1.17	(0.12)	0.99	(0.74)	77.88	(13.63)
1986 Aug. 7						
H	1.35	(0.09)	2.62	(5.23)	74.70	(31.35)
I	0.87	(0.04)	1.31	(1.67)	45.38	(20.74)
B	1.00	(0.06)	0.31	(0.75)	132.34	(21.31)

Table A1 : Continued.

Filter	Flux density (mJy)		Polarization (%)		Position angle (deg)	
2223-052 3C 446						
E(B-V) = 0.03						
1986 Aug. 4						
H	0.58	(0.08)	3.65	(20.99)	116.30	(28.41)
I	0.27	(0.02)	2.80	(7.93)	105.49	(23.25)
B	0.15	(0.01)	0.75	(5.65)	142.91	(28.84)
2230+114 4C 11.69						
E(B-V) = 0.03						
1986 Aug. 3						
H	1.18	(0.10)	8.29	(4.76)	154.21	(14.60)
I	0.64	(0.05)	3.77	(1.97)	52.35	(12.08)
B	0.42	(0.04)	0.00	(1.20)		
1986 Aug. 4						
H	1.02	(0.05)	7.70	(7.49)	136.84	(23.37)
I	0.64	(0.03)	3.86	(2.13)	109.45	(16.37)
B	0.39	(0.03)	0.00	(1.89)	100.39	(34.85)
2251+158						
E(B-V) = 0.06						
1986 Aug. 5						
H	1.97	(0.16)	6.40	(2.91)	152.90	(14.99)
I	1.12	(0.05)	1.11	(1.31)	27.84	(19.01)
B	0.65	(0.04)	0.00	(0.68)		
2254+074 OY 091						
E(B-V) = 0.06						
1986 Jul. 31						
H	2.08	(0.19)	7.06	(4.13)	46.26	(12.00)
I	0.93	(0.09)	10.09	(1.30)	57.36	(3.64)
B	0.20	(0.03)	18.91	(2.53)	57.23	(3.77)
1986 Aug. 1						
H	1.78	(0.12)	7.90	(5.62)	45.31	(12.85)
I	0.85	(0.08)	10.77	(1.48)	52.72	(4.24)
B	0.16	(0.02)	14.75	(1.57)	43.95	(3.99)

Table A1 : Continued.

Filter	Flux density (mJy)		Polarization (%)		Position angle (deg)	
1986 Aug. 3						
H	2.50	(0.12)	10.54	(1.37)	52.66	(4.66)
J	1.75	(0.08)	12.91	(1.55)	41.11	(5.37)
I	0.84	(0.06)	11.80	(1.08)	47.70	(2.50)
R	0.52	(0.05)	12.28	(0.93)	43.97	(2.91)
V	0.23	(0.02)	15.40	(1.93)	45.59	(4.41)
B	0.18	(0.02)	18.71	(1.12)	42.44	(1.48)
1986 Aug. 4						
H	2.30	(0.06)	10.31	(1.15)	44.45	(3.18)
J	1.72	(0.08)	9.03	(1.30)	43.38	(3.54)
I	0.85	(0.04)	8.99	(0.90)	48.91	(2.77)
R	0.52	(0.03)	10.27	(0.63)	45.69	(1.84)
V	0.36	(0.03)	10.92	(0.87)	47.60	(2.92)
B	0.18	(0.02)	19.17	(0.95)	44.17	(1.40)
U	0.12	(0.01)	18.36	(4.04)	47.46	(5.98)
1986 Aug. 5						
H	2.39	(0.11)	7.69	(2.40)	55.64	(6.75)
I	0.90	(0.04)	8.44	(1.31)	40.39	(3.05)
B	0.20	(0.01)	15.80	(1.33)	48.81	(2.32)
1986 Aug. 6						
H	2.48	(0.11)	4.22	(2.19)	59.06	(14.98)
I	1.18	(0.11)	7.38	(0.98)	57.42	(3.80)
B	0.21	(0.01)	11.63	(1.21)	55.39	(3.22)
1986 Aug. 7						
H	2.01	(0.11)	7.91	(4.38)	60.36	(11.00)
I	0.44	(0.02)	10.74	(3.18)	4.26	(7.83)
B	0.11	(0.01)	2.30	(3.42)	54.50	(26.31)

Table A2 : The Observations of 1987 July 27 – 1987 July 30

Filter	Flux density (mJy)		Polarization (%)		Position angle (deg)	
0048-097 OB-081						
E(B-V) = 0.00						
1987 Jul. 27						
J	4.98	(0.32)	15.53	(1.30)	107.73	(1.95)
I	2.30	(0.11)	17.25	(0.82)	104.74	(1.27)
R	1.68	(0.09)	16.50	(0.80)	104.89	(1.22)
V	1.48	(0.08)	16.12	(0.86)	105.73	(2.43)
B	1.30	(0.08)	16.76	(0.71)	102.56	(1.04)
U	0.95	(0.10)	14.56	(0.75)	102.90	(1.46)
1987 Jul. 29						
K	9.64	(0.89)	19.34	(1.83)	68.56	(2.80)
H	6.24	(0.58)	21.72	(1.13)	68.18	(1.71)
I	2.55	(0.24)	21.17	(1.02)	69.15	(1.45)
R	1.94	(0.18)	21.32	(0.70)	67.18	(1.38)
V	1.59	(0.15)	20.54	(1.41)	67.50	(2.39)
B	1.17	(0.12)	22.69	(0.66)	67.74	(1.14)
U	0.79	(0.08)	23.03	(0.81)	68.34	(1.30)
1987 Jul. 30						
K	8.02	(0.44)	12.08	(1.53)	115.22	(3.67)
H	5.80	(0.11)	11.72	(0.98)	115.47	(2.50)
I	2.33	(0.11)	12.92	(0.59)	115.59	(1.71)
R	1.63	(0.08)	13.55	(0.57)	117.00	(1.32)
V	1.38	(0.07)	13.65	(0.86)	118.35	(2.12)
B	1.05	(0.06)	13.56	(0.57)	113.95	(1.56)
U	0.68	(0.07)	14.48	(1.16)	111.16	(2.42)
PKS 0106+013						
E(B-V) = 0.00						
1987 Jul. 28						
H	0.65	(0.03)	0.00	(13.02)		
I	0.29	(0.02)	17.44	(5.83)	138.64	(8.52)
R	0.19	(0.01)	11.30	(5.55)	146.86	(15.43)
V	0.17	(0.02)	0.00	(8.75)		
B	0.16	(0.01)	7.12	(3.39)	146.48	(9.67)
U	0.11	(0.01)	14.37	(2.39)	130.09	(5.03)

Table A2 : Continued.

Filter	Flux density (mJy)		Polarization (%)		Position angle (deg)	
GC 0109+224						
E(B-V) = 0.06						
1987 Jul. 27						
H	4.81	(0.22)	13.63	(1.10)	100.66	(2.25)
I	1.77	(0.08)	14.04	(0.90)	103.58	(1.57)
R	1.19	(0.06)	13.79	(0.60)	104.61	(1.74)
V	0.94	(0.05)	15.04	(1.67)	107.92	(2.04)
B	0.73	(0.04)	15.24	(0.60)	105.83	(1.48)
U	0.51	(0.05)	14.15	(0.99)	107.34	(2.19)
1987 Jul. 30						
H	4.86	(0.23)	9.37	(1.12)	109.42	(3.73)
I	1.92	(0.09)	8.91	(0.85)	108.91	(2.25)
R	1.29	(0.07)	9.51	(0.49)	109.15	(2.28)
V	1.01	(0.05)	9.08	(0.94)	104.22	(3.96)
B	0.72	(0.04)	9.12	(0.57)	110.09	(1.60)
U	0.43	(0.03)	8.35	(1.04)	113.16	(4.37)
0118-272						
E(B-V) = 0.00						
1987 Jul. 27						
H	9.02	(0.42)	12.53	(0.71)	25.62	(1.73)
I	2.65	(0.13)	12.96	(1.15)	29.58	(2.29)
R	2.25	(0.11)	13.92	(0.98)	27.80	(1.83)
V	2.09	(0.11)	14.18	(0.86)	24.41	(1.92)
B	1.89	(0.11)	15.90	(0.57)	26.59	(1.23)
U	1.37	(0.14)	16.02	(1.08)	28.05	(1.97)
1987 Jul. 30						
K	11.48	(0.53)	12.31	(1.15)	28.51	(2.85)
H	8.62	(0.40)	12.82	(0.86)	29.04	(2.20)
I	3.62	(0.17)	14.19	(0.53)	30.66	(1.19)
R	2.68	(0.14)	13.58	(0.50)	30.47	(1.36)
V	2.25	(0.12)	13.94	(0.64)	27.20	(1.85)
B	1.78	(0.11)	15.03	(0.39)	28.54	(1.08)
U	1.44	(0.15)	15.01	(0.39)	27.58	(1.48)

Table A2 : Continued.

Filter	Flux density (mJy)		Polarization (%)		Position angle (deg)	
0138-097						
E(B-V) = 0.00						
1987 Jul. 28						
H	3.49	(0.16)	14.76	(3.03)	104.72	(3.90)
I	1.34	(0.06)	19.09	(1.33)	103.14	(3.28)
R	1.03	(0.05)	20.56	(1.24)	107.72	(1.83)
V	0.87	(0.05)	19.95	(1.65)	104.91	(2.60)
B	0.71	(0.04)	19.99	(1.01)	104.83	(1.33)
U	0.50	(0.05)	20.88	(1.41)	103.47	(1.92)
1987 Jul. 30						
H	3.07	(0.14)	21.05	(2.94)	104.76	(3.58)
I	1.35	(0.06)	22.86	(2.04)	99.90	(2.08)
R	1.01	(0.05)	18.38	(1.81)	80.35	(2.08)
V	0.85	(0.05)	20.71	(2.38)	105.77	(2.19)
B	0.69	(0.05)	22.29	(1.45)	102.91	(2.26)
U	0.43	(0.04)	20.18	(1.73)	106.91	(2.83)
0219-164						
E(B-V) = 0.00						
1987 Jul. 28						
K	13.31	(0.61)	14.83	(2.46)	160.96	(4.55)
H	11.15	(0.52)	13.67	(1.84)	170.47	(3.04)
J	7.67	(0.71)	12.85	(1.06)	159.53	(1.54)
I	5.48	(0.26)	12.45	(0.42)	159.96	(1.21)
R	4.14	(0.21)	12.65	(0.34)	161.33	(1.07)
V	3.64	(0.20)	12.37	(0.50)	160.92	(1.52)
B	3.00	(0.18)	12.70	(0.33)	161.16	(1.14)
U	2.10	(0.13)	12.83	(0.68)	160.19	(1.29)
0219+428 3C 66A						
E(B-V) = 0.09						
1987 Jul. 27						
H	11.17	(0.52)	12.53	(0.61)	164.20	(1.65)
I	3.92	(0.19)	11.20	(1.02)	162.63	(1.93)
R	2.47	(0.15)	12.52	(0.72)	162.87	(1.98)
V	2.34	(0.13)	14.25	(0.69)	161.93	(1.70)
B	1.81	(0.14)	13.16	(0.62)	163.65	(1.63)
U	1.34	(0.14)	14.47	(1.02)	165.89	(2.02)

Table A2 : Continued.

Filter	Flux density (mJy)		Polarization (%)		Position angle (deg)	
1987 Jul. 30						
H	9.55	(0.44)	13.30	(0.99)	159.89	(2.39)
I	4.58	(0.22)	11.72	(1.34)	158.10	(2.97)
R	3.29	(0.17)	12.54	(0.88)	159.94	(2.13)
V	2.64	(0.14)	13.93	(0.76)	164.56	(1.63)
B	2.02	(0.12)	14.39	(0.50)	162.82	(1.20)
U	1.34	(0.14)	12.15	(1.53)	158.73	(2.19)
AO 0235+164						
E(B-V) = 0.15						
1987 Jul. 28						
K	11.79	(0.54)	12.05	(1.04)	42.55	(2.92)
H	6.97	(0.32)	11.77	(1.02)	45.41	(3.25)
J	3.26	(0.30)	14.73	(4.42)	33.01	(9.88)
I	0.96	(0.05)	15.52	(1.59)	49.44	(3.04)
R	0.41	(0.02)	10.18	(1.58)	56.00	(3.80)
V	0.22	(0.01)	14.52	(3.67)	50.30	(9.31)
B	0.09	(0.01)	12.08	(3.73)	43.43	(8.36)
U	0.03	(0.00)	33.02	(10.17)	47.91	(8.59)
1253-055 3C 279						
E(B-V) = 0.03						
1987 Jul. 28						
K	21.88	(2.02)	26.69	(0.77)	108.71	(1.15)
H	13.96	(1.29)	27.53	(0.68)	109.21	(1.12)
J	7.77	(0.72)	31.01	(0.84)	108.87	(1.17)
I	4.45	(0.42)	32.43	(0.77)	110.57	(0.95)
R	2.89	(0.27)	34.10	(0.61)	110.90	(0.94)
V	1.92	(0.19)	34.78	(1.14)	106.41	(1.14)
B	1.26	(0.13)	35.56	(1.43)	109.41	(1.11)
U	0.63	(0.06)	35.43	(2.29)	107.74	(1.50)
1418+546 OQ 530						
E(B-V) = 0.03						
1987 Jul. 30						
H	8.49	(0.39)	2.50	(0.64)	54.32	(7.65)
J	5.79	(0.27)	4.12	(2.29)	41.04	(5.74)
I	2.94	(0.04)	3.69	(0.44)	52.71	(3.63)
R	2.00	(0.19)	5.17	(0.39)	64.37	(2.02)
V	1.46	(0.14)	5.71	(0.71)	64.43	(3.86)
B	1.05	(0.10)	7.31	(0.41)	65.58	(1.86)
U	0.69	(0.07)	8.68	(0.96)	60.93	(2.70)

Table A2 : Continued.

Filter	Flux density (mJy)		Polarization (%)		Position angle (deg)	
1514-241 AP Libra						
E(B-V) = 0.15						
1987 Jul. 27						
K	23.09	(0.07)	5.11	(0.72)	19.56	(4.28)
H	19.01	(1.76)	3.70	(0.62)	16.72	(3.85)
J	14.21	(1.32)	5.42	(0.44)	14.28	(2.05)
I	6.87	(0.64)	4.76	(0.30)	12.37	(1.61)
R	4.07	(0.39)	5.12	(0.24)	15.40	(1.35)
V	2.86	(0.28)	4.83	(0.34)	18.72	(2.25)
B	1.39	(0.14)	6.13	(0.23)	17.41	(1.22)
U	0.86	(0.04)	6.92	(0.65)	16.50	(2.56)
1641+399 3C 345						
E(B-V) = 0.00						
1987 Jul. 28						
K	2.66	(0.12)	1.52	(2.19)	179.39	(17.65)
H	1.92	(0.09)	0.00	(1.93)		
J	1.15	(0.05)	2.32	(3.51)	72.37	(23.98)
I	.0.58	(0.03)	2.32	(1.28)	50.69	(13.47)
R	0.47	(0.02)	3.41	(0.95)	123.12	(7.39)
V	0.43	(0.02)	3.47	(1.24)	119.39	(9.18)
B	0.44	(0.03)	1.76	(0.46)	131.81	(7.22)
U	0.25	(0.02)	2.62	(0.81)	127.29	(8.41)
1987 Jul. 30						
H	1.69	(0.08)	2.74	(1.78)	30.62	(13.86)
I	0.58	(0.05)	0.86	(1.97)	131.75	(26.86)
R	0.47	(0.04)	1.61	(1.29)	127.34	(16.72)
V	0.44	(0.04)	0.00	(3.39)		
B	0.43	(0.04)	1.38	(0.77)	123.69	(12.96)
U	0.24	(0.02)	1.99	(1.09)	73.13	(13.91)
1717+178 OT 129						
E(B-V) = 0.06						
1987 Jul. 30						
H	0.55	(0.10)	16.85	(11.90)	103.02	(13.86)
I	0.16	(0.02)	0.00	(11.88)		
R	0.10	(0.01)	6.33	(7.03)	150.64	(19.41)
V	0.08	(0.01)	10.37	(11.63)	34.78	(20.79)
B	0.04	(0.01)	7.11	(7.81)	134.50	(21.14)
U	0.02	(0.00)	0.00	(16.81)		

Table A2 : Continued.

Filter	Flux density (mJy)		Polarization (%)		Position angle (deg)	
1749+096 OT 081						
E(B-V) = 0.15						
1987 Jul. 27						
J	1.34	(0.09)	4.06	(2.23)	18.99	(16.94)
I	0.41	(0.02)	9.96	(3.87)	35.57	(12.25)
R	0.22	(0.01)	9.71	(4.01)	13.91	(10.32)
V	0.14	(0.01)	18.96	(6.76)	171.65	(9.63)
B	0.07	(0.00)	23.85	(3.78)	0.71	(5.88)
U	0.04	(0.00)	13.87	(7.20)	171.95	(13.11)
1921-293 OV-236						
E(B-V) = 0.12						
1987 Jul. 27						
J	1.11	(0.06)	6.01	(3.86)	85.18	(15.94)
I	0.79	(0.05)	3.91	(2.92)	130.94	(17.44)
R	0.69	(0.07)	5.60	(2.26)	105.55	(10.49)
V	0.19	(0.02)	0.00	(5.44)		
B	0.15	(0.01)	0.00	(3.32)		
2032+107						
E(B-V) = 0.12						
1987 Jul. 27						
J	8.61	(0.40)	0.56	(0.47)		
I	4.36	(0.21)	0.86	(0.40)		
R	1.98	(0.19)	1.08	(0.44)		
V	1.03	(0.06)	1.38	(1.08)		
B	0.28	(0.02)	0.00	(1.15)		
U	0.04	(0.00)	0.00	(7.18)		
PKS 2155-304						
E(B-V) = 0.00						
1987 Jul. 27						
K	67.94	(3.14)	9.16	(0.24)	175.89	(1.11)
H	60.73	(2.81)	9.40	(0.70)	176.16	(1.51)
J	55.58	(3.61)	10.14	(0.97)	172.93	(1.01)
I	36.52	(2.74)	10.29	(0.23)	171.83	(1.07)
R	27.07	(2.56)	10.46	(0.23)	171.20	(1.07)
V	26.13	(2.06)	10.69	(0.21)	170.48	(1.03)
B	24.29	(1.81)	10.91	(0.15)	169.39	(0.94)
U	18.10	(1.85)	10.93	(0.16)	169.14	(0.96)

Table A2 : Continued.

Filter	Flux density (mJy)		Polarization (%)		Position angle (deg)	
2200+420 BL Lacerta						
E(B-V) = 0.15						
1987 Jul. 27						
K	28.53	(1.32)	10.42	(0.26)	16.50	(1.11)
H	20.84	(1.35)	9.60	(0.35)	16.44	(1.44)
J	13.32	(0.62)	8.52	(0.40)	16.12	(1.74)
I	5.12	(0.25)	7.83	(0.35)	15.57	(1.41)
R	3.12	(0.16)	8.40	(0.23)	14.93	(1.12)
V	1.60	(0.11)	8.50	(0.56)	10.96	(1.96)
B	0.67	(0.07)	8.30	(0.44)	10.56	(1.57)
U	0.30	(0.03)	8.32	(1.05)	11.59	(2.99)
1987 Jul. 28						
K	32.76	(1.51)	13.23	(0.42)	22.96	(1.24)
H	23.49	(1.09)	11.93	(0.19)	19.73	(0.91)
J	14.88	(1.10)	12.12	(0.41)	17.12	(1.31)
I	5.36	(0.31)	10.26	(0.40)	16.80	(1.16)
R	2.55	(0.13)	10.56	(0.41)	14.99	(1.12)
V	1.55	(0.08)	9.77	(0.70)	9.98	(1.82)
B	0.69	(0.04)	12.27	(0.59)	9.47	(1.46)
U	0.28	(0.02)	11.42	(1.20)	5.74	(2.79)
1987 Jul. 30						
H	23.28	(1.08)	13.85	(0.32)	18.81	(1.25)
I	5.56	(0.27)	12.57	(0.62)	16.96	(1.29)
R	2.84	(0.14)	12.01	(0.55)	12.54	(1.16)
V	1.60	(0.09)	10.36	(1.10)	15.46	(2.48)
B	0.74	(0.04)	13.25	(0.60)	10.06	(1.34)
U	0.29	(0.02)	13.04	(1.54)	4.75	(1.96)
2223-052 3C 446						
E(B-V) = 0.03						
1987 Jul. 27						
J	1.38	(0.09)	12.99	(3.11)	76.27	(6.18)
I	0.65	(0.03)	11.64	(1.87)	70.41	(4.34)
R	0.47	(0.02)	13.21	(1.24)	76.03	(2.95)
V	0.33	(0.02)	17.42	(2.35)	75.44	(4.28)
B	0.22	(0.01)	11.59	(1.20)	68.41	(2.77)
U	0.16	(0.02)	9.75	(1.84)	71.52	(6.29)

Table A2 : Continued.

Filter	Flux density (mJy)		Polarization (%)		Position angle (deg)	
1987 Jul. 29						
H	2.06	(0.19)	9.29	(1.48)	88.83	(5.65)
I	0.61	(0.06)	5.87	(2.05)	87.07	(9.47)
R	0.44	(0.04)	7.90	(1.35)	82.59	(4.89)
V	0.33	(0.03)	7.35	(2.75)	73.49	(7.78)
B	0.24	(0.02)	9.57	(1.15)	73.00	(4.41)
U	0.17	(0.02)	8.34	(2.17)	78.73	(6.83)
1987 Jul. 30						
H	1.98	(0.11)	9.04	(1.83)	77.89	(5.61)
I	0.64	(0.03)	7.23	(2.44)	55.10	(8.95)
R	0.45	(0.02)	7.02	(1.88)	71.52	(7.08)
V	0.31	(0.02)	7.80	(3.33)	84.66	(11.35)
B	0.22	(0.01)	9.77	(1.88)	68.42	(5.38)
U	0.15	(0.01)	6.08	(2.51)	60.98	(10.71)
2251+158						
E(B-V) = 0.06						
1987 Jul. 28						
H	2.41	(0.16)	4.62	(2.06)	10.28	(9.32)
I	1.16	(0.06)	0.55	(1.18)	61.84	(22.04)
R	0.98	(0.05)	1.38	(0.87)	24.86	(14.17)
V	0.85	(0.05)	0.00	(1.21)		
B	0.60	(0.04)	0.00	(0.63)		
U	0.36	(0.03)	1.17	(0.97)	155.83	(24.63)
2254+074 OY 091						
E(B-V) = 0.06						
1987 Jul. 28						
H	2.46	(0.11)	11.55	(1.19)	136.59	(3.17)
I	1.04	(0.05)	9.07	(0.94)	138.02	(3.07)
R	0.67	(0.03)	11.87	(0.83)	142.79	(2.18)
V	0.45	(0.02)	13.76	(1.51)	148.83	(2.17)
B	0.24	(0.01)	17.40	(1.16)	141.65	(2.19)
U	0.12	(0.01)	14.28	(1.82)	146.91	(4.89)

Table A2 : Continued.

Filter	Flux density (mJy)		Polarization (%)		Position angle (deg)	
1987 Jul. 30						
H	2.74	(0.13)	13.62	(1.48)	139.19	(2.72)
I	1.06	(0.05)	12.06	(1.26)	143.84	(3.05)
R	0.67	(0.03)	9.89	(1.09)	142.96	(2.96)
V	0.47	(0.03)	12.09	(1.72)	141.55	(4.19)
B	0.24	(0.01)	15.76	(1.30)	148.76	(2.21)
U	0.13	(0.01)	17.52	(2.94)	139.69	(4.49)

Table A3 : The Observations of 1987 September 18 – 1987 September 21

Filter	Flux density (mJy)	Polarization (%)	Position angle (deg)
0048-097 OB-081			
E(B-V) = 0.00			
1987 Sep. 18			
H		5.40 (0.84)	81.26 (4.09)
I		3.64 (0.76)	78.81 (5.89)
R		4.52 (0.50)	88.50 (3.03)
V		3.60 (1.26)	87.11 (6.75)
B		4.09 (0.41)	94.10 (3.04)
U		3.12 (0.73)	95.17 (9.28)
1987 Sep. 19			
H	8.15 (0.75)	4.52 (0.60)	94.86 (4.07)
J	5.31 (0.49)	4.50 (0.75)	90.39 (4.22)
I	2.80 (0.26)	5.35 (0.50)	97.69 (5.21)
R	2.34 (0.22)	5.93 (0.30)	90.39 (1.37)
V	1.91 (0.18)	6.18 (0.70)	94.85 (2.29)
B	1.55 (0.15)	5.76 (0.44)	92.14 (1.76)
U	0.95 (0.10)	5.71 (0.51)	92.43 (2.25)
1987 Sep. 20			
H		3.18 (0.60)	90.70 (4.31)
I		4.17 (0.54)	86.53 (3.93)
R		4.15 (0.41)	89.69 (2.50)
V		2.46 (0.90)	83.31 (9.45)
B		5.23 (0.50)	88.92 (2.50)
U		4.08 (0.72)	94.61 (5.36)
PKS 0106+013			
E(B-V) = 0.00			
1987 Sep. 21			
H	0.43 (0.10)	36.73 (13.65)	119.33 (9.98)
I	0.28 (0.04)	0.00 (40.86)	
R	0.19 (0.02)	5.64 (4.43)	95.11 (24.59)
V	0.21 (0.03)	0.00 (10.99)	
B	0.15 (0.01)	0.54 (4.57)	56.51 (29.35)
U		0.00 (7.61)	

Table A3 : Continued.

Filter	Flux density (mJy)		Polarization (%)		Position angle (deg)	
GC 0109+224						
E(B-V) = 0.06						
1987 Sep. 19						
H	7.22	(0.67)	4.12	(0.70)	117.86	(5.10)
I	2.58	(0.24)	3.92	(0.69)	124.48	(3.95)
R	1.88	(0.18)	4.02	(0.40)	115.87	(2.84)
V	1.34	(0.13)	3.89	(1.22)	123.55	(8.53)
B	1.03	(0.10)	3.66	(0.54)	121.28	(4.32)
U	0.67	(0.07)	3.88	(0.81)	123.90	(5.81)
1987 Sep. 20						
H			13.16	(1.03)	107.82	(2.92)
I			11.64	(1.16)	105.58	(2.25)
R			15.01	(0.98)	107.98	(1.41)
V			15.90	(1.66)	110.97	(3.01)
B			14.37	(0.98)	112.02	(1.39)
U			17.26	(1.81)	109.32	(1.80)
1987 Sep. 21						
H	5.48	(0.51)	13.87	(0.74)	105.70	(1.51)
I	1.95	(0.18)	13.81	(0.57)	103.46	(1.54)
R	1.36	(0.13)	15.29	(0.50)	100.78	(0.76)
V	1.02	(0.10)	17.27	(1.37)	98.60	(2.35)
B	0.71	(0.07)	16.44	(0.64)	105.38	(1.14)
U			16.14	(0.82)	102.34	(1.79)
0118-272						
E(B-V) = 0.00						
1987 Sep. 20						
H			14.68	(0.54)	150.70	(1.26)
I			16.77	(0.68)	150.14	(1.04)
R			16.21	(0.56)	150.42	(0.73)
V			18.69	(1.01)	151.92	(1.37)
B			18.92	(0.99)	149.22	(0.72)
U			15.23	(1.37)	150.95	(1.84)

Table A3 : Continued.

Filter	Flux density (mJy)		Polarization (%)		Position angle (deg)	
1987 Sep. 21						
H	7.44	(0.69)	15.25	(0.66)	148.50	(1.39)
I	3.07	(0.29)	16.00	(0.72)	149.91	(1.30)
R	2.34	(0.22)	15.81	(0.47)	150.33	(0.79)
V	1.91	(0.18)	17.94	(0.96)	152.33	(1.42)
B	1.48	(0.15)	17.95	(0.53)	151.56	(0.64)
U			16.54	(0.88)	150.45	(1.57)
0138-097						
E(B-V) = 0.00						
1987 Sep. 19						
K	4.21	(0.39)	21.61	(2.98)	74.36	(2.34)
H	3.40	(0.31)	20.60	(1.62)	73.96	(2.26)
I	1.34	(0.12)	24.80	(1.08)	71.11	(1.29)
R	1.02	(0.10)	25.86	(0.67)	72.81	(0.77)
V	0.83	(0.08)	26.04	(1.22)	74.30	(1.39)
B	0.62	(0.06)	29.25	(0.92)	71.62	(0.83)
U	0.38	(0.04)	26.81	(1.35)	74.89	(1.49)
1987 Sep. 20						
H	2.96	(0.27)	22.23	(1.34)	70.40	(1.66)
I	1.61	(0.15)	21.45	(0.99)	74.33	(1.34)
R	1.23	(0.12)	24.51	(0.66)	73.32	(0.81)
V	1.00	(0.10)	27.33	(1.59)	73.54	(1.66)
B	0.81	(0.08)	27.07	(0.87)	73.53	(0.89)
U			27.05	(1.48)	74.69	(1.58)
1987 Sep. 21						
H	2.96	(0.27)	23.95	(1.44)	72.70	(1.72)
I	1.47	(0.14)	23.53	(1.41)	73.40	(1.80)
R	1.12	(0.11)	24.75	(0.96)	72.79	(1.12)
V	0.91	(0.09)	23.08	(1.82)	71.63	(2.31)
B	0.71	(0.07)	26.63	(1.07)	73.13	(1.13)
U			24.95	(1.47)	76.01	(1.70)

Table A3 : Continued.

Filter	Flux density (mJy)	Polarization (%)	Position angle (deg)
0219+428 3C 66A E(B-V) = 0.09			
1987 Sep. 18			
H		14.80 (0.49)	22.16 (0.98)
I		13.38 (0.78)	22.86 (1.71)
R		13.49 (0.43)	24.04 (0.89)
V		15.43 (0.73)	24.19 (0.37)
B		14.59 (0.73)	23.28 (1.17)
U		12.15 (1.07)	22.06 (2.16)
1987 Sep. 19			
H		14.11 (0.53)	22.86 (1.06)
I		14.19 (0.80)	24.47 (1.69)
R		13.73 (0.38)	24.06 (0.76)
V		15.14 (0.74)	26.87 (1.48)
B		15.29 (0.53)	24.75 (0.95)
U		13.98 (0.61)	24.79 (1.18)
1987 Sep. 20			
H	11.27 (1.04)	14.11 (0.43)	23.50 (0.95)
I	4.71 (0.44)	15.46 (0.55)	26.52 (1.05)
R	3.68 (0.35)	14.30 (0.37)	25.95 (0.76)
V	3.09 (0.30)	15.94 (0.69)	25.80 (1.35)
B	2.30 (0.23)	14.38 (0.46)	26.50 (0.96)
U		14.25 (0.64)	28.47 (1.39)
1987 Sep. 21			
H		12.50 (0.55)	24.90 (1.25)
I		12.82 (0.69)	27.53 (1.54)
R		13.31 (0.37)	27.40 (0.84)
V		14.26 (0.60)	28.07 (1.21)
B		13.43 (0.35)	28.92 (0.73)
U		12.10 (0.68)	30.04 (1.64)

Table A3 : Continued.

Filter	Flux density (mJy)		Polarization (%)		Position angle (deg)	
AO 0235+164						
E(B-V) = 0.15						
1987 Sep. 18						
H			2.47	(1.06)	10.46	(13.90)
I			1.90	(1.48)	169.90	(19.42)
R			2.30	(0.90)	14.73	(13.22)
V			9.06	(3.46)	18.29	(10.93)
B			0.61	(1.89)	33.82	(27.69)
U			6.97	(5.29)	36.60	(18.18)
1987 Sep. 20						
K	5.80	(0.54)	1.66	(1.90)	47.71	(18.00)
H	3.97	(0.37)	5.78	(0.95)	52.70	(4.58)
J	2.47	(0.23)	8.59	(1.26)	56.59	(4.42)
I	0.99	(0.09)	11.04	(0.83)	55.91	(1.59)
R	0.56	(0.05)	10.10	(0.70)	55.26	(1.84)
V	0.31	(0.03)	10.00	(2.24)	57.95	(5.46)
B	0.14	(0.01)	11.65	(1.34)	60.67	(3.26)
U			8.28	(3.42)	68.16	(9.88)
0300+470 4C 47.08						
E(B-V) = 0.15						
1987 Sep. 20						
H			9.55	(1.16)	9.00	(3.39)
I			9.44	(1.52)	1.76	(4.48)
R			8.69	(1.02)	13.96	(2.97)
V			5.05	(4.91)	167.70	(20.97)
B			6.58	(2.12)	8.84	(8.92)
U			7.53	(5.37)	4.07	(11.70)
0323+022						
E(B-V) = 0.06						
1987 Sep. 21						
H			4.65	(1.63)	8.60	(6.61)
I			3.84	(1.02)	3.53	(8.40)
R			3.78	(0.70)	14.46	(5.13)
V			0.00	(1.84)		
B			3.49	(0.90)	177.22	(7.43)
U			5.27	(0.86)	11.59	(6.65)

Table A3 : Continued.

Filter	Flux density (mJy)	Polarization (%)	Position angle (deg)
0338-214			
E(B-V) = 0.00			
1987 Sep. 19			
H	11.48 (1.60)	70.46 (3.69)	
I	11.07 (1.56)	62.59 (3.88)	
R	10.62 (0.95)	65.86 (2.00)	
V	15.58 (2.90)	65.05 (6.33)	
B	12.37 (1.13)	64.02 (3.21)	
U	8.15 (3.39)	60.82 (11.61)	
PKS 0403-132			
E(B-V) = 0.00			
1987 Sep. 19			
H	7.14 (3.93)	151.46 (14.00)	
I	0.00 (3.24)		
R	0.94 (1.16)	87.96 (23.69)	
V	0.00 (3.10)		
B	0.62 (1.19)	27.87 (21.39)	
U	0.00 (2.04)		
0414+009			
E(B-V) = 0.12			
1987 Sep. 21			
H	1.99 (3.15)	30.90 (24.90)	
I	0.00 (3.13)		
R	2.09 (1.30)	62.84 (20.17)	
V	0.00 (4.57)		
B	0.70 (1.74)	29.90 (25.78)	
U	0.00 (2.73)		
PKS 0735+178			
E(B-V) = 0.03			
1987 Sep. 19			
H	6.64 (0.68)	144.76 (2.88)	
I	8.08 (0.88)	132.34 (3.03)	
R	6.77 (0.61)	137.22 (2.85)	
V	7.44 (1.52)	131.02 (5.49)	
B	6.59 (0.93)	130.39 (3.66)	
U	5.68 (1.59)	129.65 (8.10)	

Table A3 : Continued.

Filter	Flux density (mJy)	Polarization (%)	Position angle (deg)
PKS 0736+017			
E(B-V) = 0.15			
1987 Sep. 19			
H	8.97 (7.45)		117.83 (17.10)
I	1.95 (4.32)		157.69 (21.99)
R	6.32 (1.50)		94.47 (20.28)
V	0.00 (10.13)		
B	5.41 (5.71)		157.70 (10.91)
U	4.06 (7.34)		118.15 (22.18)
1987 Sep. 20			
H	2.32 (1.16)		133.40 (11.80)
I	1.44 (0.99)		50.40 (21.32)
R	0.00 (0.80)		
V	0.00 (2.05)		
B	0.50 (0.85)		51.76 (20.59)
U	0.00 (1.36)		
1418+546 OQ 530			
E(B-V) = 0.03			
1987 Sep. 20			
H	8.21 (0.99)		3.96 (2.42)
I	15.37 (2.82)		3.45 (4.35)
R	11.30 (2.23)		15.26 (5.02)
V	17.53 (4.76)		179.34 (12.40)
B	0.00 (6.11)		
U	0.00 (35.16)		
1987 Sep. 21			
H	7.22 (1.46)		15.39 (7.78)
I	8.99 (1.48)		7.56 (5.26)
R	12.83 (1.12)		3.12 (2.95)
V	13.13 (3.13)		14.46 (4.09)
B	9.78 (2.52)		8.53 (6.39)
U	12.93 (7.57)		19.81 (15.08)

Table A3 : Continued.

Filter	Flux density (mJy)		Polarization (%)		Position angle (deg)	
1641+399 3C 345						
E(B-V) = 0.00						
1987 Sep. 19						
H	1.55	(0.14)	4.02	(3.28)	169.86	(18.80)
I	0.49	(0.05)	11.15	(3.89)	82.71	(8.74)
R	0.37	(0.04)	0.00	(1.62)		
V	0.36	(0.04)	0.00	(1.47)		
B	0.39	(0.04)	0.00	(1.41)		
U	0.24	(0.03)	1.49	(2.13)	138.80	(26.06)
1987 Sep. 20						
H			11.35	(3.33)	13.56	(8.49)
I			3.62	(6.74)	138.24	(33.19)
R			8.59	(3.64)	174.29	(10.87)
V			1.58	(9.13)	121.54	(27.23)
B			3.67	(3.02)	115.25	(17.74)
U			12.91	(13.28)	17.04	(12.31)
1652+398 Mkn 501						
E(B-V) = 0.00						
1987 Sep. 21						
K			1.34	(0.26)	138.09	(4.81)
H			1.24	(0.19)	125.70	(4.83)
J			1.57	(0.20)	124.98	(3.85)
I			1.56	(0.16)	126.94	(2.52)
R			1.95	(0.11)	122.09	(1.55)
V			2.50	(0.18)	124.08	(2.06)
B			3.53	(0.14)	124.06	(1.18)
U			3.76	(0.22)	119.20	(1.62)
1717+178 OT 129						
E(B-V) = 0.06						
1987 Sep. 20						
H			2.03	(2.31)	168.16	(21.80)
I			6.32	(5.30)	2.81	(16.84)
R			3.68	(2.74)	12.80	(15.29)
V			5.82	(10.94)	12.32	(17.70)
B			8.91	(3.23)	1.15	(9.69)
U			3.70	(11.70)	68.59	(23.92)

Table A3 : Continued.

Filter	Flux density (mJy)	Polarization (%)	Position angle (deg)
1727+502 I Zw 186			
E(B-V) = 0.00			
1987 Sep. 21			
H	1.55 (1.62)		118.80 (20.70)
I	0.00 (0.84)		
R	0.92 (0.41)		95.85 (12.45)
V	1.10 (1.92)		126.27 (25.93)
B	3.14 (1.02)		96.91 (6.26)
U	5.96 (1.30)		110.38 (6.50)
1749+096 OT 081			
E(B-V) = 0.15			
1987 Sep. 19			
H	5.86 (1.45)		131.03 (8.35)
I	0.00 (2.69)		
R	3.81 (1.12)		133.90 (8.20)
V	0.61 (4.41)		100.91 (29.10)
B	3.50 (2.41)		87.31 (17.96)
U	6.41 (3.64)		135.93 (14.12)
MC 2032+107			
E(B-V) = 0.12			
1987 Sep. 19			
H	0.00 (0.79)		
I	1.54 (0.48)		58.38 (10.74)
R	0.80 (0.47)		115.41 (14.56)
V	3.73 (1.77)		33.62 (12.96)
B	2.07 (1.70)		75.38 (18.37)
U	0.00 (9.29)		
PKS 2155-304			
E(B-V) = 0.00			
1987 Sep. 21			
K	7.14 (0.42)		170.19 (1.82)
H	7.60 (0.21)		170.00 (0.75)
I	8.33 (0.17)		170.41 (0.62)
R	8.52 (0.12)		169.67 (0.41)
V	9.05 (0.18)		169.96 (0.60)
B	8.61 (0.10)		169.91 (0.44)
U	8.35 (0.16)		171.62 (0.58)

Table A3 : Continued.

Filter	Flux density (mJy)	Polarization (%)	Position angle (deg)
2200+420 BL Lacertae			
E(B-V) = 0.15			
1987 Sep. 19			
H	13.15 (1.21)	8.35 (0.61)	31.50 (2.36)
I	3.00 (0.28)	8.11 (0.59)	40.95 (1.84)
R	1.70 (0.16)	8.37 (0.35)	38.41 (1.38)
V	0.95 (0.09)	8.35 (1.24)	45.04 (3.82)
B	0.38 (0.04)	14.04 (0.69)	37.46 (1.42)
U	0.18 (0.02)	10.53 (1.60)	37.37 (4.74)
1987 Sep. 20			
H		6.96 (0.29)	25.96 (1.21)
I		8.43 (0.55)	32.97 (1.87)
R		9.07 (0.39)	31.05 (1.24)
V		10.52 (0.94)	38.75 (3.07)
B		13.09 (0.87)	38.30 (2.03)
U		19.57 (2.06)	31.48 (3.00)
2223-052 3C 446			
E(B-V) = 0.03			
1987 Sep. 20			
H		6.55 (0.91)	92.16 (3.88)
I		7.98 (1.12)	91.95 (3.90)
R		9.03 (0.59)	94.03 (1.77)
V		12.35 (2.00)	97.50 (4.37)
B		10.30 (0.86)	92.58 (2.30)
U		8.89 (1.24)	99.50 (4.12)
21st. Sep 1987			
H		9.29 (1.09)	97.70 (3.28)
I		11.90 (1.21)	98.72 (2.58)
R		9.76 (0.59)	101.84 (2.04)
V		11.64 (2.03)	106.59 (3.92)
B		10.86 (0.83)	100.67 (2.06)
U		8.92 (1.19)	103.30 (4.37)

Table A3 : Continued.

Filter	Flux density (mJy)	Polarization (%)	Position angle (deg)
2251+158			
E(B-V) = 0.06			
1987 Sep. 20			
H	7.35 (1.22)	161.96 (4.66)	
I	4.18 (0.96)	160.62 (6.32)	
R	3.92 (0.45)	162.27 (3.31)	
V	3.72 (1.10)	159.21 (7.36)	
B	3.49 (0.47)	161.95 (4.52)	
U	2.37 (0.79)	163.02 (9.09)	
2254+074 OY 091			
E(B-V) = 0.06			
1987 Sep. 18			
H	3.34 (3.89)	45.57 (22.10)	
I	9.65 (1.45)	47.85 (4.14)	
R	11.81 (0.75)	38.76 (1.82)	
V	14.12 (2.43)	58.38 (5.14)	
B	14.26 (1.13)	39.71 (2.57)	
U	13.74 (2.16)	56.63 (4.34)	
1987 Sep. 21			
H	7.01 (1.83)	50.27 (6.09)	
I	8.10 (1.55)	42.91 (5.73)	
R	9.76 (0.85)	42.30 (2.62)	
V	14.37 (3.06)	30.83 (5.90)	
B	14.63 (1.31)	38.52 (2.67)	
U	13.47 (2.73)	40.60 (6.88)	
PKS 2345-167			
E(B-V) = 0.00			
1987 Sep. 20			
H	25.16 (5.91)	145.00 (6.40)	
I	8.62 (6.67)	165.26 (17.66)	
R	0.00 (3.17)		
V	0.00 (15.24)		
B	5.75 (3.94)	134.87 (12.36)	
U	5.16 (8.33)	85.85 (23.20)	

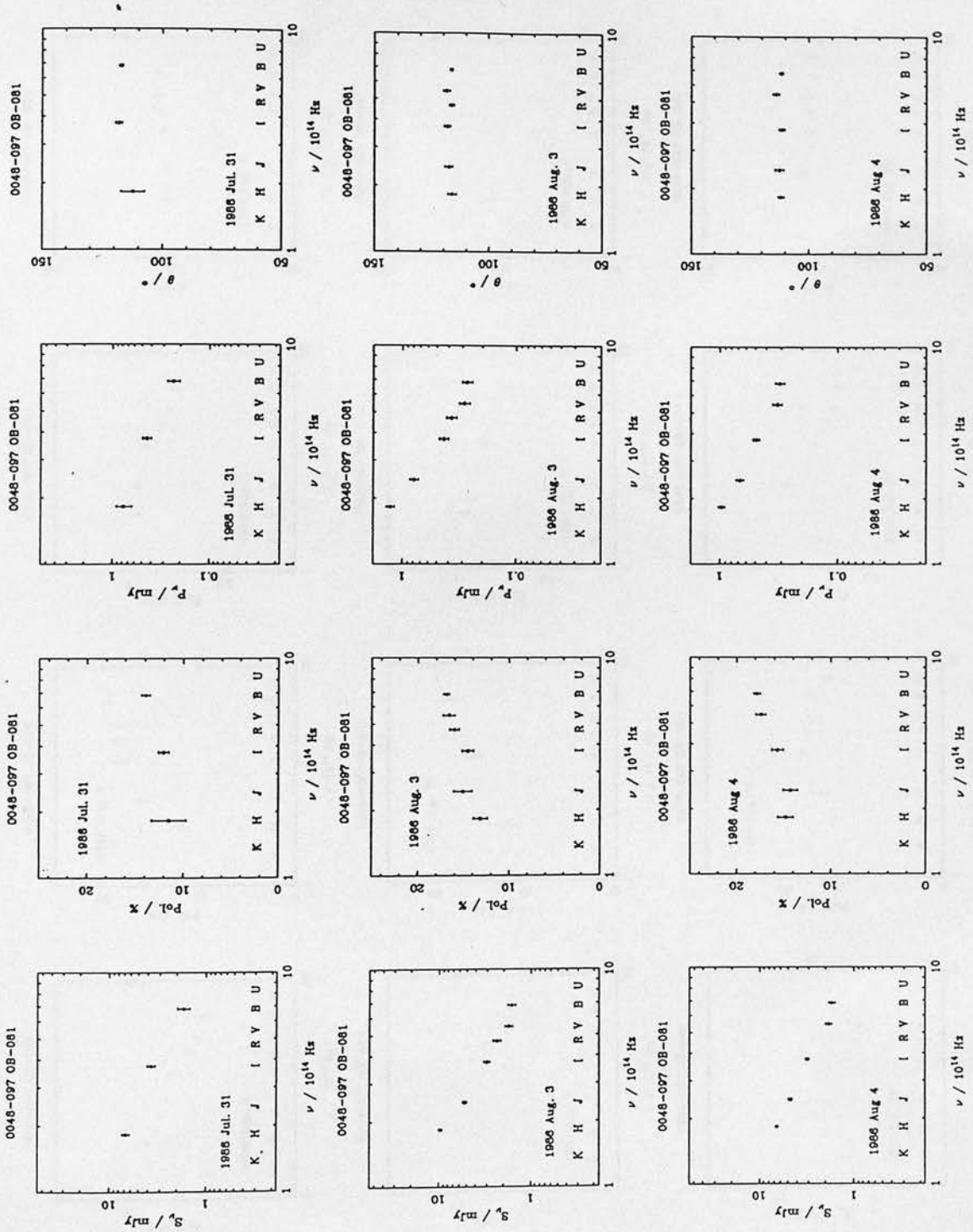

Figure A.1: Plots of the polarization data.

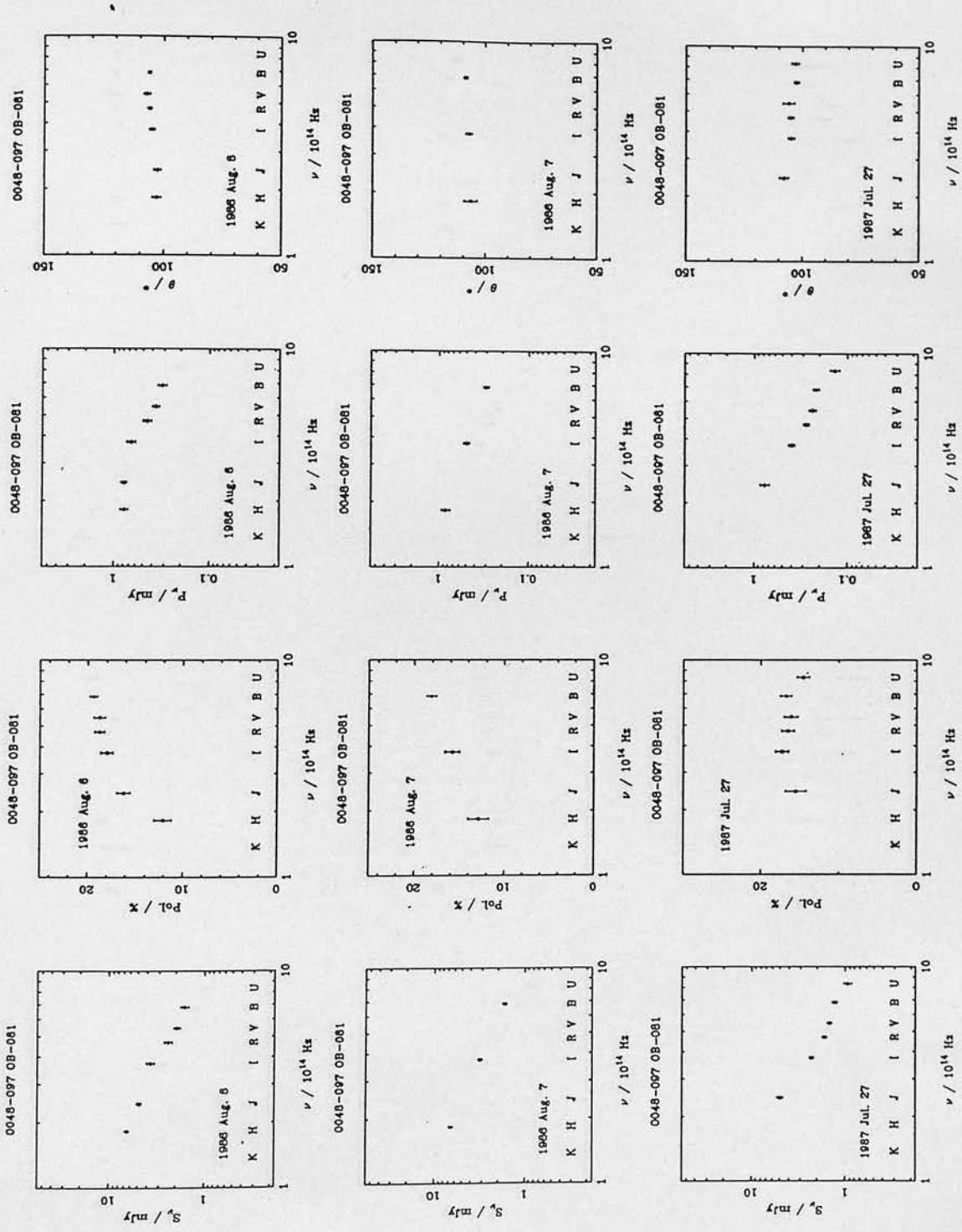

Figure A.1: *(Contd.)* Plots of the polarization data.

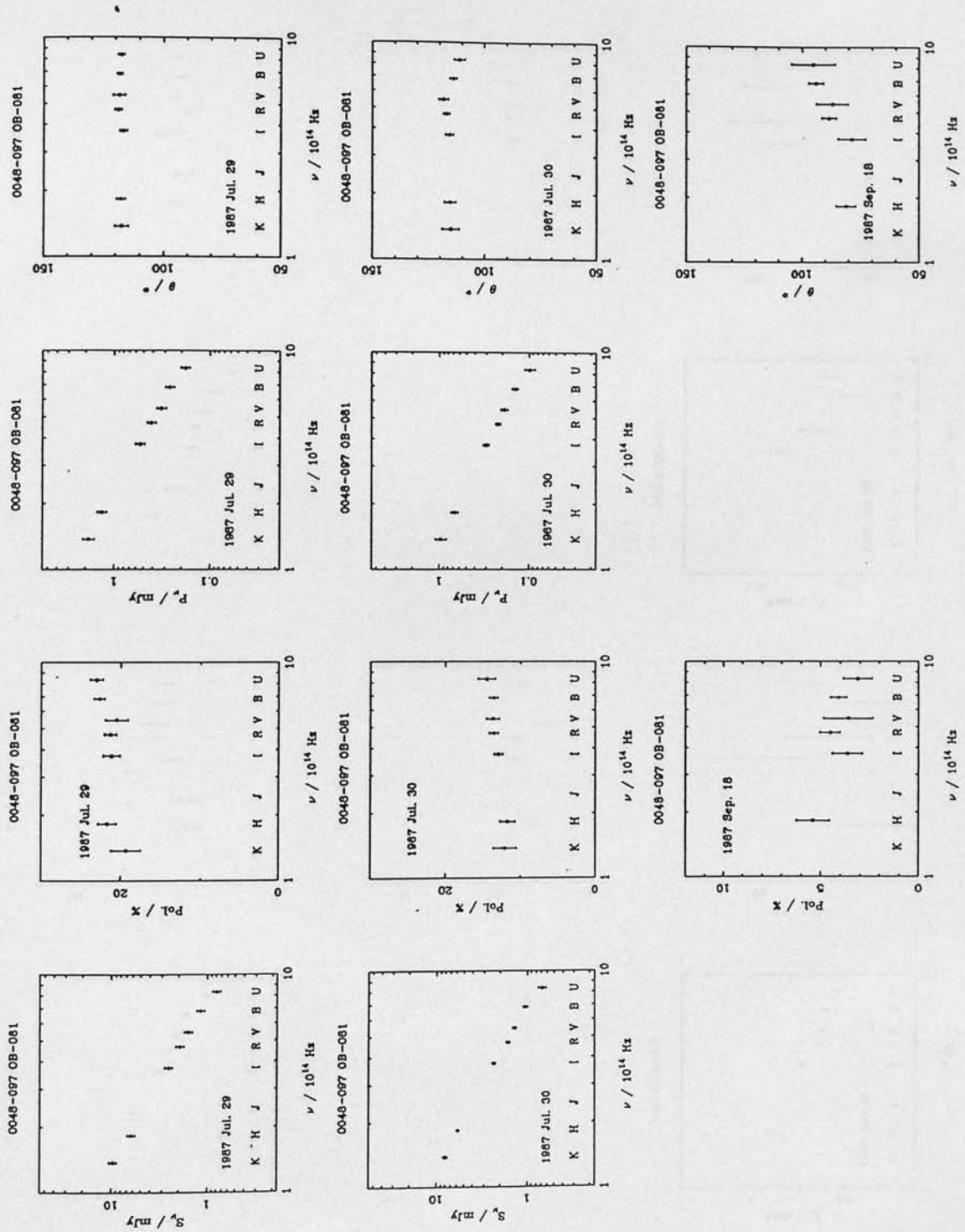

Figure A.1: *(Contd.)* Plots of the polarization data.

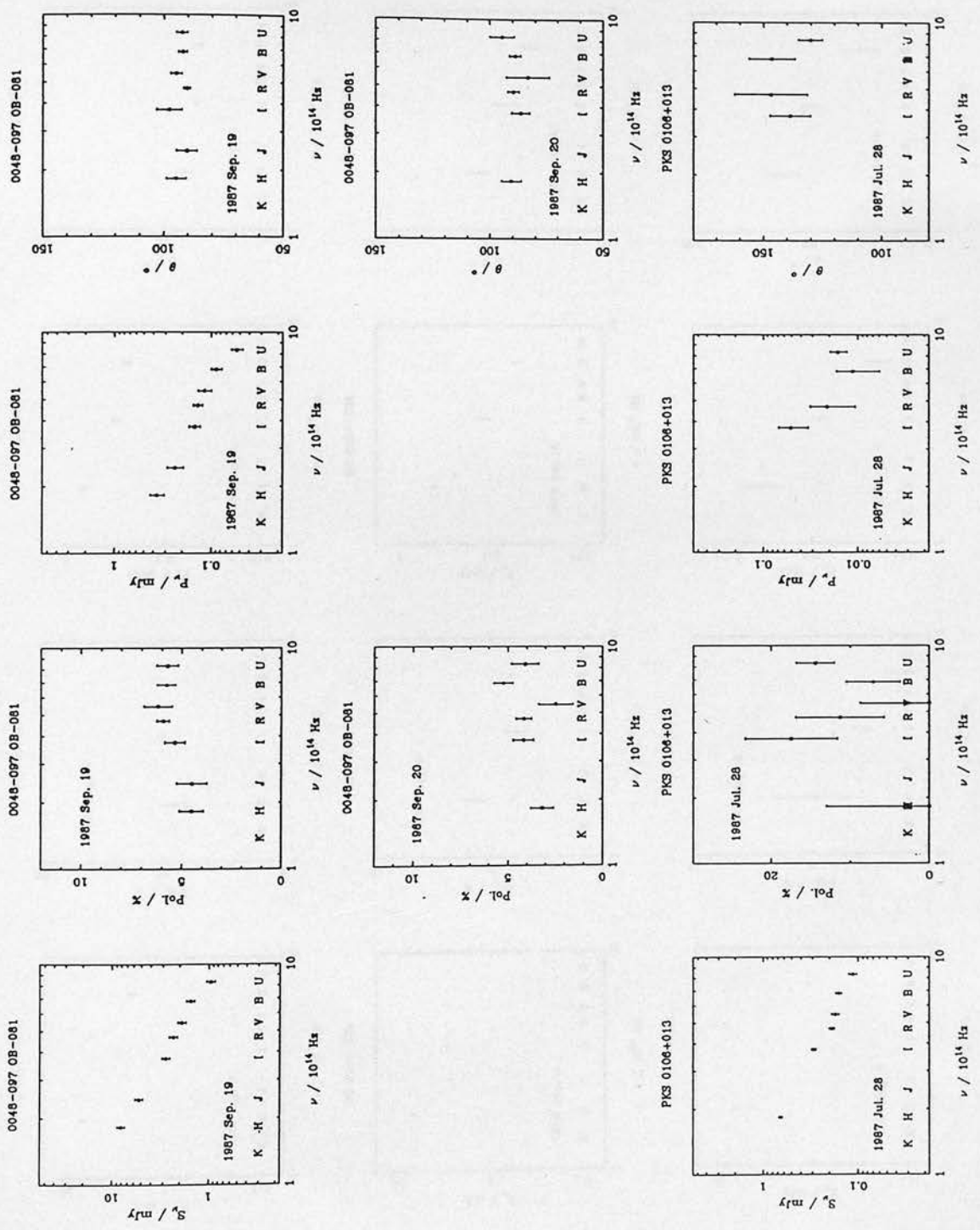

Figure A.1: *(Contd.)* Plots of the polarization data.

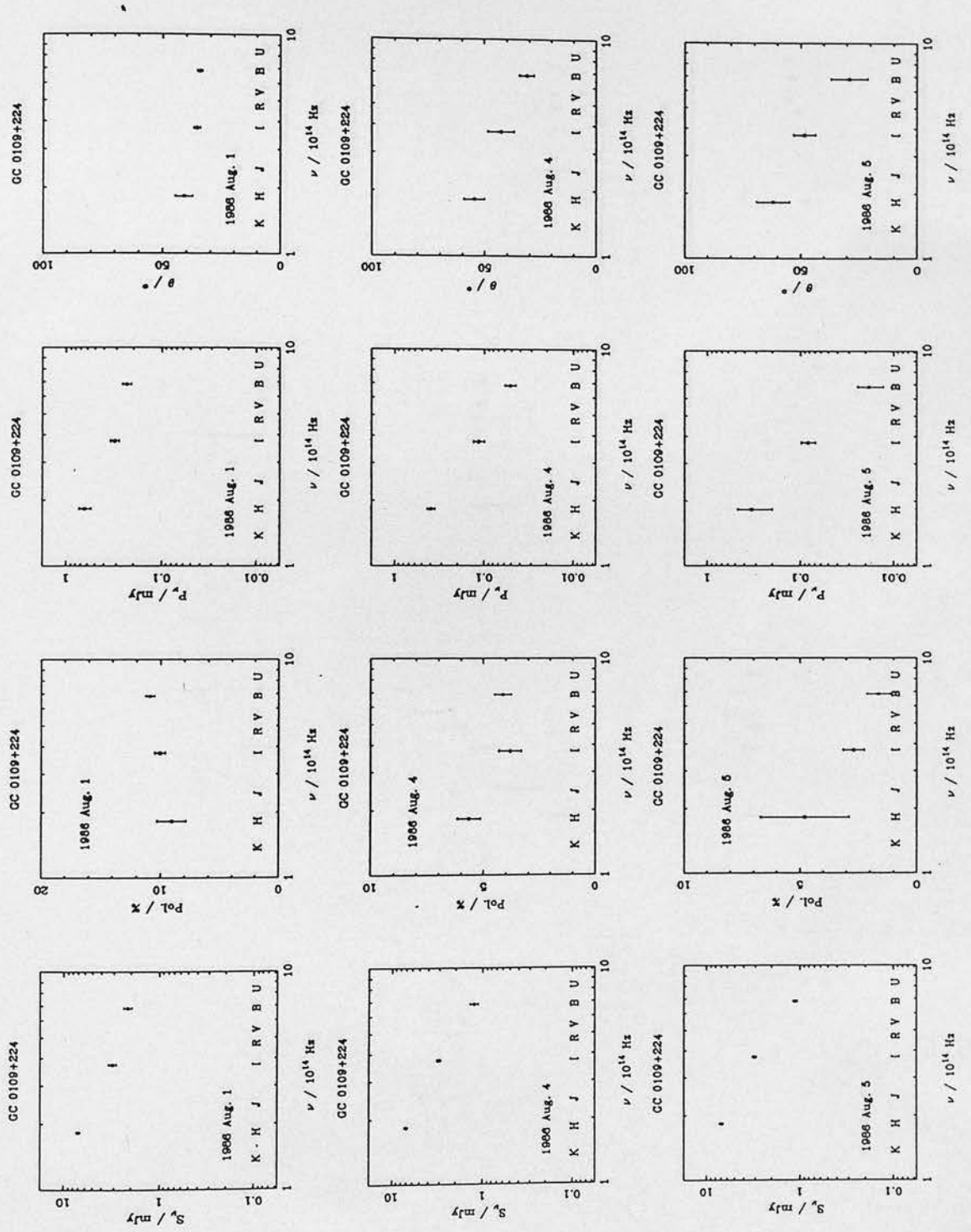

Figure A.1: *(Contd.)* Plots of the polarization data.

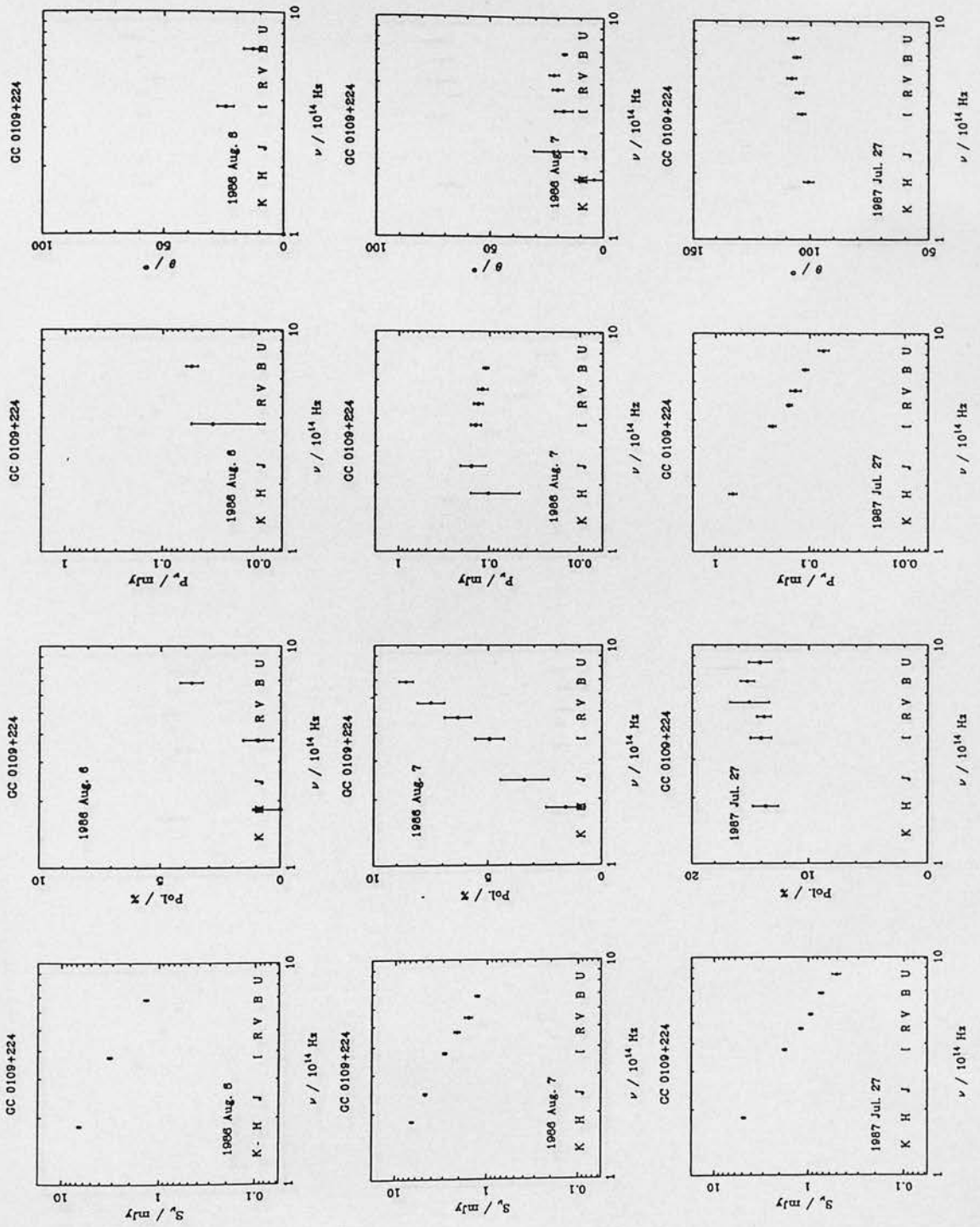

Figure A.1: *(Contd.)* Plots of the polarization data.

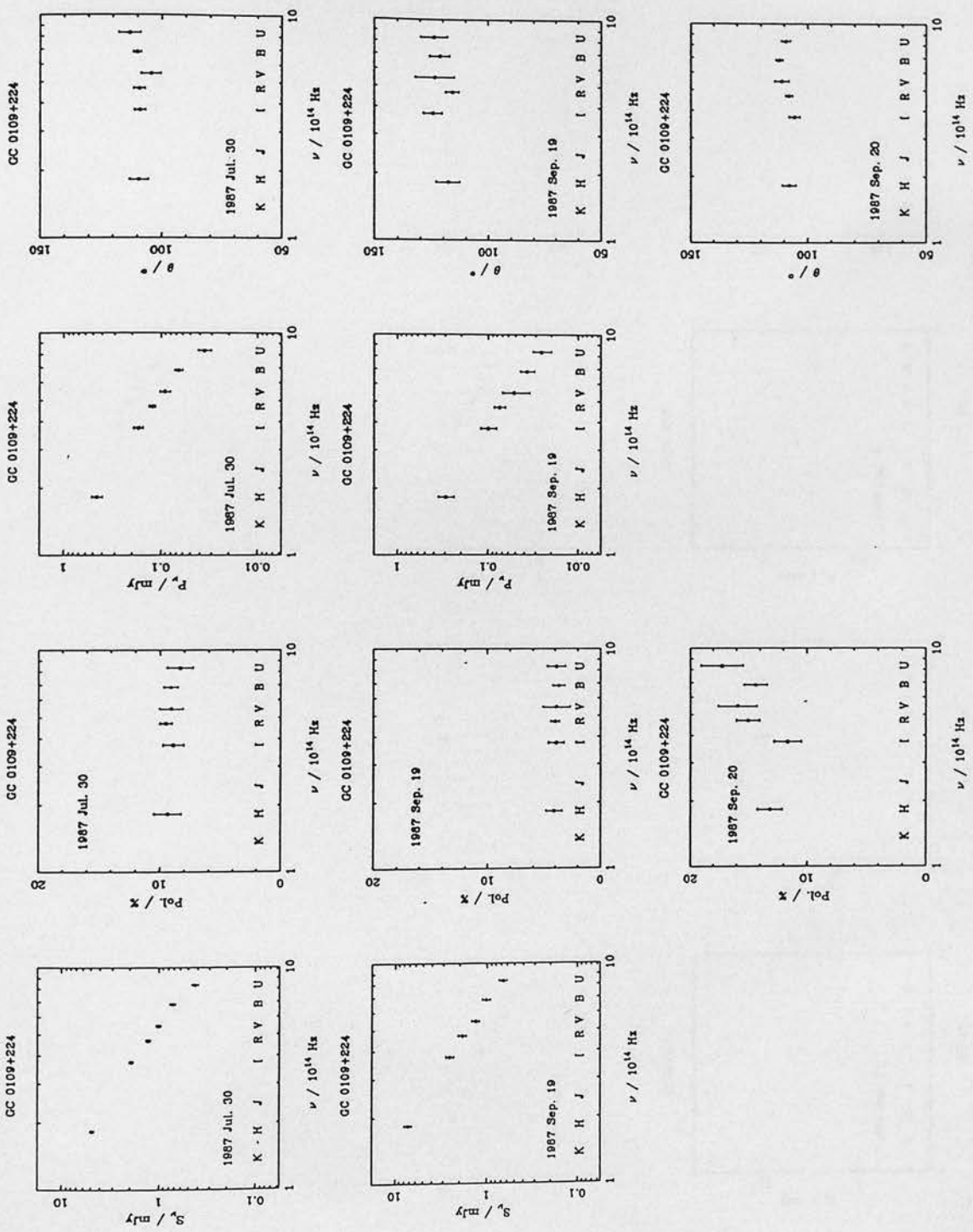

Figure A.1: *(Contd.)* Plots of the polarization data.

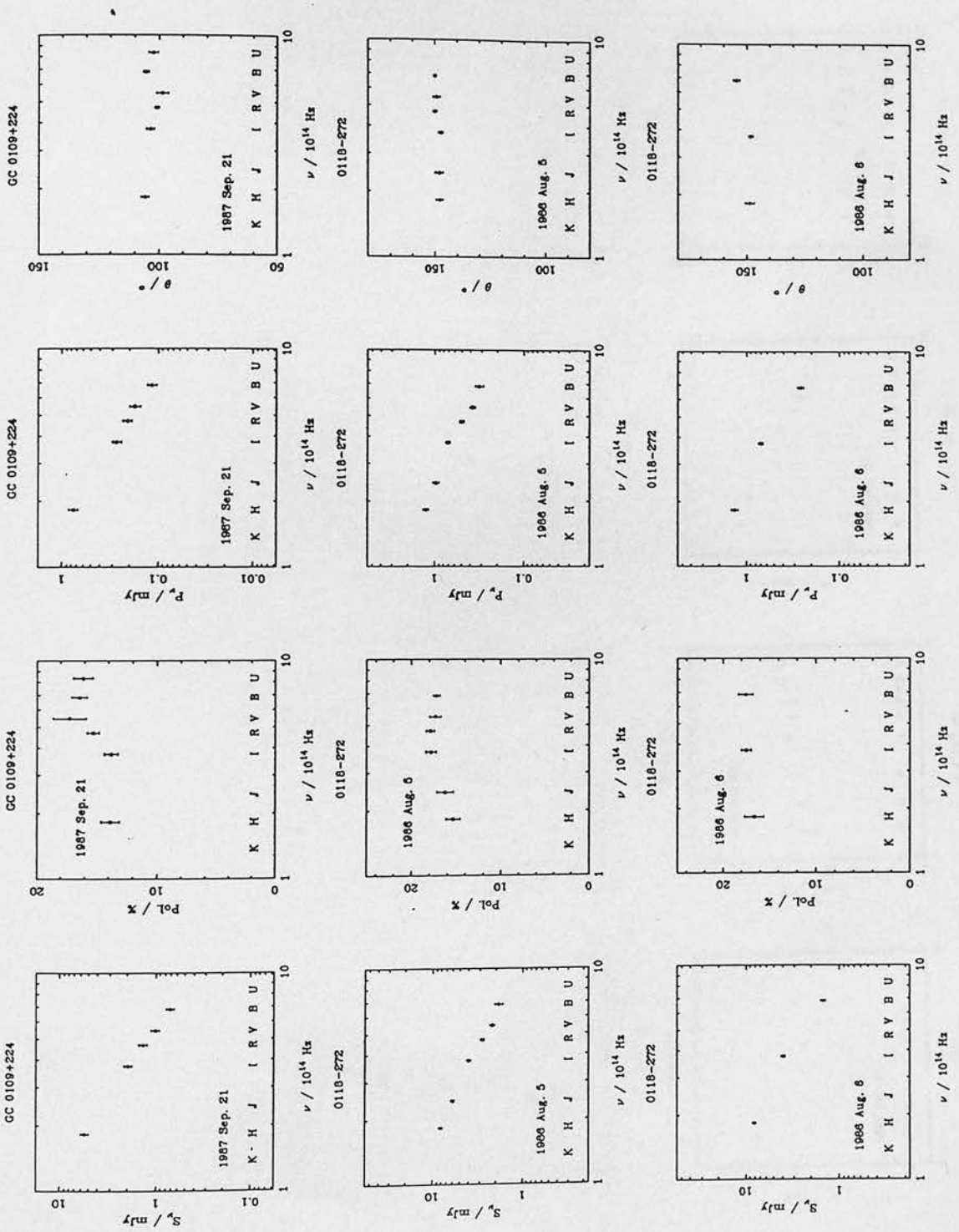

Figure A.1: *(Contd.)* Plots of the polarization data.

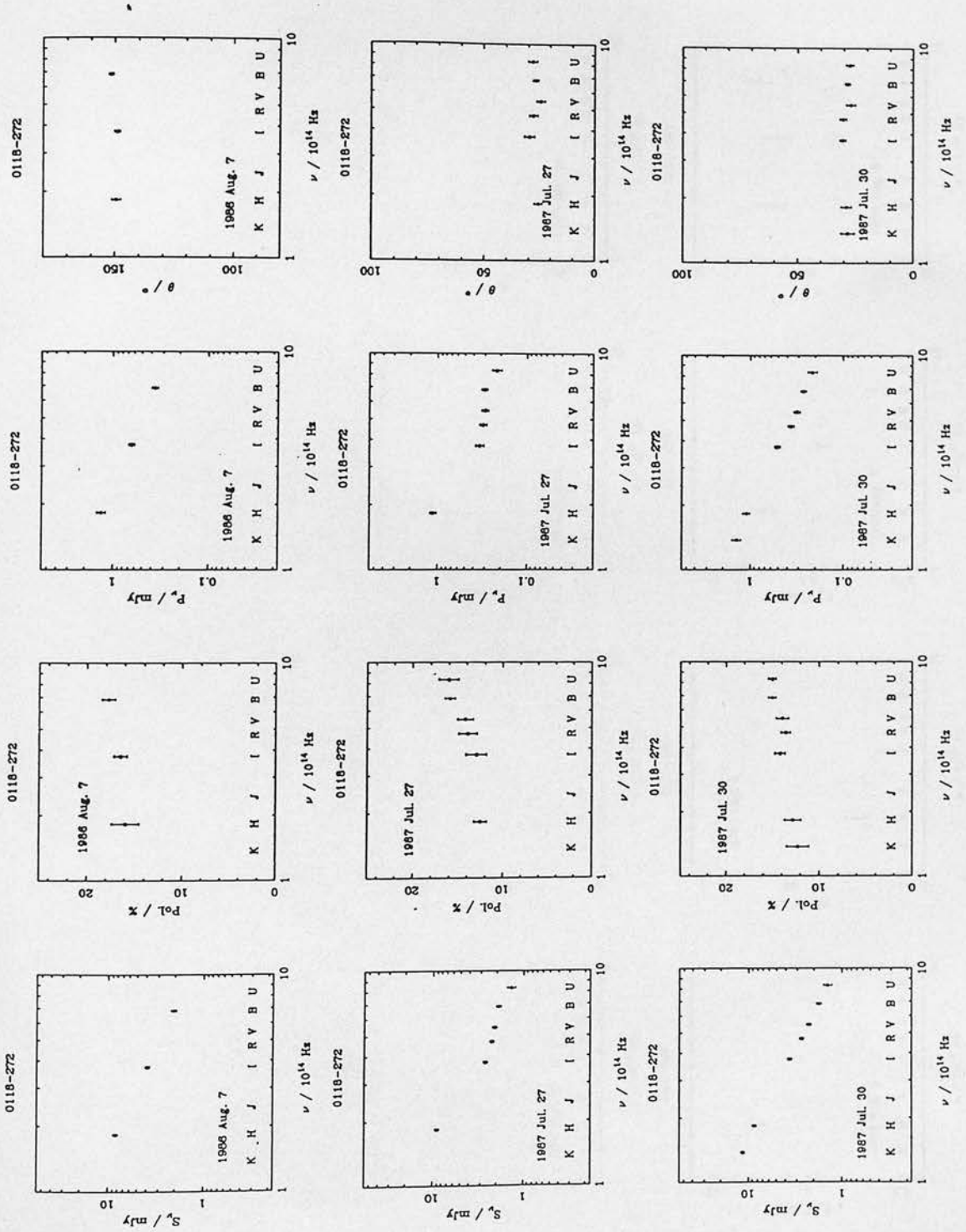

Figure A.1: *(Contd.)* Plots of the polarization data.

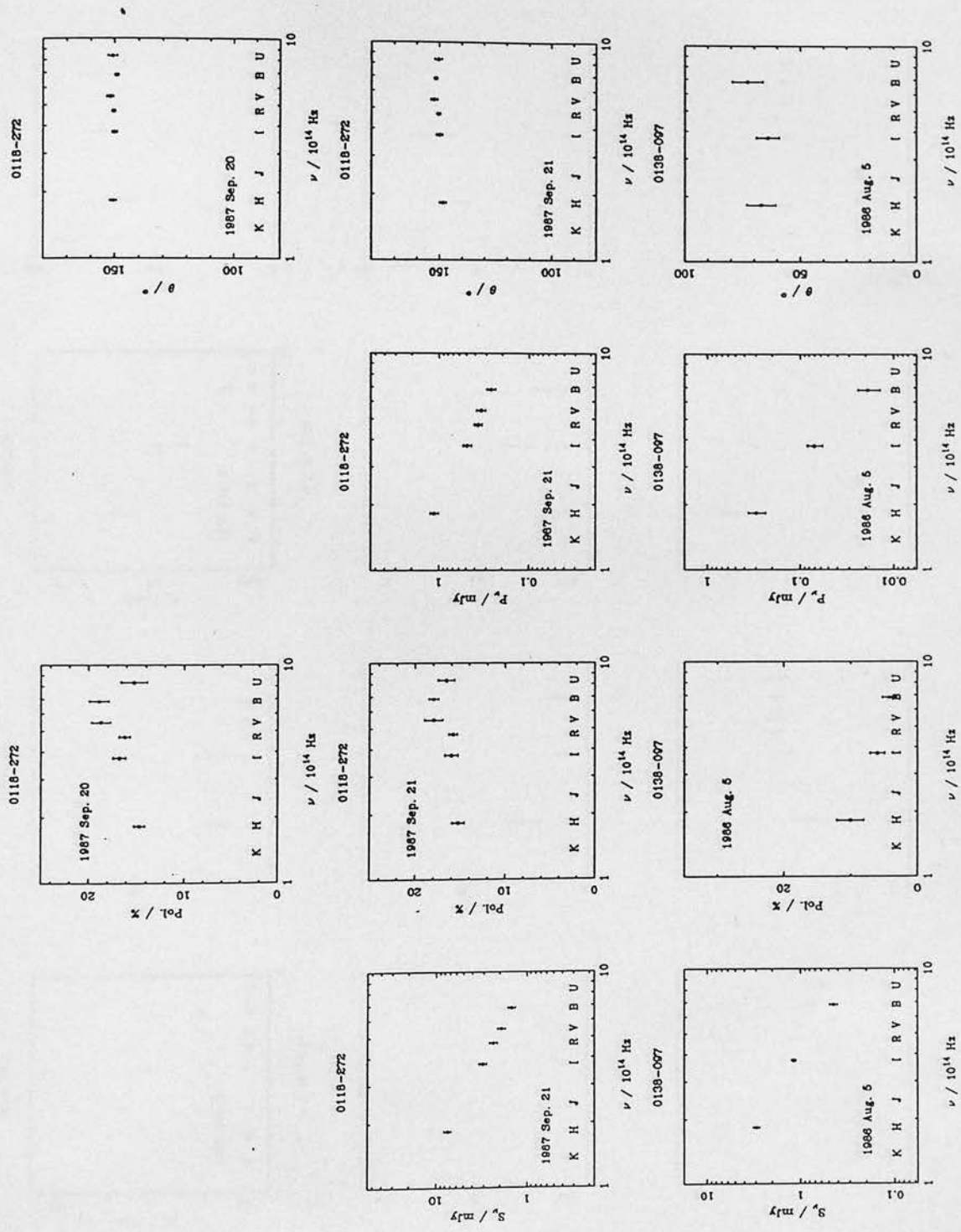

Figure A.1: *(Contd.)* Plots of the polarization data.

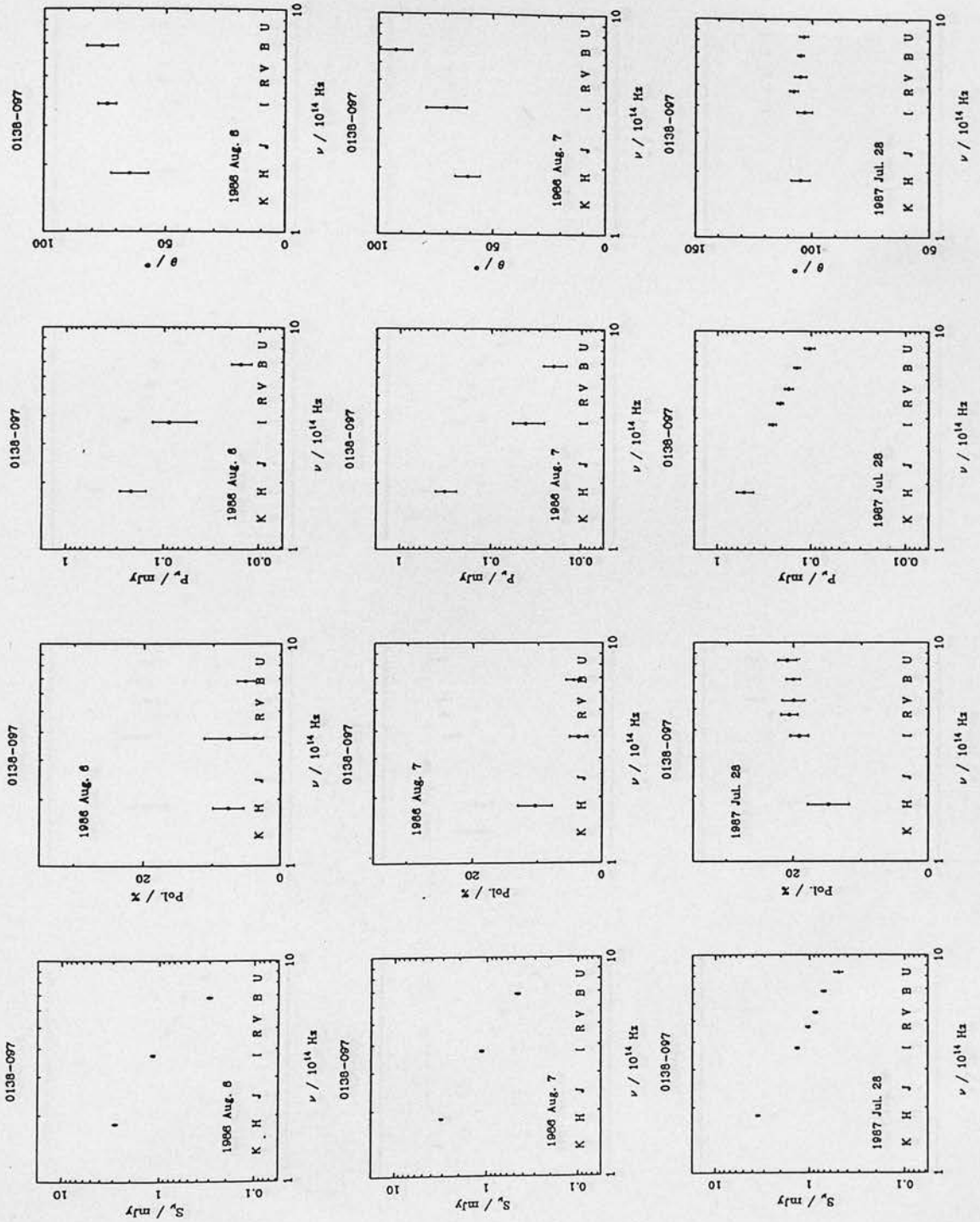

Figure A.1: *(Contd.)* Plots of the polarization data.

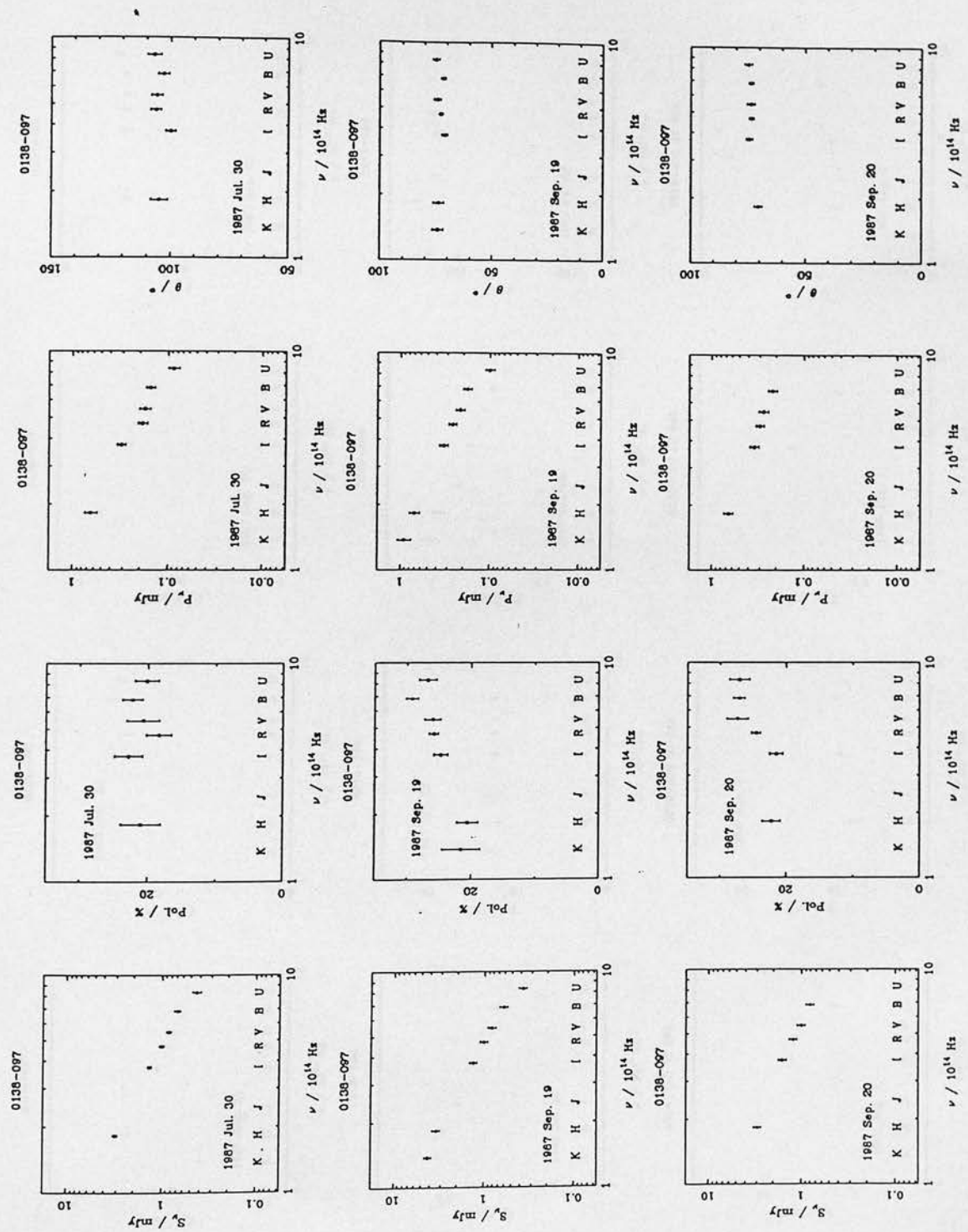

Figure A.1: *(Contd.)* Plots of the polarization data.

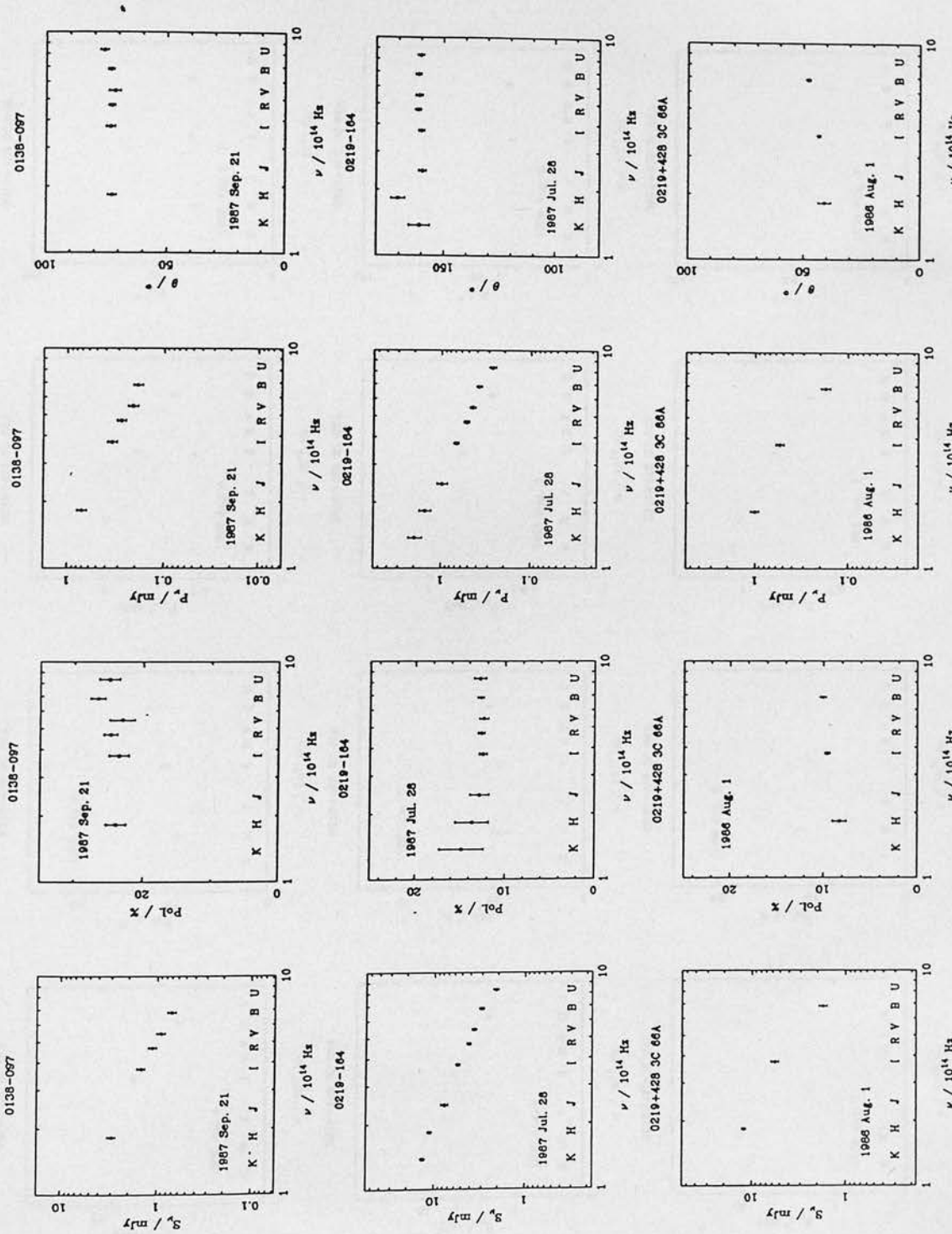

Figure A.1: *(Contd.)* Plots of the polarization data.

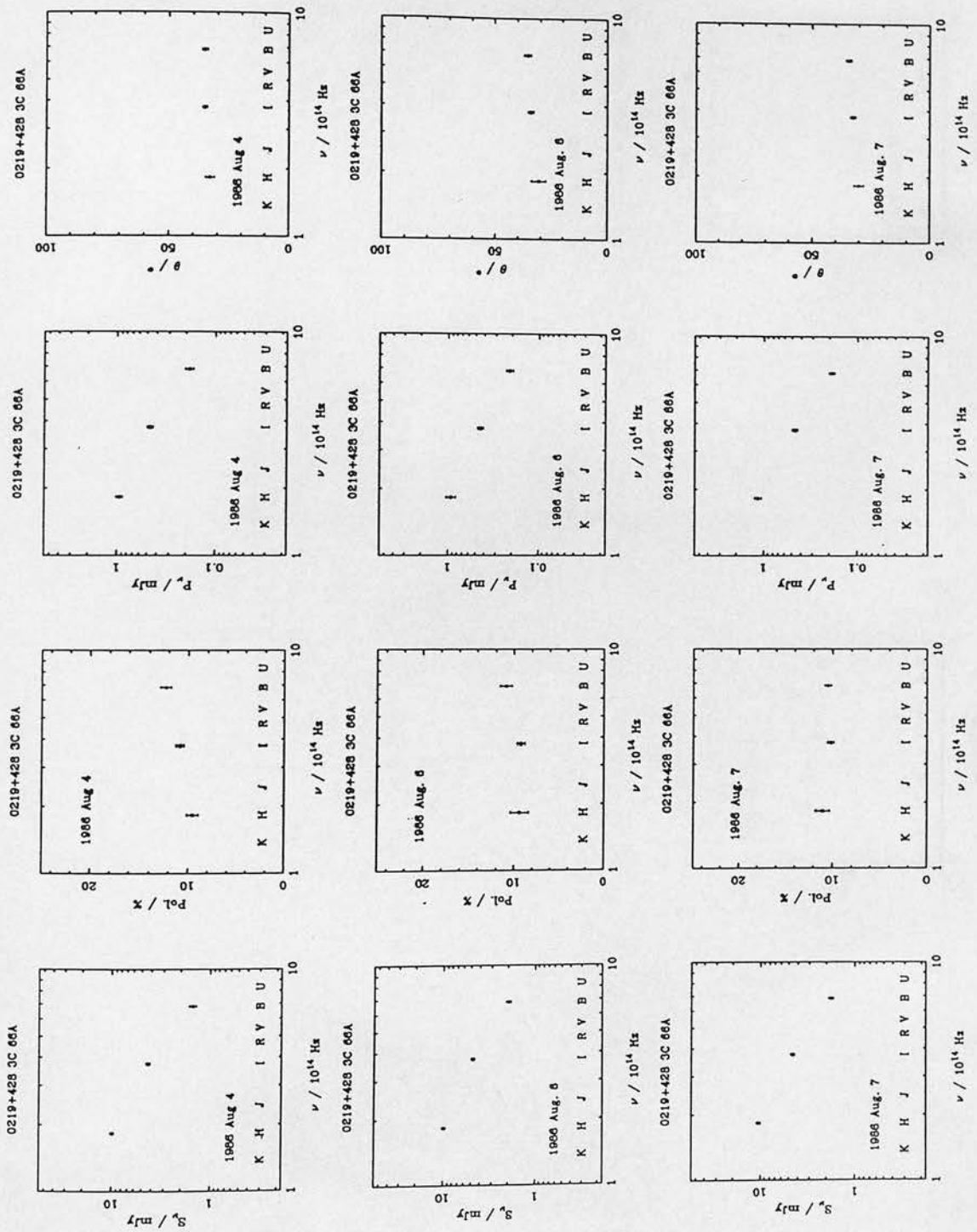

Figure A.1: *(Contd.)* Plots of the polarization data.

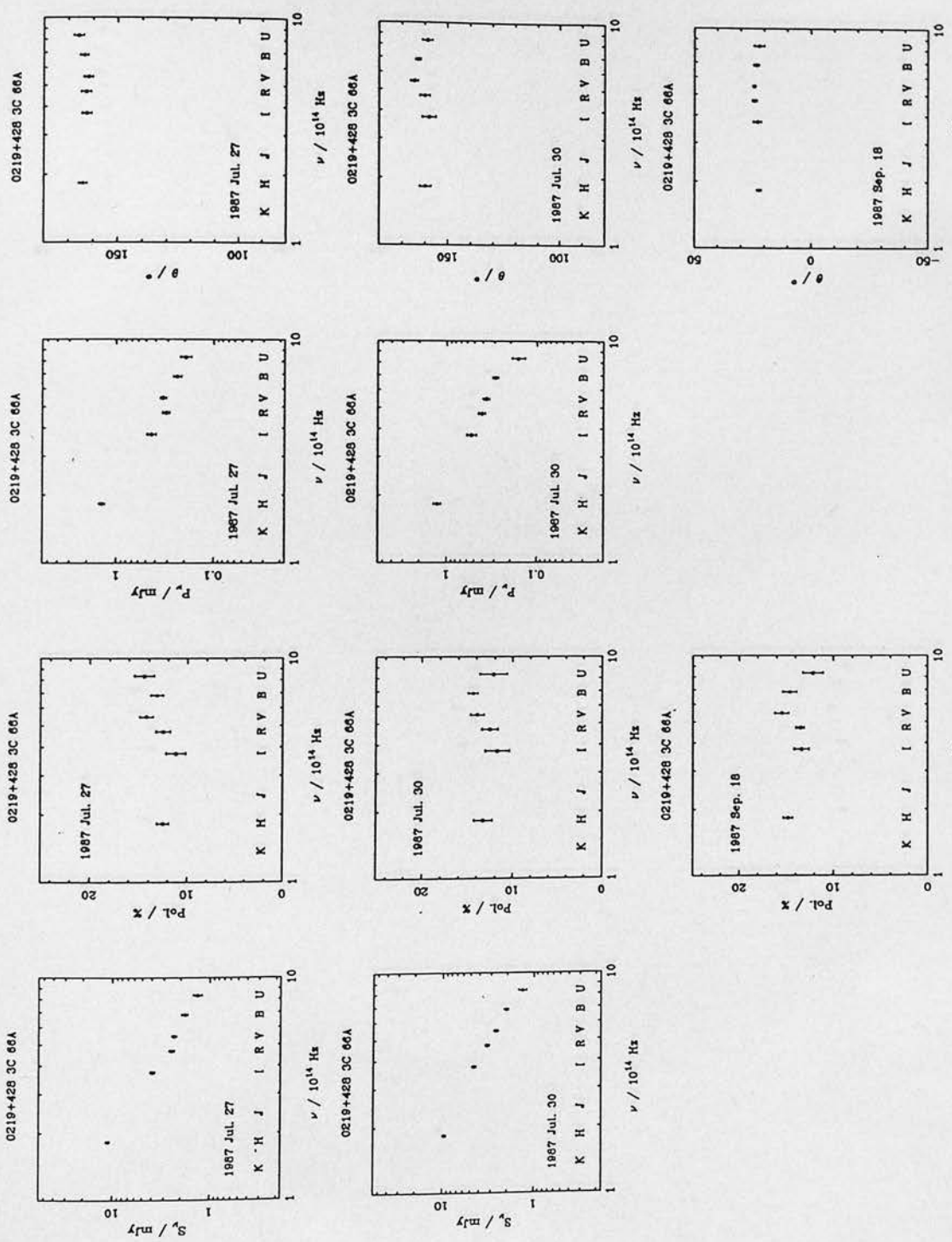

Figure A.1: *(Contd.)* Plots of the polarization data.

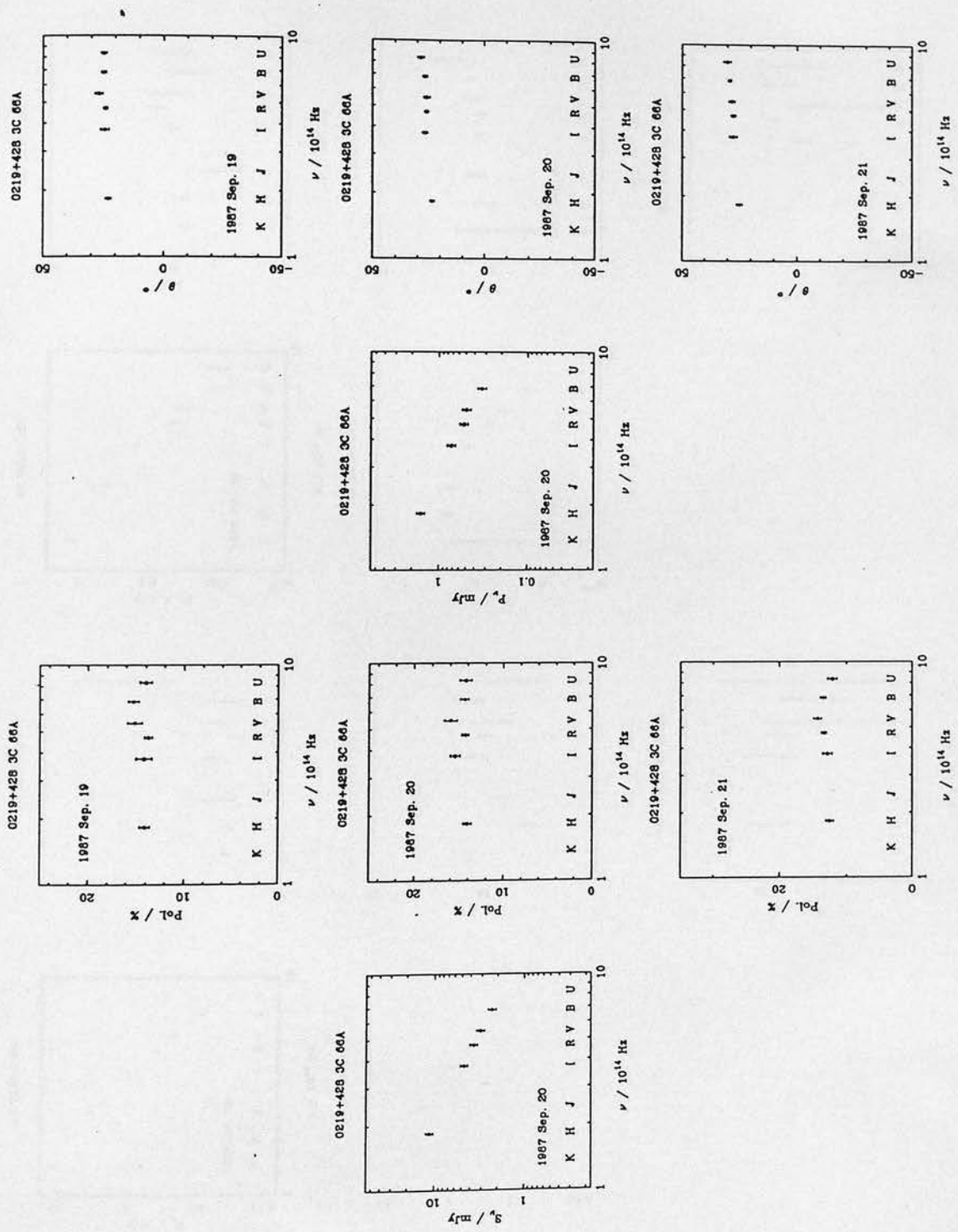

Figure A.1: *(Contd.)* Plots of the polarization data.

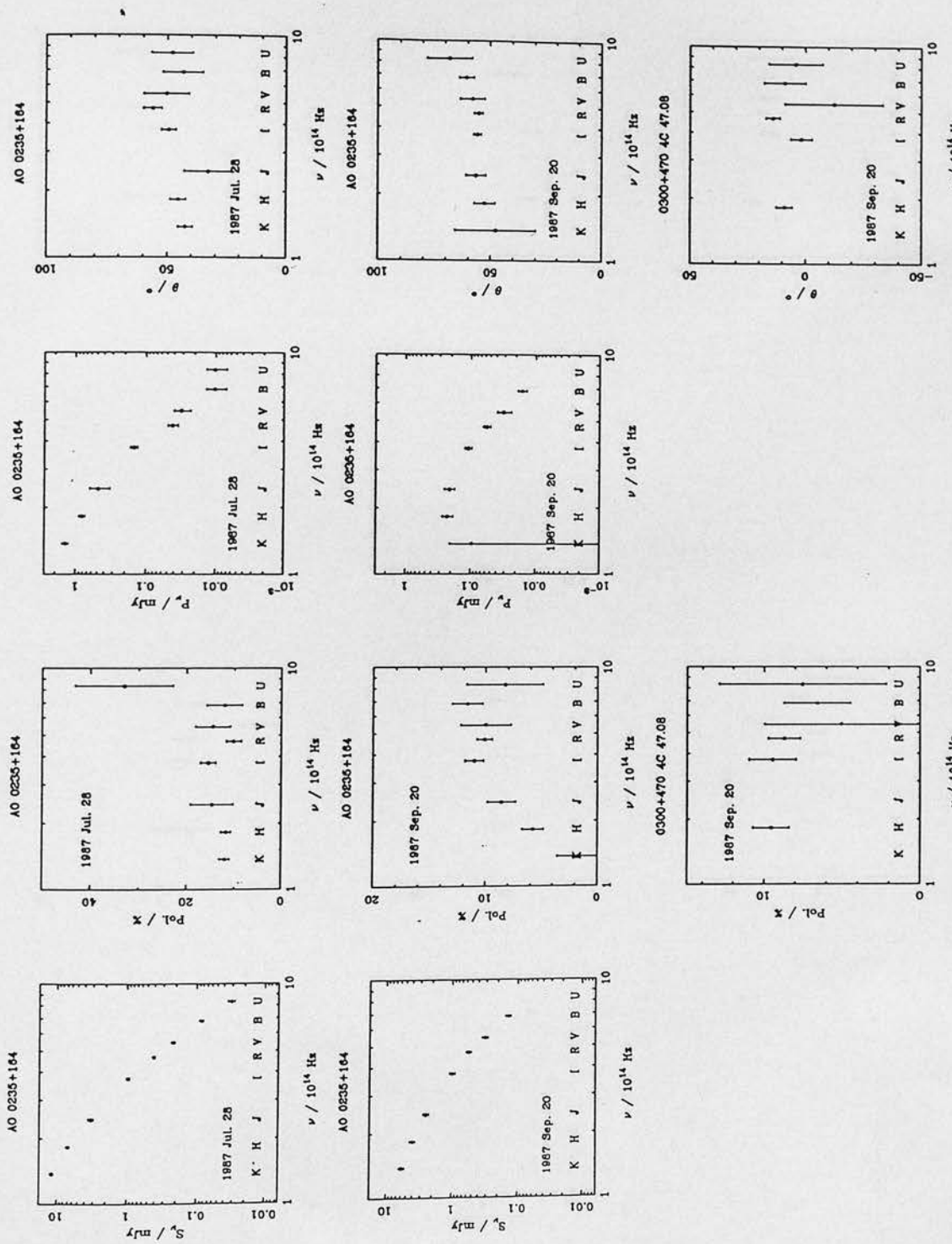

Figure A.1: *(Contd.)* Plots of the polarization data.

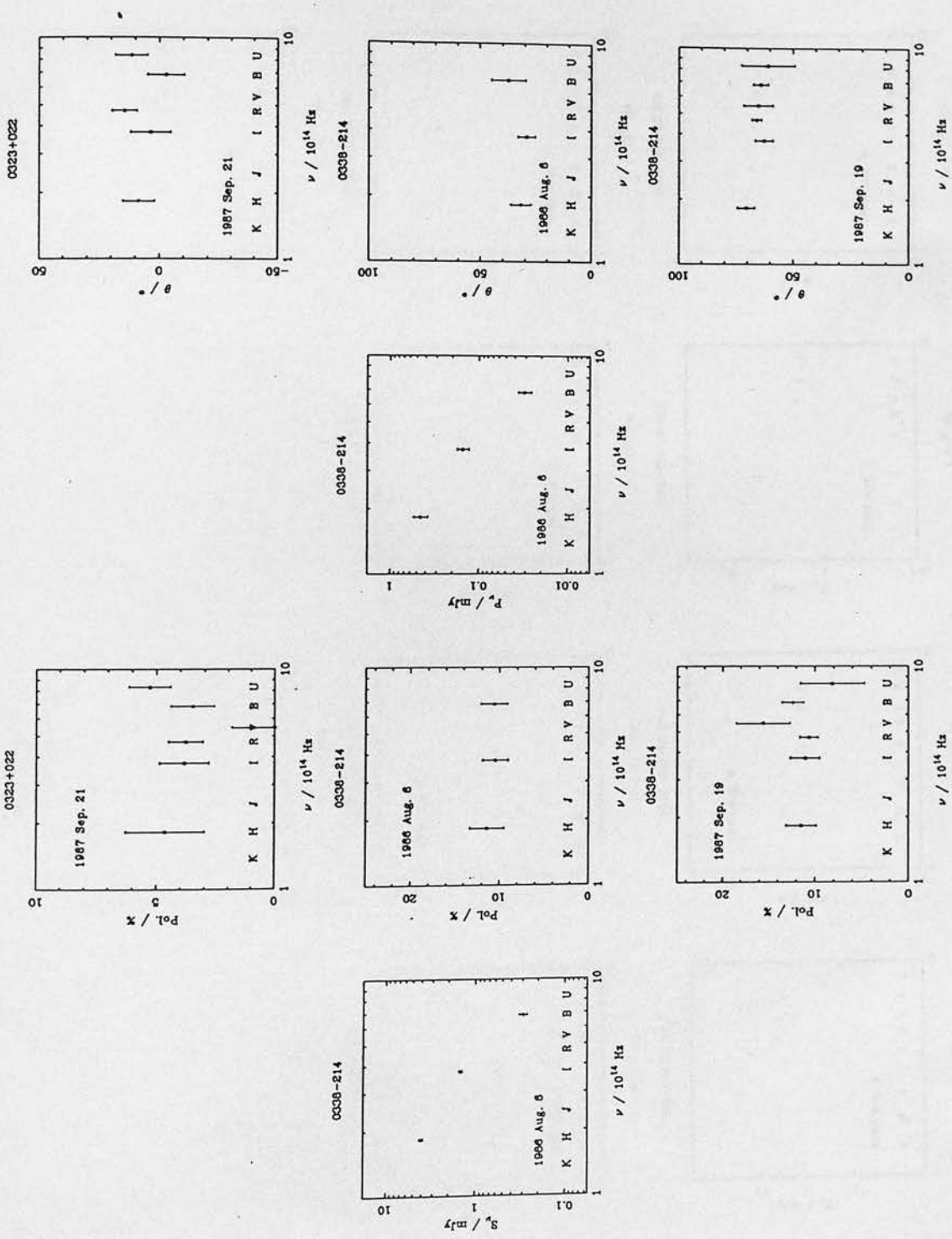

Figure A.1: *(Contd.)* Plots of the polarization data.

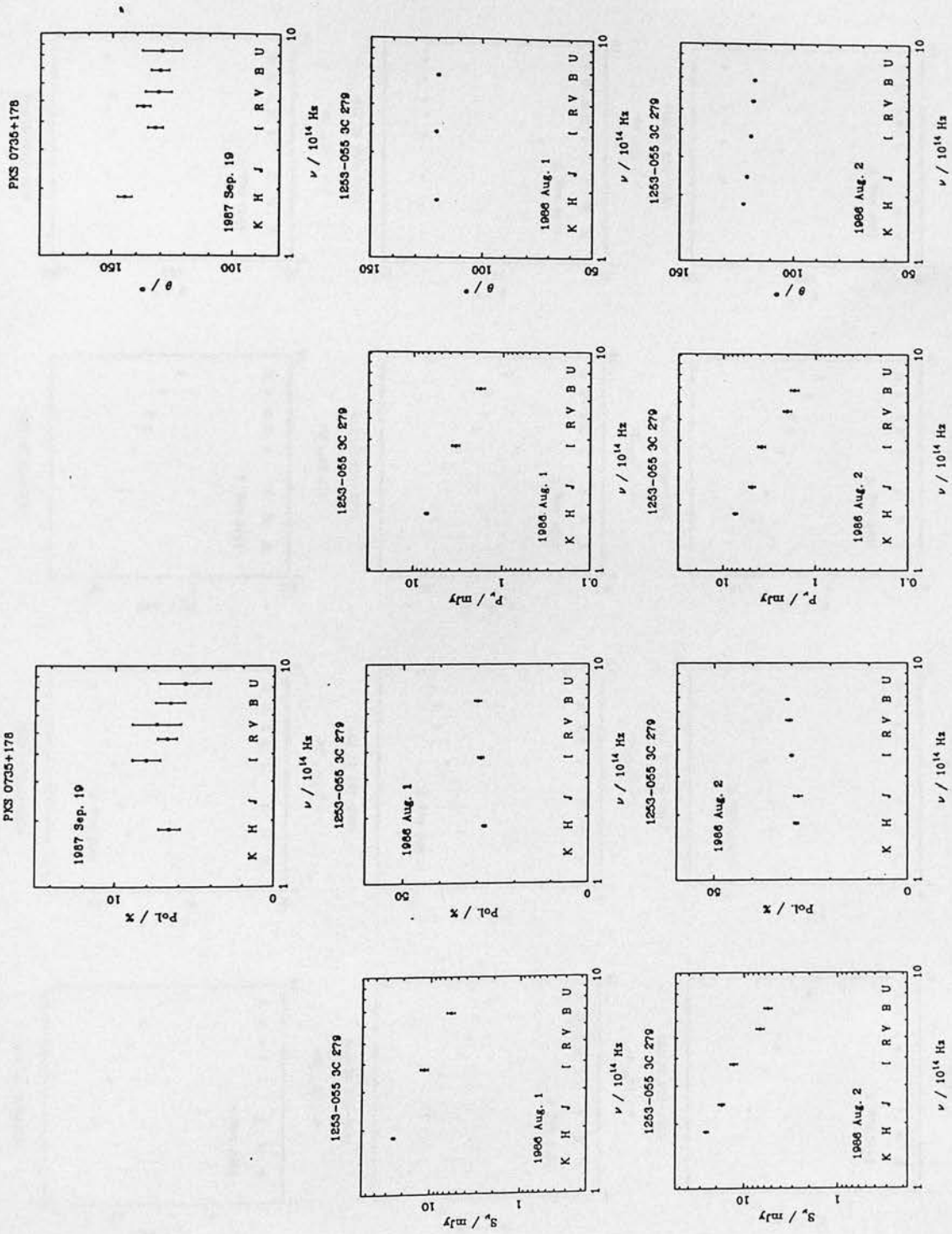

Figure A.1: *(Contd.)* Plots of the polarization data.

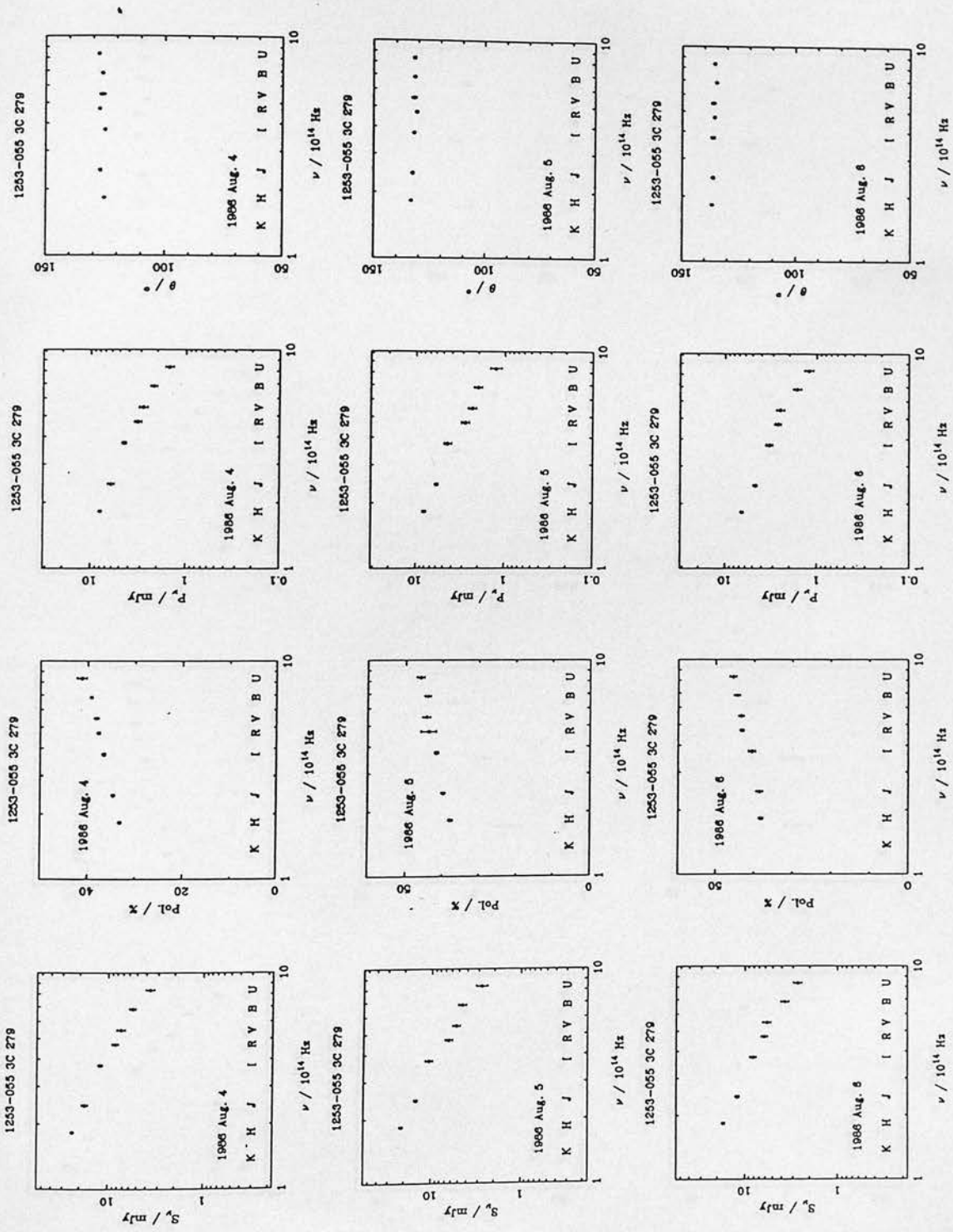

Figure A.1: *(Contd.)* Plots of the polarization data.

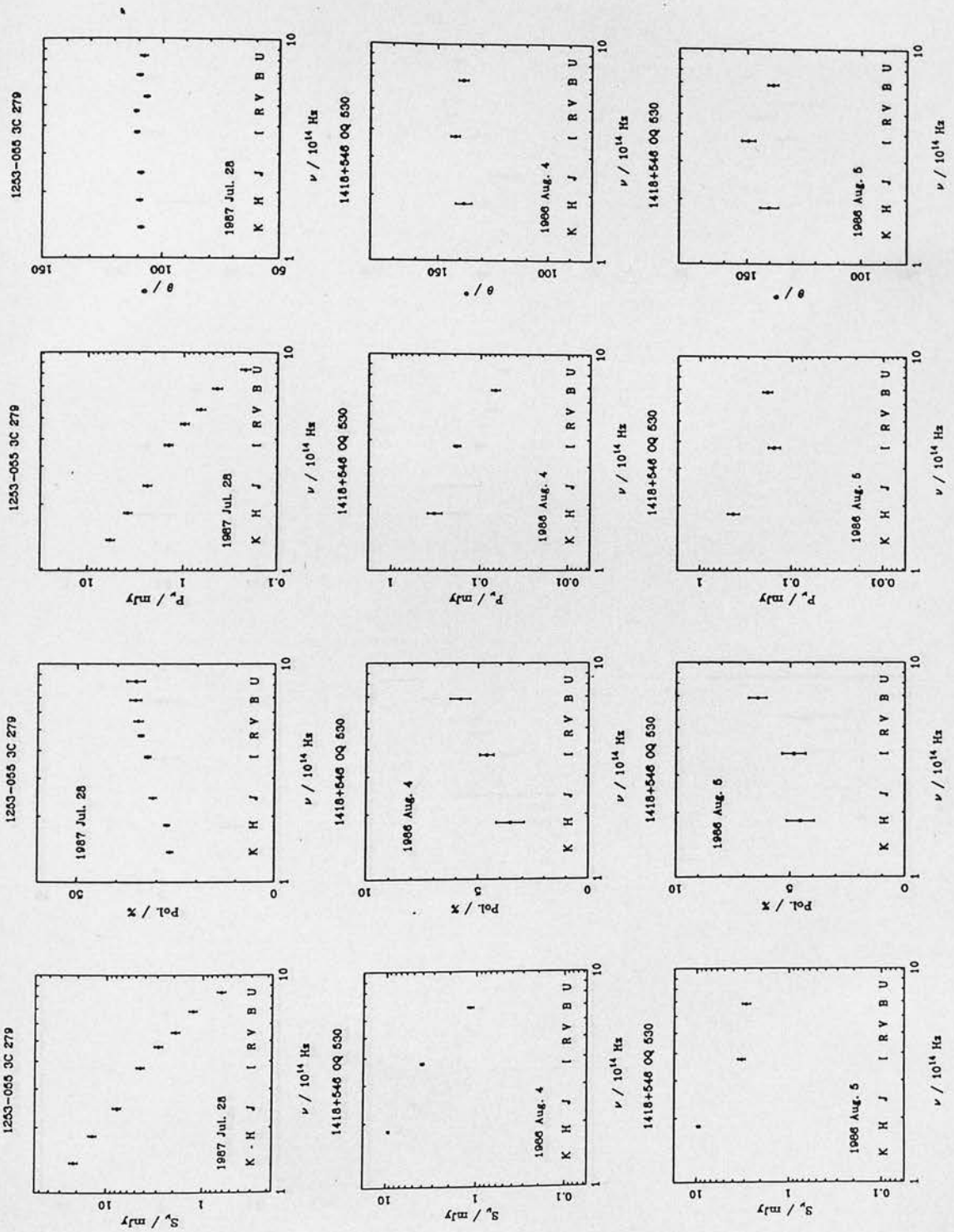

Figure A.1: *(Contd.)* Plots of the polarization data.

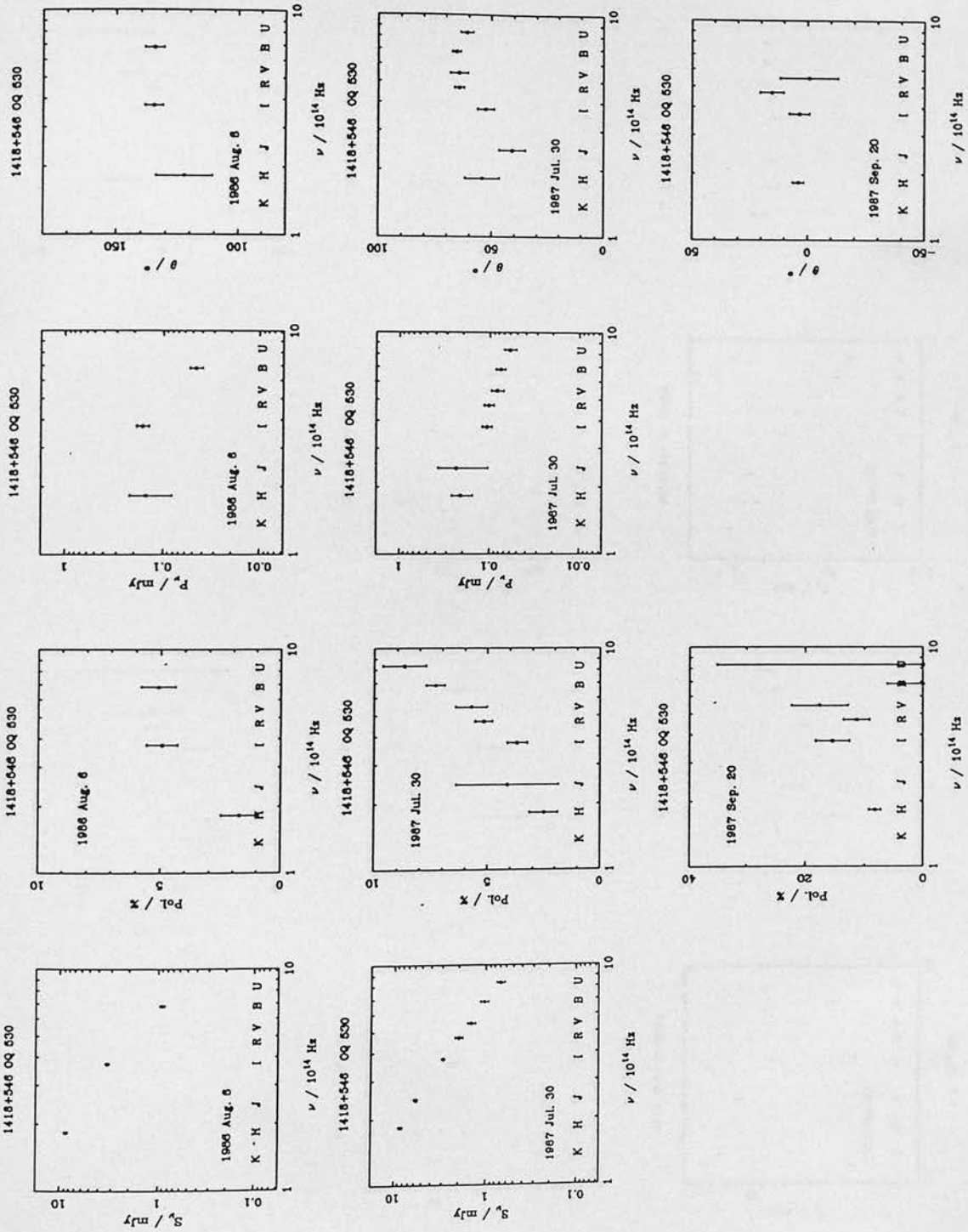

Figure A.1: *(Contd.)* Plots of the polarization data.

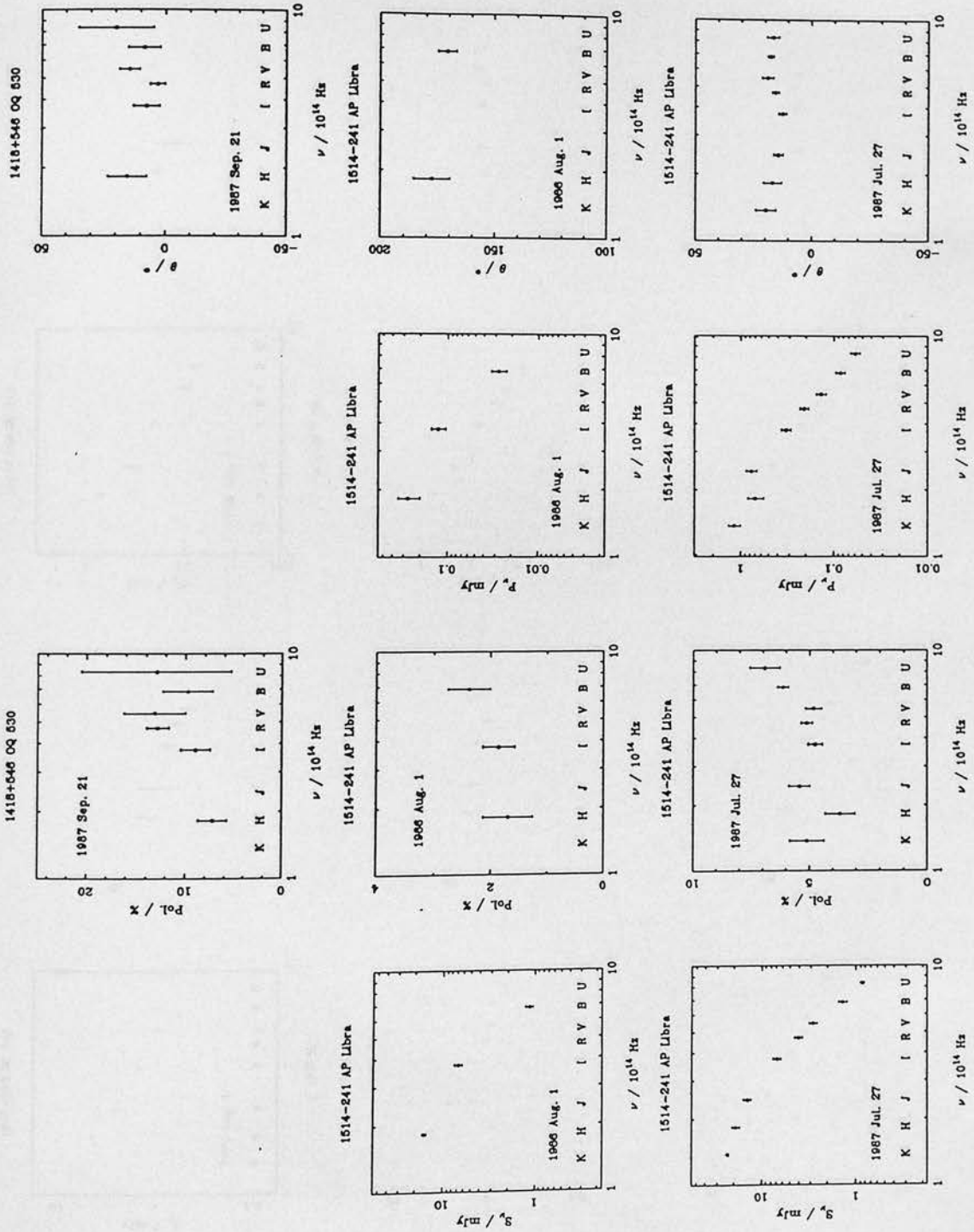

Figure A.1: *(Contd.)* Plots of the polarization data.

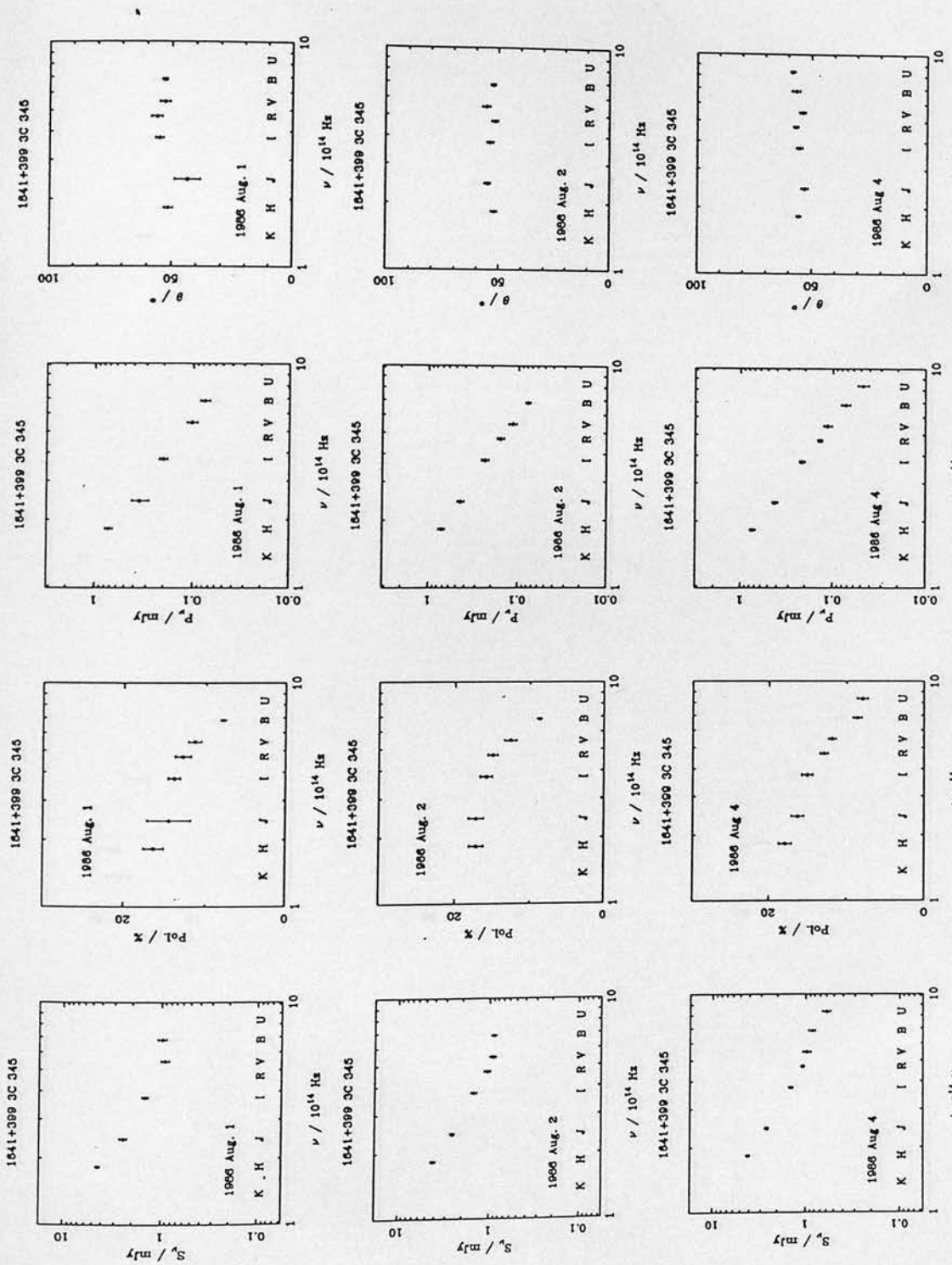

Figure A.1: *(Contd.)* Plots of the polarization data.

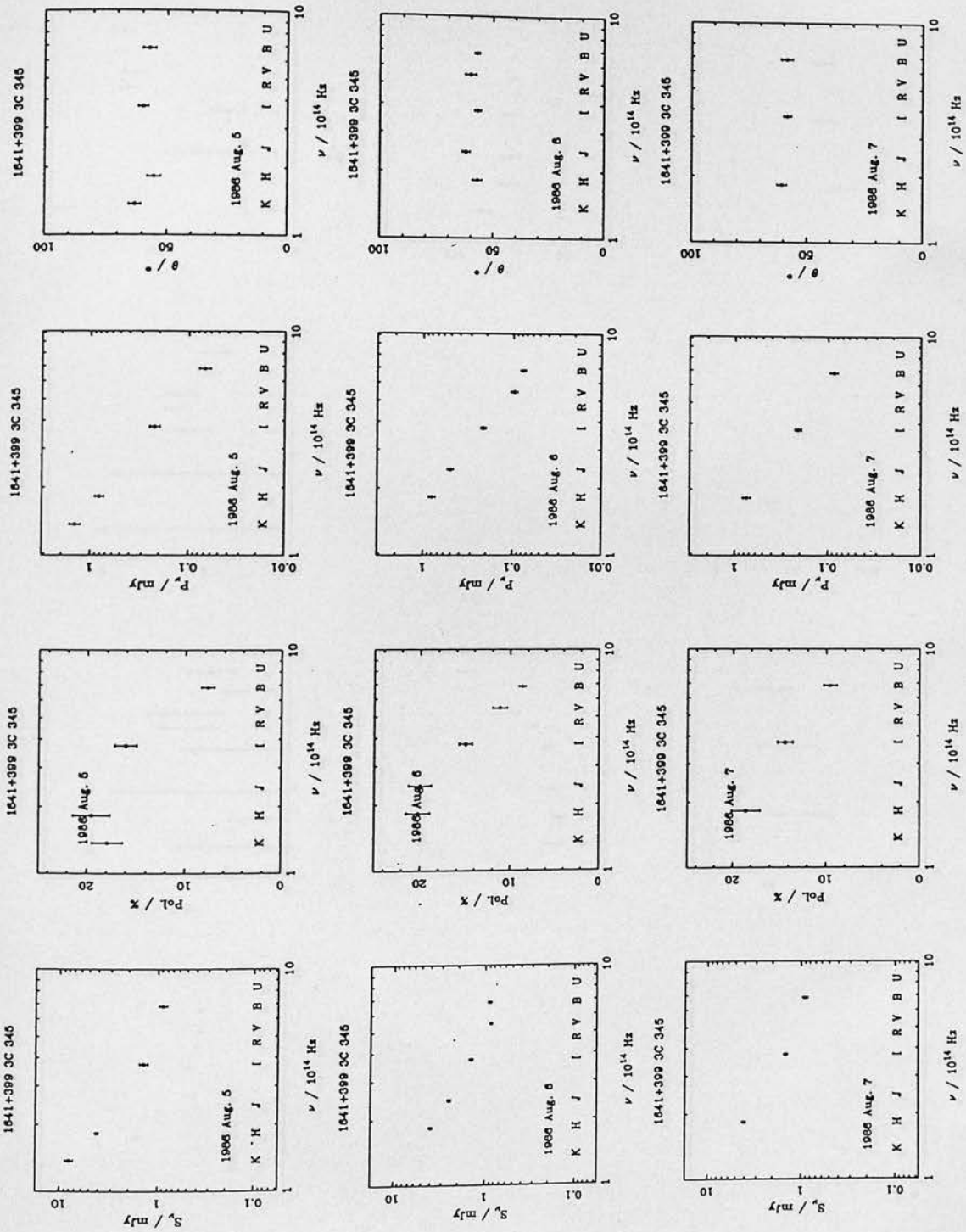

Figure A.1: *(Contd.)* Plots of the polarization data.

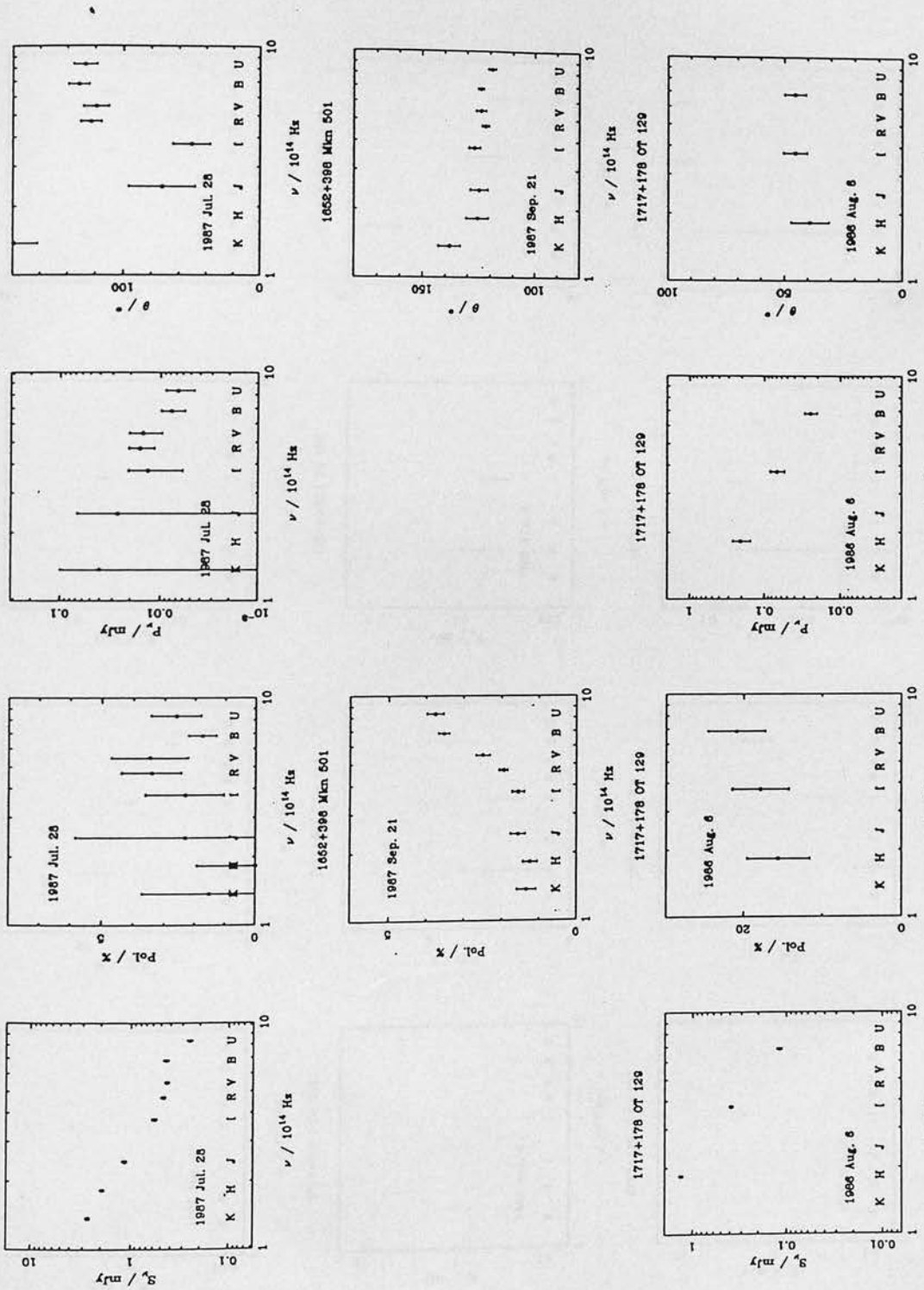

Figure A.1: *(Contd.)* Plots of the polarization data.

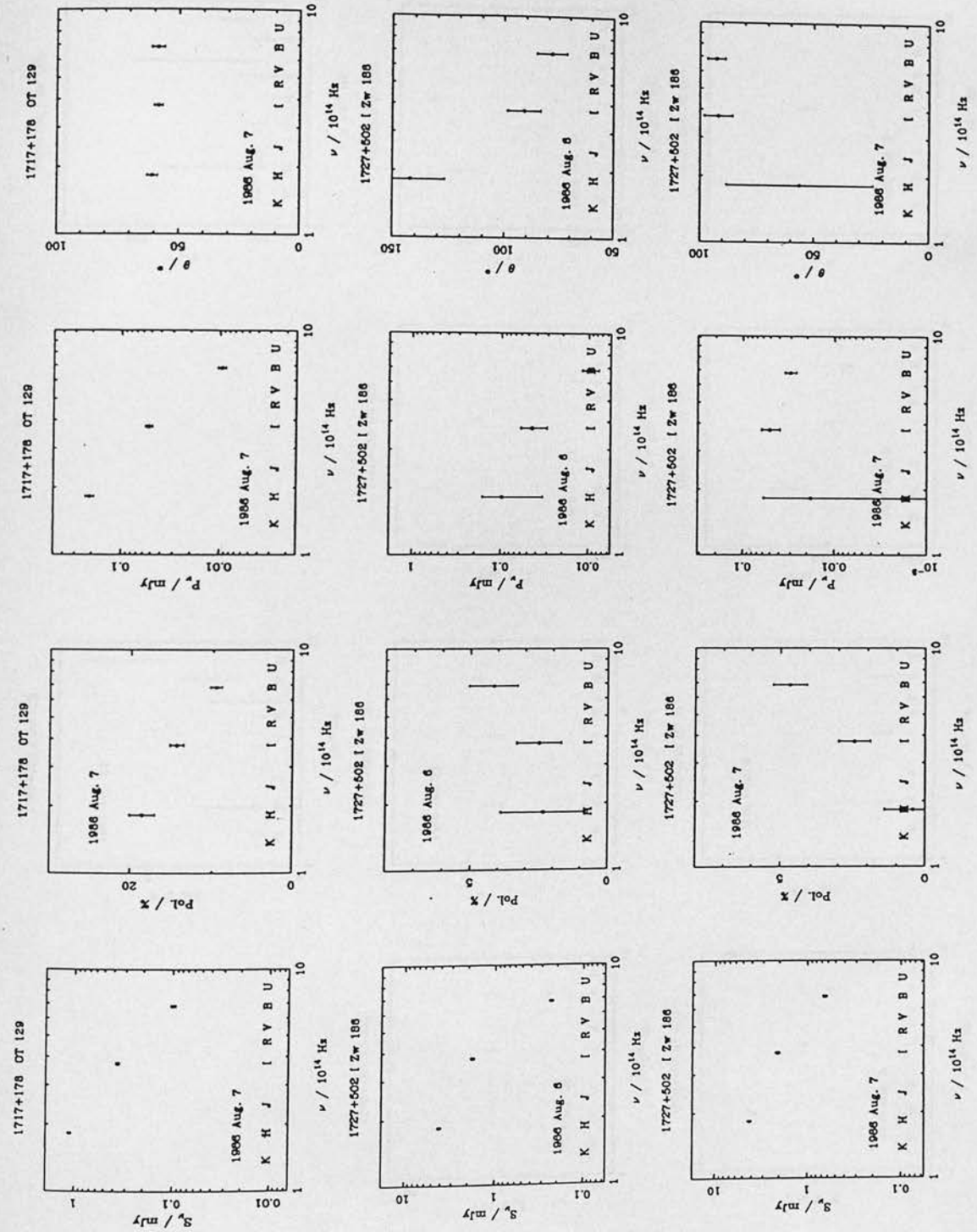

Figure A.1: *(Contd.)* Plots of the polarization data.

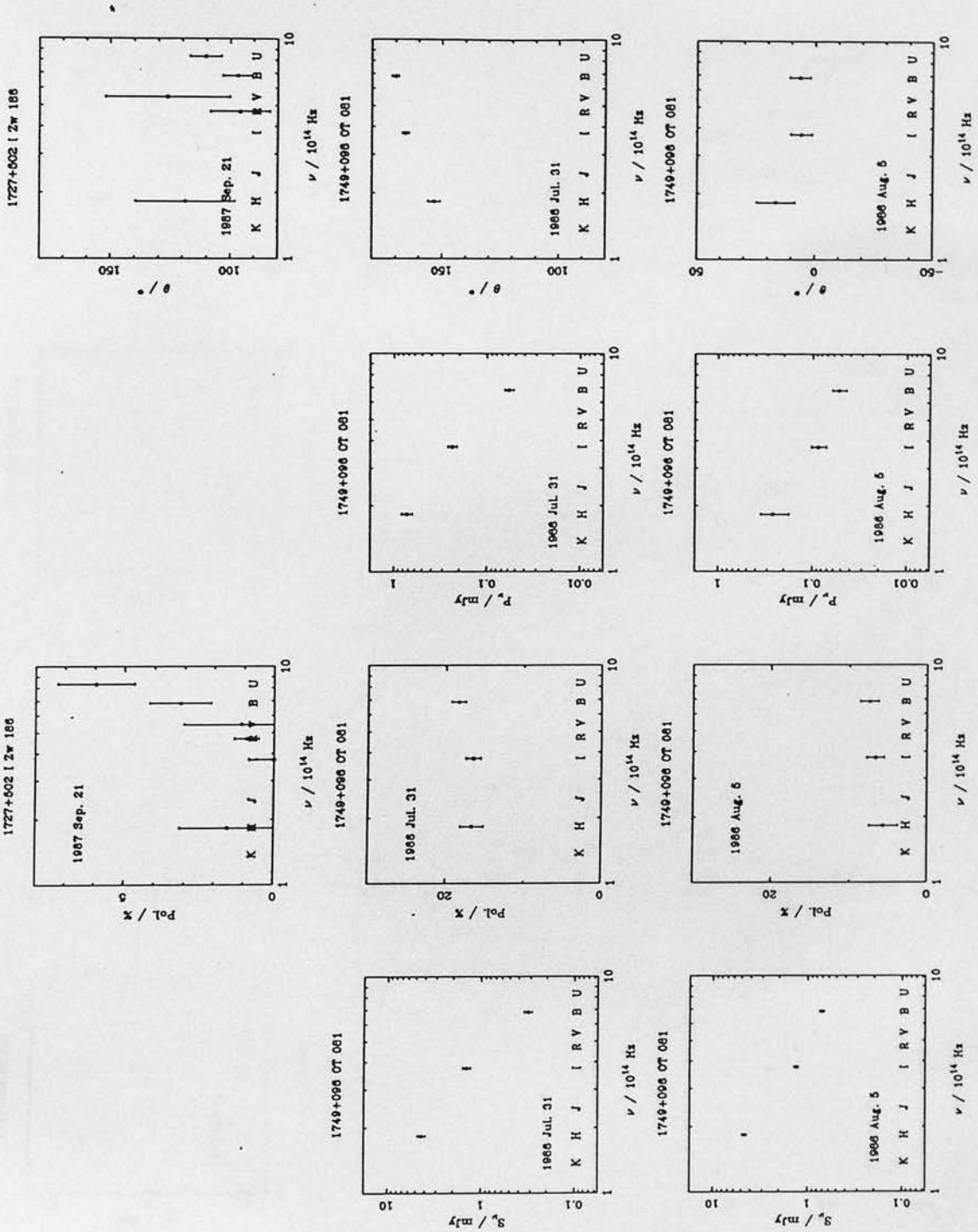

Figure A.1: *(Contd.)* Plots of the polarization data.

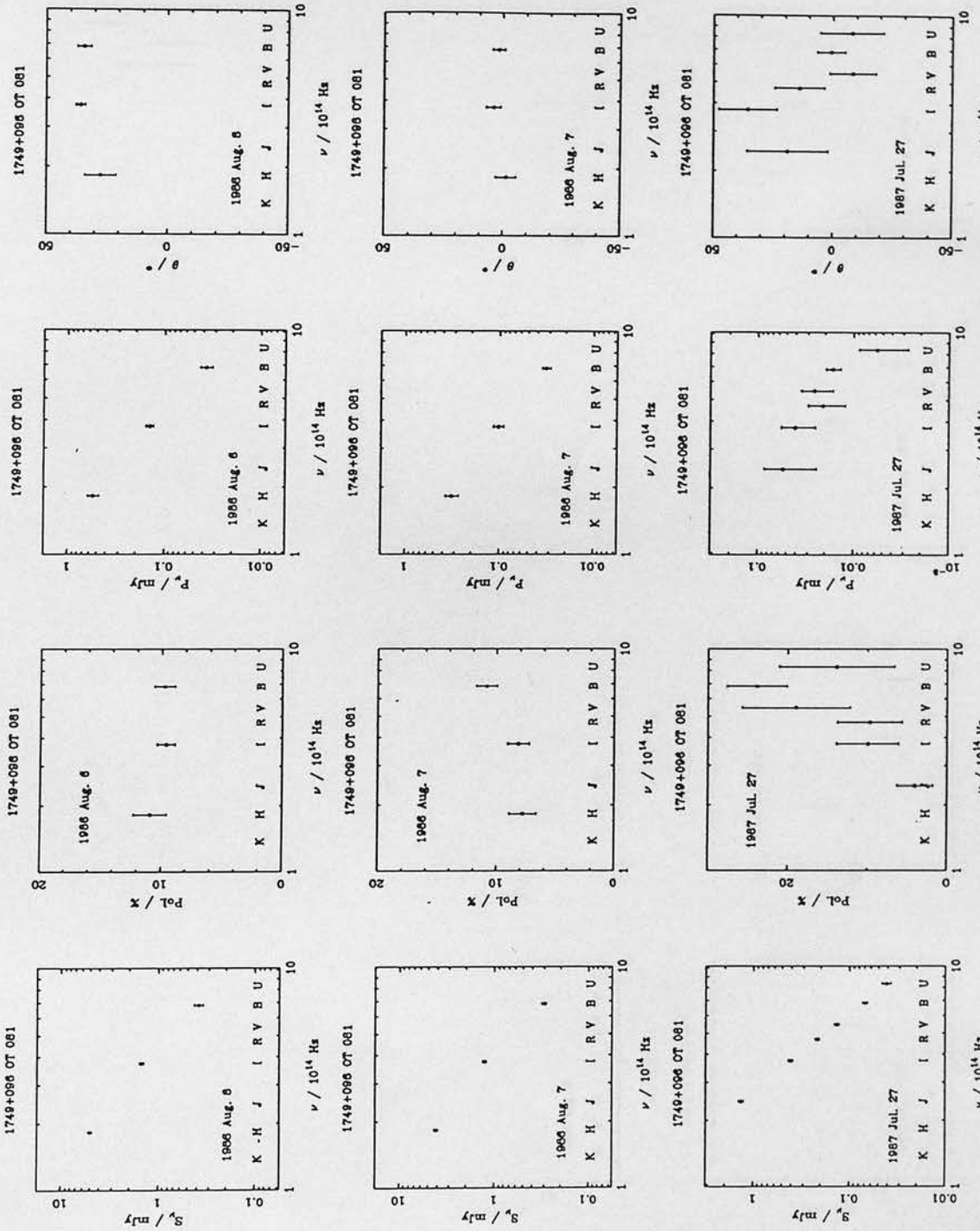

Figure A.1: *(Contd.)* Plots of the polarization data.

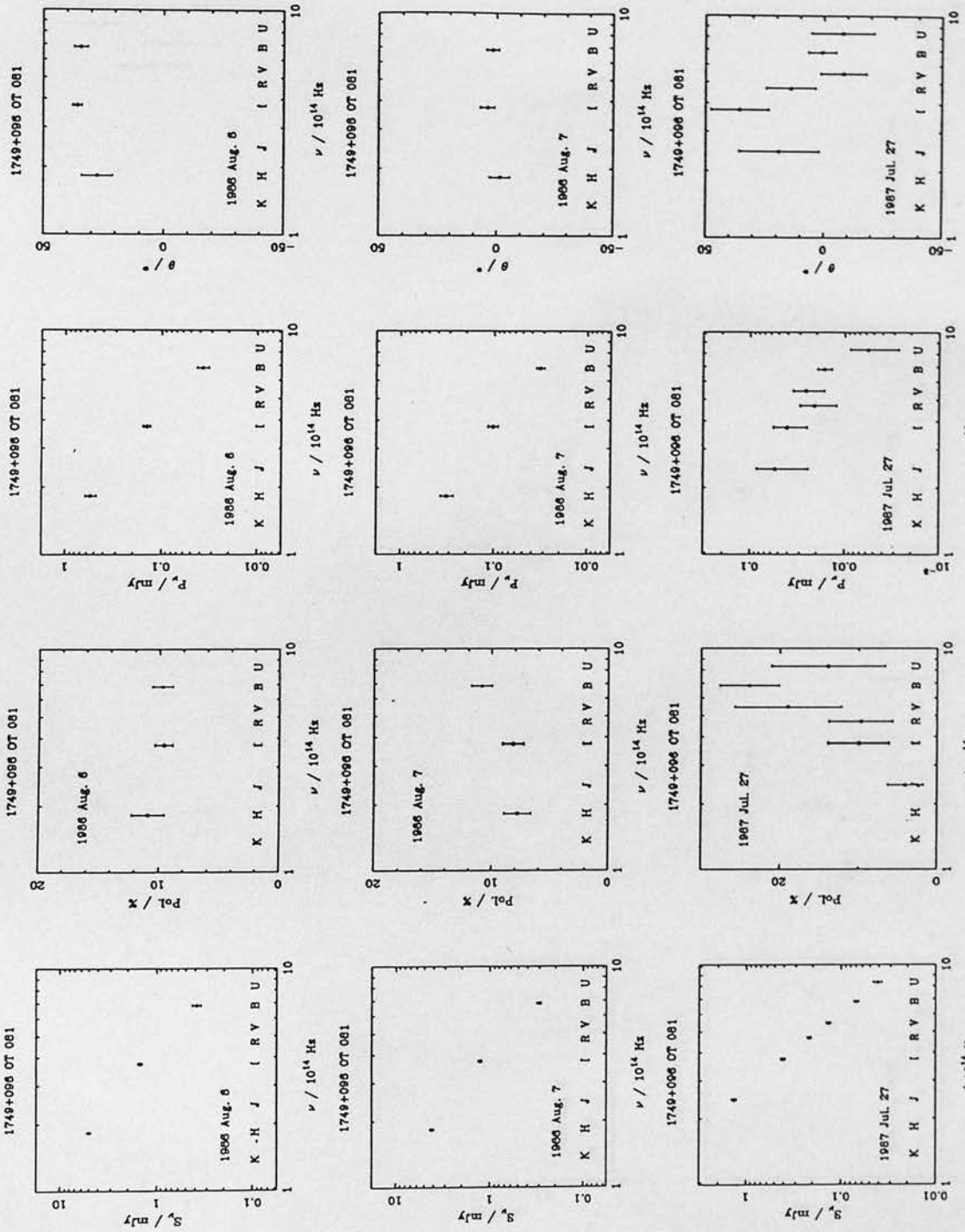

Figure A.1: *(Contd.)* Plots of the polarization data.

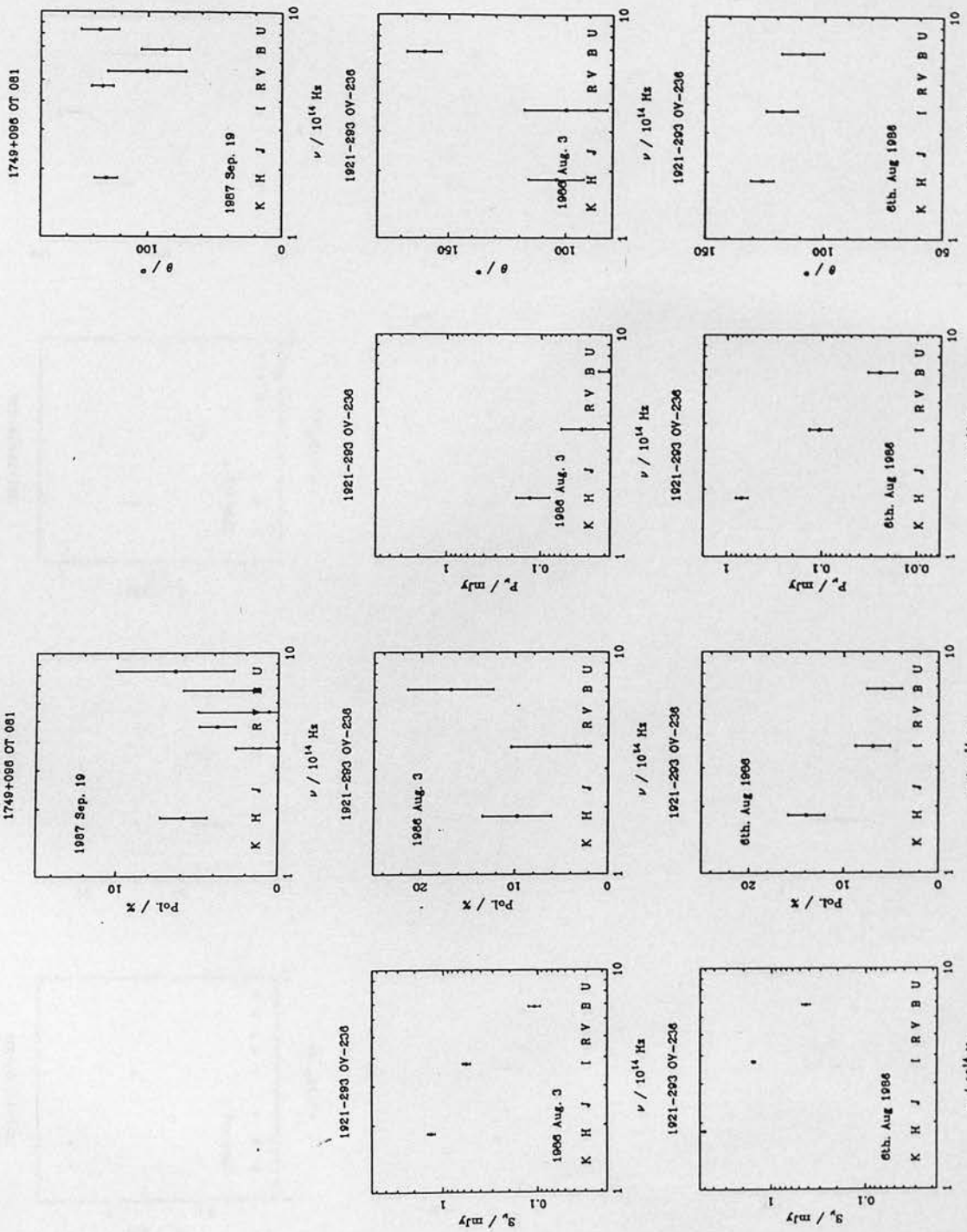

Figure A.1: *(Contd.)* Plots of the polarization data.

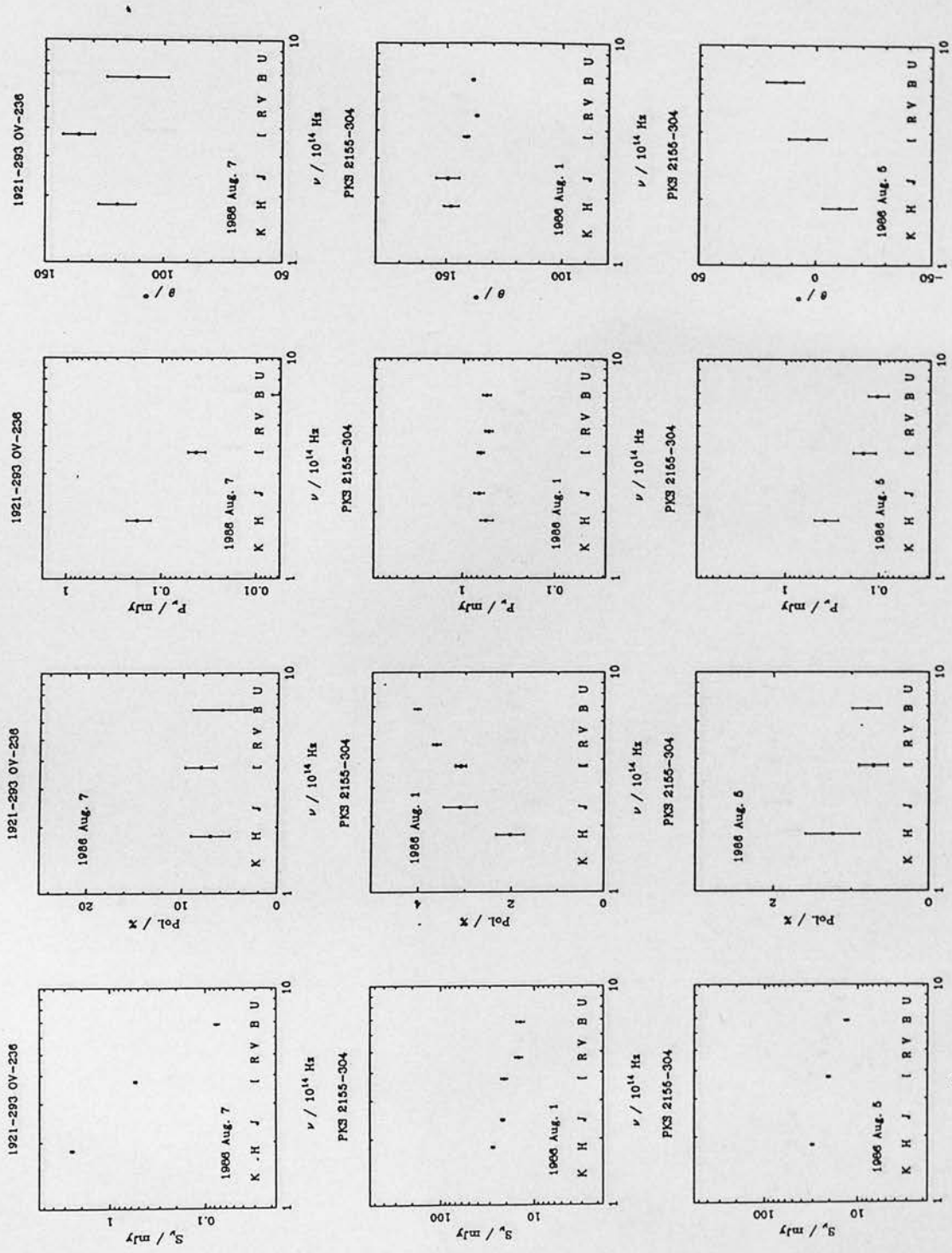

Figure A.1: *(Contd.)* Plots of the polarization data.

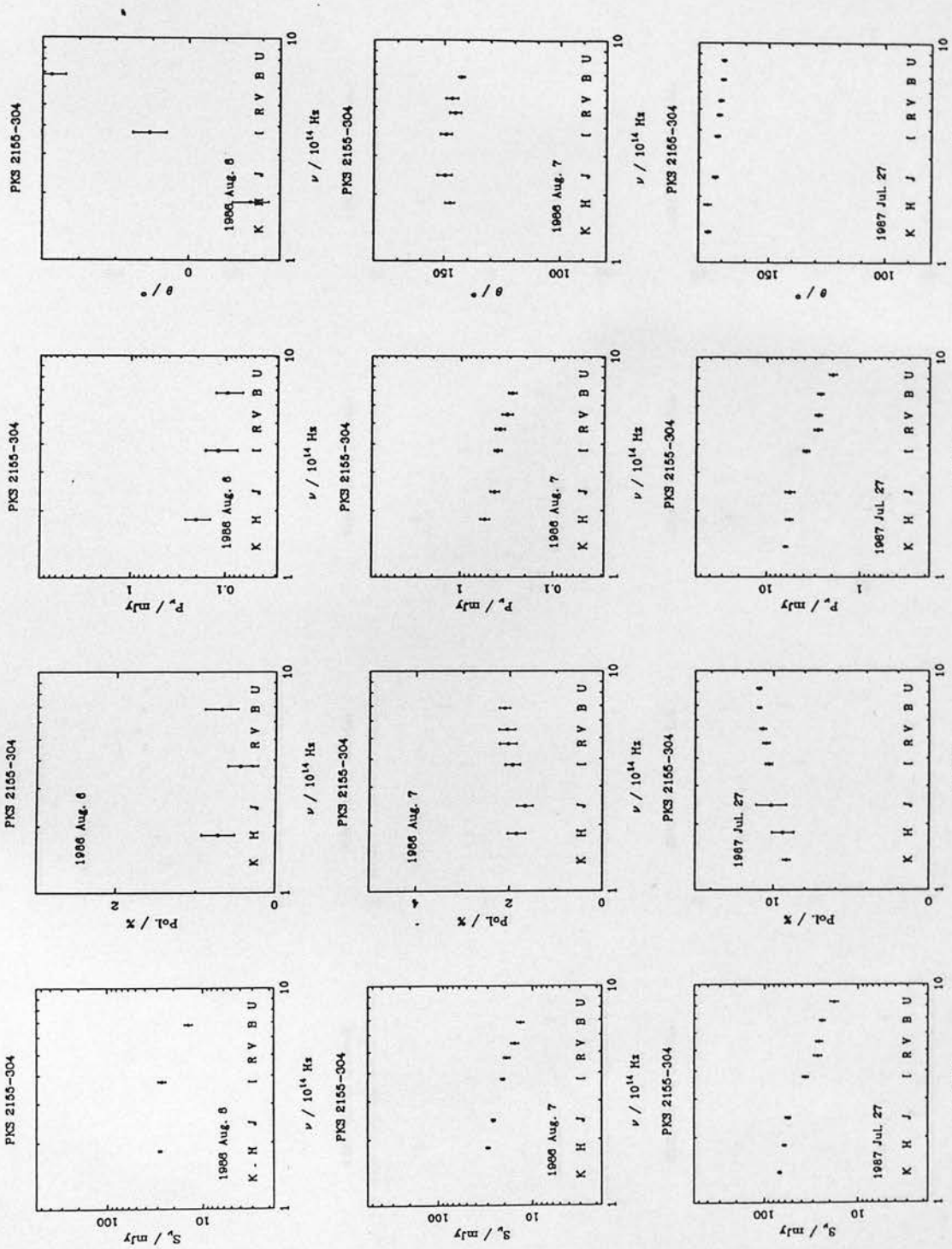

Figure A.1: *(Contd.)* Plots of the polarization data.

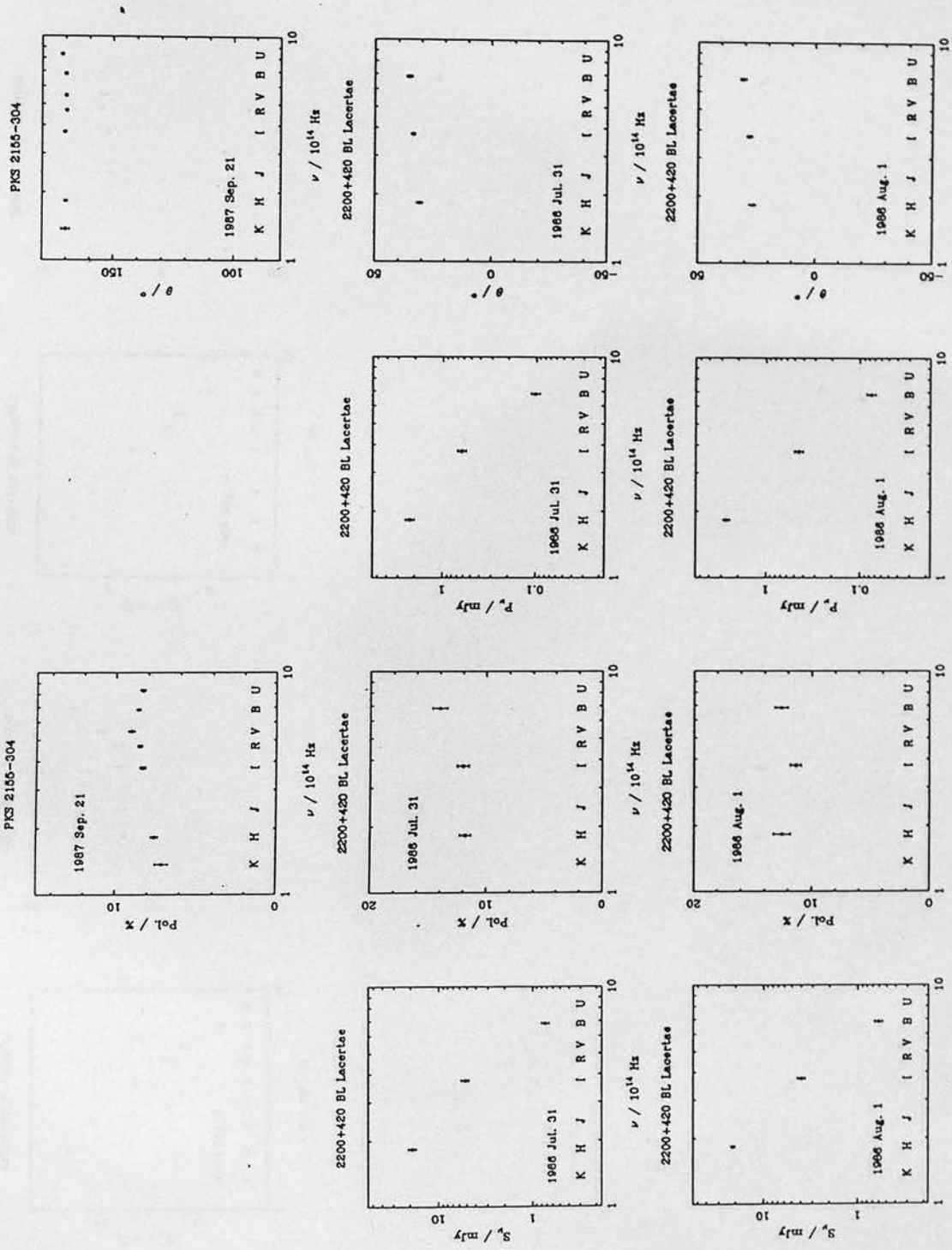

Figure A.1: *(Contd.)* Plots of the polarization data.

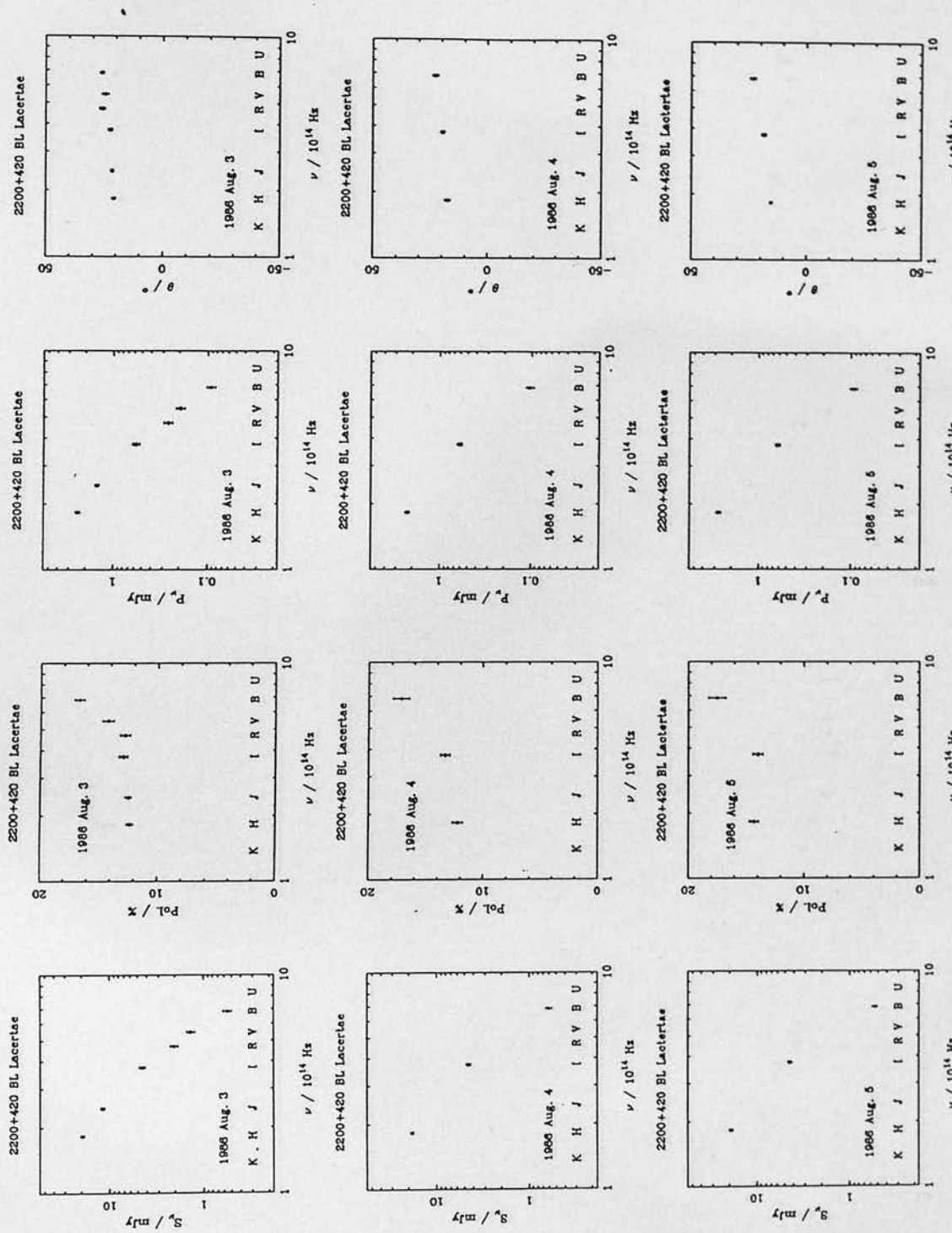

Figure A.1: *(Contd.)* Plots of the polarization data.

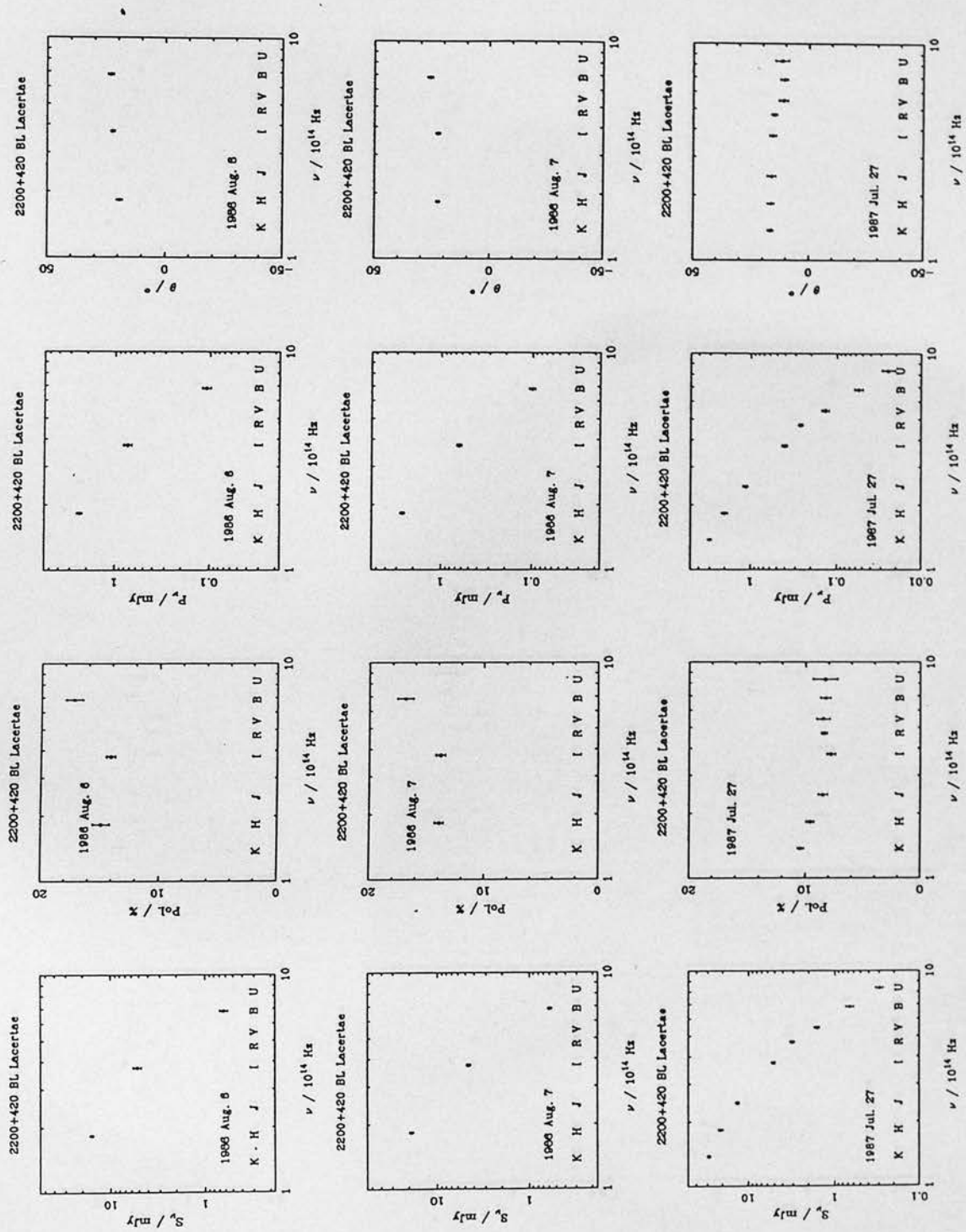

Figure A.1: *(Contd.)* Plots of the polarization data.

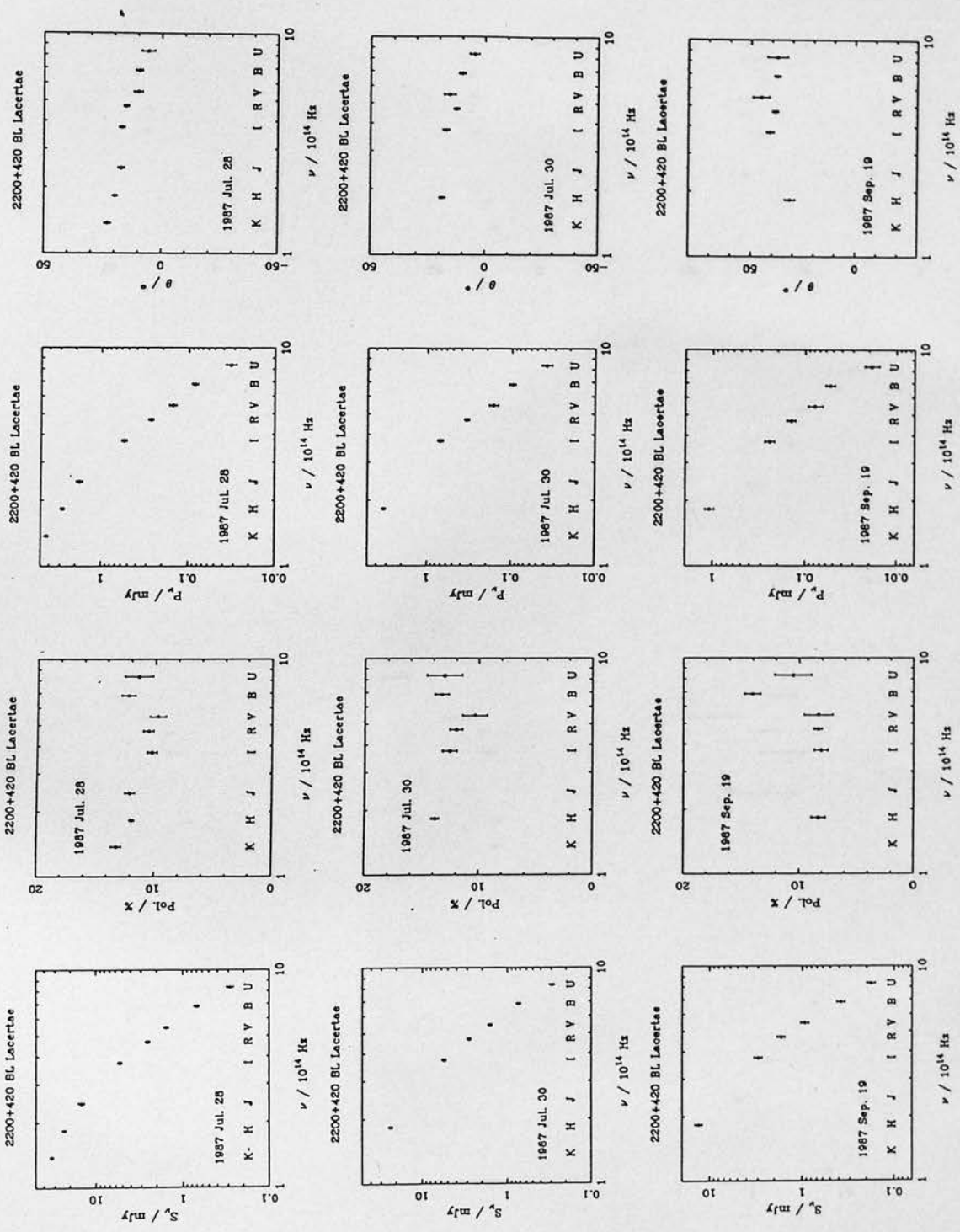

Figure A.1: *(Contd.)* Plots of the polarization data.

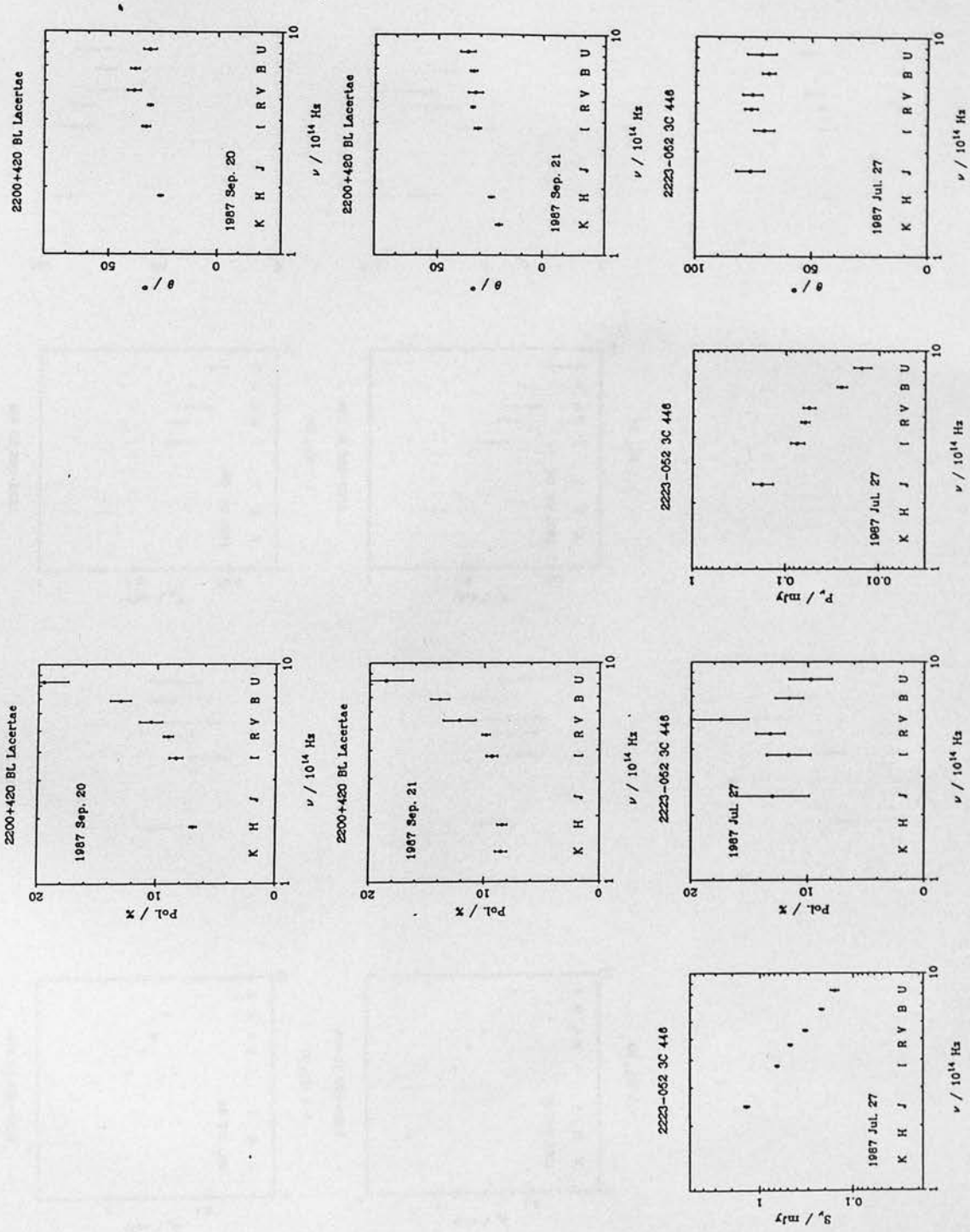

Figure A.1: *(Contd.)* Plots of the polarization data.

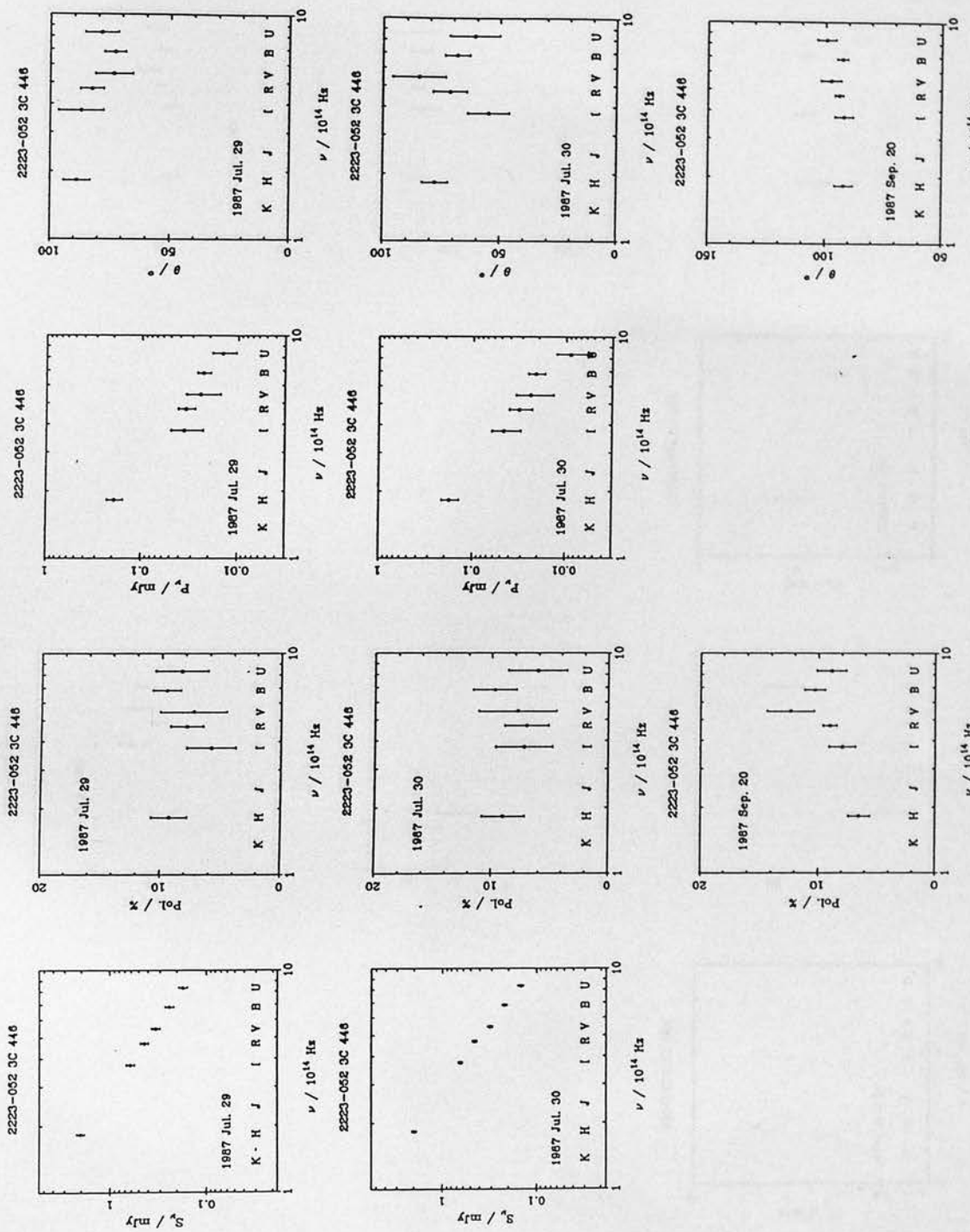

Figure A.1: *(Contd.)* Plots of the polarization data.

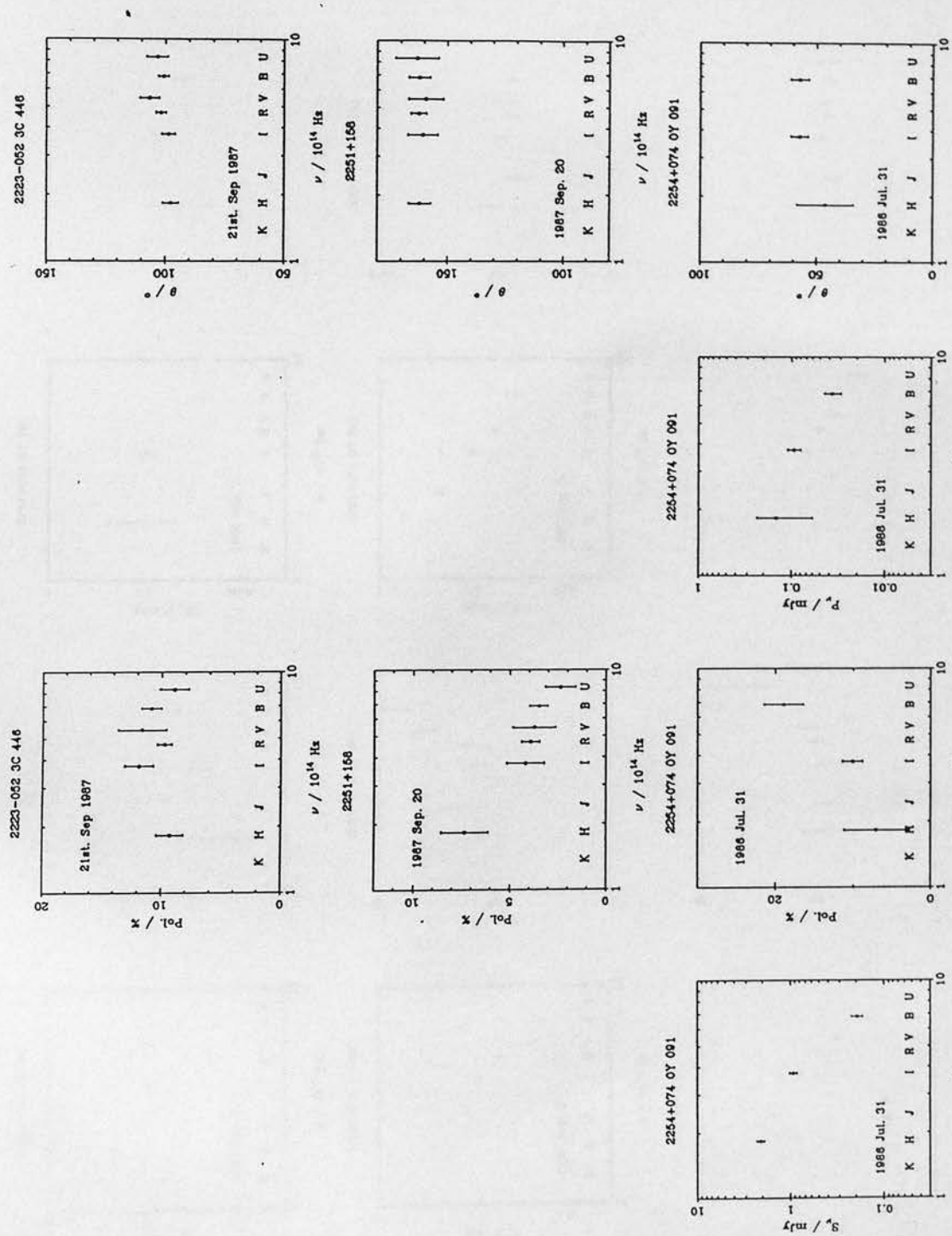

Figure A.1: *(Contd.)* Plots of the polarization data.

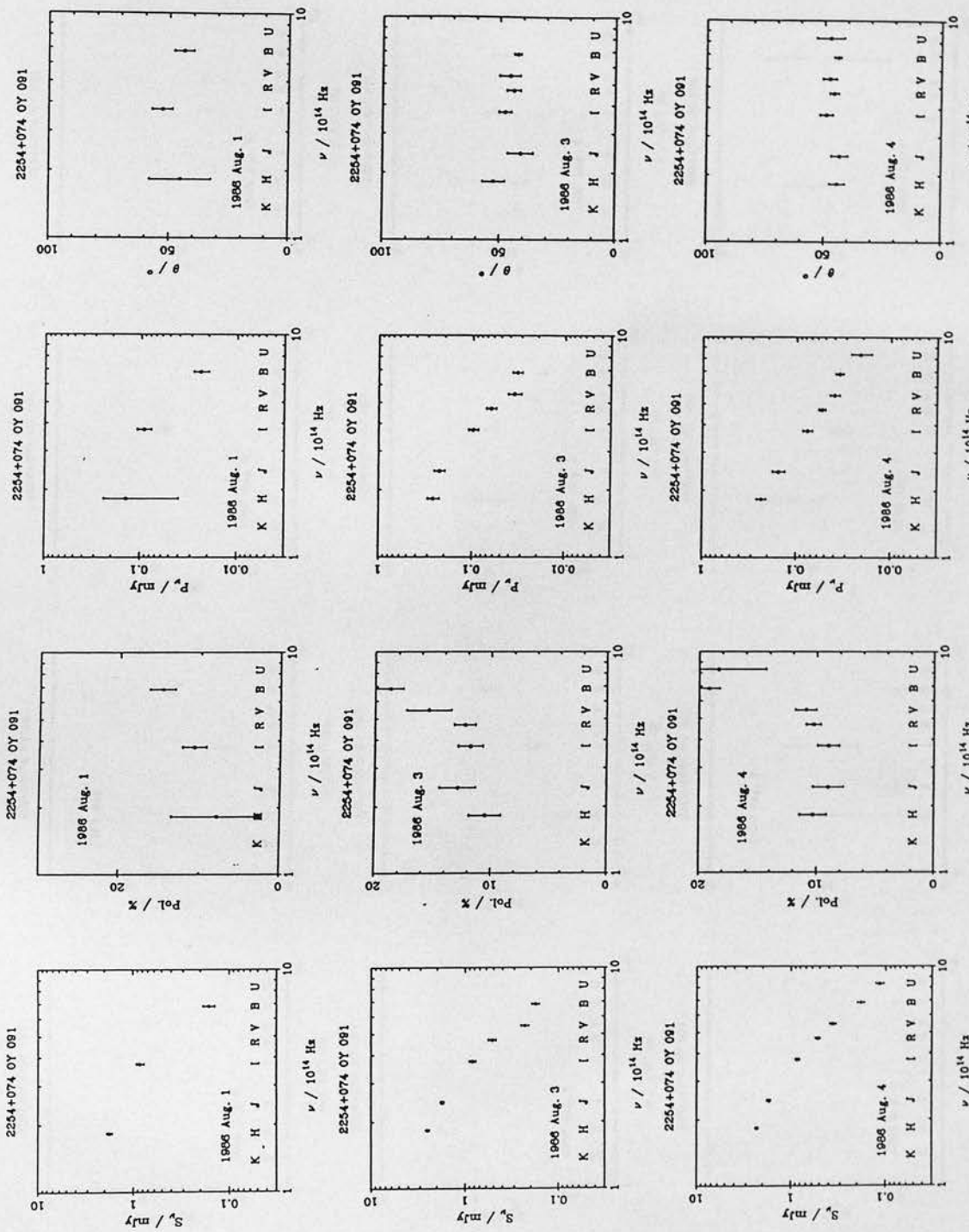

Figure A.1: *(Contd.)* Plots of the polarization data.

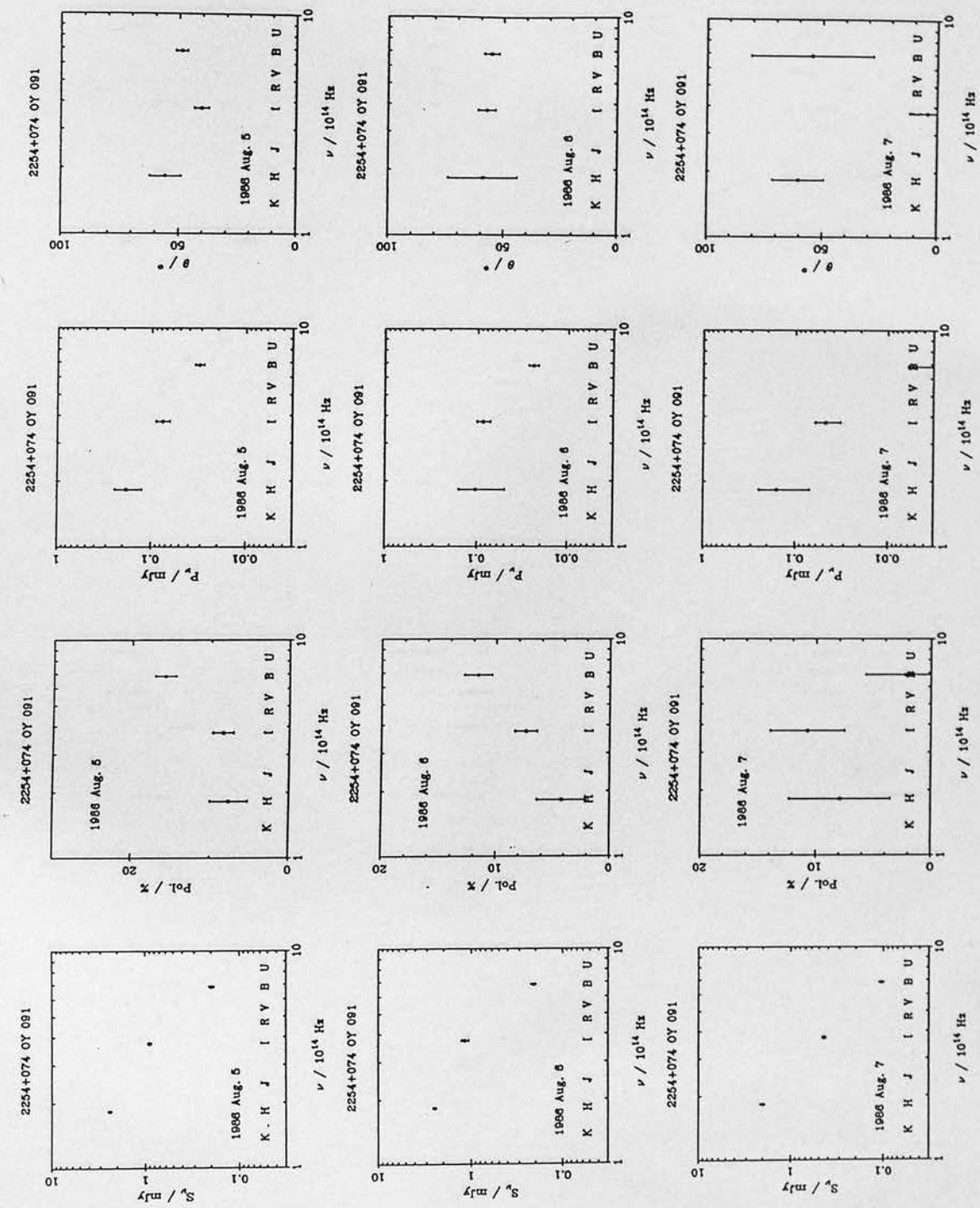

Figure A.1: *(Contd.)* Plots of the polarization data.

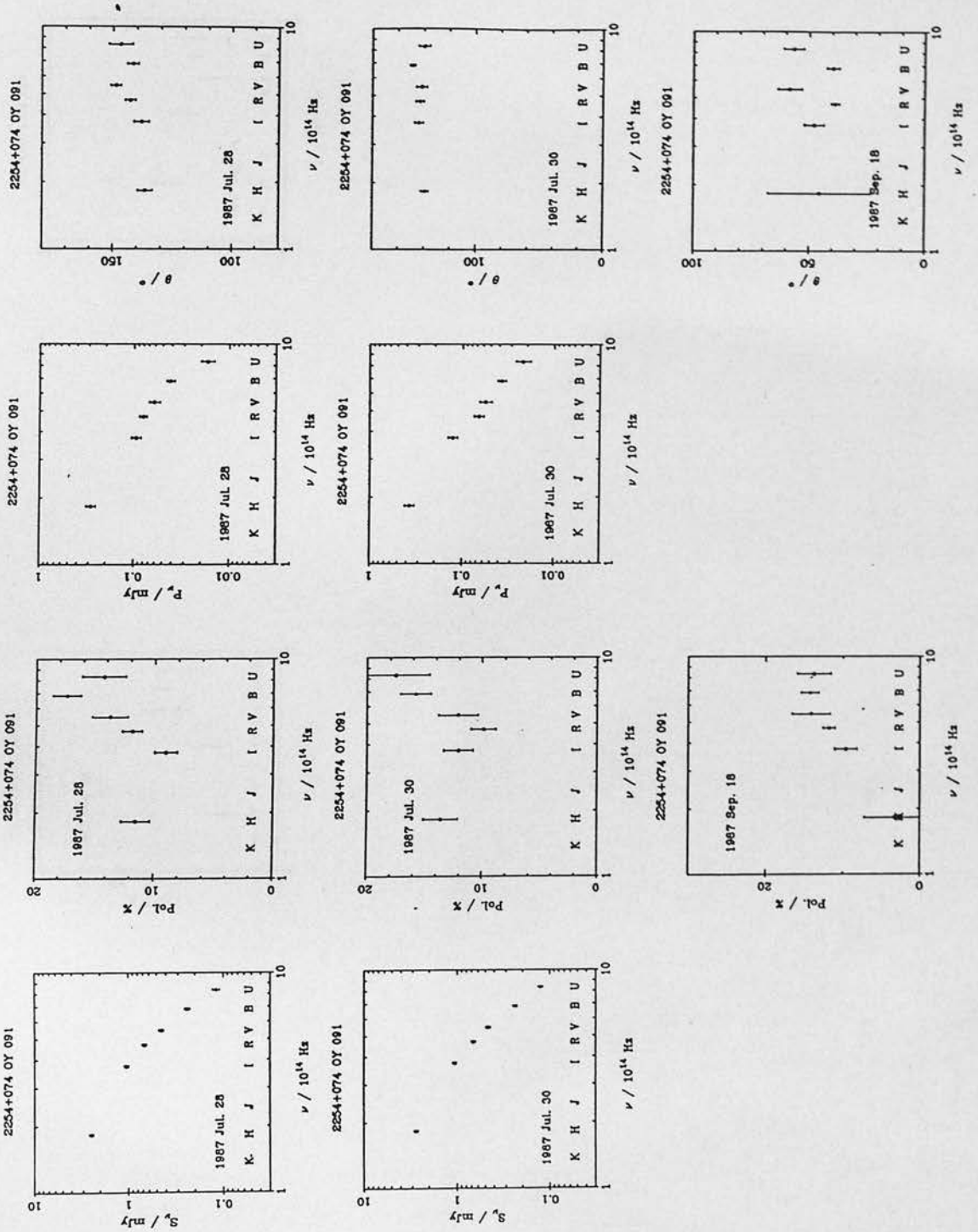

Figure A.1: *(Contd.)* Plots of the polarization data.

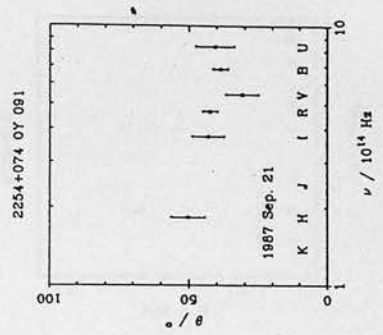

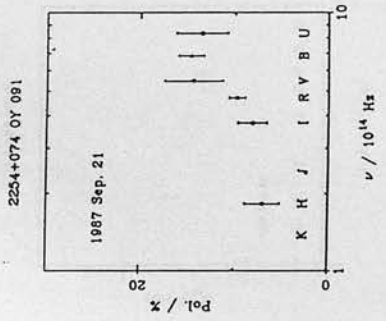

Figure A.1: *(Contd.)* Plots of the polarization data.

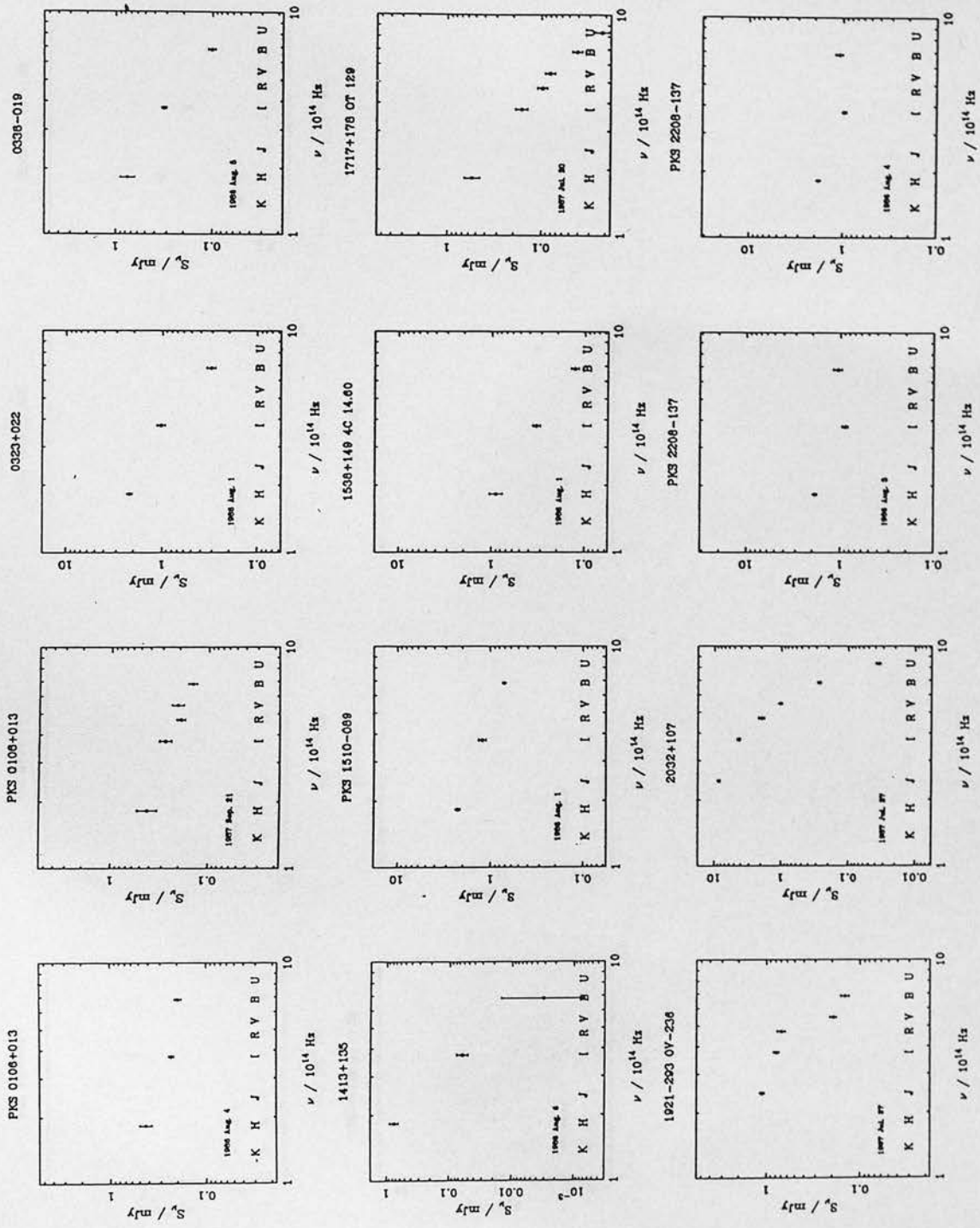

Figure A.2: Plots of the flux density data for those objects where no polarization was measured.

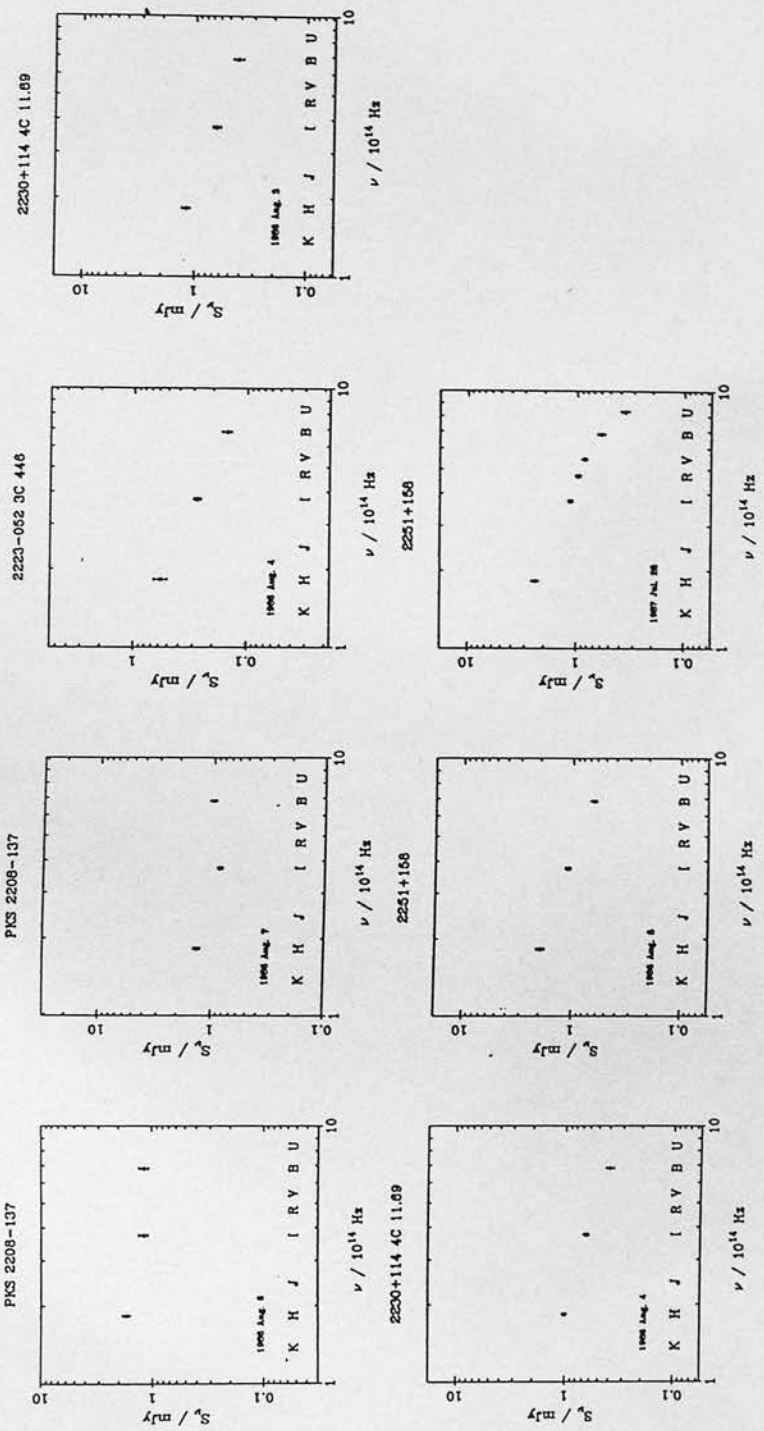

Figure A.2: *(Contd.)* Plots of the flux density data for those objects where no polarization was measured.